Cove-Edge Graphene Nanoribbon Semiconductors: from Molecules to Devices

Grisha Etkin

Submitted in partial fulfillment of the
requirement for the degree of
Doctor of Philosophy
in the Graduate School of Arts and Sciences

COLUMBIA UNIVERSITY

2018

ABSTRACT

Cove-Edge Graphene Nanoribbon Semiconductors: from Molecules to Devices

Grisha Etkin

This dissertation presents research conducted on the structure-property relationships of cove-edge graphene nanoribbon (GNR) semiconductors from the scale of molecular conformation to device performance. The ribbons described here are made derived from perylene-3,4,9,10-tetracarboxylic acid diimide (PDI) and adopt a helical conformation so we call them helical PDI (hPDI). They are n-type semiconductors with exceptional performance in field-effect transistors (FETs), organic photovoltaics (OPVs), narrowband photodetectors, and electron transporting materials in perovskite solar cells. In this work, reaction chemistry is used to design and synthesize new derivatives of hPDI to shine light on their molecular, bulk, and device properties.

The first chapter concerns the incorporation of hPDI into alternating donor-acceptor (D-A) macromolecules to create materials with internal charge transfer (CT). Computational and spectroscopic techniques, including femtosecond transient absorption spectroscopy (fsTA), are used to probe the CT character of these materials. A large dihedral angle between donor and acceptor portions limits orbital overlap, leading to lowest energy excited state with HOMO localized on the donor and LUMO localized on the acceptor. Notably, internal CT improves the OPV performance of these oligomers over their parent hPDI, while analogous macromolecules without internal CT exhibit reduced OPV performance.

Chapter 2 details a method for side chain engineering of hPDI by installing the side chain in the final step of the synthesis, rather than the first. The aromatic core of hPDI is built up with esters, rather than imides, appending the edges of the ribbons. The ester-appended ribbons are readily transformed into a late-stage intermediate for divergent installation of any desired side chains, including those that pose synthetic challenges when they are introduced into the parent PDI from the beginning. These side chains have a profound effect on the optical, thermal, and charge transport properties of hPDI in the solid state. This strategy of introducing imide side-chains into PDI-based materials in the final step can be generalized to other systems.

Chapter 3 demonstrates a method for controlling the conformation of cove-edge GNRs by changing the chemical substitution pattern at their edges. All-sp^2 substituents that lock adjacent edge positions into a ring rigidify the aromatic core of these ribbons. When substituents at adjacent edge positions are no longer locked into a ring, the aromatic core becomes flexible. Modulating this flexibility dictates how these ribbons contort to accommodate their cove-edges, with rigid cores contorting into chiral helixes, and flexible cores contorting into a butterfly conformation. This may point the way forward for the use of GNRs in applications that rely on precise control of molecular conformation

Table of Contents

List of Figures, Schemes, and Tables

Acknowledgments

First and foremost I thank Colin Nuckolls for acting as my graduate advisor. Through his mentorship and the opportunities provided by working in his lab, Colin has taught me how to work through and effectively communicate my research. More than that, his relentless optimism has been source of inspiration and motivation throughout my time in his lab. I am grateful to Fay Ng and Mike Steigerwald for their priceless guidance these last five years. Fay, the driving force behind our group's work on PDI-based materials, was always willing to talk through synthetic challenges and new ideas. Mike graciously walked me through the nuts and bolts of quantum mechanical calculations and electronic structure theory. His advice and interest in my projects has been invaluable. Jim Leighton and Luis Campos have provided thoughtful feedback as members of my thesis committee, and John Kymissis generously agreed to evaluate this dissertation as an external committee member.

I thank my colleagues and collaborators for their contributions to the work in this dissertation, and for the pleasure of working with them. Yu Zhong patiently taught me the basic principles of device performance and materials design. Boyuan Zhang has always been a bright presence in the lab and happily made many, many devices from the materials I prepared in the lab. Kiyoshi Miyata and Felisa Conrad-Burton performed extensive femtosecond transient absorption experiments on the materials presented in Chapter 1. More heroically, they explained their results to me. Florian Geyer had several valuable discussions with me about excited states and charge transfer. Neil Foegen and I worked closely together on the work presented in Chapter 2. With his enthusiasm and

Chapter 1. Internal Charge Transfer in Donor-Acceptor Perylene Diimide

Macromolecules
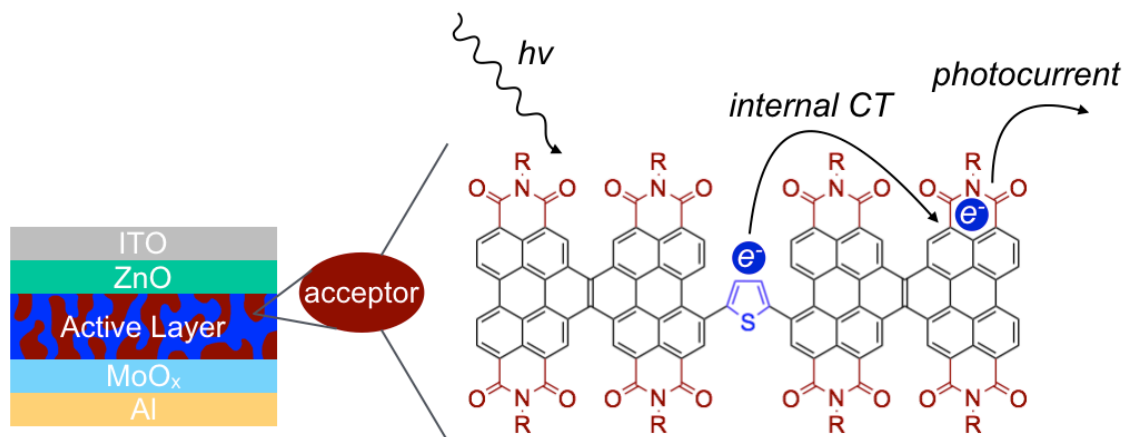
1.1 Preface

This chapter presents work on alternating donor-acceptor macromolecules based on the electron acceptor perylene-3,4,9,10-tetracarboxylic acid diimide (PDI) for use in organic photovoltaics (OPVs). This chapter begins with a summary of the state of the art of PDI-based materials for OPVs including discussion of important design criteria and strategies for new materials. Recent work from the Nuckolls group has focused on helical graphene nanoribbons of PDI that we call hPDI. Here we present acceptor-donor-acceptor dimers of hPDI linked with electron-donating thiophenes. The resulting materials exhibit internal charge transfer character that we characterize using density functional theory calculations, UV-Vis spectroscopy, fluorescence spectroscopy, and femtosecond transient absorption spectroscopy. These materials show improved OPV performance over their parent hPDI and over negative control molecules in which internal charge transfer is repressed.

This chapter is based on a manuscript in preparation entitled "Internal Charge Transfer in Perylene Diimide Materials for Organic Photovoltaics" by Grisha Etkin, Boyuan Zhang, Kiyoshi Miyata, Felisa S. Conrad-Burton, Fay Ng, Michael L. Steigerwald, Xiaoyang Zhu, and Colin Nuckolls. For this work, I synthesized all the compounds. I performed all theoretical calculations with significant advice from Dr. Michael L. Steigerwald. Boyuan Zhang fabricated all of the devices and performed all AFM experiments. Prof. Kiyoshi Miyata and Felisa S. Conrad-Burton of Prof. Xiaoyang Zhu's group performed all femtosecond transient absorption experiments.

1.2. Perylene Diimide-Based Materials as Acceptors in Organic Photovoltaics

Since the proliferation of machine-automated labor and the use of electric power, the energy for these activities has been primarily derived from fossil fuels. Extracting energy from these sources presents several problems. (1) Burning fossil fuels releases pollutants that harm the environment and negatively affect human health.[1] (2) Chief among these pollutants is CO_2. The greenhouse effect of anthropogenic CO_2 has lead to sudden changes in climate that reduce the human habitability of many regions, including changes in land arability, increasing extreme weather events, and rising sea levels.[2] (3) Fossil fuels are renewed by processes many orders of magnitude slower than human activity. Global reserves of oil and natural gas are predicted to last just over 50 years, while coal is predicted to last approximately 150 years.[3] (4) As easily extracted sources of fossil fuels are depleted, meeting human demand for energy has increased the use of extractive techniques such as fracking that harm the environment and human health.[4] To address these problems, numerous alternative energy sources have been explored. Photovoltaic devices (solar cells), which convert incident photons into electrical current, are especially appealing on account of the abundant and long-lasting source of light provided by the sun.

Commercial inorganic solar cells, primarily those made from silicon, dominate the field of photovoltaics because they achieve high power conversion (PCE) of greater than 20% and because the technology for their manufacture is mature.[5] However, organic materials have several potential advantages over inorganic silicon as the active layer in photovoltaics. (1) Organic materials can be readily processed as solutions, potentially

reducing the cost and energy expenditure of fabricating organic photovoltaics (OPVs). (2)

The electronic and materials properties of organic small molecules and polymers can be

tuned using reaction chemistry. (3) Organic thin films can be incorporated into

mechanically flexible devices, which is superior to silicon in applications that benefit

from physical impact resistance or flexibility. Single-junction OPVs now have certified

PCEs approaching 12%.[6]

Until recently, OPV research has been dominated by polymer-fullerene devices in

which the active layer is composed of a P-type (donor) polymer and an N-type (acceptor)

fullerene derivative, typically [6,6]-phenyl-C_{61}-butryic acid methyl ester (PC$_{61}$BM)

(Figure 1.1.a) or its C_{71} analog (PC$_{71}$BM). Fullerenes have several advantageous

properties as acceptors for OPVs, including high electron mobility and isotropic charge

transport.[7] Furthermore, on blending with polymer donors, they readily form active layers

with ideal morphological features for charge separation and charge extraction.[8] However,

fullerenes have weak absorptivity across most of the solar spectrum and most generated

charges must originate from absorption by the donor polymer. They are also expensive to

produce and difficult to chemically modify. It is therefore challenging to tune their

materials properties to enhance device performance. A variety of molecular and

polymeric acceptors have appeared as competitors to fullerenes in OPVs. Among these

are derivatives of perylene-3,4,9,10-tetracarboxylic acid diimide (PDI) that now have

PCEs nearing 11%.[9] PDI is an attractive parent material for electron acceptors because it

is made from inexpensive perylene-3,4,9,10-tetracarboxylic acid dianhydride (PTCDA),

it has high molar absorptivity in a large part of the solar spectrum, it readily accepts and

transports electrons, and its electronic and materials processing properties can be readily tuned through chemical reactions.

1.2.1. Limits on Current Generation in Organic Photovoltaics

Photocurrent is generated in OPVs in four steps (Figure 1.1.b). (1) Exciton generation: active layer material absorbs a photon, creating an excited state (2) Exciton diffusion: excitons travel to the interface between donor and acceptor in the active layer by diffusion or by Förster resonance energy transfer (FRET). (3) Charge separation: excitons at the donor-acceptor interface separate into holes in the donor layer and electrons in the acceptor layer. (4) Charge extraction: free charges travel to their respective charge transport and charge collection layers, generating current. Numerous unproductive pathways can capture excitons or free charge carriers, reducing the efficiency of each of these fundamental steps.
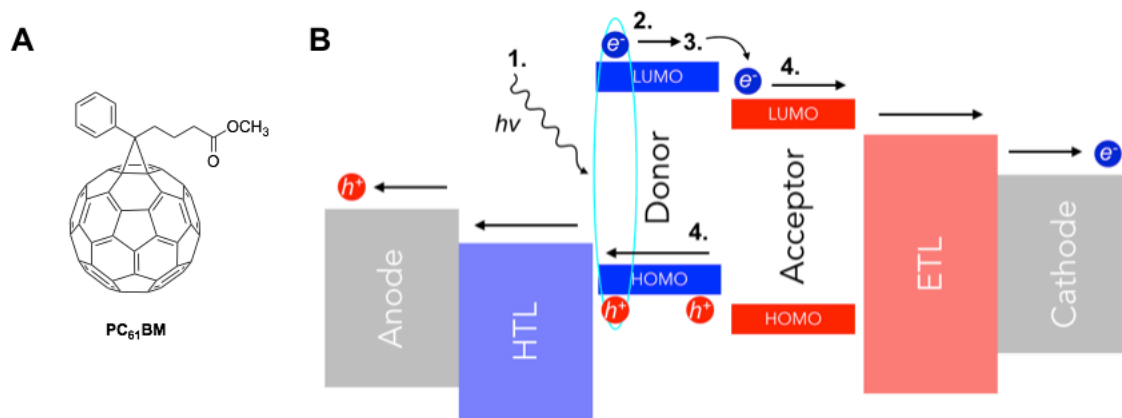
Figure 1.1. (A) Structure of fullerene acceptor PC$_{61}$BM. (B) Schematic representation of exciton generation (1), diffusion to (2) and separation at (3) the donor-acceptor interface, and charge collection (4) via an electron transporting layer (ETL) to the cathode and via a hole transporting layer (HTL) to the anode. Excitons can also be generated in the acceptor, which can then transfer a hole to the donor, also leading to current generation.

The active layer must efficiently absorb incident light. Active layers as thin as 100 nm can absorb up to 90% of incident light when made of highly absorbent donor and acceptor with complementary UV-Vis spectra.[10] The facile chemical functionalization of PDI allows it to be incorporated into a wide range of acceptors with high molar absorptivities ranging from the UV up to 550-650 nm. PDI-based acceptors are usually partnered with low bandgap donors with absorption up to 700-750 nm, effectively covering most of the high-energy portion of the solar spectrum. This broad coverage can result in high external quantum efficiency (EQE) of incident photons converted to photocurrent that matches the absorption spectrum of blend films of donor and acceptor.

Exciton diffusion to the donor-acceptor interface is limited by the short lifetimes of excitons in organic materials. The effective diffusion radius of these materials is typically 5-20 nm, which is much smaller than the film thickness required to sufficiently absorb incident sunlight.[9,11–14] Therefore, most high-performance OPVs use a bulk heterojunction (BHJ) architecture for the active layer, consisting of interpenetrating networks of donor and acceptor domains. With effective processing conditions, these domains are 10-30 nm in size. Small domain size and large interfacial surface areas minimize the loss of excitons through geminate recombination before they reach the donor-acceptor interface.[8,15–18]

Inefficient charge separation at the donor-acceptor interface can reduce PCE either through excitons failing to separate into isolated charges (reduced current) or through the driving force required for this separation (reduced voltage). The contact distance between donor and acceptor must be balanced so that the tightly bound charge

transfer state is not lower in energy than the corresponding pair of free charge carriers, which would make charge separation endothermic.[19] Some of the most successful donor materials for OPVs are polymers composed of alternating donor and acceptor subunits, leading to a lowest-energy excited state in which the hole is localized on the donor portion and the electron is localized on the acceptor portion.[20–22] Separately modifying the steric bulk of the side chains on the donor and acceptor portions of these polymers shows that efficient free charge carrier generation depends on favorable contact between the acceptor portion of the donor material and the electron-accepting material.[23] i.e., if the lowest-energy excited state of the donor localizes electrons to a particular segment of the donor material, then the side chains on that segment should be engineered to create favorable contact with the acceptor material in the solid state. The frontier orbitals of the donor and acceptor in the solid state must provide sufficient driving force to separate charges at the interface. Typically, the LUMO of the donor should be at least 0.3 eV higher in energy than the LUMO of the acceptor to efficiently separate excitons generated in the donor into free charge carriers.[24] (The same guideline applies to the HOMO of both materials for efficient generation of free charge carriers from excitons generated in the acceptor, as well as to prevent recombination at the interface.) This limit on the energy of free charge carriers limits the open-circuit voltage (V_{OC}) of devices.

Lastly, the collection of free charge carriers is limited by their potential for recombination at the interfaces between donor and acceptor, and by inefficient injection of free charges into their respective charge transport layers. Efficient extraction of free charge carriers is mediated by the contact between the active layer and the charge

7

transporting layers. For example, one of the benefits of the PTB class of donor polymers is their ability to self-organize with respect to the hole-transporting layer.[25] After processing, the π-surface of PTB-class materials is aligned parallel to the hole-transporting layer, facilitating charge extraction.

1.2.2. Design of Perylene Diimide Acceptors for Organic Photovoltaics

Given the physical processes involved in generating photocurrent, several criteria can be established for designing new PDI-based acceptors for OPVs.

(1) The acceptor should have a high absorptivity. The absorption spectrum should complement that of the donor material to ensure efficient absorption across the high-energy portion of the solar spectrum. The single visible light excitation of PDI has a molar absorptivity of 8×10^5 M^{-1} cm^{-1}. This excitation at 525 nm exhibits a vibronic progression extending to 450 nm. Materials made from PDI commonly have high absorptivity from the UV up to 550-650 nm.

(2) The acceptor should be photochemically stable and should be reversibly reducible. PDI-based molecules typically reversibly accept $2n$ electrons where n is the number of PDI subunits incorporated into the molecule. PDI is highly stable to light and is commonly used as a commercial pigment.

(3) The energy levels of the acceptor should be aligned with the donor to allow for charge separation at the donor-acceptor interface. Typically, the HOMO and LUMO of the acceptor should both be ~ 0.3 eV lower in energy than the corresponding orbitals of the donor to provide the driving force for charge separation.[24] PDI can be readily functionalized and incorporated into larger

structures using reaction chemistry, tuning the frontier orbitals to better match a variety of donor materials.

(4) The mixture of donor and acceptor should form a bulk heterojunction with favorable morphology. The segregated phases of donor and acceptor should be 10-30 nm in size to ensure efficient diffusion of excitons to their interface. The interfaces should between donor and acceptor domains should be arranged to promote charge separation. The orientation of materials within a domain should facilitate hole transport through the donor and electron transport through the acceptor. The interfaces between donor and acceptor domains with their respective charge transporting layers should promote charge extraction. Typically, these morphological features are tuned by modifying the solubilizing chains of the donor and acceptor, and by modifying the film casting and processing conditions. The imide position of PDI can be functionalized with a wide variety of side chains to tune the processing characteristics of PDI-based materials. (Chapter 2 of this text presents a general process for installing the imide solubilizing chain in the last step of synthesizing a PDI-based material, allowing for facile screening of solubilizing chains.) The molecular structure of PDI-based materials influences their conformation, with contorted materials typically being more soluble and less prone to forming large aggregates in thin films than their more planar counterparts.[8,15–18]

The properties of PDI and PDI-based materials can be tuned through a wide variety of chemical reactions to meet the above criteria. **PDI** is prepared from perylene-

3,4,9,10-tetracarboxylic acid dianhydride (**PTCDA**) and a primary amine (Scheme 1.1).
The solubilizing characteristics of this side chain installed via a primary amine have a
large influence over the film morphology of the resulting PDI (and of any materials made
from that PDI). Most high-performance PDI-based materials use a symmetrical alpha-
branched alkyl chain at the imide position to limit aggregation in thin films. PDIs with
linear alkyl chains form well-ordered domains with long-range crystallinity, leading to
the formation of excimers and charge traps.[26–30] With proper donor pairing and fine-
tuning of processing conditions, unfunctionalized monomeric PDI with alpha-branched
alkyl chains can achieve PCE up to 5.1%.[31] Short circuit current (J_{SC}) decreased linearly
with observed phase size, reinforcing the importance of BHJ morphology in driving
charge separation and collection.[8,32,33]
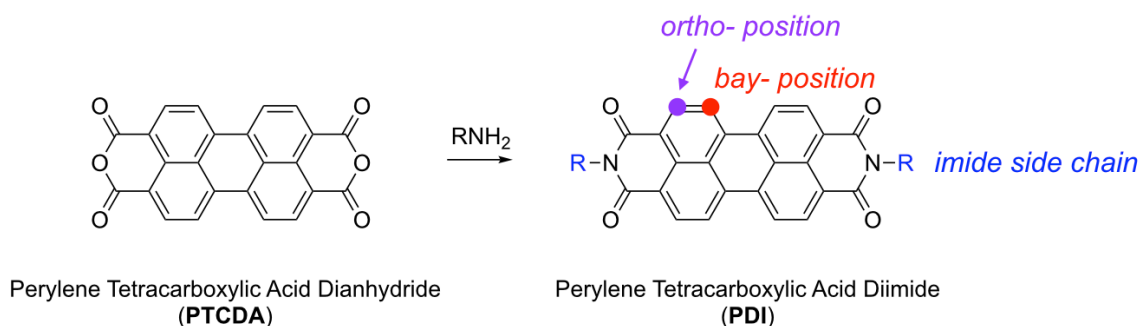
Scheme 1.1. Synthesis of **PDI** from **PTCDA** and a primary amine. The imide, 1,6,7,12- (bay-), and
2,5,8,11- (ortho-) positions can each be selectively functionalized.

PDI can be functionalized selectively at either the ortho or bay positions. Several
techniques stand out as the most useful in the context of acceptor materials for OPVs.
PDI is readily brominated at the bay position, producing a mixture of mono- and di-
brominated material (Scheme 1.2). These materials are highly active in organometallic

cross-coupling and homo-coupling reactions, which is the basis for the incorporation of PDI into many larger PDI-based materials. The di-brominated material is produced as a mixture of 1,6- and 1,7- regioisomers. Separating the two regioisomers requires preparative HPLC, limiting the use of di-brominated PDI as a building block in applications that are sensitive to this regiochemistry. Bromide functionalities can be readily displaced by methoxide, yielding the corresponding methyl ether.[34] The resulting methyl ether acts as a directing group for further bromination and can be transformed into a triflate, producing a library of regioisomerically pure PDI derivatives (Figure 1.2.a) and extended structures with absolute control over regiochemistry (Figure 1.2.b).
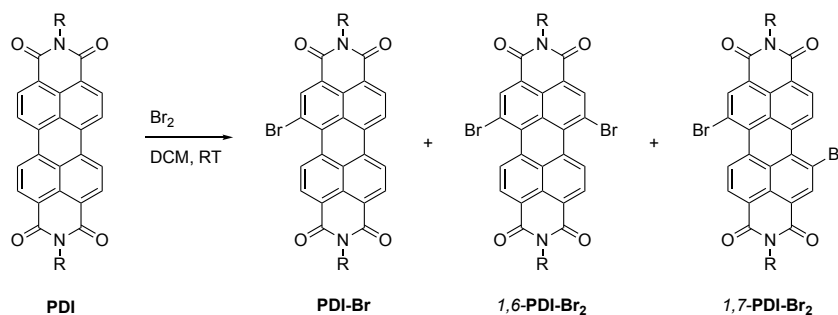
Scheme 1.2. Synthesis of brominated PDI for incorporation into PDI-based materials. The yield and ratio of mono-brominated to di-brominated material is controlled by reaction time and concentration. The ratio of *1,6*-**PDI-Br₂** to *1,7*-**PDI-Br₂** is approximately 1:5, necessitating alternative procedures or alternative building blocks for materials that depend on a regioisomerically pure PDI precursor.
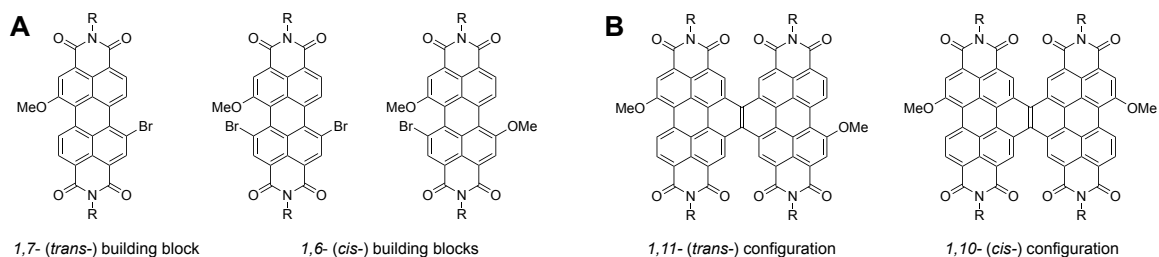
Figure 1.2. (A) Example of regioisomerically pure functionalized PDI building blocks for transformation into (B) regioisomerically pure extended PDI materials.
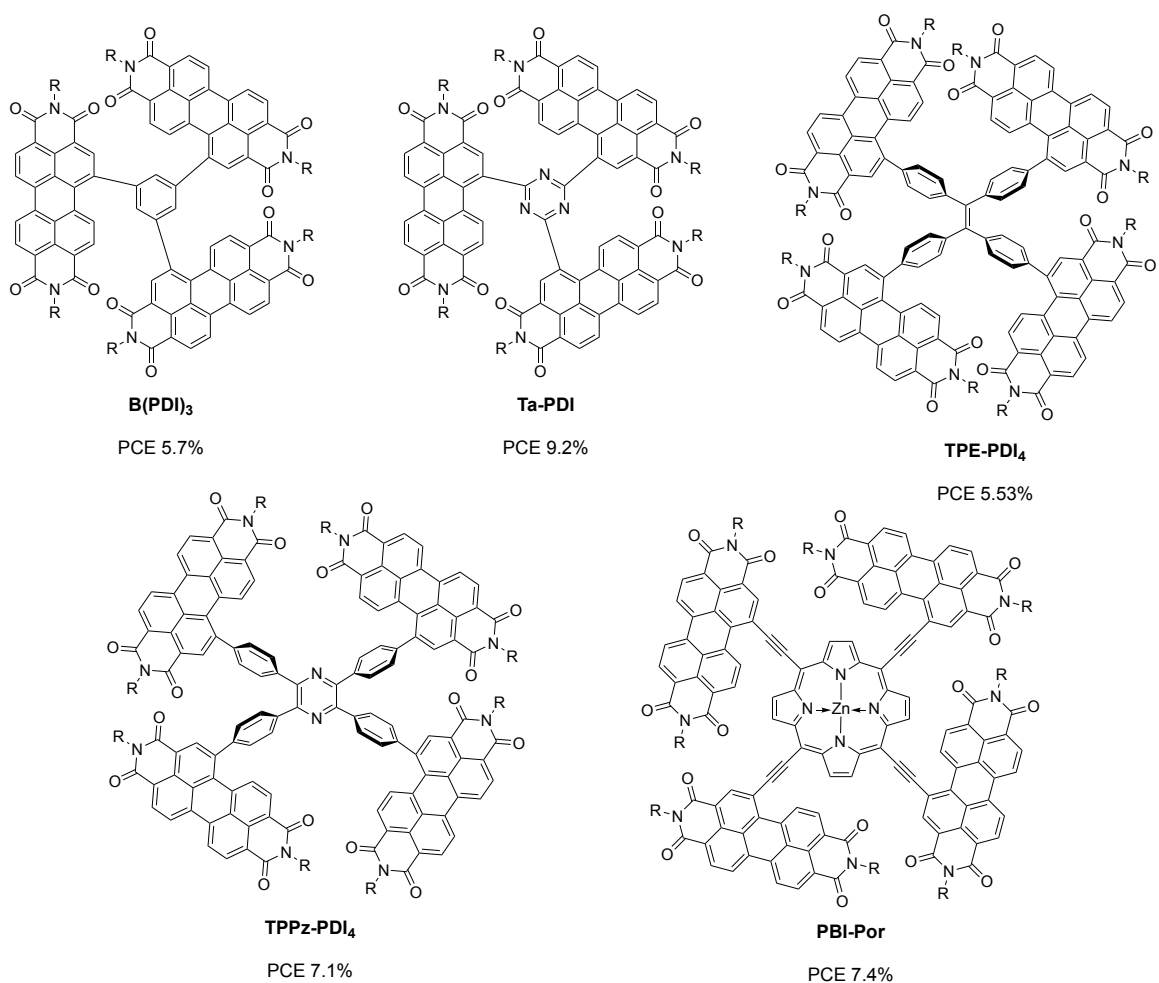
Figure 1.3. Clusters of PDI joined at the bay- position to a central linker. Conformational twisting limits aggregation in these materials, leading to small domain sizes in BHJs and efficient charge separation and extraction in OPVs.

One of the simplest strategies for creating high-performance PDI-based acceptors is to link multiple subunits of PDI to a central aromatic linker with biaryl bonds using organometallic cross-coupling (Figure 1.3).[11,12,35–37] Conformational twisting around the biaryl bonds makes these structures highly non-planar. Highly planar extended oligomers show evidence of aggregation in thin films even with alpha-branched imide side chains.[38] The conformational twisting of structures like those in Figure 1.3 reduces aggregation in

thin films and leads to appropriately small domain sizes in BHJs. Although this leads to improved PCE in devices up to 9.2%, there is no direct correlation between the degree of twisting and BHJ features or performance parameters.[39]

Selective activation of the ortho positions of PDI can be achieved either through C-H activation or through a Grignard reaction (Figure 1.4). Both techniques can be used for exhaustive arylation.[40,41] Ortho-aryl substituents have a large torsion angle with respect to the PDI core, limiting their ability to tune the frontier orbital energy of the PDI material. However, exhaustively ortho-arylated PDI derivatives prefer a slip-stacked orientation in thin films, which maintains sufficient π-stacking for charge transport while limiting excimer formation.[42] The best materials in this class achieve PCE up to 5.1%.[41] C-H activation of the ortho positions can also be used to install boronic esters or halide substituents.[43–45] This can be done either exhaustively or in moderate yield at just one ortho position by controlling the stoichiometry of the activation. Like their bay-brominated counterparts, ortho-functionalized PDI derivatives are highly active in organometallic cross-coupling reactions. Incorporating PDI into larger structures via ortho substitution leads to materials in which the PDI substituents are more planar than those in their bay-linked analogs (**αPBDT**, **βPBDT**, Figure 1.5).[46] The increased planarity of the PDI substituents improves contact between acceptor molecules and at the donor-acceptor interface, improving charge separation and charge transport over the bay-linked linked analogs. This results in PCE increase from 3.5% in **βPBDT** to 4.9% in **αPBDT**. Presumably, contortion about the biaryl bonds between the PDI subunits and the central linker of **αPBDT** limits the size of aggregates in BHJ phases. Exhaustively

substituting the central linker with ortho-linked PDI (**TPB**, Figure 1.5) yields a cluster type electron acceptor that performs with 8.5 % PCE and $J_{SC} > 18$ mA cm^{-2} in OPVs.[13]
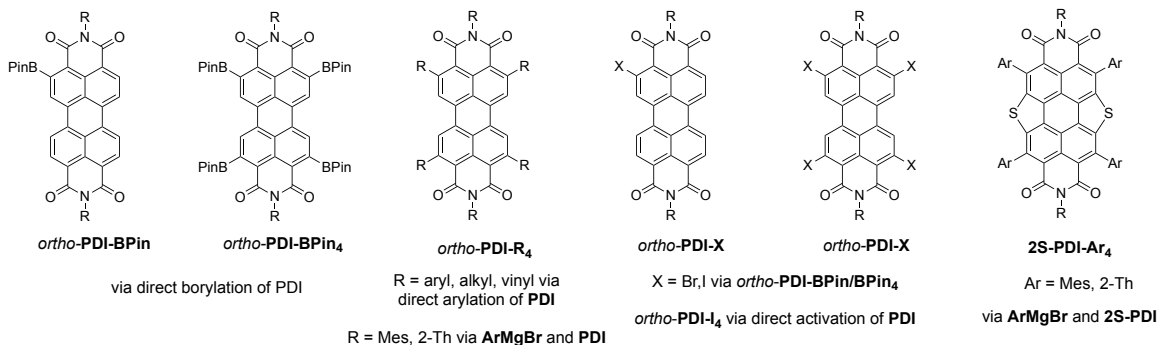
Figure 1.4. Ortho-functionalized PDI building blocks.
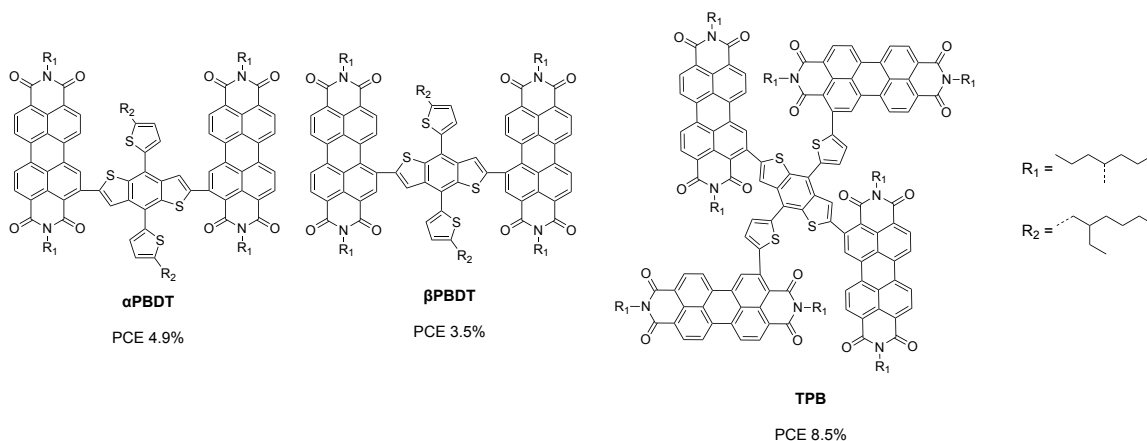
Figure 1.5. Ortho- linkage of PDI in acceptor materials. These materials exhibit similar conformational twisting to the bay- linked structures in Figure 1.3, but increased planarity of the PDI subunits improves charge carrier mobility.

The bay position of PDI can be annulated to include a fused pyrrole, thiophene, or selenophene ring via a nitrated precursor (Scheme 1.3). The pyrrole position can be alkylated, adding a second handle in addition to the imide position for tuning the solubility and processing characteristics of pyrrole-annulated PDI.[47] Chalcogen annulation produces higher-performing PDI acceptors than their unfunctionalized analogs, up to a near doubling of PCE in **tetra-PBI-S** (Figure 1.6).[48,49] This is attributed

to closer packing in thin films resulting from Se···O interactions[48,50] and to better charge

transport and charge transfer resulting from more diffuse frontier orbitals.[14,51]
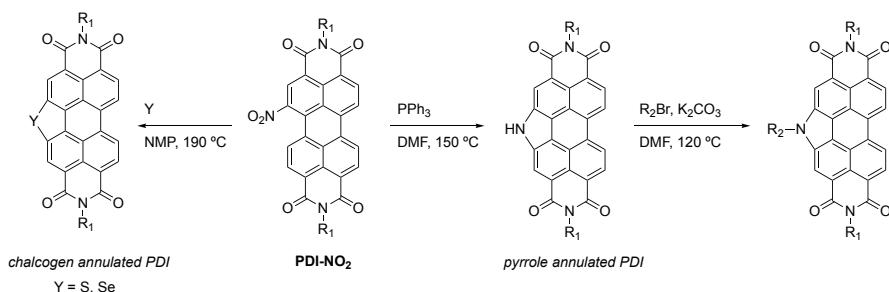
Scheme 1.3. Synthesis of pyrrole, thiophene, and selenophene fused PDI building blocks.
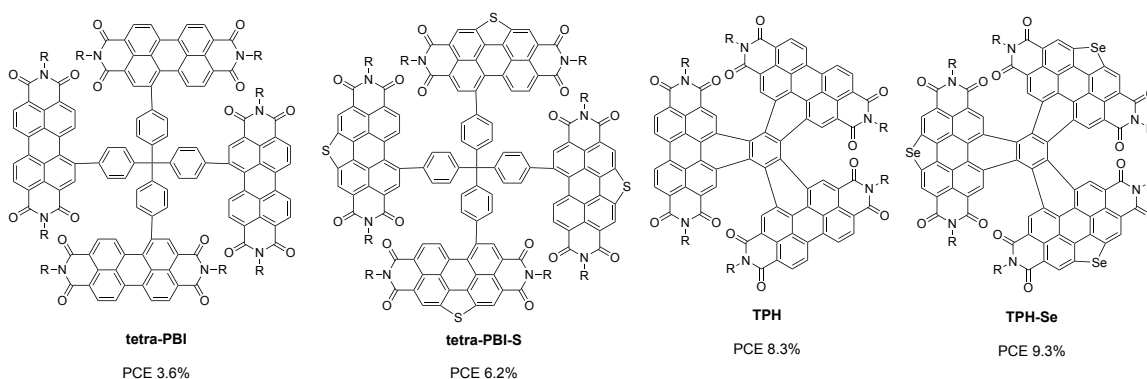
Figure 1.6. Enhanced PCE in chalcogen annulated PDI materials compared to their unfunctionalized analogs. **Tetra-PBI** and **tetra-PBI-S** devices are fabricated under similar conditions with the same donor. **TPH** and **TPH-Se** devices are fabricated under similar conditions with the same donor.

The last important functionalization strategy involves the oxidative cyclization of PDI that has been linked to an unsaturated carbon scaffold at the bay position (Figure 1.7).[9,52,53] This is achieved either via a Mallory photocyclization or via a Scholl reaction. In both of these reactions, the highly electron-deficient nature of PDI limits unwanted oxidations such as oxygenation or coupling reactions. The products of these reactions incorporate multiple PDI units into continuously fused π-systems with several

advantageous properties. These systems typically feature contortion between the PDI units, improving solubility and helping to limit aggregation in the solid state.[54] Highly absorbent PDI-to-PDI transitions are retained in the UV-Vis spectrum of these materials, and are usually bathochromically shifted due to increased conjugation. Furthermore, new transitions are incorporated, resulting from transitions between PDI subunits and the aromatic scaffold. As a result, these materials have high absorptivity from the UV region up to 550-650 nm, improving their ability to harvest photons. The increased rigidity of these materials reduces their reorganization energy compared to their unfused counterparts, facilitating exciton diffusion and charge transport. Together, these electronic features improve the photovoltaic performance of fused PDI materials, in some cases nearly doubling PCE over their unfused analogs in direct comparative studies (Figure 1.7).
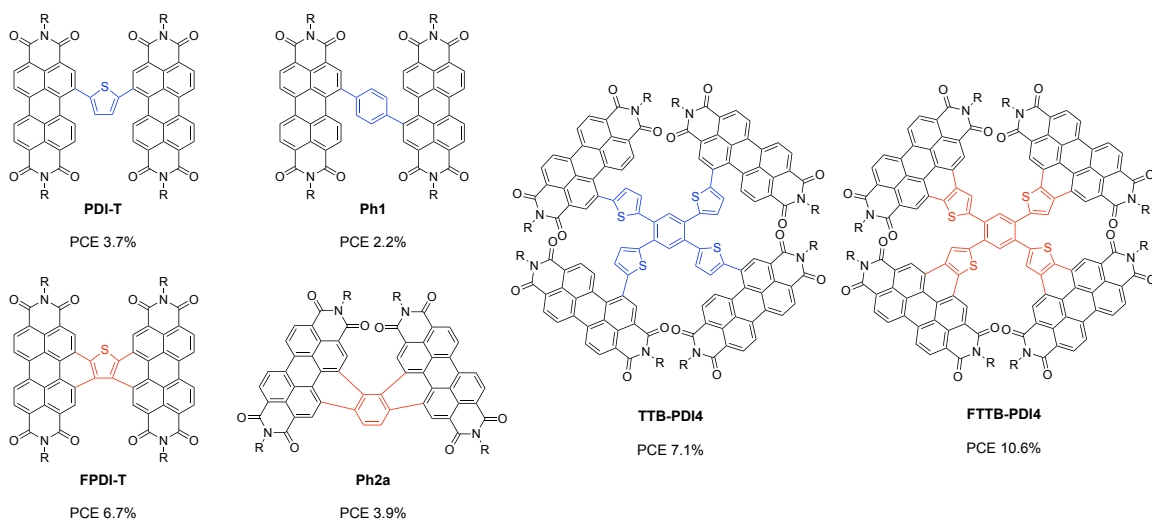
Figure 1.7. Ring-fusion in PDI-based acceptors. Unfused linkers are denoted in blue. Fused cores are denoted in red. In these cases, PCE comparisons between fused materials and their unfused analogs are for devices made under identical conditions.

1.2.3. Donor Materials in Perylene Diimide-Based OPVs

The aforementioned molecular design strategies represent the current state of the art for PDI-based acceptors in OPVs. The donor materials in these devices are typically donor-acceptor polymers based on thiophene or fused thiophene derivatives. Figure 1.8.a shows the structure of the three most successful of these materials in the context of PDI-based OPVs and their record PCE values. The most widely used of these in high-performance devices is the commercially available low-band-gap polymer poly[4,8-bis(5-(2-ethylhexyl)thiophen-2-yl)benzo[1,2-b;4,5-b']dithiophene-2,6-diyl-alt-(4-(2-ethylhexyl)-3-fluorothieno[3,4-b]thiophene)-2-carboxylate-2,6-diyl] (**PTB7-Th**).[55] **PTB7-Th** has several structural features that drive performance. Electron-withdrawing fluorine atoms and a highly quinoidal structure (Figure 1.8.b) reduce the bandgap of **PTB7-Th**,[56] leading to a UV-Vis absorption profile that complements that of most PDI-based acceptors. The large central benzodithiophene unit improves π-π stacking over simpler polythiophenes, leading to better hole mobility.[57,58] In devices, **PTB7-Th** forms a face-on orientation with the poly(3,4-ethylenedioxythiophene):poly(styrenesulfonate) (PEDOT:PSS) hole transport layer, facilitating charge transport to the anode.[59–61] The Stille polycondensation used to synthesize **PTB7-Th** can lead to high weights with low polydispersity.[62] The placement of fluorine within the PTB backbone influences the internal polarizability of the polymer (Figure 1.8.c). Fluorine placement on the alternating acceptor subunit helps to isolate charges in the excited state, leading to improved charge separation at the donor-acceptor interface.[63,64]
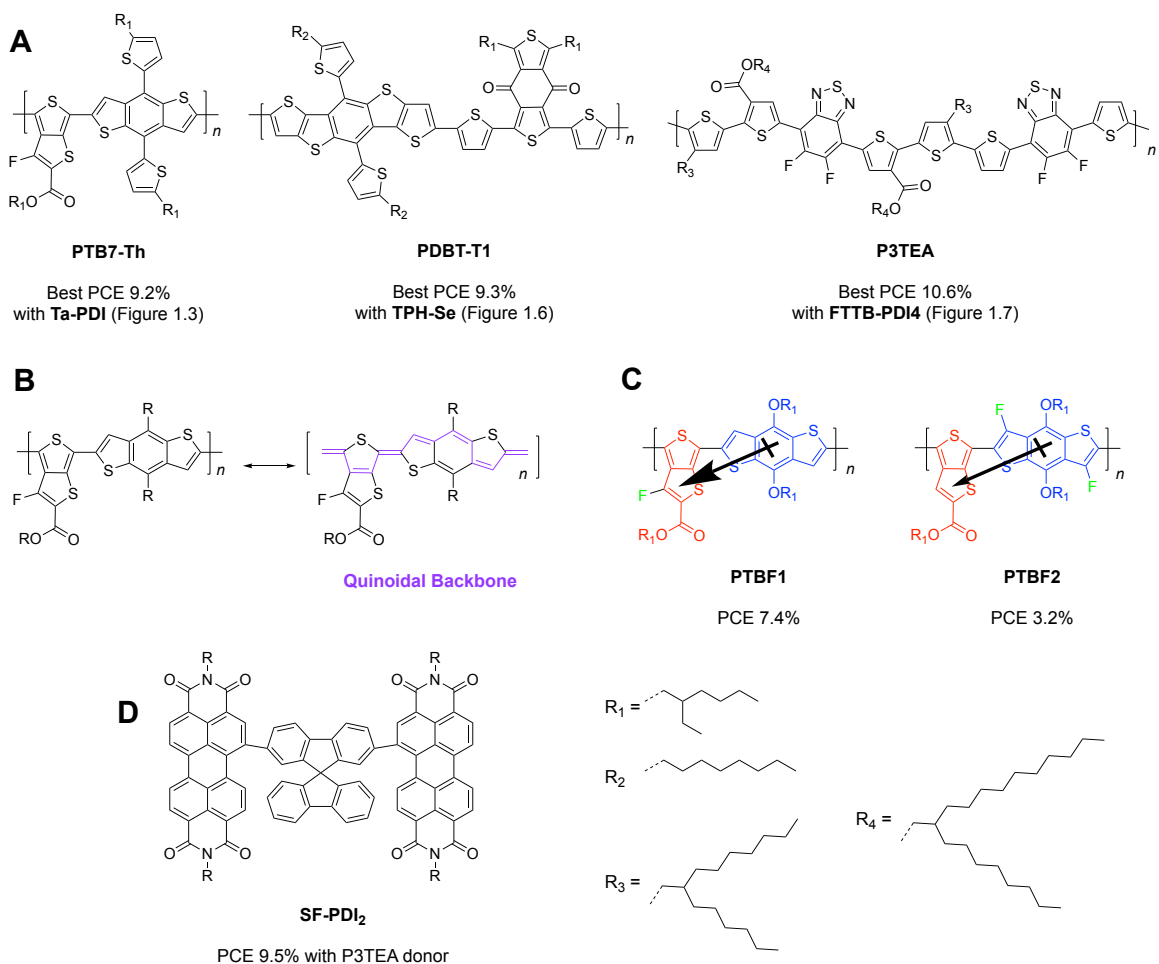
Figure 1.8. Donor polymers for PDI-based OPVs. (A) Structures and best PCEs of the most successful donors for PDI-based OPVs. (B) Quinoidal character of the PTB backbone in **PTB7-Th** and other PTB polymers highlighted in purple. (C) Dependence of internal polarizability and resultant PCE on fluorine placement (green) in PTB polymers. Placement of fluorine on the acceptor unit (red) amplifies polarizability, while placement on the donor unit (blue) reduces the polarizability. (D) Structure of **SF-PDI₂** as an acceptor for **P3TEA** polymer.

While the PTB-class of polymers has been investigated for several years, newer classes of high-performance donors are not as well understood. Recently, the wide-bandgap polymer poly{dithieno[2,3-d:2′,3′-d′]benzo[1,2-b:4,5-b′]dithio- phene-co-1,3-bis(thiophen-2-yl)-benzo-[1,2-c:4,5-c′]dithiophene- 4,8-dione} (**PDBT-T1**,

Figure 1.8.a) was reported as a high-performance donor.[65] The high PCE of devices from PC$_{71}$BM/**PDBT-T1** devices was attributed to the formation of long, fibrous domains of polymer in the BHJ leading to efficient exciton dissociation and charge transport. The PCE of devices from **PDBT-T1/TPH-SE** (Figure 1.6) have PCE up to 9.3%.[48] The current record-holding PDI-based OPVs used donor **P3TEA** (Figure 1.8.a) and acceptor **FTTB-PDI4** (Figure 1.7).[9] **P3TEA** was found to have efficient charge separation with an exceptionally small driving force when incorporated in devices with **SF-PDI$_2$** (Figure 1.8.d).[21] Typically, a large driving force (the difference between the bandgap and the energy of the charge transfer state) in organic materials is a major source of voltage losses in OPVs.[66–70] **P3TEA** has a negligible driving force, leading to V$_{OC}$ up to 1.13 V while maintaining high J$_{SC}$ and fill factor (FF). So far, the structure-property relationships leading to the beneficial properties of **P3TEA** and **PDBT-T1** have yet to be thoroughly explored like the PTB class of materials.

1.2.4. hPDI: Helical Graphene Nanoribbons Derived from Perylene Diimide

Recent work in the Nuckolls group has focused on helical graphene nanoribbons of PDI made by fusing together PDI monomers at the bay- position with ethylene linkers that we call **hPDI** (Figure 1.9.a).[54] Each fusion point between PDI subunits features two fused [4]helicenes (Figure 1.9.b), leading to a helical twist down the ribbon axis (Figure 1.9.c). This conformation was originally determined using density functional theory (DFT) calculations.[54,71] Chapter 3 of this dissertation presents single crystal x-ray diffraction data that confirm this prediction, and presents a synthetic method for controlling the conformation of cove-edge graphene nanoribbons.
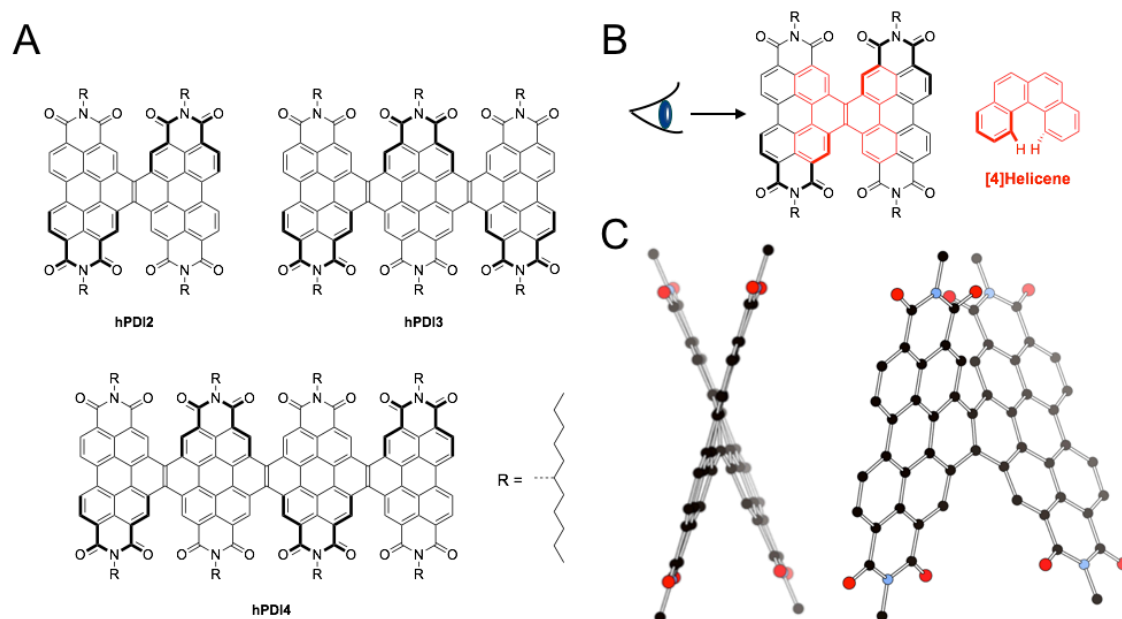
Figure 1.9. (A) Structure of **hPDI**, emphasizing the helical contortion resulting along the ribbon axis. (B) Structure of **hPDI2**, emphasizing in red the two [4]helicene subunits at each PDI-PDI fusion point in **hPDI**. Steric repulsion of the internal "cove" protons of [4]helicene bend it away from planarity. (C) DFT-predicted conformation of **hPDI2** showing the helical twist along the ribbon axis. The imide side chains are reduced to methyl substituents to simplify calculations, which were performed at B3LYP/6-31G** level.

The dimeric **hPDI2** is synthesized using the strategies discussed above: linking halogenated PDI subunits using organometallic cross-coupling followed by Mallory photocyclization (Scheme 1.4.a). **hPDI2** is amenable to the same reactions as the parent PDI, facilitating the synthesis of higher order oligomers **hPDI3** and **hPDI4**, as well as donor-acceptor ribbons incorporating a central pyrene subunit (Scheme 1.4.b).[72] **hPDI** retains the useful properties of parent PDI for OPVs, such as high electron mobility, high molar absorptivity, the ability to reversibly accept multiple electrons, and frontier orbital energies that complement donor materials. Lateral π-conjugation bathochromically shifts the absorption spectrum of **hPDI** and leads to new electronic transitions between the ethylene linker and the PDI subunits, leading to high absorptivity from the absorption

edge to the UV region. The helical contortion of these ribbons improves their solubility and limits aggregation in thin films that is unfavorable for BHJ OPVs. Chapter 2 of this dissertation presents a synthetic strategy for modulating the thin film properties of **hPDI** by easily varying its imide side chains. As a result of the favorable properties described above, PCE of up to 8.3% is achieved in **hPDI4/PTB7-Th** OPVs.[73,74] Besides its utility as an acceptors in OPV, **hPDI** materials are useful as electron transporting materials in perovskite photovoltaics[75] and as thin films for ultranarrowband photodetectors.[76] The work presented in this and the other chapters of this dissertation use chemical synthesis to study the relationship between the structure, properties, and performance of **hPDI** materials.
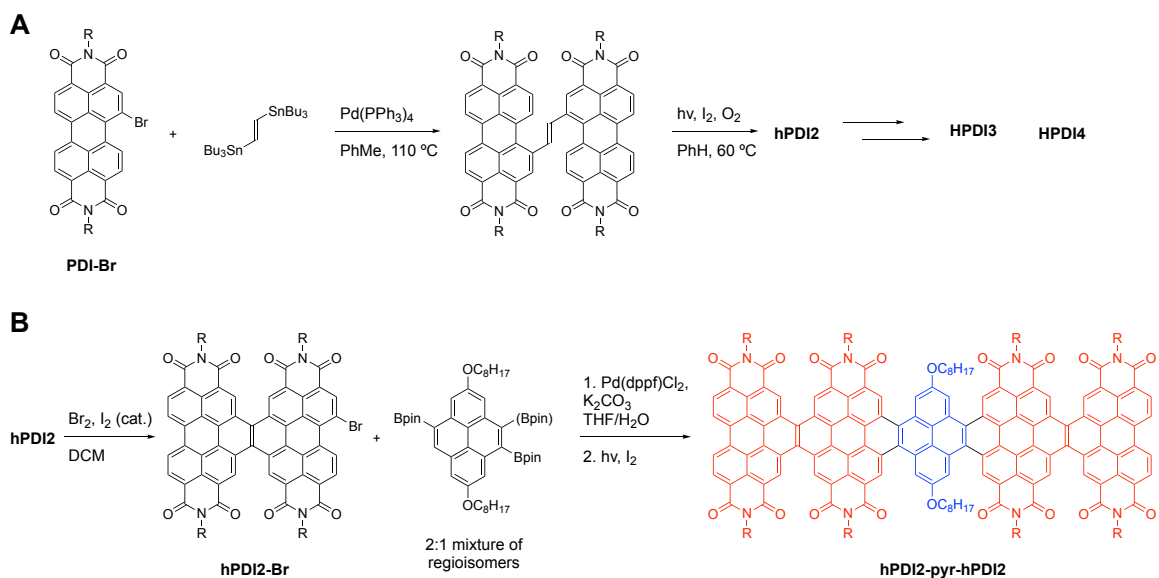
Scheme 1.4. (A) Synthesis of **hPDI2**. R = 6-undecyl. **hPDI3** and **hPDI4** are prepared by a similar sequence of halogenation of **hPDI2**, organometallic cross-coupling, and Mallory photocyclization. (B) Synthesis and structure of a donor-acceptor PDI nanoribbon with the central pyrene donor highlighted in blue and hPDI acceptors highlighted in red. R = 6-undecyl.

1.3. Internal Charge Transfer Character in PDI Materials for Organic Photovoltaics

Here is presented a class of materials based on linking **hPDI** into alternating acceptor-donor-acceptor macromolecules. The resulting materials exhibit internal charge transfer (CT) character and outperform their parent materials in OPVs. **hPDI** acceptors are linked together with electron donating thiophene rings, leading to internal CT upon excitation with light. The photophysics are probed using femtosecond transient absorption spectroscopy, revealing that the initial excited states evolve to a CT state that is not seen in the parent hPDI. Notably, these new materials outperform the parent **hPDI** in OPVs, achieving PCEs of 7.4% despite forming large domains in a BHJ. Deactivating internal CT by replacing the electron donating thiophene linker with an electronically neutral phenyl linker leads to a drastic reduction in PCE, highlighting the importance of internal CT in the performance of these materials.

Although the molecular properties of PDI-based materials can be readily tuned using the principles outlined above, the rules relating molecular properties to device performance are not well understood. One common feature of these high performance materials is that they form device active layers consisting of interpenetrating phases of polymer donor and PDI acceptor with 10-30 nm domains. In cases where the analogs of these high performance materials form much larger domains of 60 nm or more, the device performance is drastically reduced.[11,77,78] For example, the materials in Figure 1.10 have similar frontier orbital energies, solubility, UV-Vis absorption spectra, and electron mobilities. However, **BP-PDI$_2$** forms much larger BHJ domains than **TPE-PDI$_4$** and exhibits drastically reduced PCE.[11] The importance of small domain size has been

more extensively studied in fullerene systems.[8,15–18] Short-lived excitons have small diffusion radii, leading to substantial geminate recombination and reduced performance in devices with larger domain sizes. Achieving an ideal domain size of 10-30 nm is thus considered essential for high performance OPVs.[9,11,13,51,79,80] However, it is difficult to predict the size of BHJ domains when fabricating devices and harder still to control the domain size when designing new materials.

TPE-PDI$_4$
PCE 5.53%
20-30 nm domains

BP-PDI$_2$
PCE 3.13%
60-80 nm domains
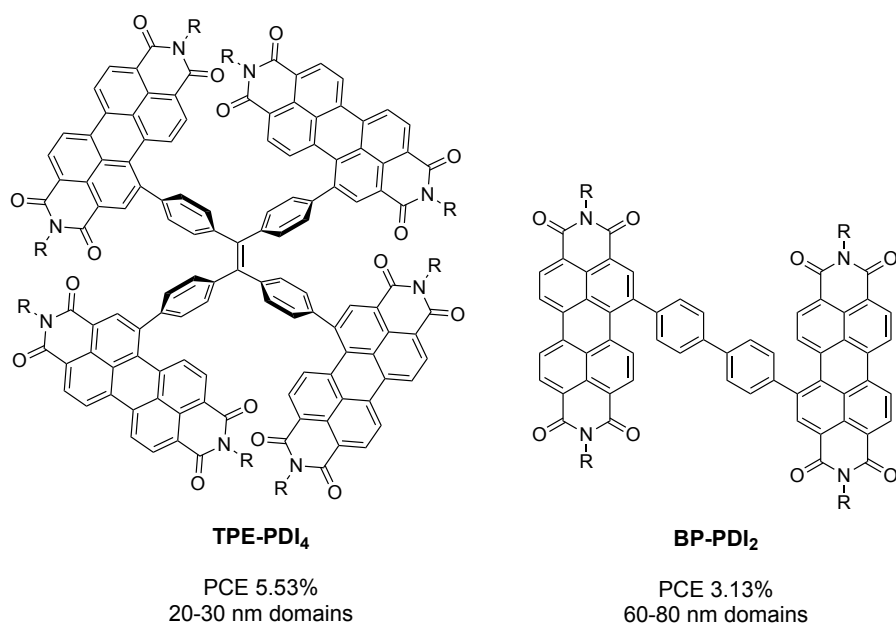
Figure 1.10. Effect of domain size on OPV performance of PDI acceptors with similar molecular properties.

As described in Chapter 1.2.3 of this text, internal CT is an important factor in the performance of many donor polymers used in OPVs. Here, we investigated the benefits of internal CT in PDI-based acceptor materials. We chose as the parent acceptor **hPDI2** (**1**) because of the beneficial properties described in chapter 1.2.4 of this text. To incorporate internal CT character two units of **hPDI2** were linked together with π-

electron rich thiophenes into an acceptor-donor-acceptor (A-D-A) system called **Bi-hPDI2-T** (Figure 1.11).

hPDI2 (1)   **Bi-hPDI2-T (2)**
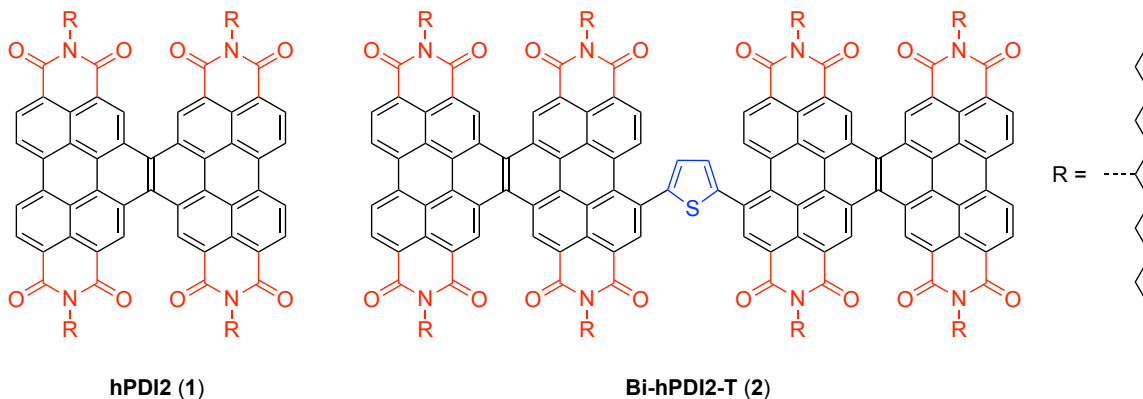
Figure 1.11. Structure of **1** and **2** with electron accepting substituents highlighted in red and electron donating substituents highlighted in blue.

This is based on a common strategy for inducing internal CT in organic materials: directly linking donor and acceptor moieties with biaryl bonds such that their respective π-orbital planes are orthogonal. This arrangement localizes the HOMO on the donor moiety and localizes the LUMO on the acceptor moiety, resulting in an excited state with localized hole and electron (Figure 1.12.a).[81–89] In studies on mesitylene-acridinium donor-acceptor dyads, the extreme steric hindrance about the biaryl bond between the two components completely isolates the HOMO on the donor mesitylene and the LUMO on the acceptor acridinium (Figure 1.12.b). Excitation with light leads to an internal CT state that is quenched in solution with bimolecular kinetics, indicating that the orthogonal HOMO and LUMO forbid vibrational relaxation of the CT state, which is only quenched by collision of two excited dyads.[85] Wasielewski's group investigated internal CT of PDI materials with porphyrin donor antennae (Figure 1.12.c).[82] Internal CT in these systems was amplified when the electron could be delocalized over two PDI subunits. This

suggests that internal CT in A-D-A materials based on π-extended **hPDI2** would be amplified over those based on simple PDI.
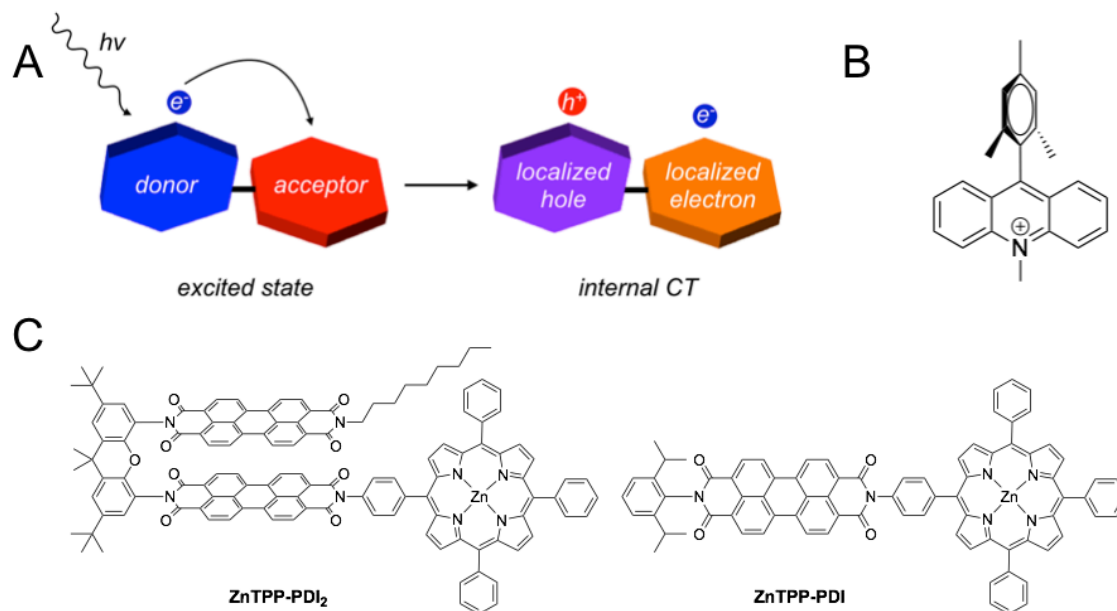
Figure 1.12. (A) Schematic representation of internal CT in donor-acceptor systems with orthogonal donor and acceptor. (B) Structure of mesitylene-acridinium systems with efficient internal CT from orthogonal arrangement of donor mesitylene and acceptor acridinium. (C) Importance of delocalization for promoting internal CT in PDI-based systems. Electron transfer from the porphyrin donor is increased 50% from **ZnTPP-PDI** to **ZnTPP-PDI₂** due to delocalization of the electron between the cofacial PDI subunits.

In **Bi-hPDI2-T**, successful incorporation of CT character was predicted by DFT calculations and confirmed by UV-Vis spectroscopy, emission spectroscopy, and femtosecond transient absorption (fsTA) spectroscopy. As a result, Bi-hPDI2-T achieves PCEs of up to 7.4% despite large BHJ domain sizes of 60±10 nm.

1.3.1. Synthesis and Characterization of Internal Charge Transfer
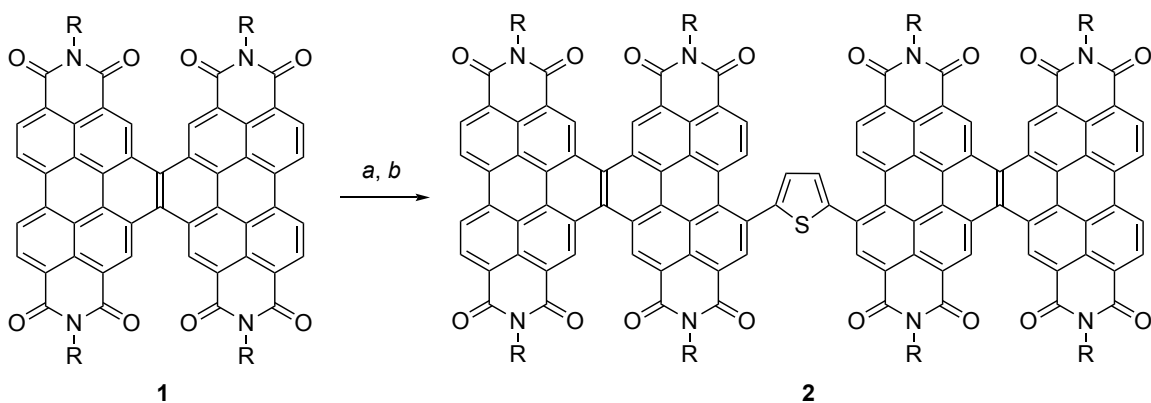
Scheme 1.5. Synthesis of Bi-hPDI2-T (**2**) from hPDI2 (**1**), R = 6-undecyl; (a) Br_2, I_2, DCM, RT, 3 days, 45% yield; (b) bis(trimethylstannyl)thiophene, Pd_2dba_3, $AsPh_3$, PhMe, 105 ºC, 2 hrs, 86% yield.

Halogenation of **hPDI2** (**1**) followed by an organometallic coupling reaction produces the A-D-A macromolecule **Bi-hPDI2-T** (**2**) in excellent yield (Scheme 1.5). **2** retains the attributes of parent **1** that are advantageous in OPVs: high solubility in common organic solvents such as chloroform and chlorobenzene, high molar absorptivity, high electron mobility, and HOMO/LUMO levels (Figure 1.13.a) complementary to common donor materials. The cyclic voltammogram of **2** is presented in Figure 1.13.b. Table 1.1 summarizes the characterization of the frontier orbitals. Figures 1.13.c and 1.13.d show the DFT-calculated HOMO and LUMO of **2**. The twist about the thiophene-PDI biaryl bonds effectively localizes the HOMO onto the donor thiophene linker and the LUMO onto the acceptor hPDIs (Figure 1.13.c and 1.13.d).
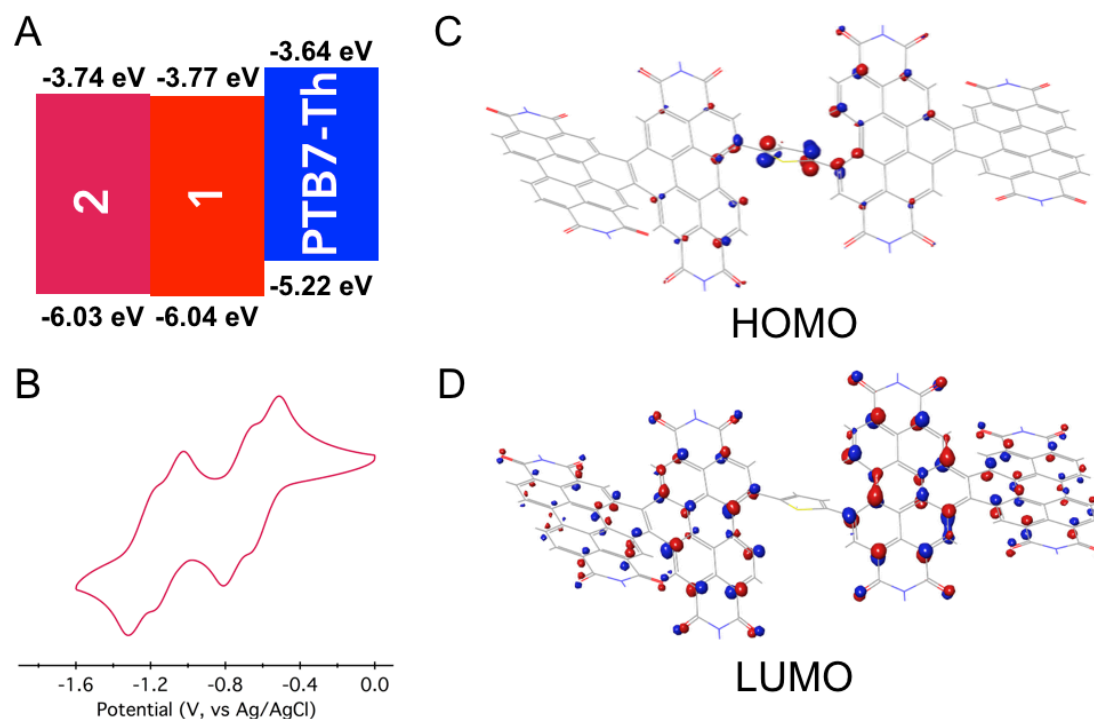
Figure 1.13. Frontier orbitals of **2**. (A) **2** has a slightly lowered HOMO and LUMO compared to **1**. The frontier orbitals complement those of donor **PTB7-Th**. LUMO level of **2** was determined by CV. HOMO energy of **2** was estimated by subtracting the energy of the optical bandgap (estimated from the wavelength of the $S_0 \rightarrow S_1$ transition) from the LUMO energy determined by CV. Data for **1** were previously reported.[73] (B) Cyclic voltammogram of **2**, showing four reversible reduction events. (C) HOMO and (D) LUMO of **2**. The central thiophene linker is out of plane with the hPDI subunits, leading to poor spatial overlap between the HOMO localized on the thiophene and the LUMO localized on the hPDI.

Table 1.1. Frontier Orbital Energies Derived from Computational, Optical, and CV data

	Computational Data[a]			Optical Data[b]		CV
	E_{HOMO} (eV)	E_{LUMO} (eV)	E_{gap} (eV)	λ_{max} (nm)	E_{gap} (eV)	E_{LUMO} (eV)
1[c]	-6.19	-3.77	2.42	547	2.27	-3.77
2	-6.15	-3.82	2.33	542	2.29	-3.74

[a] Calculations were performed at the B3LYP/6-31G** level. [b] The optical bandgap was estimated from the wavelength of the $S_0 \rightarrow S_1$ transition. [c] Data were previously reported.[54]

The conformational flexibility of **2** was screened using a series of calculations in which one or both of these dihedral angles was restricted in increments as detailed in Table 1.2. The lowest energy structure is presented in Figure 1.13.c and 1.13.d. Notably, a wide range of conformations were found to be isoenergetic to each other, and less than 2 kcal mol^{-1} from the lowest energy structure. Time-dependent DFT (TD-DFT) revealed that the energy and oscillator strength of the lowest energy excited state, representing internal CT, varies with changes in these dihedral angles (Table 1.2). Figure 1.14 shows the variable temperature ^{1}H NMR of **2** as it is cooled. Although there are only four chemically distinct protons representing the [4]helicene coves of **2**, more than four signals are distinguishable at 260 K, indicating the presense of multiple conformations. This conformational flexibility accounts for the broadening of the electronic transitions in **2** compared to **1** (Figure 1.15.a).

Table 1.2. Conformational Flexibility of **2**.[a]

Dihedral Angle[b] °	Dihedral Angle[b] °	Relative Gas Phase Energy (kcal mol^{-1})	Lowest Energy Transition (eV)	Lowest Energy Transition (nm)	Oscillator Strength
64.1[c]	43.4	1.40	1.89	657	0.150
61.3	43.4*	1.37	1.87	665	0.196
67.9	13.3*	4.74	1.83	676	0.360
65.9	16.9*	8.49	1.92	646	0.375
63.9	47.0*	9.68	2.07	600	0.300
71.5	77.1*	5.48	2.11	587	0.347
75.2	107.3*	1.81	2.13	582	0.220
80.2	137.4*	1.85	2.15	577	0.165
107.3*	48.1*	1.01	2.03	611	0.344
107.3*	84.9*	1.56	2.13	583	0.359
43.4*	54.9*	1.18	1.85	672	0.241
43.4*	61.3*	1.36	1.86	665	0.196
137.4*[d]	**50.2***	**0**	**1.92**	**647**	**0.467**
137.4*	80.2*	1.81	2.02	614	0.212

[a] Calculations were performed at the B3LYP/6-31G** level. [b] Dihedral angle about the biaryl bonds between thiophene linker and PDI core. Angles denoted with * were restricted. [c] Initially optimized geometry. [d] Final optimization. This is the geometry displayed in Figure 1.13.c and 1.13.d, and used for all other calculations.
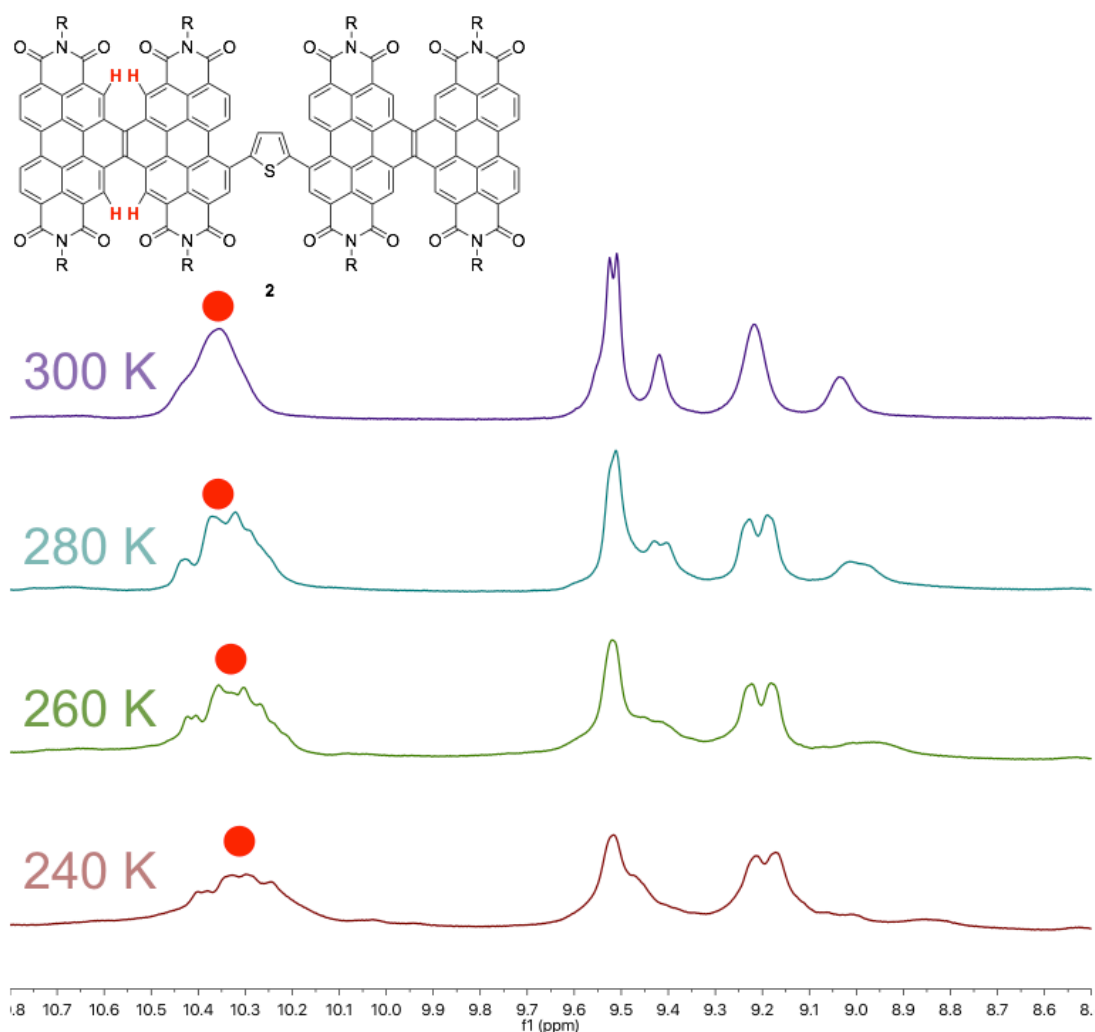
Figure 1.14. VT NMR of **2** with cove protons highlighted in red. As the sample is cooled, at least eight signals are clearly present in the cove region, despite **2** only having four chemically distinct cove positions.

Spatial isolation of HOMO and LUMO has been shown in other donor-acceptor systems to create a CT state,[82,85,90,91] so **2** was probed for internal CT using UV-Vis and fluorescence spectroscopy. **2** has a similar UV-Vis absorption profile to its parent **1**. However, a broad, low-energy shoulder is seen in **2** (Figure 1.15.a). Time-dependent DFT (TD-DFT) calculations assign this new transition in **2** as being a HOMO to LUMO transition from thiophene to PDI. The poor spatial overlap between these orbitals

accounts for the weakness of this absorption. Furthermore, because this lowest-energy excited state arises from a transition between poorly overlapping orbitals we expect nonradiative decay to predominate over fluorescence. Indeed, the photoluminescence quantum yield (PLQY) of **2** is greatly reduced and more dependent on solvent polarity than **1**, diminishing almost entirely in highly polar solvent (Figure 1.15.b). Low-energy emission of **2** shifts bathochromically with increasing solvent polarity before being impossible to distinguish from the tails of high-energy emission (Figure 1.15.d). This strong dependence of PLQY on solvent polarity is common in donor-acceptor chromophores with internal CT caused by spatial isolation of HOMO and LUMO from twisting about a biaryl bond.[92]
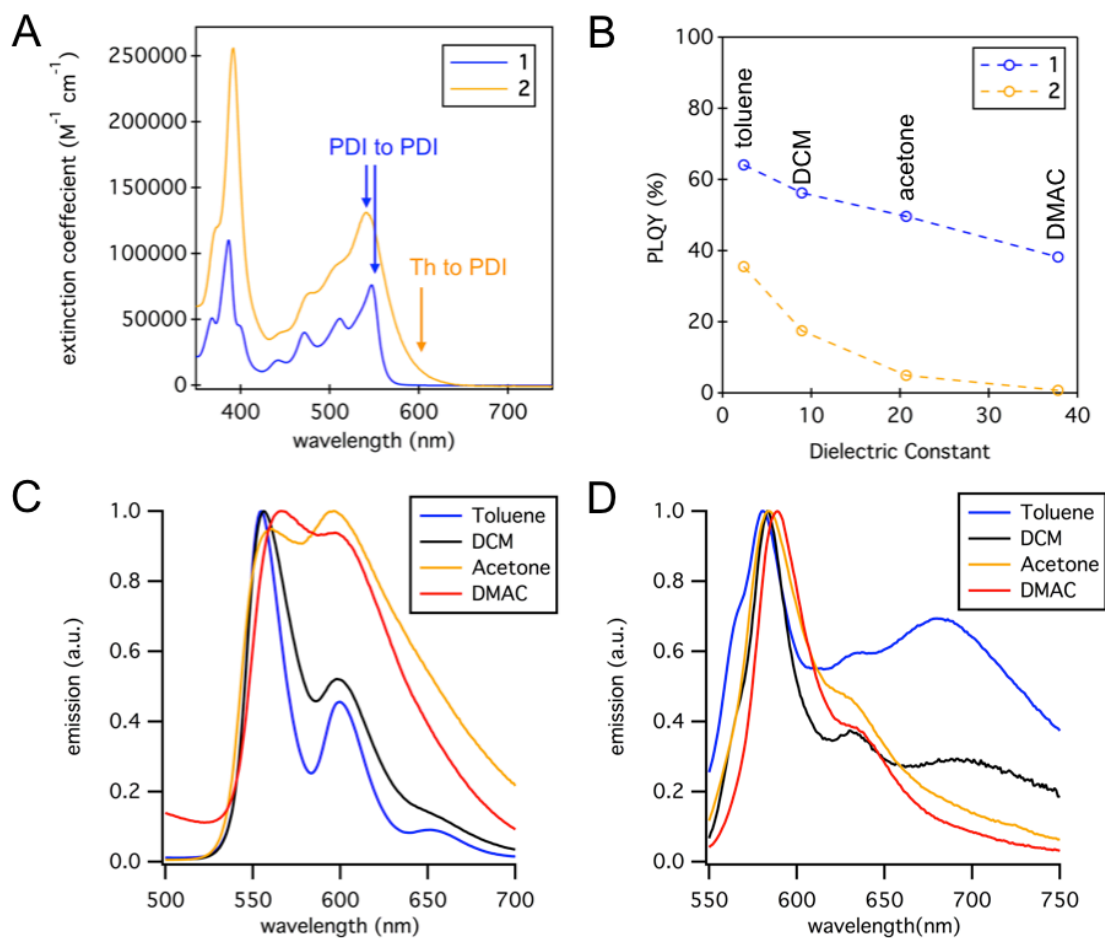
Figure 1.15. (A) UV-Vis spectra of **1** and **2**, highlighting the PDI to PDI $S_0 \rightarrow S_1$ transition and the thiophene to PDI CT shoulder. (B) PLQY data for **1** and **2** in solvents of varying dielectric constant. Fluorescence spectra of **1** (C) and **2** (D) in solvent of varying dielectric constant. The low-energy emission of **2** in toluene at 680 nm is reduced and more bathochromically shifted than higher-energy emissions in DCM, before being indistinguishable in highly polar acetone and DMAC.

To quantify the internal charge-transfer character, we utilize femtosecond transient absorption (fsTA). Figure 1.17.a and 1.17.b show fsTA spectra of **1** and **2** in dilute solution. The bleaching features with peaks at 520, and 560 nm in **1** (Figure 1.16.a) and that with a peak at 540 nm in **2** (Figure 1.16.b) are assigned to the bleaching of the ground-state absorption. The induced absorption signals in the wavelengths longer than

570 nm in **1** are the excited-state absorption (ESA) of the photogenerated excitons. In both samples, the TA spectra just after excitation show similar features with a broad absorption centered at ~720 nm, indicating the common nature of the initial excitations. The ESA can be assigned to the singlet $S_1 \rightarrow S_N$ transitions of an hPDI2 unit. The TA spectra in **2** evolve into broad absorption with almost no peak structure between 600-740 nm within 10 ps. Note that the transition is quantitative since the bleaching signal stays constant during the transition.
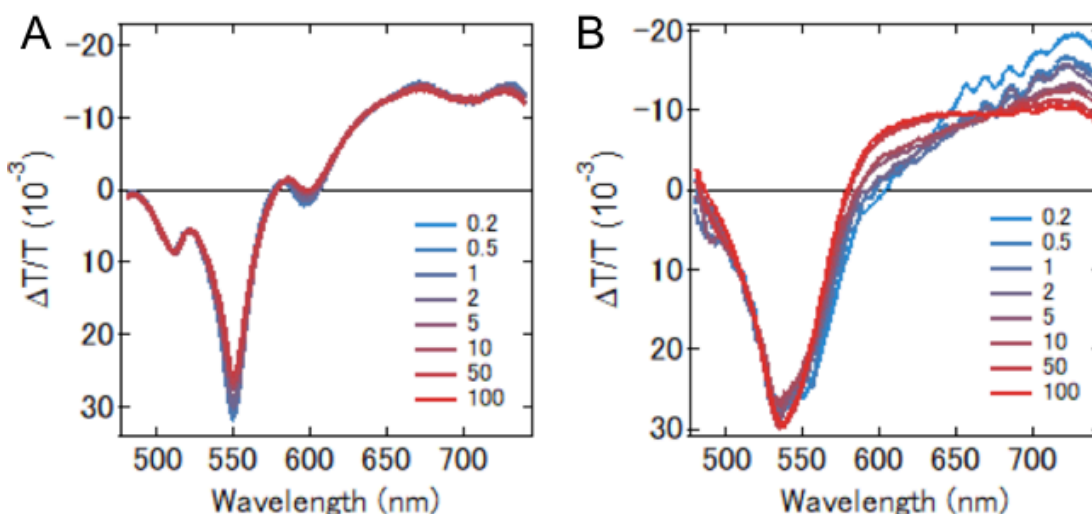
Figure 1.16. Solution fsTA spectra of **1** (A) and **2** (B) showing the evolution of internal CT in **2**. Spectra are recorded in chloroform after pumping at 530 nm. Time scale is in ps.

There are two possible explanations for the long-lived excited state: internal CT state or triplet generation. Triplet excitons can be generated via intersystem crossing or singlet fission. However, intersystem crossing in organic systems without heavy atoms is very slow (>ns) and cannot account for the observed dynamics.[93] Singlet fission is also unlikely because the energy of the triplet exciton is more than half that of the singlet and is thus too high to meet the requirement for singlet fission (Figure 1.17.a).[94,95] An internal

CT state is the most likely explanation for these behaviors. We also measured the lifetime of the excitons in thin films of **1** and **2**, which shows more than factor of two longer lived excited states in **2** (Figure 1.17.b). While the excited states for the **hPDI2** components decay with a time constant of 2.0 ± 0.1 ps (59%), 31.6 ± 1.8 ps (21%), 559 ± 50 ps (20%) in **1**, those for **2** have much longer lifetime: 5.7 ± 1.0 ps (34%), 71.7 ± 13.1 ps (24%), 466 ± 54 ps (42%) in **1**. Importantly, the fastest component is less dominant in the film of **2** (34%) than in that of **1** (59%). The longer excited state lifetime assisted by internal CT character is likely beneficial in OPVs.
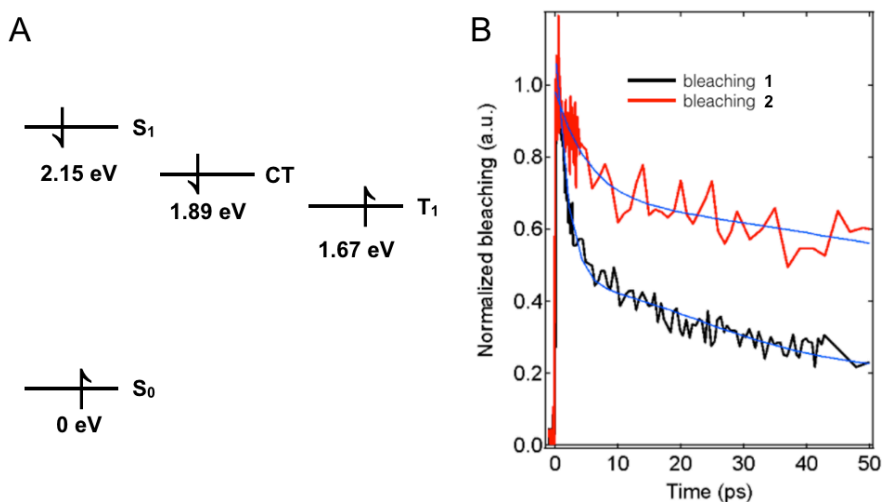
Figure 1.17. (A) DFT-calculated energy diagram of excited states in **2**. S_1 is assigned as the lowest energy PDI→PDI transition. CT state is assigned as the lowest energy Th→PDI transition. The thermodynamic requirement for intramolecular singlet fission requires the lowest energy singlet state to be double the energy of the T_1 state. (B) Decay dynamics of **hPDI2** (**1**) and **Bi-hPDI2-T** (**2**) in fsTA experiment on thin films after pumping at 530 nm.

1.3.2. Acceptors with Internal Charge Transfer in OPVs
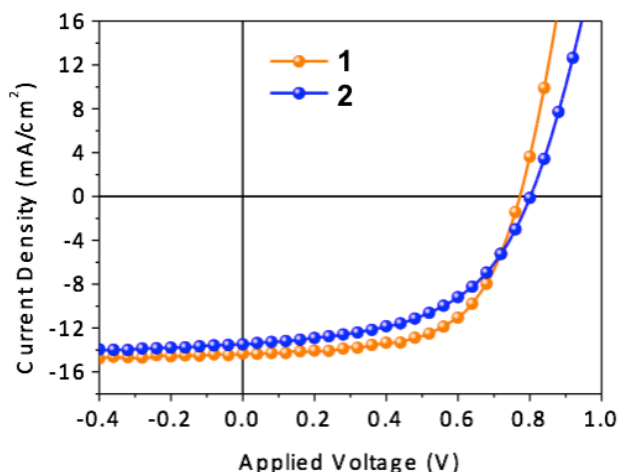
Figure 1.18. Current-voltage characteristics of **hPDI2** (**1**) and **Bi-hPDI2-T** (**2**) in OPVs using **PTB7-Th** as the donor.

We find that **2** is much more efficacious in OPVs than the parent nanoribbon **1** in OPVs made from blended films with the commercially available low-band-gap polymer **PTB7-Th**.[55] We fabricate the devices in an inverted structure with a configuration of ITO/ZnO(20 nm)/PTB7-Th:acceptor/MoO$_x$(7 nm)/Al(100 nm). The active layers were spin cast from a solution of a mixture of the donor and acceptor. Figure 1.18 displays current-density (J-V) curves of these devices, and Table 1.3 contains the extracted parameters for the solar cells made from **1**/**2**:**PTB7-Th**. Incorporation of solvent additives chloronaphthalene (CN) and diiodooctane (DIO) improved PCE.[96–98] Compared to devices made from parent **1**, V$_{OC}$ decreased slightly but short circuit current J$_{SC}$ and fill factor FF increased for **2**. Notably, optimized devices from **2** achieve a high PCE of 7.4%, which is substantially improved from optimized devices from **1** (PCE = 6.1%).[73]

Table 1.3. Device characteristics for OPVs made from **1/2**:**PTB7-Th**.

	Jsc (mA/cm^2)	Voc (V)	FF (%)	PCE (%)
1 (**hPDI2**) w no additive	13.6	0.80	51	5.59
1 w 1% DIO + 1% CN (optimized)	**13.5**	0.80	**55**	**6.05**
2 (**Bi-hPDI2-T**) w no additive	14.3	0.77	60	6.64
2 w 1% CN + 1% DIO additive (optimized)	**14.6**	0.79	**64**	**7.36**

Of particular of interest is improvement in Jsc, indicating better charge separation and collection that is most related to the morphology of BHJ active layers.[8,32,33] To investigate the morphology of our active layers, we use atomic force microscopy (AFM) to probe the topography and surface roughness of these blended films in tapping mode (Figure 1.19.a). From the height images, all the films show smooth surfaces with no detectable long-range crystallinity. Notably, these films show phase separation with domain sizes of 60±10 nm, much larger than the typical BHJ feature size for efficient charge carrier extraction in OPVs (10-30 nm).[17]
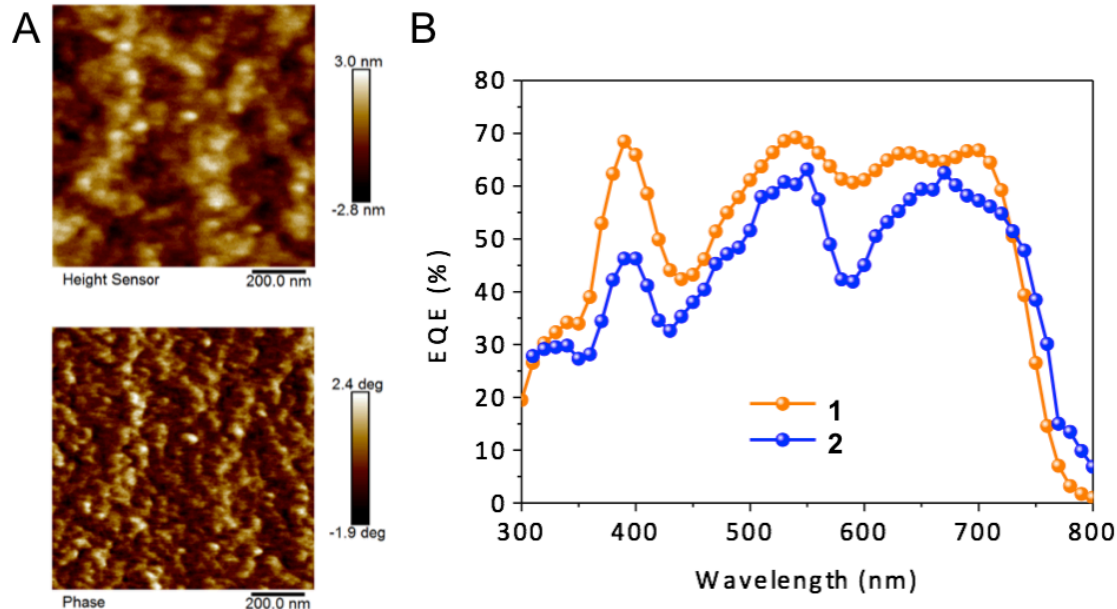
Figure 1.19. (A) AFM measurement performed on blend films of **2**:**PTB7-Th** showing the smooth surface of films and phase separation. (B) EQE measurements of **hPDI2** (**1**) and **Bi-hPDI2-T** (**2**) showing improved EQE at 390 nm and 580 nm as a result of charge carriers originating from absorption by **2**.

The external quantum efficiency (EQE) spectra of **1** and **2** (Figure 1.19.b) hint at the origin of this improved device performance. Compared to the parent **1**, **2** shows substantially higher EQE across most of the spectrum. First, the EQE around 390 nm is much higher in **2** than in **1**. Comparison of neat and blended thin film absorption spectra (Figure 1.21.a) shows that absorption at this wavelength is almost exclusively from the acceptor. Second, there is a decrease in the EQE centered at 580 nm for **1**, while **2** has consistently high EQE in this region. The donor **PTB7-Th** is only weakly absorbing at wavelengths shorter than 600 nm. **1** has a sharp absorption edge at 570 nm, right where **1/PTB7-Th** devices show reduced EQE. **2** has a broad absorption tail extending to 620 nm, increasing the absorption of **2/PTB7-Th** films and improving EQE around 580 nm (Figure 1.19.b, 1.20.a). Increased EQE, especially in regions resulting from absorption by

2, suggests that this acceptor efficiently converts photogenerated excitons into photocurrent. This efficient intermolecular charge transfer from acceptor **2** to donor PTB7-Th is supported by fsTA on blended films (Figure 1.21.b).
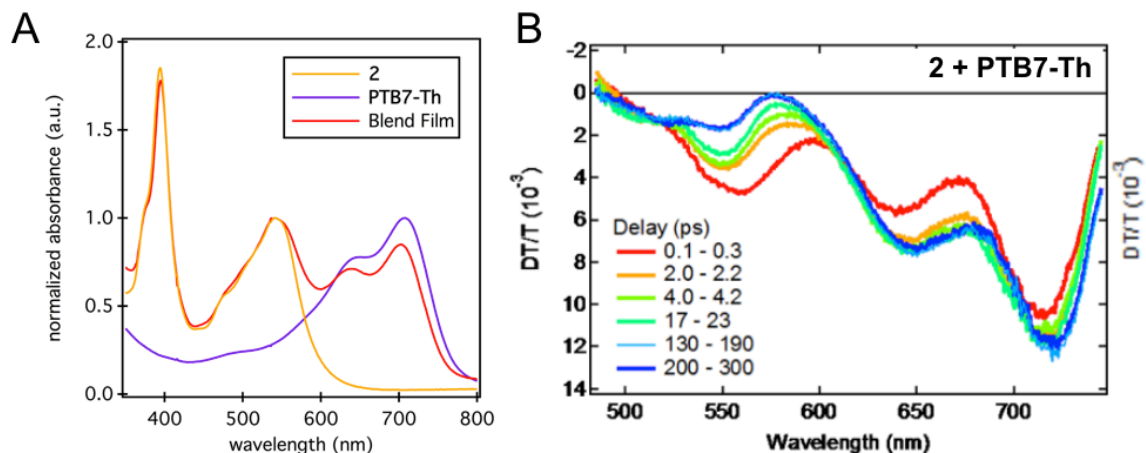
Figure 1.20. (A) Blend film absorption of **Bi-hPDI2-T** (**2**). The absorption tail of **2** improves the absorbance in regions of the spectrum where **PTB7-Th** is weakly absorbing. (B) Blend film fsTA of **Bi-hPDI2-T** (**2**) pumping at 520 nm, leading primarily to excitation of the acceptor **2**. The ESA peak for **2** at 550 nm rapidly decays, leading to a long-lived ESA at 720 nm representing hole transfer to the donor.
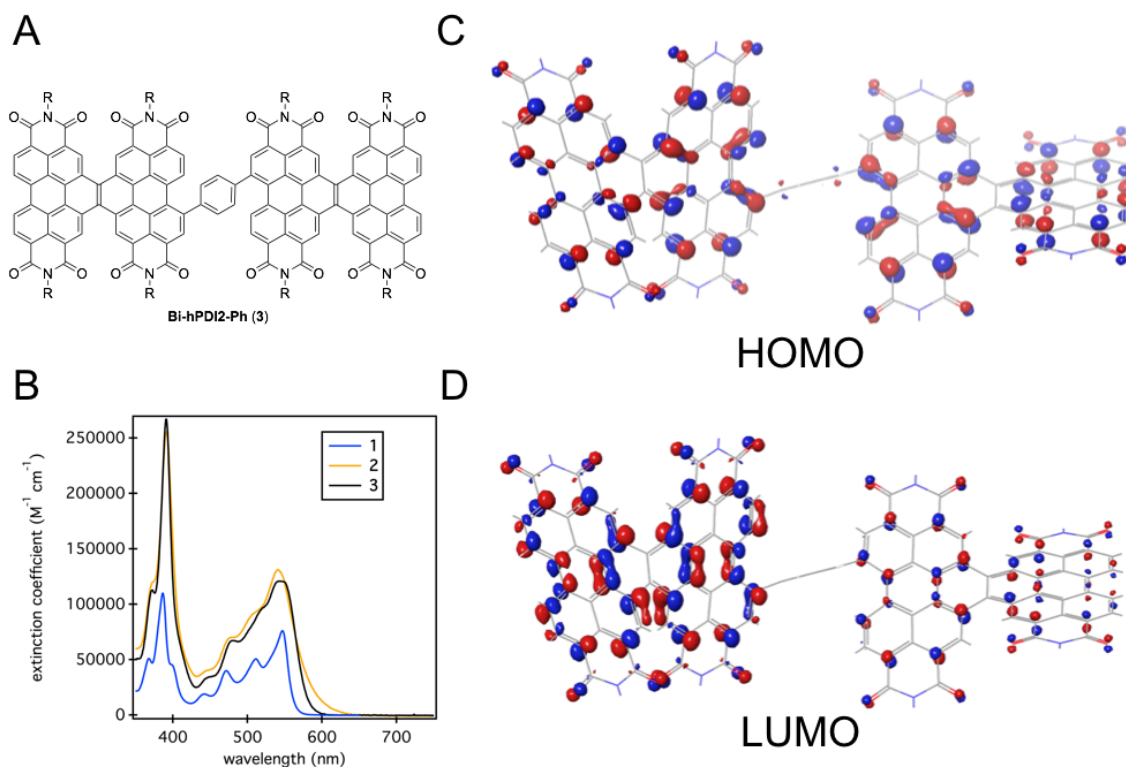
Figure 1.21. (A) Structure of **2** analog with an electronically neutral phenyl linker **Bi-hPDI2-Ph** (**3**). (B) Solution UV-Vis comparison of **1-3**. Although **3** absorption peaks are broadened compared to **1**, **3** lacks the distinct tail of **2**. HOMO (C) and LUMO (D) of **3**, showing that the frontier orbitals representing the $S_0 \rightarrow S_1$ transition are delocalized over the PDI subunits, with nearly no orbital density on the phenyl linker.
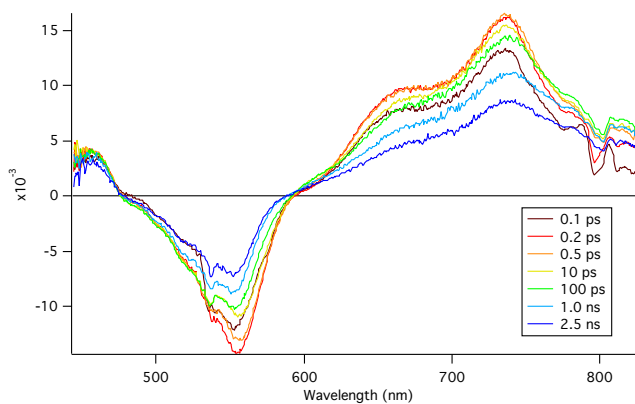
Figure 1.22. Solution fsTA spectrum of **3**. Just as with **1** (Figure 1.16.a), **3** shows no evolution in its bleaching or ESA besides a gradual decay.

To further understand the importance of internal CT character in **2**, we replaced the donor thiophene linker with an electronically neutral phenyl linker (Figure 1.21.a). The resulting molecule, **Bi-hPDI2-Ph** (**3**), has an almost identical absorption spectrum to parent **1**, without the low-energy absorption shoulder seen in **2** (Figure 1.21.b). TD-DFT calculations assign the lowest energy transition of **3** as a HOMO to LUMO transition with both orbitals delocalized over the hPDI2 subunits (Figure 1.21.c, 1.21.d). Indeed, fsTA shows similar results with **1** and shows no significant CT character (Figure 1.22). Although **3** lacks the CT character of **2**, it does retain many of the useful electronic properties of **1**: high molar absorptivity, good electron mobility, reversible reduction (Figure 1.23.a), and complementary absorption profile (Figure 1.23.b) and HOMO/LUMO alignment (Figure 1.23.c) to common donor materials (Table 1.4). Furthermore, AFM studies of BHJ films made from **3** and PTB7-Th show domain sizes 40±10 nm, much closer to the ideal range than high-performance **2** (Figure 1.23.d, 1.23.e). Despite that, **3** performs poorly in OPVs compared to **2** and even the parent **1**. Devices fabricated from **3** under the same conditions as **2** using the same PTB7-Th donor have a PCE of 2.2% (Figure 1.24.a, 1.24.b). The performance comparison is plotted in Table 1.5. Although **3** has similar electronic properties to **2**, the HOMO and LUMO are not spatially isolated from each other via an electron rich linker. These negative control experiments unambiguously indicate the importance of CT character from an A-D-A configuration for overcoming unfavorably large domains in OPVs.
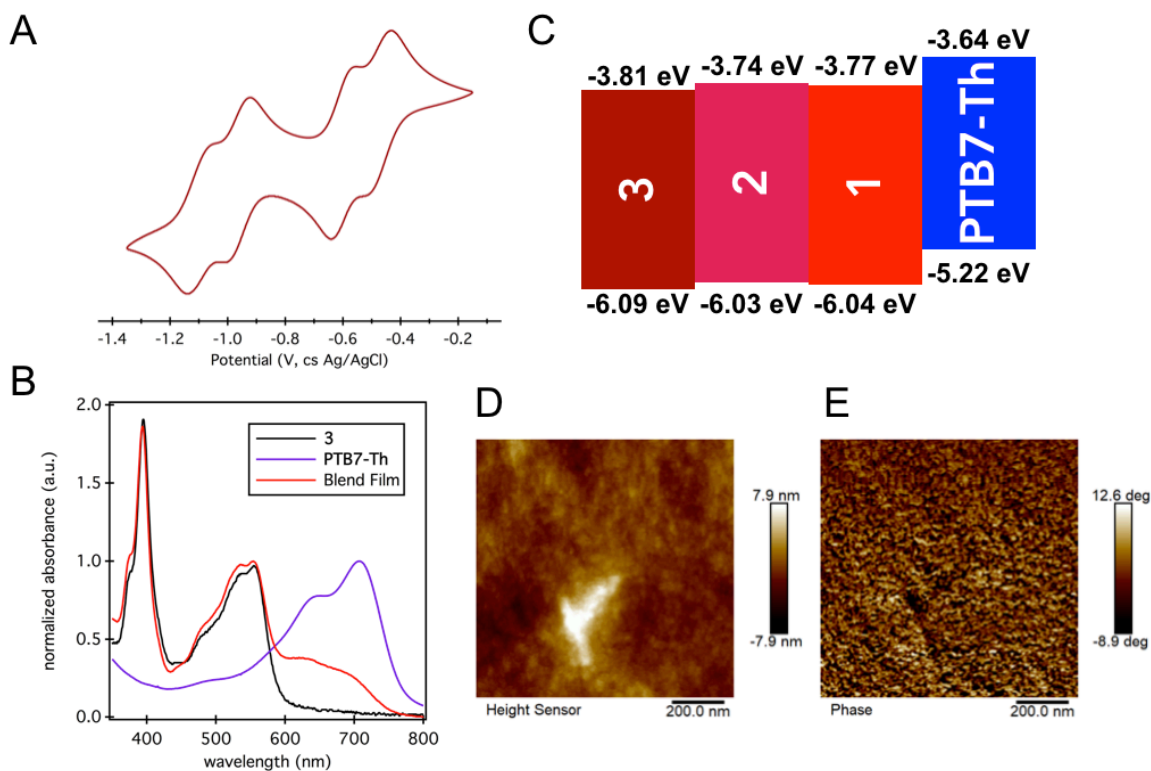
Figure 1.23. (A) CV of **3** showing reversible reduction. (B) Thin film UV-Vis spectra of **3**, **PTB7-Th**, and **3**/**PTB7-Th** blend showing similar complementary absorption to **2**/**PTB7-Th** blends (Figure 1.20.a). (C) HOMO/LUMO levels of **1-3** and **PTB7-Th** showing that **1-3** all have complementary energy levels to **PTB7-Th**. LUMO level of **3** was determined by CV. HOMO energy of **3** was estimated by subtracting the energy of the optical bandgap (estimated from the wavelength of the $S_0 \rightarrow S_1$ transition) from the LUMO energy determined by CV. AFM height (D) and phase (E) images of **3**/**PTB7-Th** blends.

Table 1.4. Frontier Orbital Energies Derived from Computational, Optical, and CV data

	Computational Data[a]			Optical Data[b]		CV
	E_{HOMO} (eV)	E_{LUMO} (eV)	E_{gap} (eV)	λ_{max} (nm)	E_{gap} (eV)	E_{LUMO} (eV)
1[c]	-6.19	-3.77	2.42	547	2.27	-3.77
2	-6.15	-3.82	2.33	542	2.29	-3.74
3	-6.18	-3.80	2.38	544	2.28	-3.81

[a] Calculations were performed at the B3LYP/6-31G** level. [b] The optical bandgap was estimated from the wavelength of the $S_0 \rightarrow S_1$ transition. [c] Data were previously reported.[54]
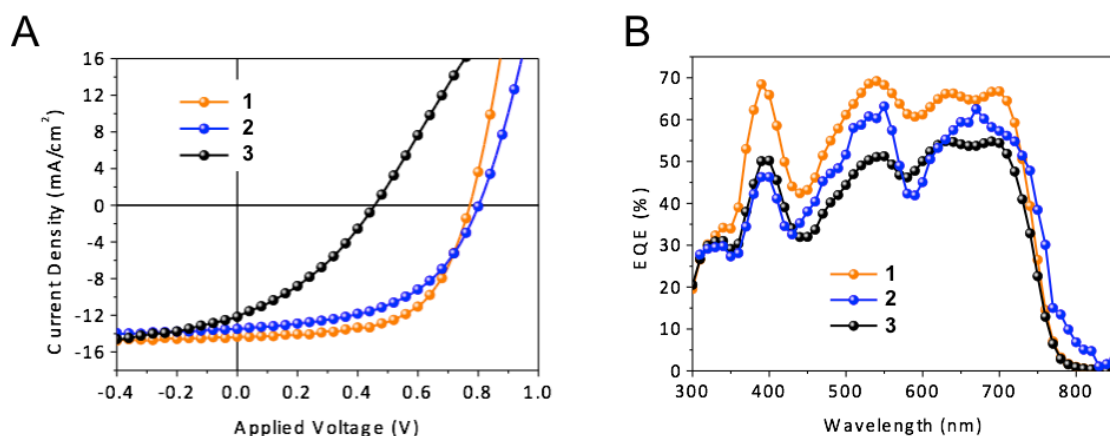
Figure 1.24. J/V characteristics (A) and EQE (B) of **1-3** in OPVs with **PTB7-Th** as the donor material.

Table 1.5. Device characteristics for OPVs made from **1/2/3**:**PTB7-Th**.

	Jsc (mA/cm^2)	Voc (V)	FF (%)	PCE (%)
1 (**hPDI2**) w no additive	13.6	0.80	51	5.59
2 (**Bi-hPDI2-T**) w no additive	14.3	0.77	60	6.64
3 (**Bi-hPDI2-Ph**) w no additive	12.3	046	39	2.21

We also find that this A-D-A motif reliably improves the performance of hPDI-based OPVs in general. We varied the thiophene linker in **2** to create the series **4-6** and incorporated them into OPVs with PTB7-Th (Figure 1.25.a). **4-6** have similar absorption spectra (Figure 1.25.b), frontier orbital energies (Table 1.6), and cyclic voltammograms (Figure 1.25.c) to **2**. J-V curves and EQE are presented in Figure 26. OPV performance of **4-6** is summarized in Table 1.7. All three of these materials performed comparably to **2** when fabricated under identical conditions. Just like **2**, they have slightly decreased V_{OC} relative to that from the parent **1**, but increased J_{SC} and FF. Overall the PCE is 0.4-0.7% higher in the devices made from **4-6** than those from **1** under identical conditions.

The use of an A-D-A structure to improve the performance of acceptors for OPVs is generalizable, suggesting room for further optimizing materials based on this motif.
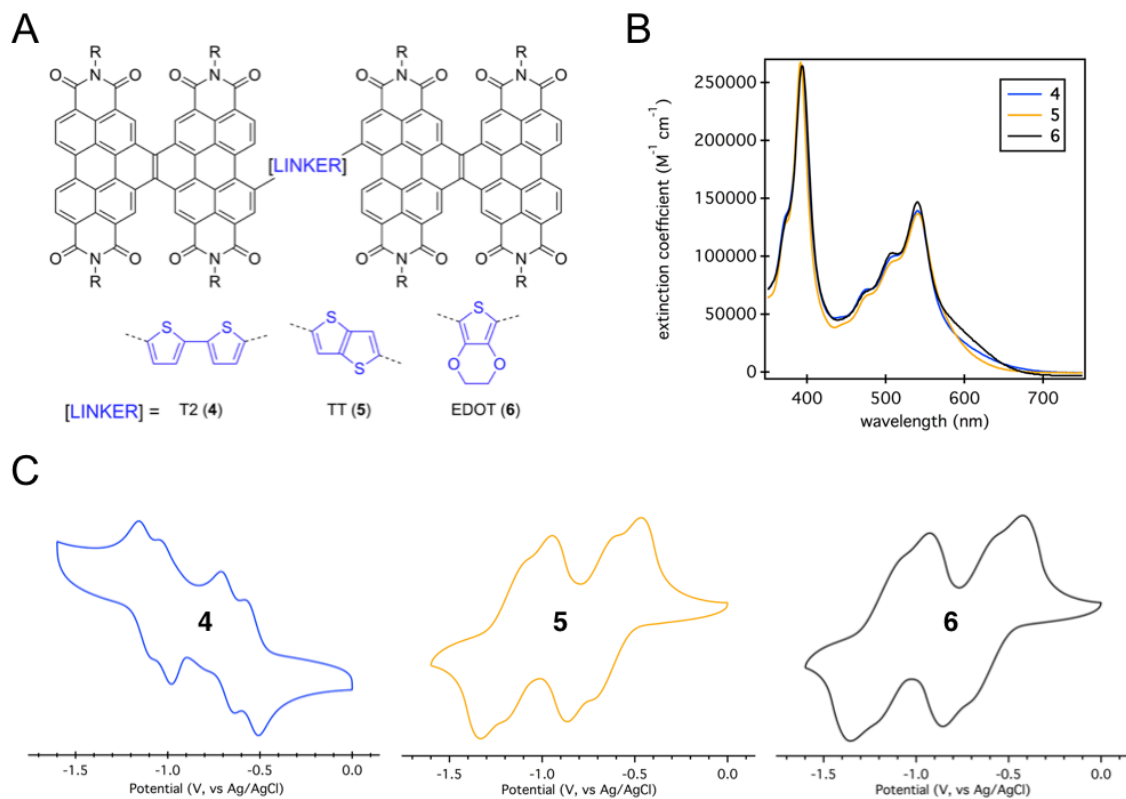
Figure 1.25. (A) Structure of **4-6**. R = 6-undecyl. (B) Solution UV-Vis spectra of **4-6** showing the same CT shoulder as in **2**. (C) Cyclic voltammograms of **4-6** showing reversible reduction.

Table 1.6. Frontier Orbital Energies Derived from Computational, Optical, and CV data for **4-6**.

	Computational Data[a]			Optical Data[b]		CV
	E_{HOMO} (eV)	E_{LUMO} (eV)	E_{gap} (eV)	λ_{max} (nm)	E_{gap} (eV)	E_{LUMO} (eV)
4	-6.12	-3.82	2.30	541	2.29	-3.77
5	-6.18	-3.81	2.36	541	2.29	-3.74
6	-6.00	-3.78	2.22	541	2.29	-3.76

[a] Calculations were performed at the B3LYP/6-31G** level. [b] The optical bandgap was estimated from the wavelength of the $S_0 \rightarrow S_1$ transition.
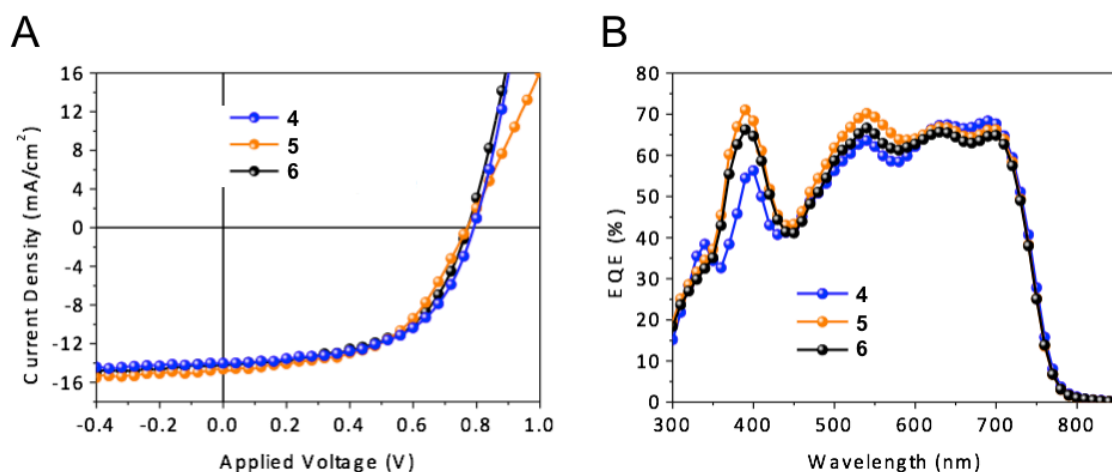
Figure 1.26. J/V characteristics (A) and EQE (B) of **4-6** in OPVs with **PTB7-Th** as the donor material.

Table 1.7. Device characteristics for OPVs made from **4/5/6**:**PTB7-Th**.

	Jsc (mA/cm^2)	Voc (V)	FF (%)	PCE (%)
4 (**Bi-hPDI2-T2**) w no additive	14.0	0.79	56.4	6.24
5 (**Bi-hPDI2-TT**) w no additive	14.6	0.77	53.5	6.01
6 (**Bi-hPDI2-EDOT**) w no additive	14.1	0.77	56.6	6.14

1.3.3. Conclusion

In this study we have presented a new design motif for OPV acceptor materials: electron-accepting nanoribbons are linked with electron-donating thiophenes to form A-D-A macromolecules. These new materials exhibit internal charge transfer between the donor and acceptor subunits and improved OPV performance despite forming large BHJ domains. The PCE increases from 2.2% in a control molecule **Bi-hPDI2-Ph** with an electronically neutral linker to 7.4% in the A-D-A dimer **Bi-hPDI2-T**. Improved performance is seen with a variety of other thiophene linkers, suggesting that this motif can be used to create a large library of high performance A-D-A dimers. Future studies to

better understand the mechanism by which this internal CT character improves

performance can guide the design of new acceptors, or even electron-donating materials.

1.4. General Experimental Details

General Synthetic Details. All reactions were performed under a nitrogen atmosphere. Anhydrous and anaerobic solvents were obtained from a Schlenck manifold with purification columns packed with activated alumina and supported copper catalyst (Glass Contour, Irvine, CA) and then sparged with nitrogen for 30 minutes before use. Reaction monitoring by thin layer chromatography (TLC) was performed on J.T. Baker Baker-flex Silica Gel IB2-F (25 mm x 75 mm) TLC plates. TLC visualization was accomplished by visible observation and irradiation with a UV lamp. Automated flash chromatography was performed with a Teledyne Isco Combiflash Rf200 using Redisep Rf Silica columns. Preparative high performance liquid chromatography (HPLC) was performed on a Waters Prep150 instrument equipped with a UV-vis detector (335 nm), an automated fraction collector, and a Nacalai Tesque COSMOSIL 5PBB column (20 mm I.D. x 250 mm, 5 μm).

Materials. **hPDI2** (**1**) and intermediate **hPDI2-Br₁** (**7**) were synthesized according to previously reported procedures.[54] All chemicals were purchased from commercial sources and used without further purification unless otherwise specified. 2,5-bis(trimethylstannyl)-3,4-ethylenedioxythiophene was generously provided by Jonathan Low.

Instrumentation. ^{1}H and ^{13}C NMR spectra were recorded on a Bruker DRX400 (400 MHz) or a Bruker DMX500 (500 MHz) spectrometer. Chemical shifts for protons are reported in parts per million downfield from tetramethylsilane and are referenced to residual protium in the NMR solvent (CHCl$_3$: δ 7.26). Chemical shifts for carbon are reported in parts per million downfield from tetramethylsilane and are referenced to the carbon resonances of the solvent (CD$_2$Cl$_2$ δ 53.0; CDCl$_3$ δ 77.0). Data are represented as follows: chemical shift, multiplicity (s = singlet, d = doublet, m = multiplet), coupling constants in Hertz, and integration.

High-resolution mass spectroscopic (HRMS) data were obtained on a Bruker UltrafleXtreme MALDI/TOF instrument using a dithranol matrix.

UV-Vis absorption spectra were obtained on Shimadzu UV 1800 UV-Vis spectrophotometer using a 1.0 cm quartz cell.

Infrared (IR) spectra were recorded on a Perkin Elmer Spectrum400 FTIR spectrometer using a PIKE ATR attachment.

Emission spectra were recorded using a Fluoromax 4 from Horiba Scientific. Photoluminescence quantum yields were determined using a quanti-phi integrating sphere accessory.

Cyclic voltammograms (CVs) were recorded on a CH166 electrochemical workstation using an Ag/AgCl electrode as the reference electrode at room temperature. 0.1 M tetrabutylammonium hexafluorophosphate (TBAPF$_6$) in dichloromethane was used as the supporting electrolyte. All cyclic voltammetry data were referenced to the known ferrocene/forrocenium couple.

1.5. Synthetic Procedures and Details of Characterization

Scheme 1.6. General synthesis of **2-6**.

hPDI2 (**1**)   hPDI2-Br$_1$ (**7**)
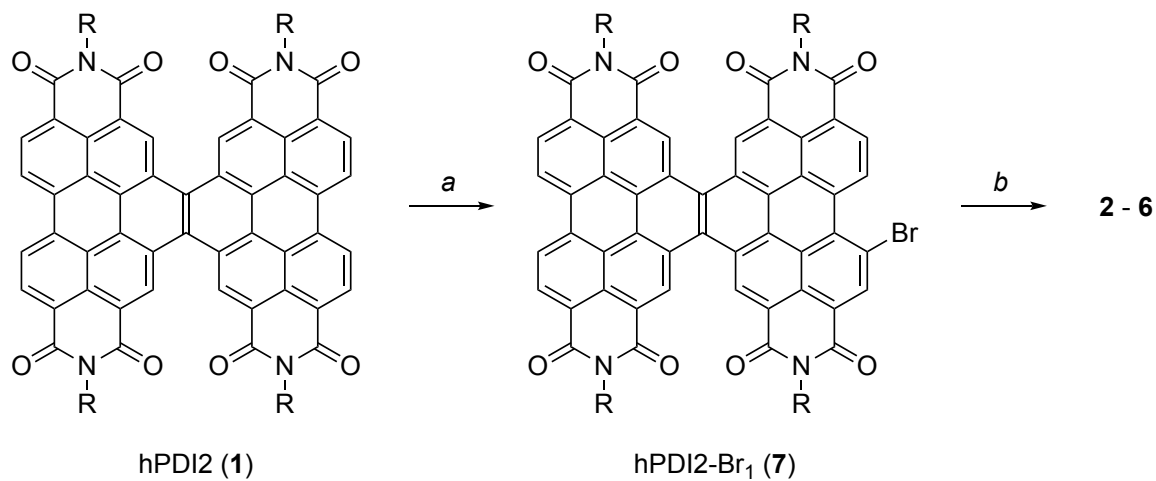
Key: R = 6-undecyl; (a) Br$_2$, I$_2$, DCM, RT, 3 days, 45% yield; (b) bis(trialkylstannyl)arene, Pd$_2$dba$_3$, AsPh$_3$, PhMe, 105 °C, 2-24 hrs, 58-86% yield.

Preparation of Pd$_2$dba$_3$/AsPh$_3$ for Stille Coupling

Triphenylarsine (0.034 g, 0.110 mmol, 2 eq) and tris(dibenzylideneacetone)dipalladium(0) (0.050 g, 0.055 mmol, 1 eq) were ground into a fine powder. The catalyst mixture was stored in a desiccator for up to 3 months with no apparent loss of catalytic activity.

Scheme 1.7. Synthesis of Bi-hPDI2-T (**2**)
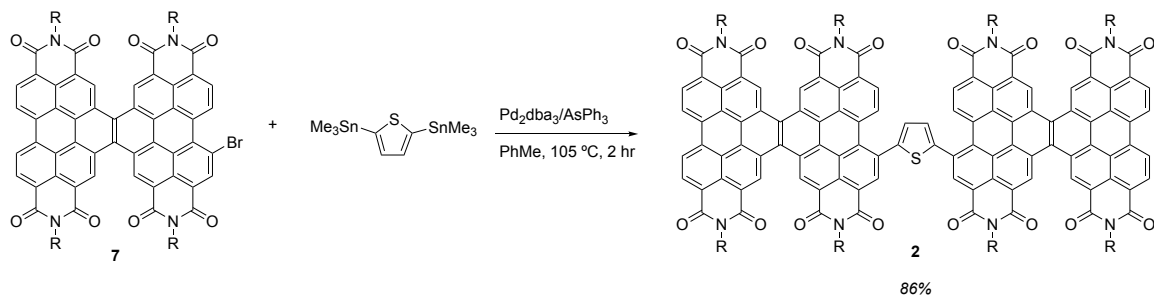
Key: R = 6-undecyl

Bi-hPDI2-T (**2**)

A round bottom flask was charged with **7** (0.500 g, 0.33 mmol, 2.2 eq), 2,5-bis(trimethylstannyl)thiophene (0.062 g, 0.15 mmol, 1 eq) and Pd$_2$dba$_3$/AsPh$_3$ mixture (0.011 g, 0.008 mmol, 5 mol%) and fitted with a rubber septum. The flask was evacuated and backfilled with nitrogen 3 times, toluene (20 mL) was added, and the reaction was stirred under a nitrogen atmosphere at 105 ºC for 2 hours. The reaction mixture was cooled to room temperature, filtered through a plug of silica gel using DCM as the eluent, and concentrated under reduced pressure. The mixture was purified by flash column chromatography (SiO$_2$, gradient mobile phase: hexane to 2:3 hexane:DCM to DCM), concentrated, triturated in methanol, filtered, and dried under vacuum to yield **2-hPDI2-Th** (**2**) as a dark red solid (0.380 g, 0.132 mmol, 86%). If necessary, samples were further purified by preparative HPLC (5PBB, eluent: 56:44 hexane:DCM). **^{1}H NMR** (500 MHz, CDCl$_3$, 323 K): δ 10.41-10.28 (overlap, 8H) 9.51-9.45 (overlap, 6H), 9.36 (s, 2H), 9.25-9.20 (overlap, 4H), 8.99 (d, 2H), 7.75 (s, 2H), 5.42-5.46 (overlap, 8H), 2.47-2.28 (overlap, 16H) 2.09-1.90 (overlap, 16H), 1.56-1.24 (overlap, 96H), 0.94-0.78 (overlap, 48H). **^{13}C NMR** (400 MHz, CDCl$_3$, 300 K): Numerous carbon resonances overlap,

leading to fewer signals than the number of chemically distinct carbon nuclei. δ 164.76, 163.69, 147.44, 134.01, 133.48, 133.41, 133.01, 130.77, 130.09, 129.74, 129.16, 127.34, 127.30, 127.05, 127.01, 126.92, 126.88, 126.73, 126.50, 126.11, 126.07, 125.86, 125.82, 125.60, 124.32, 123.91, 122.45, 55.26, 55.06, 32.45, 31.82, 31.77, 31.74, 26.79, 26.73, 22.59, 22.52, 14.13, 14.10, 14.07, 14.03. **IR** (ATR, cm^{-1}): 2922, 2856, 1703, 1699, 1658, 1596, 1446, 1320, 1236, 1182. **HRMS** (MALDI$^-$) m/z (M$^-$) calculated for $C_{192}H_{208}N_8O_{16}S = 2913.542$; found 2913.546

Scheme 1.8. Synthesis of Bi-hPDI2-Ph (**3**)
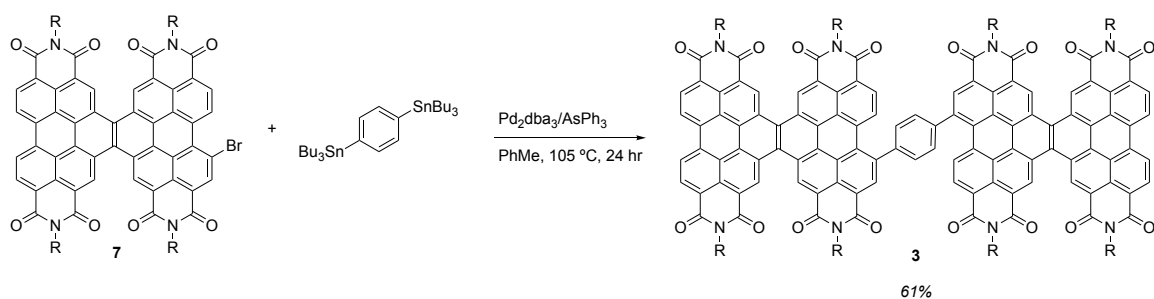
Key: R = 6-undecyl

Bi-hPDI2-Ph (3)

A round bottom flask was charged with **7** (0.407 g, 0.271 mmol, 2.2 eq), 2,5-bis(tributylstannyl)thiophene (0.081 g, 0.123 mmol, 1 eq) and Pd$_2$dba$_3$/AsPh$_3$ mixture (0.009 g, 0.006 mmol, 5 mol%) and fitted with a rubber septum. The flask was evacuated and backfilled with nitrogen 3 times, toluene (20 mL) was added, and the reaction was stirred under a nitrogen atmosphere at 105 ºC for 24 hours. The reaction mixture was cooled to room temperature, filtered through a plug of silica gel using DCM as the eluent, and concentrated under reduced pressure. The mixture was purified by flash column

chromatography (SiO$_2$, gradient mobile phase: hexane to 2:3 hexane:DCM to DCM), concentrated, triturated in methanol, filtered, and dried under vacuum to yield **2-hPDI2-Ph** (**3**) as a bright red solid (0.218 g, 0.072 mmol, 61%). If necessary, samples were further purified by preparative HPLC (5PBB, eluent: 60:40 hexane:DCM). **^{1}H NMR** (500 MHz, CDCl$_3$, 323 K): δ 10.44-10.30 (overlap, 8H), 9.51-9.44 (overlap, 4H), 9.36 (broad, 2H), 9.23 (overlap, 4H), 9.10-8.76 (broad, overlap 4H), 8.11 (4H), 5.48-5.25 (overlap, 8H), 2.52-2.27 (overlap, 16H) 2.12-1.87 (overlap, 16H), 1.62-1.22 (overlap, 96H), 0.95-0.76 (overlap, 48H). **^{13}C NMR** (400 MHz, CDCl$_3$, 300 K): Numerous carbon resonances overlap, leading to fewer signals than the number of chemically distinct carbon nuclei. δ 164.88, 163.73, 143.84, 141.32, 134.26, 134.01, 133.49, 132.00, 131.11, 130.81, 130.06, 127.33, 126.97, 126.53, 126.26, 126.10, 126.00, 125.80, 125.53, 124.34, 124.19, 123.90, 123.51, 123.09, 122.46, 55.06, 32.45, 31.78, 26.74, 22.58, 14.09. **IR** (ATR, cm^{-1}): 2955, 2925, 2858, 1702, 1700, 1660, 1598, 1447, 1323, 1241. **HRMS** (MALDI$^-$) m/z (M$^-$) calculated for C$_{194}$H$_{210}$N$_8$O$_{16}$ = 2907.586; found 2907.590

Scheme 1.9. Synthesis of **Bi-hPDI2-T2** (**4**).
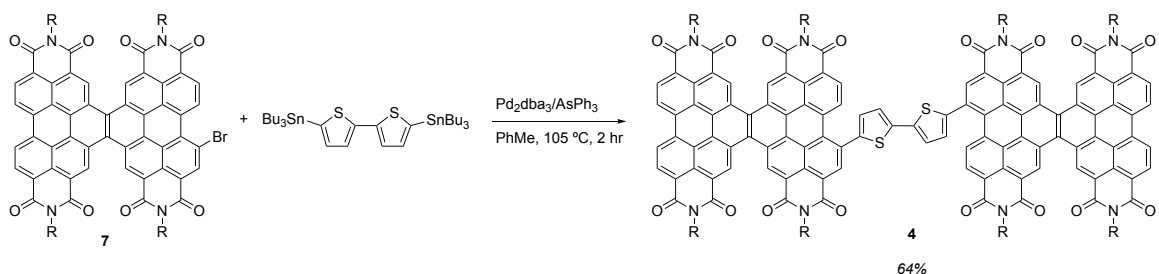
Key: R = 6-undecyl

Bi-hPDI2-T2 (4)

A scintillation vial was charged with **7** (0.100 g, 0.066 mmol, 2.1 eq), 5,5'-bis(tributylstannyl)-2,2'-bithiophene (0.024 g, 0.032 mmol, 1 eq) and Pd$_2$dba$_3$/AsPh$_3$ mixture (0.002 g, 0.0016 mmol, 5 mol%) and fitted with a PTFE septum cap. The vial was evacuated and backfilled with nitrogen 3 times, toluene (4 mL) was added, and the reaction was stirred under a nitrogen atmosphere at 105 ºC for 2 hours. The reaction mixture was cooled to room temperature, filtered through a plug of silica gel using DCM as the eluent, and then concentrated under reduced pressure. The mixture was purified by flash column chromatography (SiO$_2$, gradient mobile phase: hexane to 2:3 hexane:DCM to DCM), concentrated, triturated in methanol, filtered, and dried under vacuum to yield **Bi-hPDI2-T2 (4)** as a dark purple solid (0.061 g, 0.020 mmol, 64%). If necessary, samples were further purified by preparative HPLC (5PBB, eluent: 56:44 hexane:DCM).

^{1}H NMR (500 MHz, CDCl$_3$, 323 K): δ 10.38-10.27 (overlap, 8H), 94.9-9.43 (overlap, 4H), 9.31-9.19 (overlap, 8H), 8.92 (d, J = 8.4 Hz, 2H), 7.56 (d, J = 3.4 Hz, 2H), 7.51 (d, J = 3.4, 2H), 5.39-5.28 (overlap, 8H), 2.44-2.30 (overlap, 16H), 2.05-1.92 (overlap, 16H), 1.53-1.26 (overlap, 96H), 0.92-0.82 (overlap, 48H). **^{13}C NMR** (400 MHz, CDCl$_3$, 300 K): δ 164.83, 163.79, 143.90, 139.56, 134.00, 133.77, 133.61, 132.97, 130.09, 129.72, 128.30, 127.34, 127.00, 126.88, 126.73, 126.62, 126.51, 126.18, 126.00, 125.93, 125.83, 125.51, 124.33, 123.90, 55.11, 32.42, 31.78, 26.73, 22.58, 14.09. **IR** (ATR, cm^{-1}): 2924, 2857, 1703, 1699, 1658, 1598, 1446, 1320, 1236, 1180. **HRMS** (MALDI$^-$) m/z (M$^-$) calculated for C$_{196}$H$_{210}$N$_8$O$_{16}$S$_2$ = 2995.5301; found 2995.5257

Scheme 1.10. Synthesis of **Bi-hPDI2-TT** (**5**).
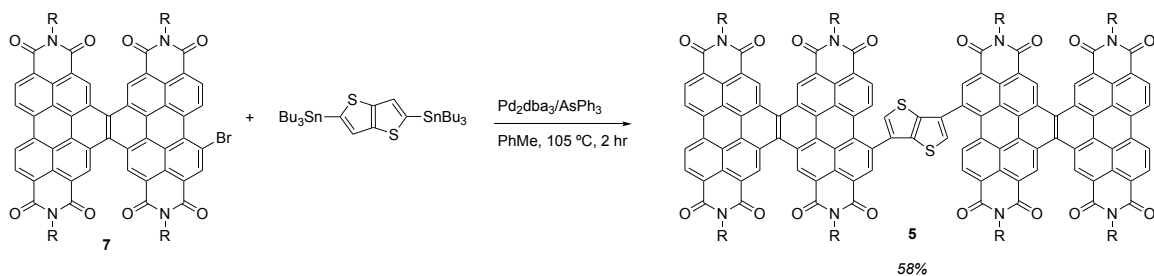
Key: R = 6-undecyl

Bi-hPDI2-TT (5)

A scintillation vial was charged with **7** (0.100 g, 0.066 mmol, 2.1 eq), 2,5-bis(trimethylstannyl)-thieno[3,2-*b*]thiophene (0.015 g, 0.032 mmol, 1 eq) and Pd$_2$dba$_3$/AsPh$_3$ mixture (0.002 g, 0.0016 mmol, 5 mol%) and fitted with a PTFE septum cap. The vial was evacuated and backfilled with nitrogen 3 times, toluene (4 mL) was added, and the reaction was stirred under a nitrogen atmosphere at 105 ºC for 2 hours. The reaction mixture was cooled to room temperature, filtered through a plug of silica gel using DCM as the eluent, and then concentrated under reduced pressure. The mixture was purified by flash column chromatography (SiO$_2$, gradient mobile phase: hexane to 2:3 hexane:DCM to DCM), concentrated, triturated in methanol, filtered, and dried under vacuum to yield **Bi-hPDI2-TT** (**5**) as a dark maroon solid (0.055 g, 0.019 mmol, 58%). If necessary, samples were further purified by preparative HPLC (5PBB, eluent: 58:42 hexane:DCM). **¹H NMR** (500 MHz, CDCl$_3$, 323 K): δ 10.42-10.30 (overlap, 8h), 9.49-9.45 (overlap, 4H), 9.38 (s, 2H), 9.30-9.20 (overlap, 6H), 8.92 (d, *J* = 10.7 Hz, 2H), 7.89 (s, 2H), 5.42-5.29 (overlap, 8H), 2.46-2.32 (overlap, 16H), 2.06-1.93 (overlap, 16H), 1.51-1.26 (overlap, 96H), 0.94-0.83 (overlap, 48H). **¹³C NMR** (400 MHz, CDCl$_3$, 300K):

δ 164.84, 163.75, 147.30, 141.75, 134.01, 133.92, 133.46, 133.05, 130.49, 129.93, 128.95, 128.37, 127.35, 127.30, 127.03, 126.92, 126.70, 126.52, 126.17, 126.00, 125.86, 125.52, 124.33, 123.91, 123.53, 123.08, 122.42, 119.95, 55.09, 32.42, 31.79, 29.71, 26.74, 22.59, 14.10. **IR** (ATR, cm^{-1}): 2922, 2858, 1703, 1699, 1658, 1597, 1446, 1320, 1234, 1181. **HRMS** (MALDI$^-$) m/z (M$^-$) calculated for $C_{194}H_{208}N_8O_{16}S_2$ = 2969.5144; found 2969.5090

Scheme 1.11. Synthesis of **Bi-hPDI2-EDOT** (**6**).
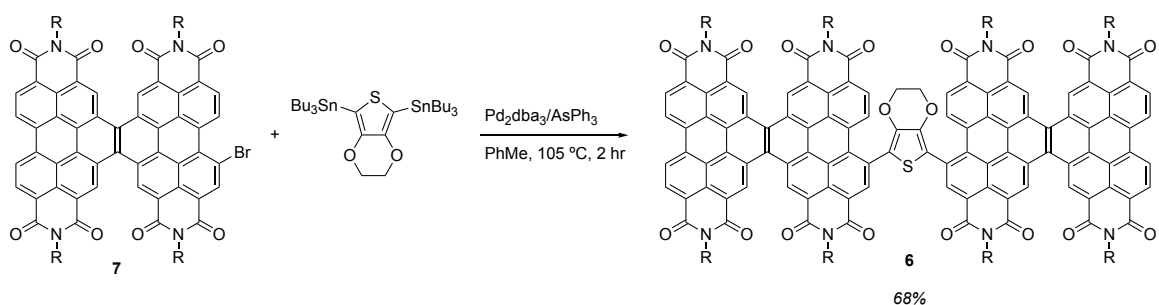
Key: R = 6-undecyl

Bi-hPDI2-EDOT (6)

A scintillation vial was charged with **7** (0.100 g, 0.066 mmol, 2.1 eq), 2,5-bis(trimethylstannyl)-3,4-ethylenedioxythiophene (0.015 g, 0.032 mmol, 1 eq) and Pd$_2$dba$_3$/AsPh$_3$ mixture (0.002 g, 0.0016 mmol, 5 mol%) and fitted with a PTFE septum cap. was evacuated and backfilled with nitrogen 3 times, toluene (4 mL) was added, and the reaction was stirred under nitrogen at 105 ºC for 2 hours. The reaction mixture was cooled to room temperature, filtered through a plug of silica gel using DCM as the eluent, and then concentrated under reduced pressure. The mixture was purified by flash column chromatography (SiO$_2$, gradient mobile phase: hexane to 2:3 hexane:DCM to DCM),

concentrated, triturated in methanol, filtered, and dried under vacuum to yield **Bi-hPDI2-EDOT** (**6**) as a dark purple solid (0.065 g, 0.022 mmol, 68%). If necessary, samples were further purified by preparative HPLC (5PBB, eluent: 56:44 hexane:DCM). **^{1}H NMR** (500 MHz, CDCl$_3$, 323 K): δ 10.45-10.27 (overlap, 8H), 9.69 (s, broad, 2H), 9.52-9.38 (overlap, 6H), 9.29-9.19 (overlap, 4H), 9.07 (s, 2H), 5.43-5.27 (overlap, 8H), 4.07 (s, 4H), 2.48-2.29 (overlap, 16H), 2.09-1.93 (overlap, 16H), 1.56-1.24 (overlap, 96H), 0.96-0.80 (overlap, 48H). **^{13}C NMR** (400 MHz, CDCl$_3$, 300 K): δ 164.85, 163.78, 138.85, 134.67, 134.22, 134.01, 133.55, 133.21, 130.88, 130.38, 130.06, 127.61, 127.35, 127.30, 127.07, 126.99, 126.92, 126.68, 126.53, 126.21, 126.08, 126.02, 125.81, 125.30, 124.34, 123.92, 123.53, 123.06, 122.40, 119.70, 64.77, 55.10, 32.43, 31.83, 31.79, 29.71, 26.80, 26.74, 22.71, 22.60, 22.54, 14.13, 14.10, 14.05. **IR** (ATR, cm^{-1}): 2922, 1859, 1702, 1699, 1658, 1596, 1446, 1350, 1321, 1236, 1181. **HRMS** (MALDI$^-$) m/z (M$^-$) calculated for C$_{194}$H$_{210}$N$_8$O$_{18}$S = 2971.5478; found 2971.5515

1.6. NMR Spectra
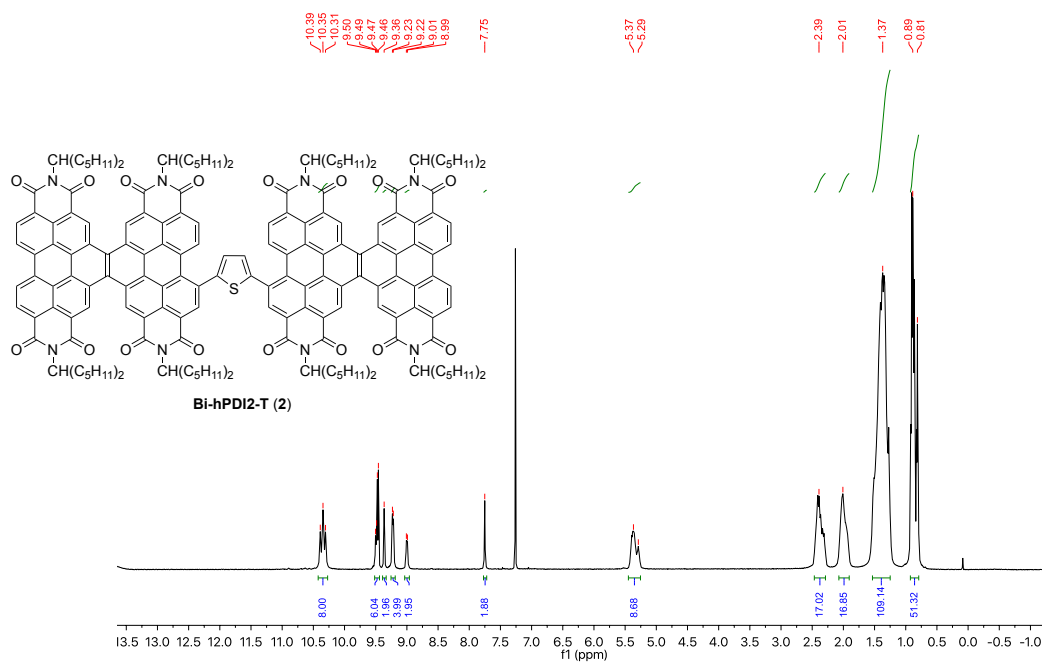
Figure 1.27. ^{1}H NMR Spectrum of **2**.
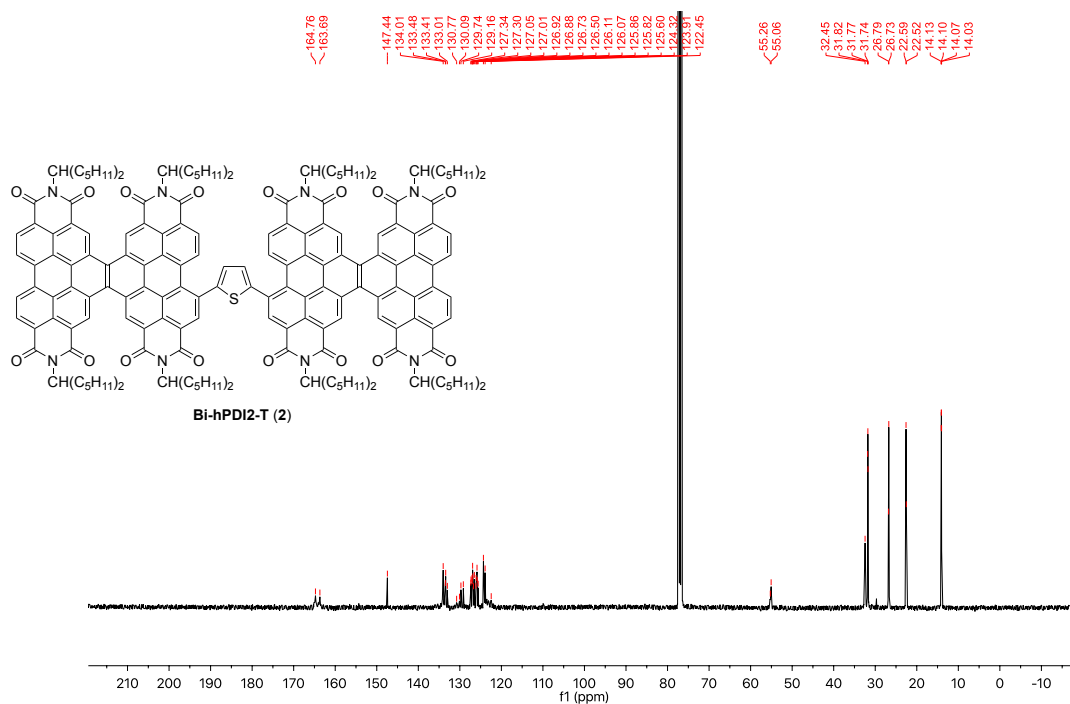
Figure 1.28. ^{13}C NMR Spectrum of **2**.
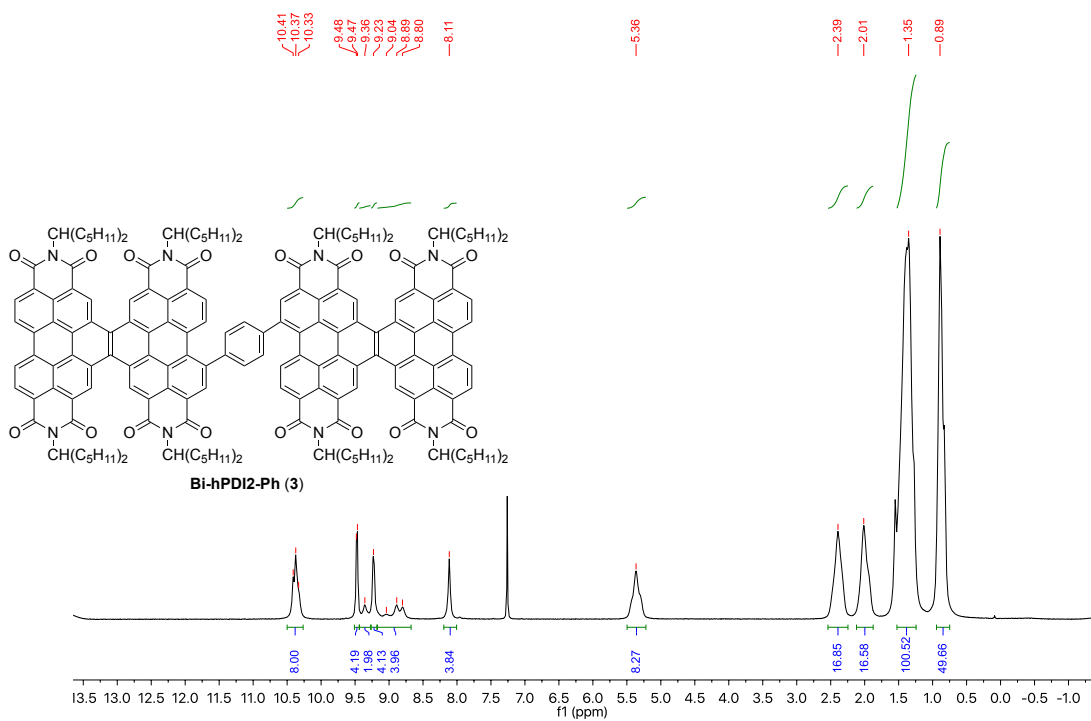
Figure 1.29. ^{1}H NMR Spectrum of **3**.
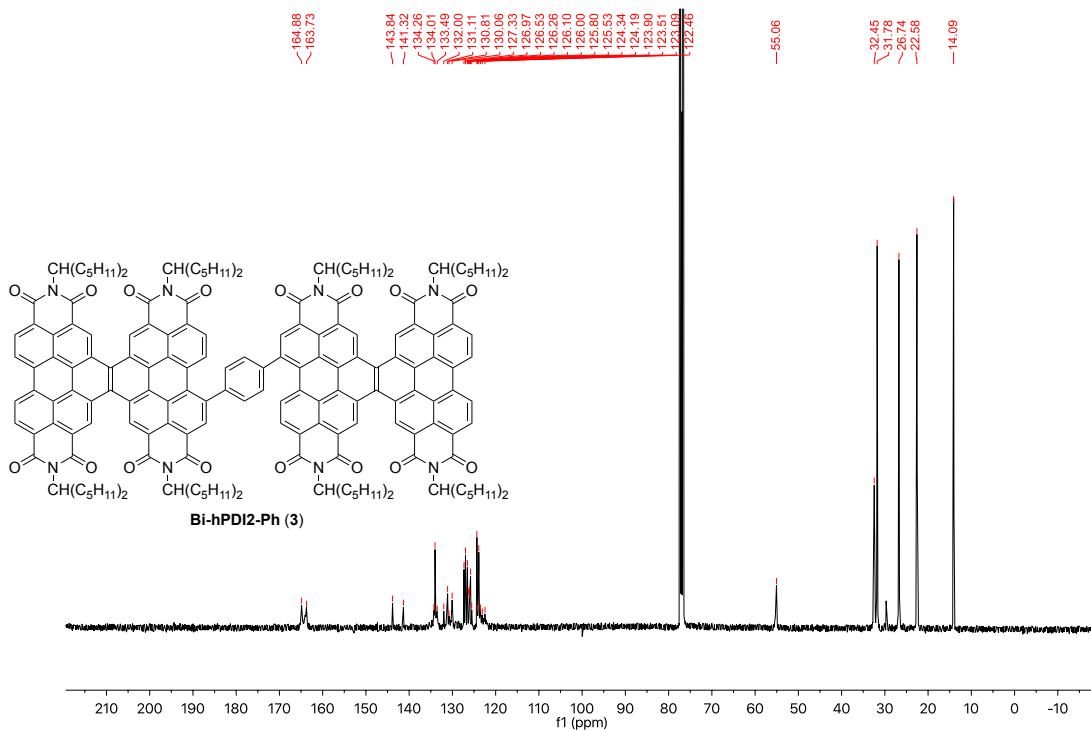
Figure 1.30. ^{13}C NMR Spectrum of **3**.
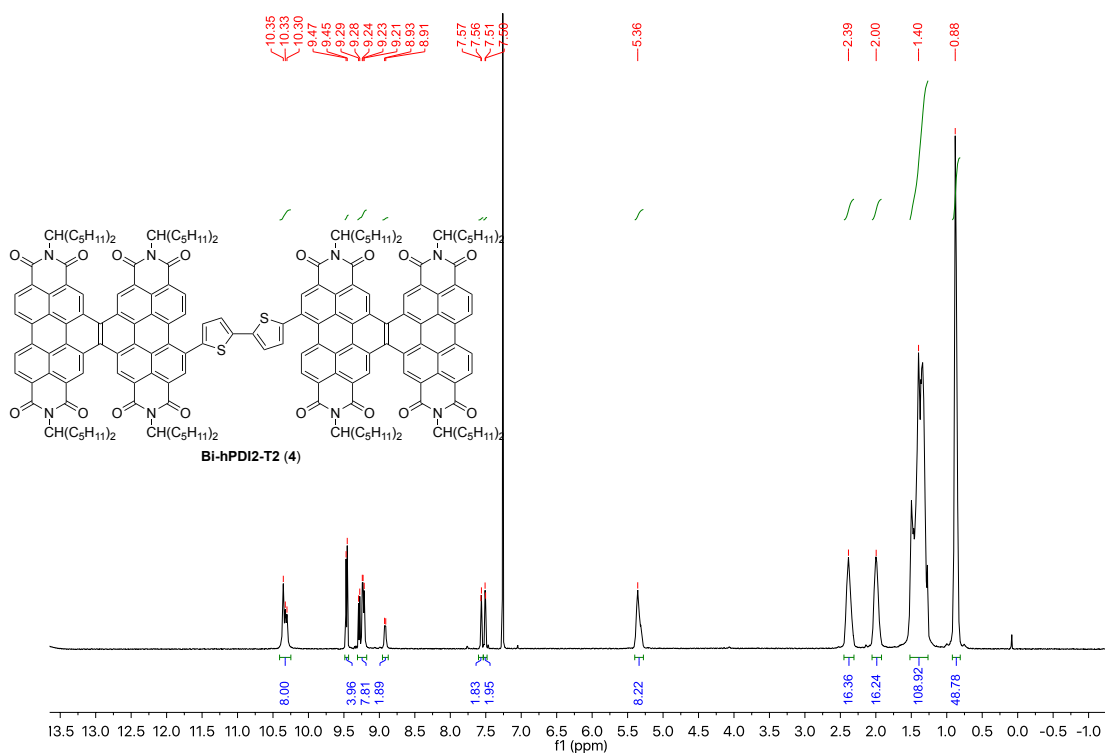
Figure 1.31. ^{1}H NMR Spectrum of **4**.
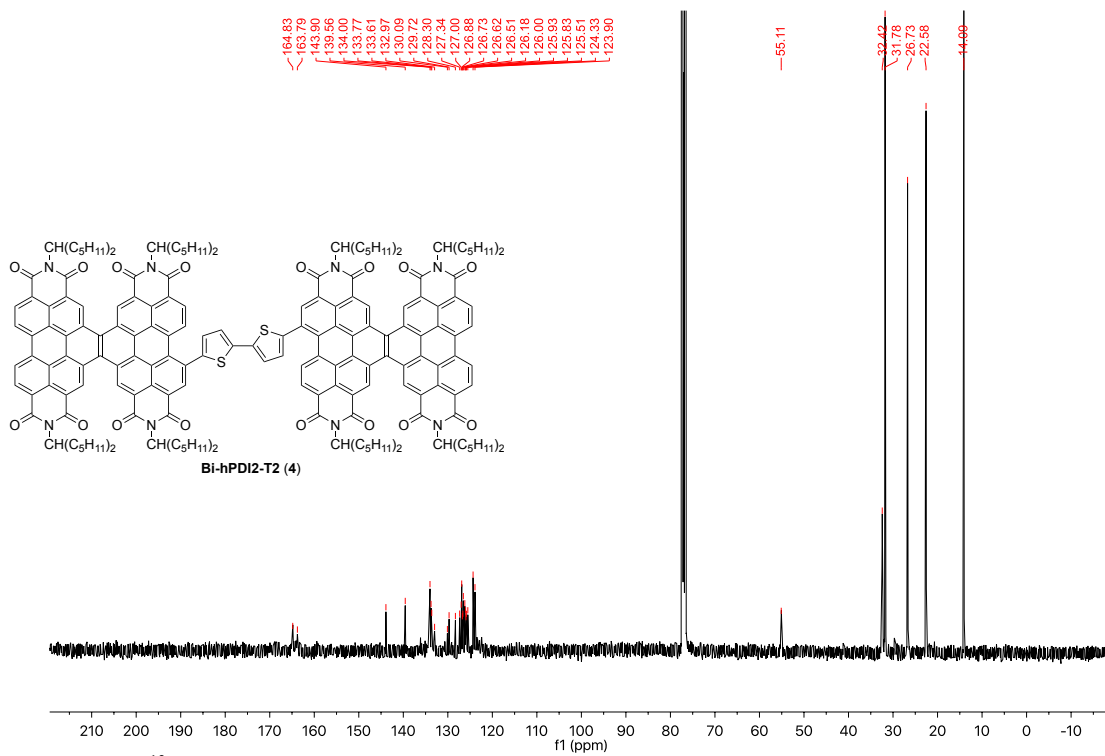
Figure 1.32. ^{13}C NMR Spectrum of **4**.

59
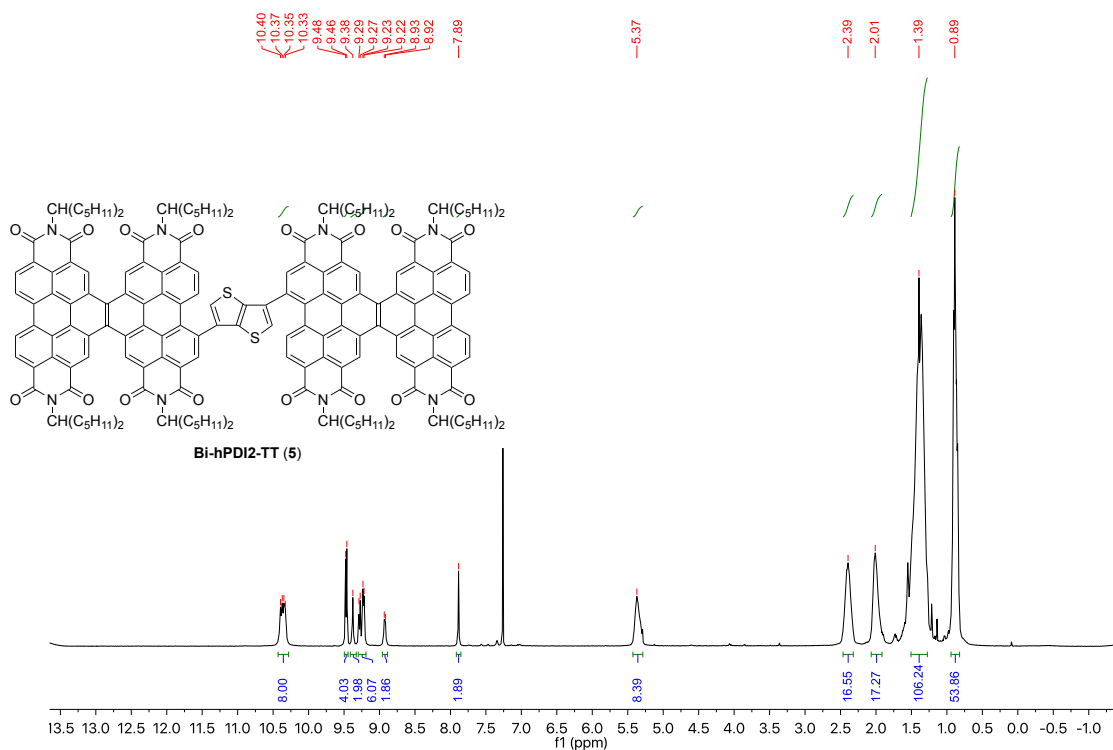
Figure 1.33. ^{1}H NMR Spectrum of **5**.
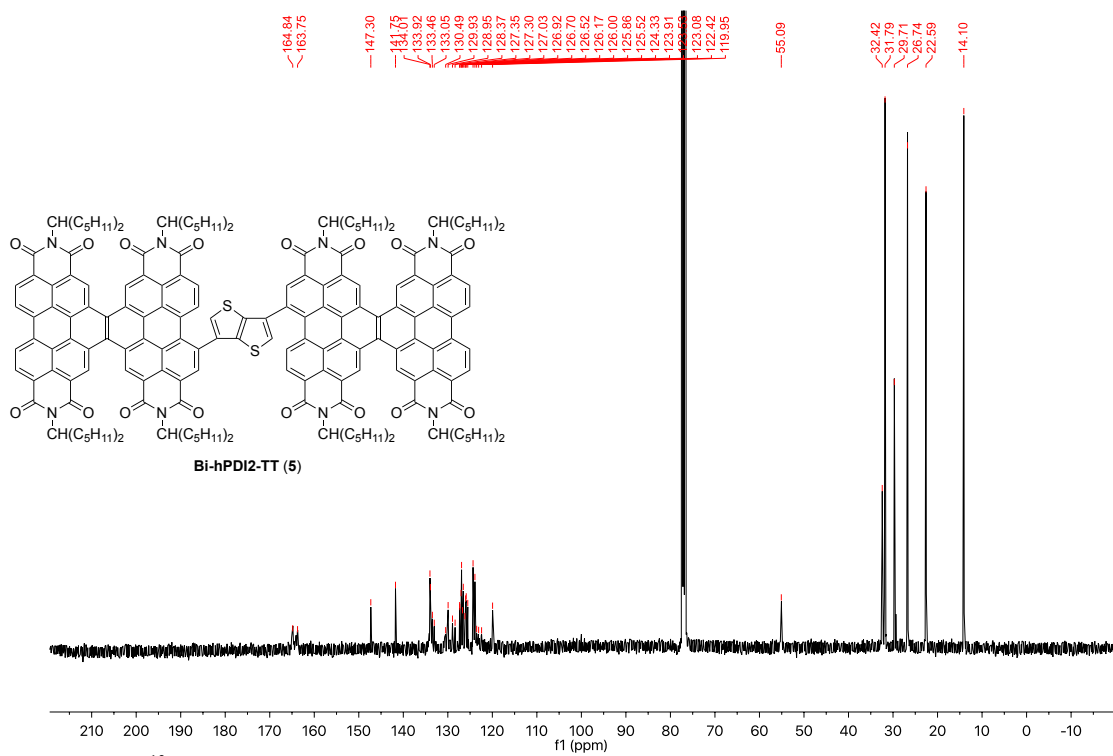
Figure 1.34. ^{13}C NMR Spectrum of **5**.
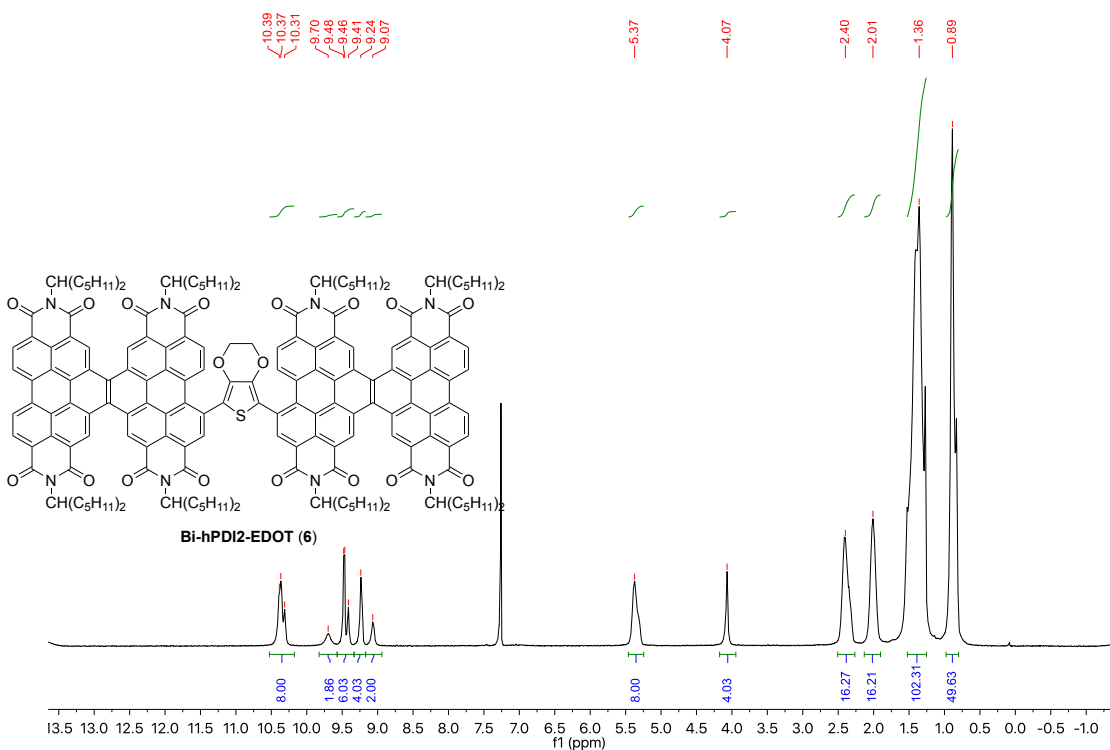
Figure 1.35. ¹H NMR Spectrum of **6**.

Figure 1.36. ¹H NMR Spectrum of **6**.

61
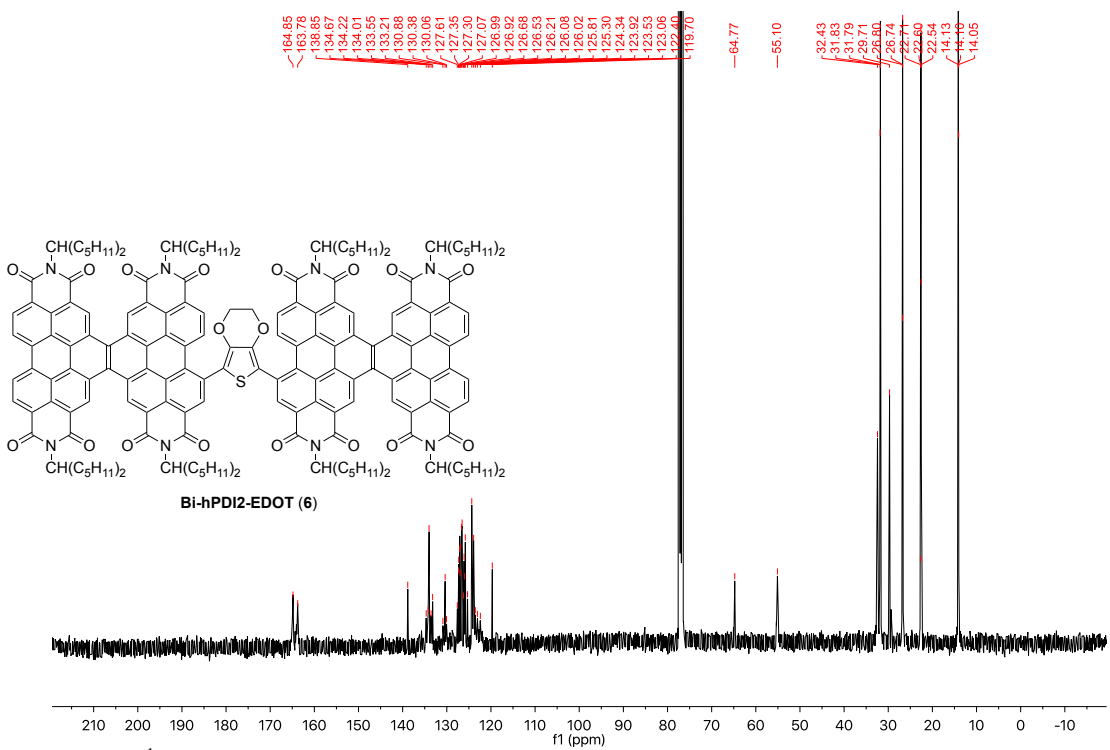
1.7. Details of DFT Calculations

Density functional theory calculations were performed using Jaguar, version 8.3, Schrodinger, Inc., New York NY, 2013. (See A. D. Bochevarov, E. Harder, T. F. Hughes, J. R. Greenwood, D. A. Braden, D. M. Philipp, D. Rinaldo, M. D. Halls, J. Zhang, R. A. Friesner, "Jaguar: A High-Performance Quantum Chemistry Software Program with Strengths in Life and Materials Sciences", Int. J. Quantum Chem., 2013, 113(18), 2110-2142).

All geometries were optimized using the B3LYP functional and the 6-31G** basis set. Table 1.2 is repeated here as Table 1.8 with each conformation assigned a reference number. The optimized geometry for each item is listed here according to that reference number. Each geometry is followed by the results of TD-DFT excited state calculations performed using the 6-31G** basis set. These calculations were performed using the package included with Jaguar. Afterwards is listed the results of calculations performed on compound **3** using the same method.

Table 1.8. Conformational Flexibility of **2**.[a]

Geometry	Dihedral Angle[b] °	Dihedral Angle[b] °	Relative Gas Phase Energy (kcal mol⁻¹)	Lowest Energy Transition (eV)	Lowest Energy Transition (nm)	Oscillator Strength	Page Number
2a	64.1[c]	43.4	1.40	1.89	657	0.150	64
2b	61.3	43.4*	1.37	1.87	665	0.196	74
2c	67.9	13.3*	4.74	1.83	676	0.360	82
2d	65.9	16.9*	8.49	1.92	646	0.375	90
2e	63.9	47.0*	9.68	2.07	600	0.300	98
2f	71.5	77.1*	5.48	2.11	587	0.347	107
2g	75.2	107.3*	1.81	2.13	582	0.220	115
2h	80.2	137.4*	1.85	2.15	577	0.165	123
2i	107.3*	48.1*	1.01	2.03	611	0.344	131
2j	107.3*	84.9*	1.56	2.13	583	0.359	139
2k	43.4*	54.9*	1.18	1.85	672	0.241	147
2l	43.4*	61.3*	1.36	1.86	665	0.196	153
2m	**137.4*[d]**	**50.2***	**0**	**1.92**	**647**	**0.467**	**159**
2n	137.4*	80.2*	1.81	2.02	614	0.212	167

[a] Calculations were performed at the B3LYP/6-31G** level. [b] Dihedral angle about the biaryl bonds between thiophene linker and PDI core. Angles denoted with * were restricted. [c] Initially optimized geometry. [d] Final optimization. This is the geometry displayed in Figure 1.13.c and 1.13.d, and used for all other calculations.

Conformation **2a** (initial optimization)

B3LYP/6-31G** optimized geometry
Final total energy = -6022.85300481104 h

angstroms

atom	x	y	z
C1	0.0033186103	-0.0103157225	0.2226593611
C2	1.4257246587	-0.0047312051	0.3543238318
C3	2.1116138437	1.2435899332	0.3875106072
C4	1.3746637470	2.4492886261	0.1930706943
C5	0.0204096113	2.4158763069	-0.0243455057
C6	-0.7055977046	1.1902235886	-0.0309131963
C7	2.1587535067	-1.2207561614	0.5199515113
C8	3.5131960096	-1.1202117180	0.8703643575
C9	4.1734908735	0.1052638722	0.9350242162
C10	3.4961833004	1.2858964683	0.6565164244
C11	-0.7051876085	-1.2392258361	0.3984497503
C12	0.0207292511	-2.4754139901	0.4458966977
C13	1.4536470312	-2.5029395259	0.3732903068
C14	-2.1199416286	-1.2164673613	0.5100365343
C15	-2.8101078238	-2.4601930012	0.5673762434
C16	-2.1380244396	-3.6562222824	0.5761453436
C17	-0.7159520634	-3.6907512221	0.5219986611
C18	-0.0368495505	-4.9254845623	0.4873659800
C19	1.3275569174	-4.9425119003	0.2833328107
C20	2.0866262497	-3.7597730609	0.1748412878
C21	3.4733529898	-3.9331669614	-0.3004809732
C22	4.0939402860	-3.2512971641	-1.3211250959
C23	5.3759039125	-3.7542463599	-1.6454237153
C24	5.7543067611	-4.8368807281	-0.8882977794
S25	4.4959538360	-5.2482506552	0.2562093062
C26	6.9908742311	-5.6263647322	-1.1083503276
C27	8.2908231623	-5.0850264700	-0.9620030104
C28	8.5894666423	-3.8723841633	-0.1944527871
C29	7.6970209702	-3.3237948459	0.7384707174
C30	9.3842014563	-5.7620609196	-1.5932229080
C31	10.6790969195	-5.1538983696	-1.6881300573
C32	10.8836855523	-3.8393870646	-1.1622672192
C33	9.8630374568	-3.2455541960	-0.3568895417
C34	6.8257680694	-6.9090333001	-1.6591866560
C35	7.8946507774	-7.6230159917	-2.1708965557
C36	9.1778911051	-7.0362133039	-2.1906999675
C37	10.2578348941	-7.6811227632	-2.8584941801

C38	11.4986738184	-7.0968505561	-2.9126639129
C39	11.7612071874	-5.8386126393	-2.2986919196
C40	10.1405743669	-2.0292942618	0.3278658747
C41	9.1910126992	-1.4908699448	1.2230418043
C42	7.9916888326	-2.1556411370	1.4365965657
C43	12.0991745921	-3.1530072398	-1.4115088841
C44	12.3360698158	-1.9298095839	-0.7167881252
C45	11.4036327951	-1.3925679645	0.1365211089
C46	-2.9252703909	-4.9212284443	0.6123655929
N47	-2.1648548735	-6.0881548027	0.6350664019
C48	-0.7781716476	-6.2112735799	0.5858696318
C49	4.2265850276	2.5799611358	0.6780896574
N50	3.4338041181	3.7101795789	0.4793144759
C51	2.0605271382	3.7718483530	0.2579820624
C52	11.7350381038	-0.1457690888	0.8831159533
N53	10.7278316839	0.3210706885	1.7249897640
C54	9.4754628532	-0.2414627702	1.9714468095
C55	7.6610311268	-8.9631598256	-2.7710529596
N56	8.7678143929	-9.5221320538	-3.4064075827
C57	10.0472901326	-8.9878486627	-3.5412739082
O58	-4.1430177126	-4.9639235000	0.6296791809
O59	-0.2407237208	-7.3048468117	0.6119979485
O60	1.4925843864	4.8429765988	0.1249880271
O61	5.4279901945	2.6796377239	0.8574488339
O62	8.6983705201	0.2732733831	2.7584596551
O63	12.7973033744	0.4435944131	0.7853294057
O64	6.5899088784	-9.5438679872	-2.7416567050
O65	10.9106907667	-9.5754592470	-4.1695279655
C66	-2.1533772166	1.1646099703	-0.1219608766
C67	-2.8331977434	0.0468042300	0.4156957446
C68	13.0526589121	-5.1837484993	-2.4205050706
C69	13.1221362217	-3.7841950086	-2.2261783560
C70	14.2774185853	-5.8960224994	-2.7332563464
C71	15.4120918911	-5.1778832148	-3.1907766011
C72	15.3496993769	-3.7543510787	-3.3194339538
C73	14.2129846553	-3.0527220531	-2.8415629581
C74	-2.9341145873	2.2309661451	-0.7145555578
C75	-4.3256575558	2.3131669496	-0.4507780976
C76	-4.9492281651	1.3445316791	0.3981121632
C77	-4.2103861861	0.2173097974	0.8420034627
C78	-5.1120451557	3.3646542439	-1.0194184141
C79	-6.4922233591	3.5190413801	-0.6863248683
C80	-7.1036130830	2.5905562778	0.2671163009
C81	-6.3172393098	1.5165443723	0.7853045714

C82	16.6197776172	-5.8673463361	-3.5331621553
C83	17.7349443218	-5.1737573177	-4.0925925902
C84	17.6329765976	-3.7298829754	-4.3175914949
C85	16.4427028168	-3.0495639963	-3.9176347667
C86	16.3401731020	-1.6438055866	-4.1158415538
C87	15.1430719328	-0.9726803490	-3.7263044590
C88	14.1261824129	-1.6547007854	-3.1066454606
C89	18.6643800488	-2.9822858431	-4.9012804326
C90	18.5529840606	-1.6079761805	-5.1000111274
C91	17.4009162048	-0.9323275785	-4.7161147302
C92	14.4295644687	-7.2876387118	-2.4639716580
C93	15.5985350896	-7.9532165878	-2.7330449697
C94	16.7095098891	-7.2702907295	-3.3109055737
C95	17.8955062345	-7.9659648822	-3.6273977316
C96	18.9707965840	-7.2794255639	-4.1781120145
C97	18.8869539145	-5.9078000373	-4.4074369447
C98	-6.9028820444	0.5989139169	1.7026798109
C99	-6.1063152105	-0.4619028937	2.2291989133
C100	-4.8139591735	-0.6436265122	1.8055454910
C101	-2.3744469459	3.1287428780	-1.6691951174
C102	-3.1264266228	4.1078809046	-2.2667365986
C103	-4.5046116976	4.2722222325	-1.9336611449
C104	-8.4357937610	2.7078310200	0.6886525590
C105	-8.9990646984	1.8094202171	1.5931078621
C106	-8.2459381505	0.7589519363	2.1059814232
C107	-5.2667419734	5.3055989693	-2.5188283609
C108	-6.6094910851	5.4429131004	-2.1884540963
C109	-7.2074299832	4.5646613174	-1.2868913159
C110	17.2946124862	0.5310838821	-4.9513460845
N111	16.0802552685	1.1042849987	-4.5756899106
C112	14.9737731828	0.4814691357	-4.0023793630
C113	15.6970731251	-9.4004049425	-2.3954426454
N114	16.8954768036	-10.0075374234	-2.7626310639
C115	18.0104456057	-9.4234551041	-3.3633141642
C116	-8.8585223932	-0.1781927776	3.0839922185
N117	-8.0021998427	-1.1618330951	3.5788286059
C118	-6.6635863453	-1.3813127228	3.2611863739
C119	-2.4854054661	4.9913070215	-3.2817497723
N120	-3.3115032816	5.9885140587	-3.7947165950
C121	-4.6504813649	6.2403238713	-3.4953752132
O122	-1.3292035782	4.8779983361	-3.6521010261
O123	-5.2471450583	7.1638037138	-4.0244164354
O124	-10.0180982499	-0.1109947882	3.4554949835
O125	-6.0269018059	-2.2712730637	3.8004967804

O126	14.8130685789	-10.0336717958	-1.8448483940
O127	18.9969894501	-10.0879433924	-3.6316755828
O128	13.9591752455	1.1093580423	-3.7524016433
O129	18.1821234684	1.2059094472	-5.4447026569
H130	-0.4868920726	3.3636181022	-0.1159745204
H131	5.2242006695	0.1590687470	1.1930488868
H132	-3.8871580495	-2.5057676637	0.5440373751
H133	1.8100296875	-5.9052015328	0.1735875649
H134	5.8348804026	-7.3386038120	-1.7384346078
H135	12.2533228492	-7.6037328364	-3.4935848838
H136	7.2957208864	-1.7466079564	2.1584711365
H137	13.2873480812	-1.4236610106	-0.7876390664
H138	-2.6828822384	-6.9596283272	0.6857224971
H139	3.9152360373	4.6034569053	0.5022760953
H140	10.9313092842	1.1761469676	2.2326726370
H141	8.6241148657	-10.4278247883	-3.8419523673
H142	13.2297690223	-1.0979043048	-2.8772552271
H143	19.5779735606	-3.4708324075	-5.2129691094
H144	19.3561773608	-1.0426036124	-5.5555034823
H145	13.6461652279	-7.8511103206	-1.9794277182
H146	19.8704503373	-7.8322263765	-4.4175839952
H147	19.7462201437	-5.4097662439	-4.8358188173
H148	-4.2491012865	-1.4316882000	2.2805576151
H149	-1.3484198725	3.0295006592	-1.9923437229
H150	-9.0549579144	3.5118505095	0.3138301681
H151	-10.0281198529	1.9120046520	1.9138380736
H152	-7.1756852523	6.2429535375	-2.6481947195
H153	-8.2551433630	4.7059164324	-1.0571105731
H154	15.9830323506	2.0999996550	-4.7464121713
H155	16.9739460154	-10.9997808901	-2.5633842517
H156	-8.4000336692	-1.7993400724	4.2610674259
H157	-2.8888651396	6.6141376689	-4.4728901335
H158	4.0723814219	-2.0153434596	1.0906082533
H159	3.6273431666	-2.4254344466	-1.8415219807
H160	6.0031744857	-3.3529305866	-2.4317981566
H161	6.7604400844	-3.8181192926	0.9405540425

Restricted Singlet Excited State   1:   1.8874 eV   656.90 nm

excitation   X coeff.
------------   ---------
426 => 429   -0.13346
428 => 429   -0.97251
428 => 431   -0.10723

Transition dipole moment (debye):
   X=   4.1935   Y= -1.8493   Z=   0.2350 Tot=   4.5892

Oscillator strength, f=   0.1507

Restricted Singlet Excited State 2:   1.9866 eV   624.11 nm

 excitation   X coeff.
------------   ---------
 426 => 430   -0.10897
 428 => 430   -0.97865

Transition dipole moment (debye):
   X= -0.4591   Y= -4.3157   Z=   0.0581 Tot=   4.3404

Oscillator strength, f=   0.1419

Restricted Singlet Excited State 3:   2.1500 eV   576.68 nm

 excitation   X coeff.
------------   ---------
 426 => 430   0.16890
 427 => 429   0.95650

Transition dipole moment (debye):
   X= -0.7922   Y= -5.2729   Z=   0.0117 Tot=   5.3321

Oscillator strength, f=   0.2318

Restricted Singlet Excited State 4:   2.2120 eV   560.50 nm

 excitation   X coeff.
------------   ---------
 426 => 429   -0.41569
 426 => 430   -0.18521
 427 => 430   -0.85379
 427 => 432   0.10192
 428 => 431   -0.11205

Transition dipole moment (debye):

X=   3.8193   Y=   -0.8933   Z=   -1.9090 Tot=   4.3623

Oscillator strength, f=   0.1596

Restricted Singlet Excited State   5:   2.2763 eV   544.68 nm

 excitation   X coeff.
 ------------ ---------
 425 => 430   -0.24504
 426 => 429   0.60936
 426 => 430   0.26521
 427 => 430   -0.30401
 427 => 432   -0.15451
 428 => 431   -0.53584
 428 => 432   0.27220

Transition dipole moment (debye):
   X=   -0.5818   Y=   -0.5344   Z=   0.2087 Tot=   0.8171

Oscillator strength, f=   0.0058

Restricted Singlet Excited State   6:   2.3134 eV   535.94 nm

 excitation   X coeff.
 ------------ ---------
 424 => 429   -0.14885
 426 => 429   0.50859
 426 => 431   0.12595
 427 => 430   -0.36565
 428 => 429   -0.17923
 428 => 431   0.65761
 428 => 432   -0.23898

Transition dipole moment (debye):
   X=   -4.1679   Y=   1.8671   Z=   0.8041 Tot=   4.6373

Oscillator strength, f=   0.1887

Restricted Singlet Excited State   7:   2.3260 eV   533.03 nm

 excitation   X coeff.

```
------------  ---------
425 => 429    0.44369
426 => 429    0.12429
426 => 430   -0.40516
427 => 431   -0.28727
428 => 431   -0.33506
428 => 432   -0.62918
```

Transition dipole moment (debye):
  X=   0.5329   Y=   1.0127   Z=   0.0142 Tot=   1.1445

Oscillator strength, f=   0.0116

Restricted Singlet Excited State   8:   2.3859 eV   519.65 nm

```
 excitation    X coeff.
------------  ---------
424 => 430   -0.13183
426 => 429   -0.18590
426 => 430    0.74088
426 => 432   -0.15320
427 => 429   -0.22951
428 => 430   -0.11196
428 => 432   -0.51820
```

Transition dipole moment (debye):
  X= -1.3010   Y=   0.7891   Z=   1.9531 Tot=   2.4759

Oscillator strength, f=   0.0555

Restricted Singlet Excited State   9:   2.4481 eV   506.45 nm

```
 excitation    X coeff.
------------  ---------
423 => 429    0.34673
423 => 430   -0.39760
424 => 429    0.65246
424 => 430    0.24888
425 => 429    0.10478
425 => 430   -0.25512
426 => 430    0.12637
427 => 432   -0.10328
```

```
427 => 433   -0.11158
427 => 434    0.11962
428 => 431    0.21458
428 => 433   -0.12834
```

Transition dipole moment (debye):
  X=   6.6366   Y= -1.7330   Z= -1.0515 Tot=   6.9392

Oscillator strength, f=   0.4470

Restricted Singlet Excited State 10:   2.4726 eV   501.43 nm

 excitation   X coeff.
 -----------   ---------
```
 423 => 429    0.53493
 424 => 429   -0.17029
 424 => 430   -0.55078
 425 => 429    0.39840
 427 => 431   -0.14820
 427 => 433   -0.16154
 428 => 432    0.28006
 428 => 434    0.18999
```

Transition dipole moment (debye):
  X= -0.8018   Y=   0.2659   Z= -2.1748 Tot=   2.3331

Oscillator strength, f=   0.0510

Restricted Singlet Excited State 11:   2.5080 eV   494.35 nm

 excitation   X coeff.
 -----------   ---------
```
 423 => 429    0.45536
 423 => 430   -0.16838
 424 => 430   -0.15092
 425 => 429   -0.49913
 425 => 430    0.22934
 426 => 429    0.24175
 426 => 430   -0.24570
 427 => 431    0.36503
 427 => 432    0.18071
 427 => 433   -0.11059
```

428 => 431   -0.20155
428 => 432   -0.26463

Transition dipole moment (debye):
  X=   2.4910   Y=   2.0469   Z= -0.5584 Tot=   3.2721

Oscillator strength, f=   0.1018

Restricted Singlet Excited State 12:   2.5796 eV   480.64 nm

 excitation   X coeff.
 ------------   ---------
 424 => 429   0.11274
 424 => 430   0.22772
 425 => 429   0.56856
 425 => 430   0.49415
 426 => 429   0.10609
 427 => 431   0.50214
 427 => 432   0.18915

Transition dipole moment (debye):
  X= -0.7012   Y= -0.7461   Z= -2.0579 Tot=   2.2985

Oscillator strength, f=   0.0517

Restricted Singlet Excited State 13:   2.5958 eV   477.63 nm

 excitation   X coeff.
 ------------   ---------
 424 => 429   0.22427
 425 => 429   -0.19142
 425 => 430   0.67988
 426 => 429   0.11465
 426 => 430   0.12585
 426 => 432   0.12170
 427 => 431   -0.60512

Transition dipole moment (debye):
  X=   0.5121   Y= -1.7303   Z=   2.1453 Tot=   2.8033

Oscillator strength, f=   0.0774

Restricted Singlet Excited State 14: 2.6342 eV 470.67 nm

```
 excitation    X coeff.
------------  ---------
 423 => 430   -0.11418
 425 => 430   -0.28205
 426 => 431   -0.17601
 426 => 432    0.13267
 427 => 430    0.10692
 427 => 431   -0.19816
 427 => 432    0.86606
```

Transition dipole moment (debye):
    X= -0.0562   Y= -0.4437   Z=   1.0237 Tot=   1.1171

Oscillator strength, f=   0.0125

Restricted Singlet Excited State 15: 2.6656 eV 465.13 nm

```
 excitation    X coeff.
------------  ---------
 423 => 429    0.36341
 423 => 430   -0.18372
 424 => 429   -0.59513
 424 => 430    0.62130
 427 => 431   -0.18509
 427 => 432   -0.12348
```

Transition dipole moment (debye):
    X=   1.1689   Y= -0.7202   Z=   1.0843 Tot=   1.7495

Oscillator strength, f=   0.0309

Conformation **2b**

B3LYP/6-31G** optimized geometry
Final total energy = -6022.852735

angstroms

atom	x	y	z
C1	-0.0263020000	0.0345830000	0.2845100000
C2	1.3923000000	0.0621110000	0.4546600000
C3	2.0520360000	1.3204000000	0.5594890000
C4	1.2923790000	2.5184400000	0.4020220000
C5	-0.0541920000	2.4672130000	0.1471100000
C6	-0.7545170000	1.2294720000	0.0633000000
C7	2.1455860000	-1.1465940000	0.5816590000
C8	3.4909390000	-1.0364770000	0.9725530000
C9	4.1224720000	0.1976670000	1.1112140000
C10	3.4271080000	1.3751110000	0.8682640000
C11	-0.7153490000	-1.2121440000	0.3869500000
C12	0.0328470000	-2.4360550000	0.3998570000
C13	1.4664870000	-2.4340900000	0.3630310000
C14	-2.1327970000	-1.2198600000	0.4621080000
C15	-2.7975890000	-2.4771630000	0.4425980000
C16	-2.1024290000	-3.6578890000	0.4197050000
C17	-0.6794080000	-3.6670570000	0.4091040000
C18	0.0282590000	-4.8844460000	0.3507520000
C19	1.3979840000	-4.8737390000	0.1858530000
C20	2.1312280000	-3.6725440000	0.1336310000
C21	3.5292540000	-3.7923820000	-0.3091360000
C22	4.1889990000	-3.0724260000	-1.2801040000
C23	5.4890910000	-3.5609310000	-1.5619070000
C24	5.8322420000	-4.6678200000	-0.8193090000
S25	4.5332890000	-5.1162220000	0.2557070000
C26	7.0505310000	-5.4828740000	-0.9864890000
C27	8.3613550000	-4.9679990000	-0.8252060000
C28	8.6854000000	-3.7443600000	-0.0777100000
C29	7.8099730000	-3.1584120000	0.8497350000
C30	9.4407050000	-5.6874940000	-1.4300680000
C31	10.7466980000	-5.1082920000	-1.5366350000
C32	10.9781740000	-3.7857380000	-1.0463150000
C33	9.9738350000	-3.1521560000	-0.2489830000
C34	6.8585260000	-6.7764980000	-1.5036850000
C35	7.9153280000	-7.5285790000	-1.9810090000
C36	9.2099240000	-6.9700720000	-2.0001270000
C37	10.2785330000	-7.6480120000	-2.6494870000

C38	11.5271900000	-7.0898930000	-2.7170560000
C39	11.8132890000	-5.8230730000	-2.1367930000
C40	10.2822340000	-1.9298160000	0.4112550000
C41	9.3528780000	-1.3546460000	1.3036870000
C42	8.1401150000	-1.9900530000	1.5340870000
C43	12.2038460000	-3.1297350000	-1.3256070000
C44	12.4693550000	-1.8985260000	-0.6599580000
C45	11.5574790000	-1.3287680000	0.1935760000
C46	-2.8644840000	-4.9345600000	0.3682200000
N47	-2.0810500000	-6.0878920000	0.3686870000
C48	-0.6901590000	-6.1834970000	0.3634340000
C49	4.1258350000	2.6804460000	0.9774700000
N50	3.3145640000	3.8030160000	0.8084660000
C51	1.9472980000	3.8474740000	0.5495670000
C52	11.9262280000	-0.0789190000	0.9145070000
N53	10.9406340000	0.4274880000	1.7596430000
C54	9.6778160000	-0.1003670000	2.0301970000
C55	7.6563470000	-8.8681040000	-2.5718210000
N56	8.7568880000	-9.4648510000	-3.1850610000
C57	10.0490800000	-8.9584740000	-3.3123230000
O58	-4.0824720000	-5.0056300000	0.3331550000
O59	-0.1355220000	-7.2700780000	0.3545370000
O60	1.3611040000	4.9131840000	0.4519090000
O61	5.3183220000	2.7999720000	1.2030950000
O62	8.9244390000	0.4464270000	2.8190670000
O63	13.0016380000	0.4850780000	0.7960850000
O64	6.5699070000	-9.4225660000	-2.5558300000
O65	10.9062350000	-9.5743840000	-3.9238030000
C66	-2.1967820000	1.1780850000	-0.0718630000
C67	-2.8702060000	0.0285720000	0.3945230000
C68	13.1080970000	-5.1916320000	-2.3010690000
C69	13.2019520000	-3.7911060000	-2.1466610000
C70	14.3037080000	-5.9319140000	-2.6507120000
C71	15.4197340000	-5.2490540000	-3.1927850000
C72	15.3694810000	-3.8293360000	-3.3578280000
C73	14.2747220000	-3.0947860000	-2.8293230000
C74	-2.9791570000	2.2486910000	-0.6524370000
C75	-4.3798690000	2.2961990000	-0.4425780000
C76	-5.0121750000	1.2834960000	0.3438990000
C77	-4.2654780000	0.1547040000	0.7679930000
C78	-5.1645190000	3.3582140000	-0.9975740000
C79	-6.5582540000	3.4753960000	-0.7085230000
C80	-7.1851360000	2.4929260000	0.1795230000
C81	-6.3980160000	1.4119800000	0.6825360000

C82	16.5889140000	-5.9721550000	-3.5942610000
C83	17.6752450000	-5.3158650000	-4.2464420000
C84	17.5813470000	-3.8788370000	-4.5070160000
C85	16.4331310000	-3.1629140000	-4.0473270000
C86	16.3385500000	-1.7628780000	-4.2824730000
C87	15.1803050000	-1.0594550000	-3.8333030000
C88	14.1951970000	-1.7031810000	-3.1272700000
C89	18.5817930000	-3.1698670000	-5.1879630000
C90	18.4765650000	-1.8014660000	-5.4249760000
C91	17.3655270000	-1.0949370000	-4.9824340000
C92	14.4470880000	-7.3177020000	-2.3525660000
C93	15.5818240000	-8.0135560000	-2.6777140000
C94	16.6659780000	-7.3707550000	-3.3436080000
C95	17.8131220000	-8.0985170000	-3.7205700000
C96	18.8613610000	-7.4494560000	-4.3602860000
C97	18.7885760000	-6.0829460000	-4.6202970000
C98	-6.9985390000	0.4430630000	1.5351880000
C99	-6.1964480000	-0.6192540000	2.0479350000
C100	-4.8861920000	-0.7551020000	1.6707610000
C101	-2.4029730000	3.1852390000	-1.5564740000
C102	-3.1507010000	4.1720510000	-2.1447890000
C103	-4.5403280000	4.3114610000	-1.8514540000
C104	-8.5364780000	2.5608960000	0.5521190000
C105	-9.1147180000	1.6112310000	1.3929660000
C106	-8.3589780000	0.5567440000	1.8902340000
C107	-5.2981970000	5.3589140000	-2.4175100000
C108	-6.6531430000	5.4638120000	-2.1260420000
C109	-7.2701070000	4.5381860000	-1.2856380000
C110	17.2628520000	0.3569300000	-5.2646620000
N111	16.0871510000	0.9660550000	-4.8231760000
C112	15.0140000000	0.3865020000	-4.1490470000
C113	15.6666070000	-9.4540700000	-2.3172500000
N114	16.8269490000	-10.0976580000	-2.7455840000
C115	17.9160150000	-9.5486080000	-3.4233620000
C116	-8.9842300000	-0.4336840000	2.8037490000
N117	-8.1226630000	-1.4179390000	3.2896800000
C118	-6.7672520000	-1.5926020000	3.0153440000
C119	-2.4926510000	5.0889970000	-3.1105320000
N120	-3.3127770000	6.0989910000	-3.6092160000
C121	-4.6605180000	6.3372350000	-3.3358250000
O122	-1.3268060000	4.9953590000	-3.4601530000
O123	-5.2455950000	7.2801230000	-3.8452720000
O124	-10.1588220000	-0.4111010000	3.1362480000
O125	-6.1304200000	-2.4910700000	3.5417500000

O126	14.8016580000	-10.0581460000	-1.7036240000
O127	18.8738210000	-10.2403970000	-3.7298430000
O128	14.0295420000	1.0441980000	-3.8521020000
O129	18.1184910000	1.0024110000	-5.8487010000
H130	-0.5788370000	3.4114550000	0.0915870000
H131	5.1664730000	0.2633810000	1.4022120000
H132	-3.8739060000	-2.5450840000	0.3792060000
H133	1.8966910000	-5.8260670000	0.0413930000
H134	5.8565220000	-7.1845620000	-1.5867080000
H135	12.2659550000	-7.6265110000	-3.2935280000
H136	7.4600050000	-1.5572430000	2.2602170000
H137	13.4316290000	-1.4121270000	-0.7500100000
H138	-2.5866750000	-6.9671340000	0.3571920000
H139	3.7793750000	4.7003450000	0.8938090000
H140	11.1757110000	1.2842870000	2.2488280000
H141	8.5896940000	-10.3685570000	-3.6142350000
H142	13.3213950000	-1.1233310000	-2.8594430000
H143	19.4624270000	-3.6847550000	-5.5492600000
H144	19.2527090000	-1.2637000000	-5.9589430000
H145	13.6841780000	-7.8567450000	-1.8090580000
H146	19.7329110000	-8.0286460000	-4.6462240000
H147	19.6265590000	-5.6150090000	-5.1209690000
H148	-4.3249990000	-1.5523790000	2.1372640000
H149	-1.3656290000	3.1095220000	-1.8533500000
H150	-9.1607220000	3.3673140000	0.1876340000
H151	-10.1594410000	1.6773200000	1.6775880000
H152	-7.2163480000	6.2774540000	-2.5703920000
H153	-8.3282520000	4.6544610000	-1.0861140000
H154	15.9979730000	1.9550230000	-5.0294470000
H155	16.8930520000	-11.0858010000	-2.5267310000
H156	-8.5342120000	-2.0884200000	3.9298450000
H157	-2.8736220000	6.7472440000	-4.2537440000
H158	4.0642540000	-1.9296370000	1.1659170000
H159	3.7365560000	-2.2325680000	-1.7930170000
H160	6.1450380000	-3.1352730000	-2.3106880000
H161	6.8617820000	-3.6288540000	1.0610950000

Restricted Singlet Excited State   1:   1.8648 eV   664.85 nm

excitation   X coeff.
------------ ---------
 426 => 429   -0.12761
 428 => 429   -0.97693
 428 => 431   -0.10112

Transition dipole moment (debye):
   X=   4.8285   Y=   -2.0985   Z=   -0.0097 Tot=   5.2648

Oscillator strength, f=   0.1960

Restricted Singlet Excited State   2:   1.9701 eV   629.34 nm

 excitation   X coeff.
------------   ---------
 426 => 430   0.10374
 428 => 430   0.98143

Transition dipole moment (debye):
   X=   0.4211   Y=   4.2560   Z=   0.1443 Tot=   4.2792

Oscillator strength, f=   0.1368

Restricted Singlet Excited State   3:   2.1433 eV   578.48 nm

 excitation   X coeff.
------------   ---------
 426 => 430   0.18500
 427 => 429   0.95571

Transition dipole moment (debye):
   X=   -1.0018   Y=   -5.2547   Z=   0.0746 Tot=   5.3499

Oscillator strength, f=   0.2326

Restricted Singlet Excited State   4:   2.2043 eV   562.46 nm

 excitation   X coeff.
------------   ---------
 426 => 429   0.47872
 426 => 430   0.15196
 426 => 431   0.10441
 427 => 430   0.82637
 427 => 432   -0.10126
 428 => 431   0.12233

Transition dipole moment (debye):
   X= -4.2978   Y=   1.1816   Z=   1.8127 Tot=   4.8118

Oscillator strength, f=   0.1935

Restricted Singlet Excited State   5:   2.2641 eV   547.60 nm

 excitation   X coeff.
 ------------   ---------
 425 => 430   0.24167
 426 => 429   0.58974
 426 => 430   0.19703
 427 => 430   -0.31303
 427 => 432   -0.15477
 428 => 431   -0.60123
 428 => 432   0.23241

Transition dipole moment (debye):
   X= -0.0409   Y= -0.5844   Z=   0.0922 Tot=   0.5931

Oscillator strength, f=   0.0030

Restricted Singlet Excited State   6:   2.3000 eV   539.07 nm

 excitation   X coeff.
 ------------   ---------
 424 => 429   0.15219
 426 => 429   -0.50276
 426 => 431   -0.11734
 427 => 430   0.42650
 428 => 429   0.17357
 428 => 431   -0.66579
 428 => 432   0.13672

Transition dipole moment (debye):
   X=   4.1157   Y= -1.4666   Z= -0.7388 Tot=   4.4312

Oscillator strength, f=   0.1713

Restricted Singlet Excited State   7:   2.3163 eV   535.27 nm

excitation   X coeff.
------------ ---------
 425 => 429   0.43050
 426 => 429   -0.13718
 426 => 430   0.39718
 427 => 431   0.26454
 428 => 431   0.22737
 428 => 432   0.70116

Transition dipole moment (debye):
  X=   0.0532   Y=   -1.4181   Z=   -0.2832 Tot=   1.4471

Oscillator strength, f=   0.0184

Restricted Singlet Excited State   8:   2.3785 eV   521.27 nm

 excitation   X coeff.
------------ ---------
 424 => 430   0.10050
 426 => 429   0.14570
 426 => 430   -0.77266
 426 => 432   0.15202
 427 => 429   0.24205
 428 => 430   0.10767
 428 => 432   0.49537

Transition dipole moment (debye):
  X=   0.6152   Y=   -0.4384   Z=   -1.8337 Tot=   1.9832

Oscillator strength, f=   0.0355

Restricted Singlet Excited State   9:   2.4493 eV   506.21 nm

 excitation   X coeff.
------------ ---------
 423 => 429   0.25644
 423 => 430   -0.42370
 424 => 429   0.70563
 424 => 430   0.14506
 425 => 430   0.27559
 427 => 431   -0.11017
 427 => 432   -0.12330

```
427 => 433    0.10286
427 => 434   -0.12294
428 => 431    0.20557
428 => 433    0.13341
```

Transition dipole moment (debye):
   X=   6.5368   Y= -1.8065   Z= -1.1937 Tot=   6.8861

Oscillator strength, f=   0.4404

Restricted Singlet Excited State 10:   2.4730 eV   501.35 nm

```
 excitation    X coeff.
------------   ---------
 423 => 429   -0.49589
 424 => 429    0.15673
 424 => 430    0.51909
 425 => 429    0.46956
 426 => 430   -0.10186
 427 => 431    0.18278
 427 => 433   -0.14752
 428 => 432   -0.29597
 428 => 434    0.18331
```

Transition dipole moment (debye):
   X=   1.3881   Y=   0.1077   Z=   2.1867 Tot=   2.5923

Oscillator strength, f=   0.0630

Conformation **2c**

B3LYP/6-31G** optimized geometry
Final total energy = -6022.847355

| | angstroms | | |
atom	x	y	z
C1	-0.8079900000	-0.5785760000	-1.2504520000
C2	0.5487910000	-0.1398320000	-1.1648670000
C3	0.8927710000	1.1492020000	-1.6622180000
C4	-0.1045850000	1.9249520000	-2.3289800000
C5	-1.3836780000	1.4469080000	-2.4803230000
C6	-1.7739920000	0.1791740000	-1.9576600000
C7	1.5453690000	-0.9426180000	-0.5298030000
C8	2.7748770000	-0.3346120000	-0.2214430000
C9	3.0956400000	0.9439390000	-0.6743770000
C10	2.1859630000	1.6694690000	-1.4357980000
C11	-1.1962730000	-1.7591660000	-0.5468180000
C12	-0.1831710000	-2.6322870000	-0.0216190000
C13	1.2127300000	-2.3201200000	-0.1504240000
C14	-2.5787180000	-2.0538300000	-0.3894730000
C15	-2.9305800000	-3.2894830000	0.2265840000
C16	-1.9760390000	-4.1548640000	0.7030440000
C17	-0.5897350000	-3.8439610000	0.5980710000
C18	0.3932820000	-4.7411020000	1.0618830000
C19	1.7272670000	-4.5010320000	0.7957610000
C20	2.1744690000	-3.3408580000	0.1247540000
C21	3.5436360000	-3.3845240000	-0.4255520000
C22	4.1264970000	-2.6711450000	-1.4545020000
C23	5.4380320000	-3.0862280000	-1.7890360000
C24	5.8909660000	-4.1385800000	-1.0298490000
S25	4.6862100000	-4.6043030000	0.1448410000
C26	7.1044470000	-4.9569430000	-1.2586720000
C27	8.4435170000	-4.4970880000	-1.1394990000
C28	8.8439560000	-3.2848560000	-0.4079770000
C29	7.9796610000	-2.5983370000	0.4608840000
C30	9.4841920000	-5.3003140000	-1.7167270000
C31	10.8404230000	-4.8341460000	-1.7755780000
C32	11.1771080000	-3.5437520000	-1.2579250000
C33	10.1936720000	-2.8165600000	-0.5148160000
C34	6.8433440000	-6.2384470000	-1.7789140000
C35	7.8489550000	-7.0438720000	-2.2775040000
C36	9.1753680000	-6.5676630000	-2.2903000000
C37	10.2018680000	-7.3242060000	-2.9240140000

C38	11.4940200000	-6.8710920000	-2.9449880000
C39	11.8655680000	-5.6437640000	-2.3289340000
C40	10.5848250000	-1.6296960000	0.1724440000
C41	9.6638620000	-0.9522150000	1.0013140000
C42	8.3791740000	-1.4560250000	1.1526570000
C43	12.4829490000	-3.0156360000	-1.4500220000
C44	12.8331040000	-1.8295550000	-0.7417170000
C45	11.9309640000	-1.1683240000	0.0543310000
C46	-2.4092320000	-5.4457240000	1.3027410000
N47	-1.3726920000	-6.2453080000	1.7859220000
C48	0.0020130000	-6.0085350000	1.7298460000
C49	2.5622280000	3.0024540000	-1.9625240000
N50	1.5377640000	3.6907570000	-2.6187690000
C51	0.2180350000	3.2874780000	-2.8291270000
C52	12.3862860000	0.0261290000	0.8201750000
N53	11.4013630000	0.6440580000	1.5893690000
C54	10.0694170000	0.2631910000	1.7542820000
C55	7.5012760000	-8.3575090000	-2.8830020000
N56	8.5606070000	-9.0221020000	-3.4994340000
C57	9.8861870000	-8.6056540000	-3.6121230000
O58	-3.5727900000	-5.8093190000	1.3888910000
O59	0.7961700000	-6.8110050000	2.1867830000
O60	-0.5813690000	4.0218890000	-3.3903580000
O61	3.6739690000	3.4966930000	-1.8445140000
O62	9.3204610000	0.8981720000	2.4807660000
O63	13.5273030000	0.4599740000	0.7970420000
O64	6.3792500000	-8.8376340000	-2.8724260000
O65	10.7031300000	-9.2718030000	-4.2276920000
C66	-3.1576890000	-0.2553640000	-1.9705100000
C67	-3.5781690000	-1.1757900000	-0.9833360000
C68	13.2278510000	-5.1515590000	-2.3980600000
C69	13.4657260000	-3.7712500000	-2.2097780000
C70	14.3533790000	-6.0216570000	-2.6751290000
C71	15.5736370000	-5.4678210000	-3.1339010000
C72	15.7030490000	-4.0474510000	-3.2619900000
C73	14.6696090000	-3.1950420000	-2.7837010000
C74	-4.1295090000	0.2421060000	-2.9215890000
C75	-5.5139860000	0.1019770000	-2.6528080000
C76	-5.9380690000	-0.5405730000	-1.4481650000
C77	-4.9832320000	-1.1851580000	-0.6166450000
C78	-6.4878320000	0.6244480000	-3.5634750000
C79	-7.8811030000	0.5977890000	-3.2503050000
C80	-8.3092600000	0.0294750000	-1.9704460000
C81	-7.3279910000	-0.5355350000	-1.0991750000

C82	16.6663140000	-6.3228190000	-3.4941110000
C83	17.8582650000	-5.7916730000	-4.0727950000
C84	17.9616130000	-4.3450730000	-4.2825570000
C85	16.8856950000	-3.5016450000	-3.8610660000
C86	16.9861170000	-2.0930820000	-4.0496610000
C87	15.8976930000	-1.2603920000	-3.6468430000
C88	14.7904970000	-1.7952980000	-3.0352310000
C89	19.0851890000	-3.7494370000	-4.8772230000
C90	19.1724970000	-2.3706890000	-5.0661270000
C91	18.1336800000	-1.5402940000	-4.6598430000
C92	14.3142740000	-7.4192960000	-2.3922450000
C93	15.3694540000	-8.2459190000	-2.6813950000
C94	16.5538760000	-7.7280860000	-3.2862840000
C95	17.6133180000	-8.5879350000	-3.6462530000
C96	18.7641850000	-8.0595010000	-4.2198020000
C97	18.8803700000	-6.6858140000	-4.4286260000
C98	-7.7377320000	-1.0983040000	0.1424720000
C99	-6.7479410000	-1.6402240000	1.0149460000
C100	-5.4288550000	-1.6852690000	0.6411490000
C101	-3.7375260000	0.7468430000	-4.1942710000
C102	-4.6608110000	1.1845190000	-5.1095230000
C103	-6.0554560000	1.1792020000	-4.8015100000
C104	-9.6530130000	0.0081810000	-1.5649450000
C105	-10.0428190000	-0.5340810000	-0.3425060000
C106	-9.0989800000	-1.0834590000	0.5150990000
C107	-7.0017730000	1.6843520000	-5.7187150000
C108	-8.3540550000	1.6622530000	-5.3973570000
C109	-8.7837400000	1.1328680000	-4.1820820000
C110	18.2335800000	-0.0772700000	-4.8910180000
N111	17.1181980000	0.6646150000	-4.4963860000
C112	15.9381240000	0.2067200000	-3.9115980000
C113	15.2587610000	-9.6945210000	-2.3584340000
N114	16.3406370000	-10.4706540000	-2.7732100000
C115	17.5155920000	-10.0497980000	-3.3992010000
C116	-9.5286090000	-1.6340130000	1.8252490000
N117	-8.4961000000	-2.1142370000	2.6321570000
C118	-7.1293220000	-2.1466660000	2.3599150000
C119	-4.1908070000	1.6440750000	-6.4427930000
N120	-5.1938930000	2.1282350000	-7.2822140000
C121	-6.5639740000	2.2228590000	-7.0327870000
O122	-3.0259190000	1.6157890000	-6.8072910000
O123	-7.3213410000	2.6922350000	-7.8680160000
O124	-10.6884940000	-1.6689090000	2.2053680000
O125	-6.3346980000	-2.5714910000	3.1825770000

```
O126      14.3035700000   -10.1986370000    -1.7882340000
O127      18.3869210000   -10.8517750000    -3.6991510000
O128      15.0285630000     0.9779140000    -3.6462880000
O129      19.2004800000     0.4702710000    -5.3986420000
H130      -2.1060260000     2.1112110000    -2.9398870000
H131       4.0613880000     1.3896010000    -0.4529870000
H132      -3.9587940000    -3.6226120000     0.2761840000
H133       2.4240750000    -5.2830860000     1.0749320000
H134       5.8217670000    -6.5990710000    -1.8376380000
H135      12.2051520000    -7.4569170000    -3.5095610000
H136       7.6973440000    -0.9448070000     1.8245090000
H137      13.8476370000    -1.4533750000    -0.7506090000
H138      -1.6554920000    -7.1198280000     2.2167480000
H139       1.7805350000     4.6061040000    -2.9806150000
H140      11.6962280000     1.4641660000     2.1093890000
H141       8.3327690000    -9.9060430000    -3.9430320000
H142      13.9812490000    -1.1131970000    -2.8071620000
H143      19.9140390000    -4.3636950000    -5.2064380000
H144      20.0423910000    -1.9209060000    -5.5334330000
H145      13.4657280000    -7.8659740000    -1.8919360000
H146      19.5655800000    -8.7378250000    -4.4947200000
H147      19.7936580000    -6.3151490000    -4.8773320000
H148      -4.7286770000    -2.0587580000     1.3750100000
H149      -2.6994420000     0.7425390000    -4.4998850000
H150     -10.4197690000     0.4265410000    -2.2044230000
H151     -11.0837400000    -0.5353410000    -0.0365900000
H152      -9.0631160000     2.0598620000    -6.1153450000
H153      -9.8460310000     1.1340360000    -3.9705610000
H154      17.1677710000     1.6640650000    -4.6687670000
H155      16.2743920000   -11.4654050000    -2.5813180000
H156      -8.7744600000    -2.4702410000     3.5397500000
H157      -4.8876040000     2.4639640000    -8.1888660000
H158       3.5057880000    -0.8786210000     0.3603340000
H159       3.6087970000    -1.9024050000    -2.0077300000
H160       6.0133040000    -2.6562950000    -2.5999240000
H161       6.9767370000    -2.9631510000     0.6185730000
```

Restricted Singlet Excited State   1:   1.8333 eV   676.29 nm

```
   excitation    X coeff.
  ------------  ---------
   426 =>  429    0.11477
   428 =>  429    0.97992
```

Transition dipole moment (debye):
   X=   -6.5565   Y=   2.5808   Z=   -1.4820 Tot=   7.2004

Oscillator strength, f=   0.3604

Restricted Singlet Excited State   2:   1.9245 eV   644.26 nm

 excitation   X coeff.
 ------------   ---------
 428 => 430   -0.98026

Transition dipole moment (debye):
   X=   0.3097   Y=   -3.6590   Z=   1.0983 Tot=   3.8328

Oscillator strength, f=   0.1072

Restricted Singlet Excited State   3:   2.1261 eV   583.15 nm

 excitation   X coeff.
 ------------   ---------
 426 => 430   -0.22785
 427 => 429   0.93740
 427 => 430   -0.14613

Transition dipole moment (debye):
   X=   1.9102   Y=   4.6858   Z=   -0.7593 Tot=   5.1169

Oscillator strength, f=   0.2111

Restricted Singlet Excited State   4:   2.1742 eV   570.25 nm

 excitation   X coeff.
 ------------   ---------
 426 => 429   0.62206
 426 => 430   0.15586
 426 => 431   -0.11432
 427 => 430   -0.72604
 427 => 432   -0.10627

Transition dipole moment (debye):
   X=   -2.9610   Y=   2.0495   Z=   2.3599 Tot=   4.3055

Oscillator strength, f=   0.1528

Restricted Singlet Excited State   5:   2.2269 eV   556.76 nm

 excitation   X coeff.
 ------------   ---------
 425 => 429   -0.13168
 425 => 430   -0.14859
 426 => 429   -0.44239
 426 => 430   -0.24703
 427 => 429   -0.17417
 427 => 430   -0.51327
 428 => 431   -0.57926
 428 => 432   0.23936

Transition dipole moment (debye):
   X=   -0.9442   Y=   1.7589   Z=   0.2670 Tot=   2.0141

Oscillator strength, f=   0.0343

Restricted Singlet Excited State   6:   2.2655 eV   547.26 nm

 excitation   X coeff.
 ------------   ---------
 424 => 429   -0.15699
 426 => 429   0.48405
 426 => 431   -0.10610
 427 => 429   0.13829
 427 => 430   0.38269
 428 => 429   -0.11885
 428 => 431   -0.67655
 428 => 432   0.22754

Transition dipole moment (debye):
   X=   -4.5066   Y=   1.5878   Z=   0.7293 Tot=   4.8335

Oscillator strength, f=   0.2007

Restricted Singlet Excited State   7:   2.3109 eV   536.51 nm

excitation   X coeff.
------------ ---------
 425 => 429   0.34068
 425 => 430   -0.19595
 426 => 429   -0.13135
 426 => 430   0.28564
 427 => 431   0.19713
 427 => 432   0.20844
 428 => 431   -0.33461
 428 => 432   -0.73035

Transition dipole moment (debye):
   X=   -0.5266   Y=   -0.2432   Z=   -0.0179 Tot=   0.5804

Oscillator strength, f=   0.0030

Restricted Singlet Excited State   8:   2.3485 eV   527.94 nm

 excitation   X coeff.
------------ ---------
 426 => 429   0.23697
 426 => 430   -0.80222
 426 => 432   -0.13826
 427 => 429   -0.22006
 428 => 430   0.11372
 428 => 432   -0.41790

Transition dipole moment (debye):
   X=   -0.1786   Y=   -0.3361   Z=   -1.2773 Tot=   1.3328

Oscillator strength, f=   0.0158

Restricted Singlet Excited State   9:   2.4298 eV   510.27 nm

 excitation   X coeff.
------------ ---------
 423 => 430   -0.24310
 424 => 429   -0.74405
 424 => 430   -0.38744
 425 => 429   -0.19177
 425 => 430   -0.24960
 427 => 434   0.10485

```
428 => 431    0.16360
428 => 433    0.15549
428 => 434    0.15127
```

Transition dipole moment (debye):
   X= -5.8317   Y= -0.0945   Z= -0.6450 Tot= 5.8680

Oscillator strength, f=   0.3173

Restricted Singlet Excited State 10:   2.4584 eV   504.33 nm

```
 excitation    X coeff.
------------  ---------
 423 => 429   -0.37548
 423 => 430    0.28650
 424 => 430   -0.25825
 425 => 429   -0.53192
 425 => 430    0.27173
 426 => 430    0.21623
 427 => 431   -0.22304
 427 => 432   -0.26660
 427 => 433    0.12985
 428 => 431   -0.14563
 428 => 432   -0.30550
```

Transition dipole moment (debye):
   X=   1.4578   Y= -2.1956   Z= -1.8230 Tot=   3.2046

Oscillator strength, f=   0.0957

Conformation **2d**

B3LYP/6-31G** optimized geometry
Final total energy = -6022.841301

angstroms

atom	x	y	z
C1	-1.2194300000	-2.0415230000	-2.2164480000
C2	0.0037510000	-1.3378610000	-2.4203570000
C3	0.0795350000	-0.3598550000	-3.4479090000
C4	-1.0262050000	-0.2019520000	-4.3342340000
C5	-2.1602180000	-0.9621550000	-4.1854370000
C6	-2.2963400000	-1.9041100000	-3.1251080000
C7	1.1186740000	-1.5391140000	-1.5506860000
C8	2.1504650000	-0.5895270000	-1.5849800000
C9	2.2029500000	0.4010600000	-2.5671130000
C10	1.2080210000	0.4843180000	-3.5328440000
C11	-1.3716850000	-2.8171080000	-1.0273530000
C12	-0.2160810000	-3.1286450000	-0.2339290000
C13	1.0869240000	-2.6435110000	-0.5925460000
C14	-2.6639250000	-3.2766800000	-0.6584470000
C15	-2.7701180000	-4.1309640000	0.4745860000
C16	-1.6715710000	-4.4680490000	1.2265720000
C17	-0.3803560000	-3.9758070000	0.8921450000
C18	0.7564000000	-4.3431190000	1.6414610000
C19	2.0149600000	-4.0090050000	1.1880150000
C20	2.2366590000	-3.2494280000	0.0115950000
C21	3.5892190000	-3.3667580000	-0.5821020000
C22	4.2354850000	-2.7450370000	-1.6336950000
C23	5.5044470000	-3.2814890000	-1.9555980000
C24	5.8732530000	-4.3429560000	-1.1681980000
S25	4.6233070000	-4.6937240000	-0.0025060000
C26	7.0792430000	-5.1837830000	-1.3517150000
C27	8.4075570000	-4.7024940000	-1.1992000000
C28	8.7641680000	-3.4722910000	-0.4780790000
C29	7.8690840000	-2.7964910000	0.3667650000
C30	9.4735600000	-5.4756900000	-1.7658260000
C31	10.8181360000	-4.9751980000	-1.8081900000
C32	11.1100500000	-3.6697300000	-1.3039720000
C33	10.0964360000	-2.9611930000	-0.5851000000
C34	6.8504550000	-6.4680120000	-1.8722280000
C35	7.8851400000	-7.2538950000	-2.3459020000
C36	9.2017820000	-6.7505440000	-2.3374400000
C37	10.2577540000	-7.4834790000	-2.9506910000

C38	11.5389570000	-6.9996780000	-2.9539000000
C39	11.8720300000	-5.7596850000	-2.3416010000
C40	10.4370160000	-1.7439260000	0.0725090000
C41	9.4839100000	-1.0778750000	0.8719020000
C42	8.2191520000	-1.6234570000	1.0294830000
C43	12.3993840000	-3.1038590000	-1.4927020000
C44	12.6997530000	-1.8899720000	-0.8098340000
C45	11.7657190000	-1.2385430000	-0.0446870000
C46	-1.8416510000	-5.3857870000	2.3850130000
N47	-0.6758350000	-5.6413520000	3.1098880000
C48	0.6198420000	-5.1967210000	2.8502000000
C49	1.3077980000	1.4952710000	-4.6127170000
N50	0.1981220000	1.5712330000	-5.4557750000
C51	-0.9854260000	0.8350340000	-5.3984260000
C52	12.1683910000	-0.0079380000	0.6915090000
N53	11.1512750000	0.5989060000	1.4254340000
C54	9.8326070000	0.1744350000	1.5866540000
C55	7.5798700000	-8.5764570000	-2.9516050000
N56	8.6656160000	-9.2195500000	-3.5436920000
C57	9.9831170000	-8.7745180000	-3.6359690000
O58	-2.9036430000	-5.8896300000	2.7132950000
O59	1.5513330000	-5.5197280000	3.5707130000
O60	-1.8944780000	1.0520840000	-6.1819010000
O61	2.2729710000	2.2237600000	-4.7782430000
O62	9.0517830000	0.8056950000	2.2811590000
O63	13.2934540000	0.4631080000	0.6720200000
O64	6.4688650000	-9.0801420000	-2.9645560000
O65	10.8239250000	-9.4244100000	-4.2357030000
C66	-3.5589940000	-2.5596920000	-2.8396460000
C67	-3.8047380000	-2.9861710000	-1.5139700000
C68	13.2211160000	-5.2292750000	-2.3984600000
C69	13.4149690000	-3.8408830000	-2.2251560000
C70	14.3785600000	-6.0657170000	-2.6440580000
C71	15.5926560000	-5.4801060000	-3.0794250000
C72	15.6825060000	-4.0601530000	-3.2247090000
C73	14.6117480000	-3.2361190000	-2.7850630000
C74	-4.5899640000	-2.7585670000	-3.8367290000
C75	-5.9196750000	-3.0333020000	-3.4296330000
C76	-6.2314980000	-3.1160660000	-2.0362230000
C77	-5.1842010000	-3.0995010000	-1.0777470000
C78	-6.9571250000	-3.2025780000	-4.4016950000
C79	-8.3206510000	-3.3590740000	-4.0067430000
C80	-8.6547900000	-3.3386850000	-2.5808720000
C81	-7.5996070000	-3.2268720000	-1.6240150000

C82	16.7212230000	-6.3027740000	-3.3980190000
C83	17.9108330000	-5.7423670000	-3.9521120000
C84	17.9755010000	-4.2984270000	-4.1792820000
C85	16.8628280000	-3.4855760000	-3.8005970000
C86	16.9253890000	-2.0792220000	-4.0067650000
C87	15.8012810000	-1.2777770000	-3.6465130000
C88	14.6965500000	-1.8389960000	-3.0565800000
C89	19.0968460000	-3.6765340000	-4.7489860000
C90	19.1469460000	-2.3002020000	-4.9553660000
C91	18.0715370000	-1.4990310000	-4.5917290000
C92	14.3770510000	-7.4589300000	-2.3446090000
C93	15.4668540000	-8.2526470000	-2.5905480000
C94	16.6491750000	-7.7058130000	-3.1714440000
C95	17.7450410000	-8.5333220000	-3.4915610000
C96	18.8918370000	-7.9776490000	-4.0437460000
C97	18.9695520000	-6.6059120000	-4.2690370000
C98	-7.9132930000	-3.2169610000	-0.2352530000
C99	-6.8531710000	-3.0870070000	0.7108020000
C100	-5.5457340000	-3.0392080000	0.2999340000
C101	-4.2829570000	-2.8271950000	-5.2267000000
C102	-5.2521730000	-3.0671860000	-6.1672230000
C103	-6.6204260000	-3.2134000000	-5.7850540000
C104	-9.9746940000	-3.4334090000	-2.1122920000
C105	-10.2739710000	-3.4089370000	-0.7509120000
C106	-9.2566630000	-3.2985610000	0.1903830000
C107	-7.6279980000	-3.3968120000	-6.7554090000
C108	-8.9525650000	-3.5379420000	-6.3598900000
C109	-9.2908480000	-3.5143210000	-5.0086240000
C110	18.1324120000	-0.0383580000	-4.8396140000
N111	16.9842080000	0.6719980000	-4.4864850000
C112	15.8031040000	0.1847820000	-3.9300820000
C113	15.3997630000	-9.6963450000	-2.2421900000
N114	16.5157960000	-10.4405380000	-2.6203810000
C115	17.6872260000	-9.9924260000	-3.2324540000
C116	-9.5930290000	-3.2462180000	1.6364920000
N117	-8.5032450000	-3.0860040000	2.4931700000
C118	-7.1530790000	-2.9768490000	2.1637170000
C119	-4.8571210000	-3.1946790000	-7.5949790000
N120	-5.9175160000	-3.3731070000	-8.4818470000
C121	-7.2821230000	-3.4538690000	-8.1969170000
O122	-3.7043640000	-3.1517830000	-7.9946740000
O123	-8.1016910000	-3.5895850000	-9.0940130000
O124	-10.7291740000	-3.3213530000	2.0776350000
O125	-6.3077960000	-2.8081840000	3.0280910000

O126	14.4531890000	-10.2234070000	-1.6803780000
O127	18.5858310000	-10.7708010000	-3.5078430000
O128	14.8631470000	0.9289080000	-3.7017030000
O129	19.0952710000	0.5325430000	-5.3267300000
H130	-2.9827940000	-0.7492880000	-4.8544140000
H131	3.0218420000	1.1119440000	-2.6021860000
H132	-3.7064230000	-4.5984280000	0.7432820000
H133	2.8518960000	-4.3959560000	1.7592210000
H134	5.8363120000	-6.8418140000	-1.9648680000
H135	12.2747620000	-7.5742540000	-3.4977810000
H136	7.5135630000	-1.1194910000	1.6810040000
H137	13.7001510000	-1.4800540000	-0.8135590000
H138	-0.7818970000	-6.2530520000	3.9123750000
H139	0.2488510000	2.2626810000	-6.1959390000
H140	11.4092890000	1.4444620000	1.9225160000
H141	8.4651270000	-10.1084950000	-3.9889300000
H142	13.8632900000	-1.1791170000	-2.8598180000
H143	19.9540870000	-4.2678490000	-5.0435400000
H144	20.0158980000	-1.8301530000	-5.4029550000
H145	13.5295400000	-7.9262810000	-1.8629290000
H146	19.7198900000	-8.6336910000	-4.2893200000
H147	19.8809360000	-6.2118740000	-4.6999560000
H148	-4.8012380000	-2.8850360000	1.0682500000
H149	-3.2614780000	-2.7575070000	-5.5761460000
H150	-10.7952870000	-3.5206530000	-2.8136760000
H151	-11.2987990000	-3.4703600000	-0.4009970000
H152	-9.7102700000	-3.6698220000	-7.1247210000
H153	-10.3335950000	-3.6278590000	-4.7418120000
H154	17.0079830000	1.6690830000	-4.6708710000
H155	16.4768310000	-11.4329170000	-2.4145830000
H156	-8.7233160000	-3.0253810000	3.4816310000
H157	-5.6675760000	-3.4444930000	-9.4621420000
H158	2.9255110000	-0.6249090000	-0.8307520000
H159	3.8118610000	-1.9386200000	-2.2069290000
H160	6.1211860000	-2.9076920000	-2.7635850000
H161	6.8812650000	-3.1930000000	0.5315480000

Restricted Singlet Excited State   1:   1.9198 eV   645.82 nm

  excitation   X coeff.
  ------------ ---------
  426 => 429   -0.13352
  428 => 429   -0.96057
  428 => 430   0.17292

Transition dipole moment (debye):
    X=   6.6547   Y=   -0.3174   Z=   2.6580 Tot=   7.1729

Oscillator strength, f=   0.3746

Restricted Singlet Excited State   2:   1.9787 eV   626.60 nm

 excitation   X coeff.
 -----------   ---------
 426 => 430   -0.11032
 428 => 429   -0.18333
 428 => 430   -0.96445

Transition dipole moment (debye):
    X=   1.5453   Y=   -2.9132   Z=   2.1902 Tot=   3.9587

Oscillator strength, f=   0.1176

Restricted Singlet Excited State   3:   2.1444 eV   578.17 nm

 excitation   X coeff.
 -----------   ---------
 426 => 430   -0.25628
 427 => 429   -0.91061
 427 => 430   0.24725

Transition dipole moment (debye):
    X=   0.8858   Y=   4.2885   Z=   -1.2505 Tot=   4.5541

Oscillator strength, f=   0.1687

Restricted Singlet Excited State   4:   2.1759 eV   569.82 nm

 excitation   X coeff.
 -----------   ---------
 426 => 429   -0.45673
 426 => 431   0.10380
 427 => 429   -0.17436
 427 => 430   -0.84142

Transition dipole moment (debye):
   X=   2.1004   Y=   -2.3355   Z=   -2.7472 Tot=   4.1729

Oscillator strength, f=   0.1437

Restricted Singlet Excited State   5:   2.2479 eV   551.57 nm

 excitation   X coeff.
 ------------ ---------
 425 => 429   0.13915
 425 => 430   0.15773
 426 => 429   0.68230
 426 => 430   0.33239
 427 => 429   -0.25438
 427 => 430   -0.38919
 428 => 429   -0.10577
 428 => 431   0.33119
 428 => 432   -0.10905

Transition dipole moment (debye):
   X=   -2.3319   Y=   -0.2545   Z=   0.3138 Tot=   2.3667

Oscillator strength, f=   0.0477

Restricted Singlet Excited State   6:   2.3177 eV   534.95 nm

 excitation   X coeff.
 ------------ ---------
 424 => 429   0.21809
 424 => 430   0.12436
 425 => 429   -0.14584
 426 => 429   0.38024
 426 => 430   -0.22458
 427 => 430   -0.18694
 427 => 431   0.14335
 428 => 429   -0.11029
 428 => 431   -0.73866
 428 => 432   0.25250

Transition dipole moment (debye):
   X=   -5.3845   Y=   1.4968   Z=   0.0926 Tot=   5.5895

Oscillator strength, f=   0.2746

Restricted Singlet Excited State   7:   2.3314 eV   531.79 nm

 excitation   X coeff.
 ------------   ---------
 425 => 429   -0.29739
 425 => 430   0.29490
 426 => 429   0.14261
 426 => 430   -0.52885
 427 => 429   0.13777
 427 => 431   0.12181
 427 => 432   0.29161
 428 => 431   0.43644
 428 => 432   0.43593

Transition dipole moment (debye):
   X=   2.4647   Y=   -0.7843   Z=   -0.3993 Tot=   2.6171

Oscillator strength, f=   0.0606

Restricted Singlet Excited State   8:   2.3677 eV   523.64 nm

 excitation   X coeff.
 ------------   ---------
 424 => 430   0.12542
 425 => 429   -0.15324
 426 => 429   -0.19068
 426 => 430   0.60180
 426 => 432   0.11547
 427 => 429   -0.18032
 428 => 430   -0.13096
 428 => 432   0.66061

Transition dipole moment (debye):
   X=   -0.3306   Y=   0.1586   Z=   0.7837 Tot=   0.8652

Oscillator strength, f=   0.0067

Restricted Singlet Excited State   9:   2.4514 eV   505.77 nm

```
 excitation    X coeff.
------------  ---------
 423 => 430   -0.12275
 424 => 429   -0.73684
 424 => 430   -0.47826
 426 => 429    0.10713
 426 => 430    0.12410
 428 => 431   -0.26435
 428 => 433   -0.19550
```

Transition dipole moment (debye):
   X=   3.9727   Y=   1.7808   Z=   0.1210 Tot=   4.3553

Oscillator strength, f=   0.1763

Restricted Singlet Excited State 10:   2.4781 eV   500.32 nm

```
 excitation    X coeff.
------------  ---------
 423 => 429   -0.52820
 423 => 430    0.55816
 424 => 430   -0.14938
 425 => 429    0.31321
 425 => 430   -0.23902
 427 => 432   -0.15193
 427 => 433    0.12657
 427 => 434   -0.16284
 428 => 431    0.12448
 428 => 432    0.28539
 428 => 434   -0.14333
```

Transition dipole moment (debye):
   X= -3.1500   Y=   1.5742   Z=   2.1295 Tot=   4.1152

Oscillator strength, f=   0.1591

Conformation **2e**

B3LYP/6-31G** optimized geometry
Final total energy = -6022.839484

angstroms

atom	x	y	z
C1	-1.4145010000	-3.8926310000	-2.2966730000
C2	-0.3761320000	-3.1484360000	-2.9309420000
C3	-0.5242140000	-2.7562830000	-4.2865520000
C4	-1.6425450000	-3.2424710000	-5.0231300000
C5	-2.5829690000	-4.0484400000	-4.4244920000
C6	-2.5072710000	-4.3959430000	-3.0437580000
C7	0.7598200000	-2.7029430000	-2.1916300000
C8	1.5530600000	-1.6959040000	-2.7536730000
C9	1.3822280000	-1.2740690000	-4.0727940000
C10	0.3877100000	-1.8396790000	-4.8574040000
C11	-1.3772520000	-4.0431850000	-0.8767760000
C12	-0.1727530000	-3.7276890000	-0.1640250000
C13	0.9829210000	-3.2176520000	-0.8461290000
C14	-2.5292330000	-4.5186890000	-0.1977490000
C15	-2.4241990000	-4.7669630000	1.1987030000
C16	-1.2677770000	-4.5090390000	1.8892170000
C17	-0.1207650000	-3.9905730000	1.2271740000
C18	1.0842340000	-3.7610550000	1.9225330000
C19	2.2319770000	-3.4482720000	1.2205310000
C20	2.2447990000	-3.2688190000	-0.1848430000
C21	3.5969840000	-3.3527990000	-0.8013930000
C22	4.3020780000	-2.7357810000	-1.8134250000
C23	5.5764020000	-3.2987730000	-2.0783050000
C24	5.8837620000	-4.3819240000	-1.2947950000
S25	4.5661500000	-4.7195550000	-0.2006300000
C26	7.0923190000	-5.2313920000	-1.4332480000
C27	8.4170400000	-4.7560600000	-1.2336990000
C28	8.7546680000	-3.5296810000	-0.4974360000
C29	7.8408110000	-2.8663820000	0.3375500000
C30	9.4992340000	-5.5248510000	-1.7765000000
C31	10.8424910000	-5.0176060000	-1.7917240000
C32	11.1161160000	-3.7097210000	-1.2827710000
C33	10.0857710000	-3.0106280000	-0.5784500000
C34	6.8804760000	-6.5160650000	-1.9613260000
C35	7.9292980000	-7.3041360000	-2.4001550000
C36	9.2450060000	-6.7995760000	-2.3560740000
C37	10.3182360000	-7.5293530000	-2.9428180000

C38	11.5972530000	-7.0386080000	-2.9210330000
C39	11.9116480000	-5.7940970000	-2.3075220000
C40	10.4074560000	-1.7945400000	0.0909440000
C41	9.4366660000	-1.1403580000	0.8795650000
C42	8.1729190000	-1.6955310000	1.0141890000
C43	12.4038420000	-3.1332670000	-1.4484570000
C44	12.6855360000	-1.9205820000	-0.7557300000
C45	11.7349230000	-1.2799200000	-0.0014020000
C46	-1.2157450000	-4.8066440000	3.3435800000
N47	-0.0160330000	-4.4651850000	3.9688750000
C48	1.1499170000	-3.9577180000	3.3923670000
C49	0.2441910000	-1.4245130000	-6.2730100000
N50	-0.8554020000	-1.9674760000	-6.9388600000
C51	-1.8396730000	-2.8208400000	-6.4374730000
C52	12.1173690000	-0.0508480000	0.7476630000
N53	11.0847020000	0.5438390000	1.4697030000
C54	9.7663330000	0.1091070000	1.6086080000
C55	7.6431420000	-8.6287550000	-3.0108130000
N56	8.7462570000	-9.2723980000	-3.5694940000
C57	10.0645170000	-8.8240100000	-3.6297820000
O58	-2.1393860000	-5.2945970000	3.9752250000
O59	2.1332110000	-3.7229150000	4.0687570000
O60	-2.7743030000	-3.1738120000	-7.1349190000
O61	1.0133640000	-0.6655730000	-6.8405490000
O62	8.9709500000	0.7311070000	2.2956510000
O63	13.2392520000	0.4288580000	0.7472510000
O64	6.5337810000	-9.1353080000	-3.0520870000
O65	10.9219230000	-9.4749120000	-4.2045980000
C66	-3.5983960000	-5.0621940000	-2.3508170000
C67	-3.7204170000	-4.8708890000	-0.9548300000
C68	13.2569400000	-5.2492180000	-2.3486690000
C69	13.4344640000	-3.8588720000	-2.1717800000
C70	14.4269650000	-6.0711190000	-2.5876670000
C71	15.6368310000	-5.4694650000	-3.0146520000
C72	15.7113230000	-4.0480250000	-3.1566790000
C73	14.6280730000	-3.2381560000	-2.7215780000
C74	-4.5839530000	-5.8838130000	-3.0222790000
C75	-5.8111740000	-6.1878070000	-2.3783310000
C76	-6.0681010000	-5.6817340000	-1.0666580000
C77	-5.0317990000	-5.0273120000	-0.3509830000
C78	-6.8043440000	-6.9796680000	-3.0397610000
C79	-8.0886120000	-7.1977330000	-2.4538200000
C80	-8.3884490000	-6.5905650000	-1.1555160000
C81	-7.3671870000	-5.8510640000	-0.4845670000

C82	16.7776850000	-6.2777820000	-3.3277430000
C83	17.9638750000	-5.7015320000	-3.8733350000
C84	18.0135710000	-4.2560710000	-4.0963570000
C85	16.8889820000	-3.4574260000	-3.7229080000
C86	16.9360970000	-2.0492920000	-3.9235070000
C87	15.8000590000	-1.2622730000	-3.5675260000
C88	14.6981460000	-1.8388240000	-2.9869230000
C89	19.1317700000	-3.6190780000	-4.6559880000
C90	19.1669190000	-2.2414730000	-4.8573530000
C91	18.0797060000	-1.4537980000	-4.4983490000
C92	14.4421410000	-7.4646840000	-2.2890830000
C93	15.5437140000	-8.2443000000	-2.5289850000
C94	16.7222580000	-7.6822460000	-3.1035900000
C95	17.8300190000	-8.4958460000	-3.4193360000
C96	18.9729800000	-7.9250910000	-3.9645280000
C97	19.0349620000	-6.5516810000	-4.1859510000
C98	-7.6455340000	-5.2658040000	0.7818250000
C99	-6.6240210000	-4.5121730000	1.4326260000
C100	-5.3690830000	-4.4090650000	0.8876710000
C101	-4.3017600000	-6.5194040000	-4.2649430000
C102	-5.2125660000	-7.3399490000	-4.8764910000
C103	-6.5025620000	-7.5562560000	-4.3051790000
C104	-9.6419240000	-6.7127550000	-0.5357900000
C105	-9.9112320000	-6.1262850000	0.6988920000
C106	-8.9261980000	-5.4013560000	1.3606170000
C107	-7.4631040000	-8.3512930000	-4.9663820000
C108	-8.7117970000	-8.5507960000	-4.3892390000
C109	-9.0181310000	-7.9808730000	-3.1556380000
C110	18.1254490000	0.0084810000	-4.7410180000
N111	16.9670420000	0.7044270000	-4.3921260000
C112	15.7877980000	0.2016160000	-3.8447380000
C113	15.4945450000	-9.6886860000	-2.1788040000
N114	16.6220440000	-10.4184510000	-2.5513600000
C115	17.7890030000	-9.9560050000	-3.1621340000
C116	-9.2363220000	-4.7570610000	2.6630350000
N117	-8.1951150000	-4.0123940000	3.2170760000
C118	-6.9130910000	-3.8064020000	2.7088090000
C119	-4.8297880000	-8.0195060000	-6.1410710000
N120	-5.8401840000	-8.7828990000	-6.7220690000
C121	-7.1444790000	-8.9877690000	-6.2678760000
O122	-3.7268340000	-7.9354460000	-6.6577290000
O123	-7.9294390000	-9.6687980000	-6.9054270000
O124	-10.3162100000	-4.8417210000	3.2272290000
O125	-6.1143370000	-3.0983090000	3.2931270000

O126	14.5529680000	-10.2275150000	-1.6198630000
O127	18.6978000000	-10.7233690000	-3.4364370000
O128	14.8388890000	0.9352360000	-3.6188240000
O129	19.0845740000	0.5921800000	-5.2201130000
H130	-3.4335810000	-4.3349720000	-5.0266490000
H131	2.0174830000	-0.5090950000	-4.5061920000
H132	-3.2319580000	-5.2263390000	1.7508530000
H133	3.1527400000	-3.3531570000	1.7823830000
H134	5.8698200000	-6.8896490000	-2.0871450000
H135	12.3459510000	-7.6113260000	-3.4490190000
H136	7.4537480000	-1.2005500000	1.6580150000
H137	13.6832650000	-1.5038380000	-0.7430720000
H138	0.0237780000	-4.6437570000	4.9666610000
H139	-0.9705860000	-1.6809650000	-7.9049510000
H140	11.3285950000	1.3880030000	1.9764470000
H141	8.5598060000	-10.1633230000	-4.0172050000
H142	13.8556730000	-1.1896980000	-2.7921220000
H143	19.9980540000	-4.1992260000	-4.9466700000
H144	20.0333490000	-1.7591220000	-5.2972450000
H145	13.5983030000	-7.9435790000	-1.8115900000
H146	19.8103440000	-8.5705880000	-4.2069030000
H147	19.9443110000	-6.1456600000	-4.6104440000
H148	-4.6614250000	-3.7802640000	1.4094590000
H149	-3.3297190000	-6.4284390000	-4.7306710000
H150	-10.4345220000	-7.2689650000	-1.0203660000
H151	-10.8878150000	-6.2188790000	1.1622420000
H152	-9.4357380000	-9.1616660000	-4.9189920000
H153	-10.0020500000	-8.1591090000	-2.7403180000
H154	16.9804730000	1.7025750000	-4.5725250000
H155	16.5954660000	-11.4113540000	-2.3454620000
H156	-8.4017180000	-3.5506380000	4.0957270000
H157	-5.6012340000	-9.2391890000	-7.5949550000
H158	2.2727910000	-1.1923920000	-2.1263720000
H159	3.9643630000	-1.8734670000	-2.3590790000
H160	6.2457640000	-2.9159640000	-2.8394900000
H161	6.8538480000	-3.2737130000	0.4853380000

Restricted Singlet Excited State   1:   2.0680 eV   599.55 nm

```
    excitation    X coeff.
    ------------  ---------
     426 => 429   -0.15161
     427 => 430   -0.11687
     428 => 429   -0.96532
```

Transition dipole moment (debye):
   X=   4.3122   Y=   3.8034   Z=   2.2805 Tot=   6.1857

Oscillator strength, f=   0.3001

Restricted Singlet Excited State   2:   2.0974 eV   591.13 nm

 excitation   X coeff.
------------ ---------
 426 => 430   0.10498
 427 => 429   0.13847
 427 => 430   0.16900
 428 => 430   0.95660

Transition dipole moment (debye):
   X= -2.1333   Y=   1.4583   Z= -3.0377 Tot=   3.9881

Oscillator strength, f=   0.1265

Restricted Singlet Excited State   3:   2.1747 eV   570.11 nm

 excitation   X coeff.
------------ ---------
 426 => 430   -0.26505
 427 => 429   0.67471
 427 => 430   0.63617
 427 => 431   -0.12021
 428 => 430   -0.18778

Transition dipole moment (debye):
   X=   0.7924   Y=   0.8615   Z= -2.8659 Tot=   3.0957

Oscillator strength, f=   0.0790

Restricted Singlet Excited State   4:   2.1885 eV   566.53 nm

 excitation   X coeff.
------------ ---------
 426 => 429   -0.31187
 427 => 429   -0.64059

427 => 430   0.67388
427 => 432   0.11069

Transition dipole moment (debye):
   X=   1.2199   Y=   -3.0509   Z=   -1.7482 Tot=   3.7219

Oscillator strength, f=   0.1150

Restricted Singlet Excited State   5:   2.3175 eV   535.00 nm

 excitation   X coeff.
 ------------ ---------
 424 => 430   -0.11980
 425 => 429   0.15108
 425 => 430   -0.27745
 426 => 429   -0.77097
 426 => 430   -0.21460
 427 => 429   0.15887
 427 => 430   -0.23171
 427 => 432   0.17201
 428 => 429   0.16277
 428 => 431   -0.19793
 428 => 432   -0.16463

Transition dipole moment (debye):
   X=   4.3378   Y=   -0.0703   Z=   0.3477 Tot=   4.3523

Oscillator strength, f=   0.1665

Restricted Singlet Excited State   6:   2.3357 eV   530.81 nm

 excitation   X coeff.
 ------------ ---------
 425 => 429   0.32624
 425 => 430   0.15664
 426 => 429   -0.17706
 426 => 430   0.74321
 427 => 429   0.20808
 427 => 430   0.10451
 427 => 431   0.24405
 428 => 430   -0.12113
 428 => 432   -0.33764

Transition dipole moment (debye):
   X=   -2.7261   Y=   -0.2071   Z=   -0.0723 Tot=   2.7350

Oscillator strength, f=   0.0663

Restricted Singlet Excited State   7:   2.4094 eV   514.59 nm

 excitation   X coeff.
 -----------   ---------
 423 => 429   -0.24905
 423 => 430   0.13297
 424 => 429   0.27913
 424 => 430   0.32111
 425 => 429   0.18095
 425 => 430   -0.26298
 426 => 429   0.23910
 427 => 431   -0.18131
 427 => 432   0.26125
 428 => 429   -0.11732
 428 => 431   -0.57110
 428 => 432   -0.28326

Transition dipole moment (debye):
   X=   -6.2587   Y=   0.4929   Z=   0.7294 Tot=   6.3203

Oscillator strength, f=   0.3650

Restricted Singlet Excited State   8:   2.4324 eV   509.71 nm

 excitation   X coeff.
 -----------   ---------
 424 => 429   0.10667
 424 => 430   0.48061
 425 => 429   -0.33714
 426 => 429   -0.24094
 426 => 430   0.31765
 426 => 432   0.10659
 427 => 429   0.11802
 427 => 431   -0.26318
 427 => 433   0.10541
 428 => 431   -0.15377

428 => 432   0.55258

Transition dipole moment (debye):
X=   -2.0334   Y=   -1.0952   Z=   1.1321 Tot=   2.5721

Oscillator strength, f=   0.0610

Restricted Singlet Excited State   9:   2.4883 eV   498.26 nm

 excitation   X coeff.
 ------------ ---------
 423 => 429   0.81712
 423 => 430   -0.30142
 424 => 430   0.19214
 426 => 429   0.17304
 427 => 433   0.11233
 427 => 434   0.12130
 428 => 431   -0.11741
 428 => 432   -0.22361
 428 => 434   -0.20921

Transition dipole moment (debye):
X=   3.6432   Y=   -0.7054   Z=   -2.0494 Tot=   4.2392

Oscillator strength, f=   0.1696

Restricted Singlet Excited State 10:   2.5010 eV   495.74 nm

 excitation   X coeff.
 ------------ ---------
 422 => 430   -0.11471
 423 => 430   0.16842
 424 => 429   0.27083
 424 => 430   0.57282
 425 => 429   0.14303
 425 => 430   0.28207
 426 => 429   -0.16328
 426 => 430   -0.37580
 426 => 431   0.10347
 427 => 433   0.12560
 428 => 431   0.43174
 428 => 432   -0.14224

428 => 433   0.11484

Transition dipole moment (debye):
  X=   -1.8301   Y=   -2.2879   Z=   0.4276 Tot=   2.9609

Oscillator strength, f=   0.0831

Conformation **2f**

B3LYP/6-31G** optimized geometry
Final total energy = -6022.852029

angstroms

atom	x	y	z
C1	-0.6191960000	-7.1769720000	-0.6098760000
C2	0.2797050000	-7.0613940000	-1.7158000000
C3	0.2383730000	-8.0476040000	-2.7434540000
C4	-0.6371200000	-9.1636390000	-2.6009910000
C5	-1.4328330000	-9.2965310000	-1.4934230000
C6	-1.4392770000	-8.3241440000	-0.4519810000
C7	1.1847140000	-5.9589960000	-1.8310000000
C8	1.9044420000	-5.8255520000	-3.0259590000
C9	1.8227710000	-6.7726870000	-4.0472580000
C10	1.0215980000	-7.8954710000	-3.9049520000
C11	-0.6994330000	-6.1070260000	0.3336340000
C12	0.2769950000	-5.0539170000	0.2983050000
C13	1.2940230000	-5.0061750000	-0.7160360000
C14	-1.7350730000	-6.1149540000	1.3054730000
C15	-1.7061600000	-5.1159800000	2.3189300000
C16	-0.7536250000	-4.1290400000	2.3357670000
C17	0.2470210000	-4.0653540000	1.3239380000
C18	1.2427300000	-3.0689980000	1.3678530000
C19	2.2825950000	-3.1011700000	0.4615560000
C20	2.3507740000	-4.0700660000	-0.5548280000
C21	3.5881820000	-3.9931920000	-1.3695890000
C22	3.9579820000	-3.0753570000	-2.3199850000
C23	5.2755870000	-3.2796960000	-2.8295620000
C24	5.9083330000	-4.3694720000	-2.2868080000
S25	4.8613350000	-5.1731650000	-1.1298300000
C26	7.2303130000	-4.9728530000	-2.5976060000
C27	8.5048900000	-4.4588850000	-2.2231330000
C28	8.7221540000	-3.3171830000	-1.3146340000
C29	7.6877720000	-2.7158040000	-0.5796910000
C30	9.6704710000	-5.1488230000	-2.7053980000
C31	10.9953600000	-4.6752860000	-2.4213420000
C32	11.1860520000	-3.4507680000	-1.7087410000
C33	10.0511260000	-2.8102880000	-1.1199270000
C34	7.1389530000	-6.1517600000	-3.3575870000
C35	8.2550130000	-6.8339350000	-3.7960160000
C36	9.5340140000	-6.3359670000	-3.4850080000
C37	10.6934020000	-7.0042500000	-3.9727000000

C38	11.9458540000	-6.5628870000	-3.6415160000
C39	12.1338620000	-5.4225550000	-2.8143870000
C40	10.2579220000	-1.6777680000	-0.2789630000
C41	9.1703540000	-1.0839400000	0.3968200000
C42	7.9017910000	-1.6224900000	0.2560340000
C43	12.4916190000	-2.9038040000	-1.5653950000
C44	12.6514400000	-1.7791030000	-0.7072420000
C45	11.5834780000	-1.1912380000	-0.0780950000
C46	-0.7531200000	-3.1480960000	3.4543220000
N47	0.2265150000	-2.1557580000	3.3699940000
C48	1.2278490000	-2.0167480000	2.4137710000
C49	0.9695890000	-8.9075980000	-4.9928400000
N50	0.1130370000	-9.9852570000	-4.7613150000
C51	-0.7119410000	-10.2077670000	-3.6620740000
C52	11.8360960000	-0.0540580000	0.8506400000
N53	10.6968670000	0.4928340000	1.4367290000
C54	9.3725690000	0.0778980000	1.2974540000
C55	8.0839420000	-8.0601570000	-4.6187610000
N56	9.2676290000	-8.6249170000	-5.0885030000
C57	10.5712720000	-8.1871460000	-4.8664490000
O58	-1.5363540000	-3.1713420000	4.3901550000
O59	2.0249690000	-1.0970170000	2.4683010000
O60	-1.4197700000	-11.1981300000	-3.5998780000
O61	1.6128610000	-8.8364940000	-6.0257980000
O62	8.4705400000	0.6441620000	1.8952650000
O63	12.9455660000	0.3909500000	1.0983290000
O64	7.0011070000	-8.5527970000	-4.8901390000
O65	11.5217950000	-8.7609830000	-5.3738290000
C66	-2.3653460000	-8.4060270000	0.6636850000
C67	-2.6862230000	-7.2137700000	1.3515690000
C68	13.4642180000	-4.9421640000	-2.5103910000
C69	13.6341500000	-3.5896120000	-2.1460540000
C70	14.6277480000	-5.7979240000	-2.5935730000
C71	15.9117650000	-5.2186890000	-2.7157320000
C72	16.0523950000	-3.7956640000	-2.6850980000
C73	14.9308980000	-2.9786820000	-2.3753700000
C74	-2.9896110000	-9.6437480000	1.0920190000
C75	-4.1286330000	-9.6077940000	1.9376180000
C76	-4.6479080000	-8.3491350000	2.3749800000
C77	-3.9406820000	-7.1540870000	2.0808030000
C78	-4.7774720000	-10.8212270000	2.3405980000
C79	-5.9731640000	-10.7986500000	3.1218380000
C80	-6.5384680000	-9.5079630000	3.5177250000
C81	-5.8673710000	-8.3079620000	3.1291380000

C82	17.0619610000	-6.0495330000	-2.9026110000
C83	18.3441910000	-5.4833610000	-3.1661780000
C84	18.4808640000	-4.0270530000	-3.2064290000
C85	17.3331590000	-3.2136800000	-2.9542290000
C86	17.4638680000	-1.7973530000	-2.9817200000
C87	16.3079850000	-0.9939810000	-2.7546180000
C88	15.0971690000	-1.5660580000	-2.4608510000
C89	19.7032910000	-3.3943740000	-3.4754220000
C90	19.8204980000	-2.0068530000	-3.5082350000
C91	18.7118560000	-1.2053700000	-3.2666970000
C92	14.5360730000	-7.2118270000	-2.4338580000
C93	15.6385210000	-8.0192890000	-2.5414430000
C94	16.9175820000	-7.4641740000	-2.8453460000
C95	18.0329500000	-8.2976740000	-3.0650130000
C96	19.2709890000	-7.7357030000	-3.3481370000
C97	19.4211990000	-6.3521440000	-3.3928220000
C98	-6.4150500000	-7.0496520000	3.5076110000
C99	-5.7556660000	-5.8560950000	3.0857090000
C100	-4.5669230000	-5.9142830000	2.4035510000
C101	-2.4187030000	-10.9151080000	0.7964520000
C102	-3.0086990000	-12.0848480000	1.1997240000
C103	-4.2239050000	-12.0720610000	1.9474150000
C104	-7.7130840000	-9.4004210000	4.2781240000
C105	-8.2401860000	-8.1653880000	4.6467100000
C106	-7.6074880000	-6.9898110000	4.2607910000
C107	-4.8547320000	-13.2764610000	2.3226470000
C108	-6.0219880000	-13.2407400000	3.0760540000
C109	-6.5674060000	-12.0206700000	3.4690650000
C110	18.8470900000	0.2699730000	-3.3293360000
N111	17.6666380000	0.9838740000	-3.1203810000
C112	16.3920220000	0.4873320000	-2.8594830000
C113	15.4890790000	-9.4838460000	-2.3326060000
N114	16.6411000000	-10.2291430000	-2.5806610000
C115	17.8951720000	-9.7717240000	-2.9901210000
C116	-8.1934850000	-5.6792030000	4.6386250000
N117	-7.5138540000	-4.5620520000	4.1499410000
C118	-6.3529500000	-4.5259600000	3.3783700000
C119	-2.3586070000	-13.3731350000	0.8473560000
N120	-3.0695660000	-14.5098700000	1.2280910000
C121	-4.2771320000	-14.5833360000	1.9241000000
O122	-1.2931260000	-13.4664250000	0.2596010000
O123	-4.7908510000	-15.6635930000	2.1735220000
O124	-9.2011980000	-5.5510360000	5.3148620000
O125	-5.8862580000	-3.4645210000	2.9995420000

O126	14.4545360000	-10.0245230000	-1.9770240000
O127	18.7985140000	-10.5552040000	-3.2321330000
O128	15.4404260000	1.2399990000	-2.7283700000
O129	19.8953640000	0.8497810000	-3.5576250000
H130	-2.1093260000	-10.1394510000	-1.4833460000
H131	2.3855240000	-6.6521010000	-4.9647470000
H132	-2.3899490000	-5.1441640000	3.1536540000
H133	3.0664680000	-2.3562760000	0.5564520000
H134	6.1633070000	-6.5419870000	-3.6257230000
H135	12.7846430000	-7.0819160000	-4.0829850000
H136	7.0821050000	-1.1783820000	0.8111060000
H137	13.6319210000	-1.3954500000	-0.4638610000
H138	0.2152750000	-1.4556580000	4.1029160000
H139	0.0835110000	-10.6939980000	-5.4917770000
H140	10.8521190000	1.2747320000	2.0636490000
H141	9.1673190000	-9.4466190000	-5.6747260000
H142	14.2569160000	-0.8942200000	-2.3581960000
H143	20.5887660000	-3.9857720000	-3.6676010000
H144	20.7687700000	-1.5280880000	-3.7241360000
H145	13.5995110000	-7.6838730000	-2.1694450000
H146	20.1124830000	-8.3966630000	-3.5255850000
H147	20.4031450000	-5.9533520000	-3.6105310000
H148	-4.1488610000	-4.9733890000	2.0728280000
H149	-1.4719550000	-10.9988010000	0.2814900000
H150	-8.2365470000	-10.2937010000	4.5955390000
H151	-9.1489920000	-8.0972140000	5.2341760000
H152	-6.4887330000	-14.1793310000	3.3510270000
H153	-7.4763390000	-12.0341510000	4.0561580000
H154	17.7439400000	1.9935560000	-3.1786640000
H155	16.5460150000	-11.2350330000	-2.4891270000
H156	-7.9155210000	-3.6626730000	4.3890010000
H157	-2.6571000000	-15.3971870000	0.9623700000
H158	2.5397950000	-4.9662080000	-3.1718520000
H159	3.3156460000	-2.2588590000	-2.6291530000
H160	5.7381130000	-2.6398810000	-3.5712410000
H161	6.6853380000	-3.0991010000	-0.6496170000

Restricted Singlet Excited State   1:   2.1132 eV   586.72 nm

```
  excitation    X coeff.
 ------------  ---------
  427 => 429   -0.11890
  427 => 430   -0.19985
  428 => 429    0.95318
```

Transition dipole moment (debye):
   X= -2.1577   Y= -5.8439   Z= -2.1168 Tot= 6.5793

Oscillator strength, f=   0.3469

Restricted Singlet Excited State 2:   2.1341 eV   580.98 nm

 excitation   X coeff.
 -----------   ---------
 427 => 429   -0.51986
 427 => 430   0.12441
 428 => 430   0.82480

Transition dipole moment (debye):
   X= -0.7351   Y=   0.7877   Z=   1.2460 Tot= 1.6472

Oscillator strength, f=   0.0220

Restricted Singlet Excited State 3:   2.1890 eV   566.40 nm

 excitation   X coeff.
 -----------   ---------
 426 => 430   0.18637
 427 => 429   0.81529
 427 => 431   -0.10716
 428 => 430   0.52150

Transition dipole moment (debye):
   X= -0.2186   Y=   0.6243   Z= -0.0179 Tot= 0.6617

Oscillator strength, f=   0.0036

Restricted Singlet Excited State 4:   2.2160 eV   559.49 nm

 excitation   X coeff.
 -----------   ---------
 426 => 429   -0.20592
 427 => 430   -0.93735
 428 => 429   -0.19685

Transition dipole moment (debye):
  X=   1.5490   Y= -3.5250   Z= -1.5649 Tot=   4.1562

Oscillator strength, f=   0.1452

Restricted Singlet Excited State   5:   2.3514 eV   527.27 nm

 excitation   X coeff.
 ------------   ---------
 425 => 429   0.16445
 425 => 430   0.32339
 426 => 429   0.76589
 427 => 430   -0.15112
 427 => 432   -0.28609
 428 => 431   0.34305
 428 => 432   0.11648

Transition dipole moment (debye):
  X= -2.0737   Y= -0.4071   Z= -0.3763 Tot=   2.1465

Oscillator strength, f=   0.0411

Restricted Singlet Excited State   6:   2.3739 eV   522.29 nm

 excitation   X coeff.
 ------------   ---------
 425 => 429   -0.45632
 425 => 430   0.17894
 426 => 430   -0.64195
 427 => 429   0.11175
 427 => 431   0.36356
 428 => 431   0.12688
 428 => 432   -0.39318

Transition dipole moment (debye):
  X= -0.2285   Y= -0.2407   Z= -0.1608 Tot=   0.3688

Oscillator strength, f=   0.0012

Restricted Singlet Excited State   7:   2.4455 eV   506.99 nm

```
 excitation    X coeff.
------------  ---------
 423 => 429    0.11284
 423 => 430    0.41113
 424 => 429   -0.61575
 425 => 429   -0.10032
 425 => 430   -0.28249
 426 => 429    0.25354
 427 => 432    0.20515
 427 => 434   -0.13075
 428 => 429   -0.10372
 428 => 431   -0.38948
 428 => 433   -0.12796
```

Transition dipole moment (debye):
   X=   -7.9132   Y=   -0.6133   Z=   1.5812 Tot=   8.0929

Oscillator strength, f=   0.6074

Restricted Singlet Excited State   8:   2.4849 eV   498.96 nm

```
 excitation    X coeff.
------------  ---------
 423 => 429   -0.50112
 423 => 430    0.18555
 424 => 430    0.54489
 425 => 429    0.32107
 425 => 430   -0.10130
 426 => 430   -0.38839
 427 => 433   -0.18073
 428 => 432    0.20360
 428 => 434   -0.17797
```

Transition dipole moment (debye):
   X=   -0.7952   Y=   -1.8938   Z=   1.4332 Tot=   2.5046

Oscillator strength, f=   0.0591

Restricted Singlet Excited State   9:   2.5063 eV   494.70 nm

```
 excitation    X coeff.
------------  ---------
```

```
422 => 429   0.17586
423 => 430   0.40488
424 => 429  -0.40241
425 => 430   0.18365
426 => 429  -0.43732
426 => 430   0.14397
426 => 431   0.11938
427 => 430   0.10461
427 => 432  -0.16418
427 => 434  -0.11723
428 => 431   0.53977
428 => 433  -0.12397
```

Transition dipole moment (debye):
   X=   -2.1526   Y=   -1.4417   Z=   2.6801 Tot=   3.7276

Oscillator strength, f=   0.1321

Restricted Singlet Excited State 10:   2.5168 eV   492.62 nm

 excitation   X coeff.
 ------------ ---------
```
422 => 430  -0.16957
423 => 429  -0.41605
424 => 429   0.13693
424 => 430   0.30058
425 => 429  -0.21894
426 => 429   0.10966
426 => 430   0.54524
426 => 432  -0.12719
427 => 431   0.20115
427 => 433  -0.10564
428 => 432  -0.46936
428 => 434  -0.11392
```

Transition dipole moment (debye):
   X=   1.2744   Y=   -0.7817   Z=   -0.0866 Tot=   1.4976

Oscillator strength, f=   0.0214

Conformation **2g**

B3LYP/6-31G** optimized geometry
Final total energy = -6022.846185

angstroms

atom	x	y	z
C1	-1.4178600000	-5.9942070000	-1.5966530000
C2	-0.5141670000	-5.6695930000	-2.6552750000
C3	-0.8231300000	-6.0951130000	-3.9803140000
C4	-1.9730920000	-6.9050150000	-4.2013630000
C5	-2.7833530000	-7.2713840000	-3.1609260000
C6	-2.5294430000	-6.8464390000	-1.8250940000
C7	0.6655740000	-4.8897600000	-2.4183610000
C8	1.3976630000	-4.4733150000	-3.5399330000
C9	1.0658260000	-4.8612230000	-4.8378150000
C10	-0.0201650000	-5.6874010000	-5.0670260000
C11	-1.1907700000	-5.4465720000	-0.2966670000
C12	0.0458960000	-4.7681550000	-0.0132100000
C13	1.0448300000	-4.5505570000	-1.0344730000
C14	-2.1900190000	-5.6101420000	0.7019210000
C15	-1.8838640000	-5.1972590000	2.0288560000
C16	-0.6904010000	-4.6002300000	2.3392570000
C17	0.2894050000	-4.3631410000	1.3321650000
C18	1.5281170000	-3.7900630000	1.6777610000
C19	2.5201390000	-3.6957450000	0.7255190000
C20	2.3298680000	-4.0919930000	-0.6128680000
C21	3.5843590000	-3.9316220000	-1.4081520000
C22	4.0144680000	-2.9878650000	-2.3096770000
C23	5.3490870000	-3.1934820000	-2.7687450000
C24	5.9413450000	-4.3136270000	-2.2439730000
S25	4.8304090000	-5.1407250000	-1.1734960000
C26	7.2603400000	-4.9378150000	-2.5245180000
C27	8.5396790000	-4.4340780000	-2.1489670000
C28	8.7675670000	-3.2963960000	-1.2388630000
C29	7.7421530000	-2.7025880000	-0.4864030000
C30	9.7002310000	-5.1343130000	-2.6285440000
C31	11.0283900000	-4.6621660000	-2.3581060000
C32	11.2272720000	-3.4331330000	-1.6553150000
C33	10.0982600000	-2.7909880000	-1.0570780000
C34	7.1621020000	-6.1273140000	-3.2672490000
C35	8.2738510000	-6.8230940000	-3.6957150000
C36	9.5567090000	-6.3278750000	-3.3955040000
C37	10.7112400000	-7.0036660000	-3.8840370000

115

C38	11.9659440000	-6.5599570000	-3.5706700000
C39	12.1629980000	-5.4123730000	-2.7563120000
C40	10.3135940000	-1.6592070000	-0.2175460000
C41	9.2330540000	-1.0682730000	0.4719080000
C42	7.9654190000	-1.6113960000	0.3496900000
C43	12.5333310000	-2.8849540000	-1.5278040000
C44	12.7008540000	-1.7570130000	-0.6751360000
C45	11.6400410000	-1.1702960000	-0.0334890000
C46	-0.4180060000	-4.2442280000	3.7588680000
N47	0.8018280000	-3.6077070000	3.9827770000
C48	1.8060070000	-3.3253810000	3.0579720000
C49	-0.3460890000	-6.1025560000	-6.4537680000
N50	-1.4654970000	-6.9241890000	-6.5786020000
C51	-2.3241010000	-7.3638950000	-5.5742150000
C52	11.9008710000	-0.0315180000	0.8913160000
N53	10.7682790000	0.5122830000	1.4918580000
C54	9.4442340000	0.0937220000	1.3700190000
C55	8.0950110000	-8.0579840000	-4.5042170000
N56	9.2739480000	-8.6324220000	-4.9728720000
C57	10.5799270000	-8.1955260000	-4.7638200000
O58	-1.1853270000	-4.4680000000	4.6798730000
O59	2.8307150000	-2.7475270000	3.3891510000
O60	-3.2769900000	-8.0830010000	-5.8334860000
O61	0.3015150000	-5.7711700000	-7.4299930000
O62	8.5501660000	0.6595220000	1.9784560000
O63	13.0104280000	0.4187010000	1.1251260000
O64	7.0105440000	-8.5517580000	-4.7646030000
O65	11.5230540000	-8.7790620000	-5.2717640000
C66	-3.4497010000	-7.1518440000	-0.7436830000
C67	-3.4177880000	-6.3340540000	0.4067720000
C68	13.4961770000	-4.9279480000	-2.4720260000
C69	13.6694240000	-3.5729000000	-2.1193390000
C70	14.6607060000	-5.7809320000	-2.5700380000
C71	15.9413420000	-5.2006770000	-2.7215500000
C72	16.0796380000	-3.7773870000	-2.7026620000
C73	14.9618400000	-2.9612020000	-2.3751170000
C74	-4.4002640000	-8.2489210000	-0.7903850000
C75	-5.4792600000	-8.2949830000	0.1295090000
C76	-5.6172280000	-7.2637320000	1.1094550000
C77	-4.6026740000	-6.2796840000	1.2459530000
C78	-6.4415790000	-9.3569990000	0.0765600000
C79	-7.5751730000	-9.3742510000	0.9426370000
C80	-7.7481490000	-8.2872450000	1.9052080000
C81	-6.7683900000	-7.2499360000	1.9630880000

C82	17.0892690000	-6.0314380000	-2.9270080000
C83	18.3645280000	-5.4653770000	-3.2216210000
C84	18.4980560000	-4.0089920000	-3.2742680000
C85	17.3546090000	-3.1955560000	-3.0014540000
C86	17.4810920000	-1.7793880000	-3.0403300000
C87	16.3281110000	-0.9770230000	-2.7925350000
C88	15.1244140000	-1.5490660000	-2.4704320000
C89	19.7126860000	-3.3766490000	-3.5752960000
C90	19.8264280000	-1.9890520000	-3.6183270000
C91	18.7219890000	-1.1871800000	-3.3557390000
C92	14.5756940000	-7.1936370000	-2.3994010000
C93	15.6769950000	-8.0010760000	-2.5255760000
C94	16.9485820000	-7.4464150000	-2.8595030000
C95	18.0590820000	-8.2808820000	-3.1017110000
C96	19.2904810000	-7.7189860000	-3.4113030000
C97	19.4379730000	-6.3353330000	-3.4649850000
C98	-6.9319500000	-6.1884170000	2.8952640000
C99	-5.9693300000	-5.1368040000	2.9195680000
C100	-4.8528900000	-5.1879470000	2.1263090000
C101	-4.2184670000	-9.3683830000	-1.6544060000
C102	-5.1157980000	-10.4032040000	-1.7021170000
C103	-6.2706130000	-10.4088710000	-0.8663260000
C104	-8.8349060000	-8.2324540000	2.7902570000
C105	-8.9805470000	-7.1956390000	3.7081480000
C106	-8.0430070000	-6.1715720000	3.7635430000
C107	-7.2166710000	-11.4513180000	-0.9491680000
C108	-8.3164920000	-11.4546810000	-0.1026730000
C109	-8.4868700000	-10.4340570000	0.8293180000
C110	18.8526780000	0.2883530000	-3.4308880000
N111	17.6752440000	1.0017020000	-3.2011730000
C112	16.4072620000	0.5039560000	-2.9085110000
C113	15.5330640000	-9.4653700000	-2.3087940000
N114	16.6785510000	-10.2119800000	-2.5818340000
C115	17.9232980000	-9.7555220000	-3.0187080000
C116	-8.2273830000	-5.0594780000	4.7289200000
N117	-7.2693530000	-4.0488880000	4.6568830000
C118	-6.1595730000	-3.9670030000	3.8172770000
C119	-4.8650900000	-11.5241940000	-2.6455260000
N120	-5.8652890000	-12.4943580000	-2.6778600000
C121	-7.0369520000	-12.5566780000	-1.9241920000
O122	-3.8793660000	-11.6107490000	-3.3581370000
O123	-7.8370510000	-13.4627040000	-2.0851160000
O124	-9.1435220000	-4.9979600000	5.5315980000
O125	-5.4125720000	-3.0017440000	3.8530440000

O126	14.5058910000	-10.0065590000	-1.9307900000
O127	18.8223310000	-10.5413050000	-3.2727300000
O128	15.4578550000	1.2578130000	-2.7620100000
O129	19.8952670000	0.8694830000	-3.6841610000
H130	-3.6676930000	-7.8353790000	-3.4166710000
H131	1.6522510000	-4.5283350000	-5.6856430000
H132	-2.5501150000	-5.4110830000	2.8526240000
H133	3.4787200000	-3.2924810000	1.0319370000
H134	6.1847280000	-6.5168010000	-3.5313850000
H135	12.7992390000	-7.0842860000	-4.0160120000
H136	7.1538270000	-1.1728160000	0.9201050000
H137	13.6828190000	-1.3704370000	-0.4446660000
H138	0.9840130000	-3.3160920000	4.9365650000
H139	-1.6876410000	-7.2331190000	-7.5174830000
H140	10.9297090000	1.2947070000	2.1166250000
H141	9.1672310000	-9.4596300000	-5.5504200000
H142	14.2854560000	-0.8777680000	-2.3539660000
H143	20.5944540000	-3.9684690000	-3.7845650000
H144	20.7682800000	-1.5095320000	-3.8593730000
H145	13.6450470000	-7.6666840000	-2.1162030000
H146	20.1285500000	-8.3803960000	-3.6032930000
H147	20.4151970000	-5.9374480000	-3.7048670000
H148	-4.1901480000	-4.3343160000	2.1607210000
H149	-3.3384070000	-9.4646940000	-2.2731290000
H150	-9.5869330000	-9.0117230000	2.7750180000
H151	-9.8219620000	-7.1644250000	4.3902980000
H152	-9.0315240000	-12.2663720000	-0.1850700000
H153	-9.3551310000	-10.4734940000	1.4721790000
H154	17.7493400000	2.0111990000	-3.2685850000
H155	16.5859310000	-11.2173640000	-2.4807280000
H156	-7.3954630000	-3.2781040000	5.3033160000
H157	-5.7259420000	-13.2479490000	-3.3433260000
H158	2.2492710000	-3.8342010000	-3.4113380000
H159	3.4276300000	-2.1153030000	-2.5708350000
H160	5.8507560000	-2.5304320000	-3.4620600000
H161	6.7412700000	-3.0928880000	-0.5421460000

Restricted Singlet Excited State   1:   2.1293 eV   582.28 nm

```
  excitation     X coeff.
  ------------  ---------
  427 => 429    0.14363
  428 => 429   -0.94987
  428 => 430    0.21091
```

Transition dipole moment (debye):
   X=   1.4433   Y=   4.8940   Z=   1.1117 Tot=   5.2221

Oscillator strength, f=   0.2202

Restricted Singlet Excited State   2:   2.1579 eV   574.55 nm

 excitation   X coeff.
 -----------   ---------
 425 => 432   -0.10520
 427 => 429   -0.38359
 427 => 430   -0.88551
 428 => 429   -0.13376
 428 => 430   -0.11202

Transition dipole moment (debye):
   X=   1.1123   Y=   3.3880   Z=   4.3681 Tot=   5.6388

Oscillator strength, f=   0.2602

Restricted Singlet Excited State   3:   2.1989 eV   563.86 nm

 excitation   X coeff.
 -----------   ---------
 426 => 430   0.17593
 427 => 430   -0.13772
 428 => 429   0.19917
 428 => 430   0.94327

Transition dipole moment (debye):
   X=   1.2932   Y=   0.7981   Z=   -0.0229 Tot=   1.5198

Oscillator strength, f=   0.0193

Restricted Singlet Excited State   4:   2.2144 eV   559.91 nm

 excitation   X coeff.
 -----------   ---------
 425 => 429   -0.11340
 427 => 429   0.89875

427 => 430   -0.39423
428 => 429   0.10154

Transition dipole moment (debye):
  X= -0.4824   Y=   0.2956   Z=   0.5866 Tot=   0.8150

Oscillator strength, f=   0.0056

Restricted Singlet Excited State   5:   2.3472 eV   528.23 nm

 excitation   X coeff.
 ------------   ---------
 426 => 429   -0.83002
 426 => 430   0.22886
 428 => 431   -0.42008
 428 => 432   -0.24263

Transition dipole moment (debye):
  X=   2.0067   Y= -0.1234   Z=   0.3208 Tot=   2.0359

Oscillator strength, f=   0.0369

Restricted Singlet Excited State   6:   2.4002 eV   516.56 nm

 excitation   X coeff.
 ------------   ---------
 425 => 429   0.24830
 425 => 430   0.71639
 427 => 431   -0.32754
 427 => 432   0.53304

Transition dipole moment (debye):
  X=   1.0267   Y=   0.6358   Z=   1.1292 Tot=   1.6533

Oscillator strength, f=   0.0249

Restricted Singlet Excited State   7:   2.4448 eV   507.14 nm

 excitation   X coeff.
 ------------   ---------
 423 => 429   0.57316

```
424 => 430     0.63304
426 => 430    -0.34333
427 => 434    -0.15797
428 => 430     0.10084
428 => 431    -0.18718
428 => 432    -0.14252
428 => 433     0.14191
```

Transition dipole moment (debye):
  X=   -8.8060   Y=   -0.9885   Z=   1.7872 Tot=   9.0398

Oscillator strength, f=   0.7576

Restricted Singlet Excited State   8:   2.4779 eV   500.36 nm

 excitation   X coeff.
 ------------   ---------
```
 423 => 429    -0.53007
 423 => 430     0.30102
 424 => 429     0.43861
 424 => 430     0.37119
 426 => 429    -0.19285
 426 => 430    -0.33632
 427 => 434    -0.15722
 428 => 431     0.20643
 428 => 433    -0.19935
```

Transition dipole moment (debye):
  X=   1.4250   Y=   -1.7853   Z=   0.7281 Tot=   2.3976

Oscillator strength, f=   0.0540

Restricted Singlet Excited State   9:   2.5280 eV   490.44 nm

 excitation   X coeff.
 ------------   ---------
```
 422 => 429     0.15521
 422 => 430     0.10400
 423 => 429     0.14301
 423 => 430    -0.25371
 424 => 429    -0.11590
 424 => 430    -0.35992
```

```
425 => 429   -0.15197
426 => 429   -0.36922
426 => 430   -0.59055
426 => 431    0.11330
427 => 431   -0.10012
427 => 434    0.11199
428 => 430    0.13737
428 => 431    0.38432
```

Transition dipole moment (debye):
  X=   1.0512   Y=   0.6801   Z=   0.5363 Tot=   1.3621

Oscillator strength, f=   0.0178

Restricted Singlet Excited State 10:   2.5383 eV   488.46 nm

 excitation   X coeff.
 ------------ ---------
 422 => 429   0.15319
 422 => 430   -0.13512
 423 => 429   0.27811
 424 => 429   0.15121
 424 => 430   0.20889
 425 => 429   -0.34195
 426 => 429   -0.23133
 426 => 430   0.48276
 426 => 432   0.10480
 427 => 431   -0.10359
 428 => 431   0.46389
 428 => 432   0.34248

Transition dipole moment (debye):
  X= -1.3304   Y= -1.1407   Z=   2.2331 Tot=   2.8386

Oscillator strength, f=   0.0776

Conformation **2h**

B3LYP/6-31G** optimized geometry
Final total energy = -6022.851974

angstroms

atom	x	y	z
C1	0.2542170000	-7.6625510000	0.7858080000
C2	1.1671290000	-7.7654380000	-0.3089230000
C3	1.4720810000	-9.0518600000	-0.8352800000
C4	0.9223290000	-10.2068190000	-0.2039940000
C5	0.1089670000	-10.0896900000	0.8934270000
C6	-0.2380820000	-8.8214780000	1.4387580000
C7	1.7442210000	-6.6012820000	-0.9081710000
C8	2.4696680000	-6.7692450000	-2.0987270000
C9	2.7314950000	-8.0306480000	-2.6321680000
C10	2.2692280000	-9.1731280000	-1.9937740000
C11	-0.1834280000	-6.3680970000	1.2036690000
C12	0.4794380000	-5.1988540000	0.6980040000
C13	1.5311000000	-5.2939260000	-0.2758930000
C14	-1.2581520000	-6.2624070000	2.1256950000
C15	-1.5846070000	-4.9693910000	2.6226270000
C16	-0.9377080000	-3.8428320000	2.1833630000
C17	0.0915330000	-3.9279640000	1.2031790000
C18	0.7722510000	-2.7684130000	0.7771660000
C19	1.8647140000	-2.8840200000	-0.0603350000
C20	2.2934630000	-4.1247670000	-0.5664710000
C21	3.5707550000	-4.0780540000	-1.3118140000
C22	3.9338930000	-3.1619070000	-2.2720130000
C23	5.2785630000	-3.2910530000	-2.7207400000
C24	5.9651560000	-4.2990000000	-2.0944390000
S25	4.9501950000	-5.0828240000	-0.8943160000
C26	7.2939820000	-4.8875310000	-2.4128470000
C27	8.5807260000	-4.3734160000	-2.0881810000
C28	8.8289950000	-3.2083230000	-1.2205210000
C29	7.8125010000	-2.5669370000	-0.4952120000
C30	9.7292600000	-5.0827500000	-2.5881410000
C31	11.0653590000	-4.6184010000	-2.3449140000
C32	11.2836080000	-3.3832070000	-1.6594480000
C33	10.1676920000	-2.7156790000	-1.0632690000
C34	7.1784110000	-6.0741450000	-3.1579700000
C35	8.2758650000	-6.7671320000	-3.6232100000
C36	9.5660750000	-6.2782180000	-3.3477200000
C37	10.7061950000	-6.9649750000	-3.8547250000

123

C38	11.9698410000	-6.5337170000	-3.5578540000
C39	12.1878910000	-5.3835870000	-2.7529670000
C40	10.4045000000	-1.5644890000	-0.2566270000
C41	9.3360680000	-0.9354150000	0.4172860000
C42	8.0564640000	-1.4531540000	0.3045050000
C43	12.5969850000	-2.8486400000	-1.5561440000
C44	12.7878040000	-1.7096420000	-0.7239610000
C45	11.7399080000	-1.0930780000	-0.0894590000
C46	-1.2990120000	-2.5309790000	2.7833060000
N47	-0.6260960000	-1.4325130000	2.2475120000
C48	0.3791440000	-1.4263410000	1.2802320000
C49	2.5827920000	-10.5105430000	-2.5562580000
N50	2.0326970000	-11.5897190000	-1.8605720000
C51	1.2154750000	-11.5644180000	-0.7333800000
C52	12.0243060000	0.0617540000	0.8069920000
N53	10.9026620000	0.6424780000	1.3939190000
C54	9.5703960000	0.2473910000	1.2816700000
C55	8.0696240000	-7.9941560000	-4.4361600000
N56	9.2356620000	-8.5797790000	-4.9235350000
C57	10.5495110000	-8.1580740000	-4.7297430000
O58	-2.1231800000	-2.3878420000	3.6725300000
O59	0.8852650000	-0.3785120000	0.9099660000
O60	0.7984060000	-12.5978970000	-0.2339860000
O61	3.2650030000	-10.6932720000	-3.5521210000
O62	8.6876220000	0.8467950000	1.8743840000
O63	13.1434970000	0.4944520000	1.0285010000
O64	6.9733780000	-8.4663430000	-4.6868950000
O65	11.4816990000	-8.7507920000	-5.2481980000
C66	-1.1927830000	-8.6912410000	2.5241760000
C67	-1.8771070000	-7.4628240000	2.6649140000
C68	13.5303610000	-4.9125130000	-2.4880650000
C69	13.7190360000	-3.5558920000	-2.1500900000
C70	14.6867430000	-5.7776670000	-2.5854280000
C71	15.9739440000	-5.2103300000	-2.7391230000
C72	16.1254060000	-3.7882830000	-2.7353070000
C73	15.0145270000	-2.9587630000	-2.4212240000
C74	-1.4882600000	-9.7613810000	3.4583460000
C75	-2.6557130000	-9.6980320000	4.2617600000
C76	-3.5317170000	-8.5726030000	4.1518170000
C77	-3.1542040000	-7.4610460000	3.3545070000
C78	-2.9775670000	-10.7617930000	5.1674310000
C79	-4.1921900000	-10.7547210000	5.9179470000
C80	-5.1219320000	-9.6354140000	5.7521220000
C81	-4.7737720000	-8.5694890000	4.8678030000

C82	17.1161430000	-6.0516550000	-2.9308690000
C83	18.3992790000	-5.4986260000	-3.2196450000
C84	18.5452760000	-4.0442580000	-3.2888910000
C85	17.4053890000	-3.2194640000	-3.0375700000
C86	17.5427830000	-1.8047080000	-3.0972240000
C87	16.3936410000	-0.9903980000	-2.8725240000
C88	15.1849970000	-1.5495410000	-2.5444080000
C89	19.7683990000	-3.4244710000	-3.5857360000
C90	19.8924610000	-2.0384860000	-3.6498070000
C91	18.7907110000	-1.2258160000	-3.4120010000
C92	14.5884740000	-7.1887160000	-2.4090180000
C93	15.6834010000	-8.0058790000	-2.5240170000
C94	16.9631220000	-7.4642220000	-2.8494640000
C95	18.0713450000	-8.3089840000	-3.0637890000
C96	19.3099380000	-7.7603130000	-3.3699560000
C97	19.4681320000	-6.3788070000	-3.4433260000
C98	-5.6730640000	-7.4782050000	4.7023030000
C99	-5.3303810000	-6.4339670000	3.7936220000
C100	-4.1180910000	-6.4305710000	3.1529460000
C101	-0.5718220000	-10.8260630000	3.6978340000
C102	-0.8464880000	-11.8321360000	4.5881360000
C103	-2.0719460000	-11.8495840000	5.3174040000
C104	-6.3424880000	-9.5608260000	6.4405770000
C105	-7.2170300000	-8.4887310000	6.2737560000
C106	-6.8966490000	-7.4515250000	5.4058280000
C107	-2.3737970000	-12.9094990000	6.2004240000
C108	-3.5612200000	-12.8936060000	6.9215010000
C109	-4.4526160000	-11.8318310000	6.7801640000
C110	18.9330910000	0.2473510000	-3.5081190000
N111	17.7580900000	0.9720020000	-3.3033240000
C112	16.4832990000	0.4874600000	-3.0164700000
C113	15.5247070000	-9.4669130000	-2.2979750000
N114	16.6689410000	-10.2238140000	-2.5430670000
C115	17.9250780000	-9.7810640000	-2.9607890000
C116	-7.8483770000	-6.3259300000	5.2206100000
N117	-7.4584530000	-5.3697580000	4.2831100000
C118	-6.2901220000	-5.3303670000	3.5230190000
C119	0.1606370000	-12.9083380000	4.7887890000
N120	-0.2352070000	-13.9268390000	5.6560490000
C121	-1.4290640000	-14.0408620000	6.3708060000
O122	1.2527080000	-12.9336840000	4.2442480000
O123	-1.6463690000	-15.0147000000	7.0795080000
O124	-8.9090670000	-6.2212760000	5.8169810000
O125	-6.1008720000	-4.4397160000	2.7121070000

O126	14.4887700000	-9.9964530000	-1.9315110000
O127	18.8223680000	-10.5750620000	-3.1903750000
O128	15.5366480000	1.2479390000	-2.8946280000
O129	19.9828950000	0.8178010000	-3.7574530000
H130	-0.3157950000	-11.0033700000	1.2827800000
H131	3.3070180000	-8.1424620000	-3.5448200000
H132	-2.3048610000	-4.8369940000	3.4167150000
H133	2.4252130000	-1.9870370000	-0.2947820000
H134	6.1940640000	-6.4605970000	-3.3969660000
H135	12.7931990000	-7.0672850000	-4.0108290000
H136	7.2519020000	-0.9753940000	0.8528540000
H137	13.7779500000	-1.3348670000	-0.5074540000
H138	-0.8886120000	-0.5266260000	2.6201430000
H139	2.2572920000	-12.5090580000	-2.2228630000
H140	11.0797220000	1.4381260000	1.9971140000
H141	9.1127300000	-9.4054700000	-5.4998250000
H142	14.3483700000	-0.8726220000	-2.4442640000
H143	20.6481520000	-4.0249600000	-3.7774760000
H144	20.8406480000	-1.5687610000	-3.8872080000
H145	13.6530350000	-7.6517570000	-2.1242860000
H146	20.1455700000	-8.4299390000	-3.5428250000
H147	20.4505010000	-5.9908760000	-3.6799390000
H148	-3.9440770000	-5.6359760000	2.4423150000
H149	0.3972950000	-10.8497200000	3.2193510000
H150	-6.6260870000	-10.3498370000	7.1248330000
H151	-8.1592030000	-8.4441160000	6.8094280000
H152	-3.7699620000	-13.7203180000	7.5927390000
H153	-5.3669910000	-11.8553540000	7.3581660000
H154	17.8403960000	1.9796450000	-3.3866750000
H155	16.5673080000	-11.2275780000	-2.4371640000
H156	-8.1083270000	-4.6038010000	4.1377900000
H157	0.4248420000	-14.6875020000	5.7768630000
H158	2.8309510000	-5.9006610000	-2.6286130000
H159	3.2447910000	-2.4217900000	-2.6618320000
H160	5.7169770000	-2.6696910000	-3.4912780000
H161	6.8020800000	-2.9323550000	-0.5481850000

Restricted Singlet Excited State   1:   2.0202 eV   613.74 nm

```
  excitation    X coeff.
  -----------   ---------
  426 => 429   -0.16410
  428 => 429    0.96404
  428 => 430    0.11197
```

Transition dipole moment (debye):
   X=   -2.4582   Y=   -4.6539   Z=   -0.1331 Tot=   5.2649

Oscillator strength, f=   0.2124

Restricted Singlet Excited State   2:   2.0733 eV   598.01 nm

 excitation   X coeff.
------------   ---------
 426 => 430   -0.10024
 427 => 429   -0.13128
 428 => 430   0.96846

Transition dipole moment (debye):
   X=   0.7871   Y=   -2.5300   Z=   0.4315 Tot=   2.6845

Oscillator strength, f=   0.0567

Restricted Singlet Excited State   3:   2.1478 eV   577.25 nm

 excitation   X coeff.
------------   ---------
 426 => 430   -0.11946
 427 => 429   0.95376
 427 => 430   -0.15091
 428 => 430   0.10913

Transition dipole moment (debye):
   X=   -1.2975   Y=   -4.2288   Z=   -0.8426 Tot=   4.5029

Oscillator strength, f=   0.1652

Restricted Singlet Excited State   4:   2.2187 eV   558.82 nm

 excitation   X coeff.
------------   ---------
 426 => 429   -0.26184
 426 => 430   -0.23209
 427 => 429   0.14036
 427 => 430   0.90634

Transition dipole moment (debye):
   X= -2.7201   Y=   2.8522   Z=   1.0033 Tot=   4.0670

Oscillator strength, f=   0.1392

Restricted Singlet Excited State   5:   2.2935 eV   540.59 nm

 excitation   X coeff.
 ----------- ---------
  425 => 430   0.19057
  426 => 429   0.62902
  426 => 430   0.52476
  427 => 430   0.33131
  428 => 429   0.10369
  428 => 431   -0.25616
  428 => 432   0.25143

Transition dipole moment (debye):
   X=   2.3920   Y=   0.3960   Z=   -0.3228 Tot=   2.4459

Oscillator strength, f=   0.0520

Restricted Singlet Excited State   6:   2.3543 eV   526.62 nm

 excitation   X coeff.
 ----------- ---------
  425 => 429   -0.45948
  426 => 429   0.49457
  426 => 430   -0.50095
  427 => 429   -0.12093
  427 => 431   -0.29062
  427 => 432   -0.14278
  428 => 429   0.12681
  428 => 431   0.10438
  428 => 432   -0.30922

Transition dipole moment (debye):
   X=   2.0597   Y=   0.6562   Z=   -0.1092 Tot=   2.1644

Oscillator strength, f=   0.0418

Restricted Singlet Excited State 7: 2.3944 eV 517.80 nm

```
 excitation    X coeff.
------------  ---------
 423 => 429   -0.14735
 423 => 430    0.12042
 424 => 429    0.32412
 424 => 430    0.18283
 425 => 429    0.27326
 425 => 430   -0.27896
 426 => 429    0.21293
 426 => 431   -0.10138
 427 => 431    0.23089
 427 => 432    0.26221
 428 => 429    0.11106
 428 => 431    0.64760
 428 => 432   -0.13768
```

Transition dipole moment (debye):
   X= 5.4271 Y= 0.8632 Z= -1.4122 Tot= 5.6739

Oscillator strength, f= 0.2923

Restricted Singlet Excited State 8: 2.4257 eV 511.13 nm

```
 excitation    X coeff.
------------  ---------
 424 => 429    0.14335
 424 => 430    0.35074
 425 => 429   -0.37688
 426 => 429   -0.30833
 426 => 430    0.49880
 426 => 432    0.11650
 427 => 431   -0.19900
 428 => 432   -0.49098
 428 => 434   -0.10466
```

Transition dipole moment (debye):
   X= 3.2265 Y= 1.7430 Z= -1.5385 Tot= 3.9768

Oscillator strength, f= 0.1455

Restricted Singlet Excited State   9:   2.4747 eV   501.01 nm

 excitation   X coeff.
------------   ---------
 423 => 429   0.30355
 423 => 430   -0.29376
 424 => 429   -0.47111
 424 => 430   -0.39196
 425 => 430   0.11996
 426 => 429   0.11890
 426 => 430   0.24684
 428 => 431   0.40333
 428 => 432   -0.31801
 428 => 434   0.12920

Transition dipole moment (debye):
  X=   -3.3912   Y=   -0.1255   Z=   3.6310 Tot=   4.9699

Oscillator strength, f=   0.2318

Restricted Singlet Excited State 10:   2.4878 eV   498.38 nm

 excitation   X coeff.
------------   ---------
 423 => 429   -0.73601
 423 => 430   0.21463
 424 => 430   -0.44671
 425 => 429   0.11299
 425 => 430   0.10697
 427 => 433   -0.22430
 428 => 432   -0.24481
 428 => 434   0.16722

Transition dipole moment (debye):
  X=   3.1505   Y=   -0.9857   Z=   0.7272 Tot=   3.3803

Oscillator strength, f=   0.1078

Conformation **2i**

B3LYP/6-31G** optimized geometry
Final total energy = -6022.853303

| | angstroms | | |
atom	x	y	z
C1	-0.0141000000	-0.0402000000	0.4153000000
C2	1.3928000000	-0.0375000000	0.6658000000
C3	2.0603000000	1.2067000000	0.8542000000
C4	1.3250000000	2.4197000000	0.6981000000
C5	-0.0054000000	2.3960000000	0.3652000000
C6	-0.7139000000	1.1714000000	0.1962000000
C7	2.1236000000	-1.2596000000	0.7881000000
C8	3.4455000000	-1.1834000000	1.2576000000
C9	4.0827000000	0.0358000000	1.4786000000
C10	3.4162000000	1.2311000000	1.2417000000
C11	-0.7230000000	-1.2806000000	0.4329000000
C12	0.0101000000	-2.5135000000	0.4404000000
C13	1.4434000000	-2.5279000000	0.4810000000
C14	-2.1429000000	-1.2720000000	0.4292000000
C15	-2.8187000000	-2.5198000000	0.3255000000
C16	-2.1353000000	-3.7081000000	0.2959000000
C17	-0.7137000000	-3.7350000000	0.3628000000
C18	-0.0154000000	-4.9577000000	0.2956000000
C19	1.3620000000	-4.9566000000	0.2026000000
C20	2.1084000000	-3.7622000000	0.2345000000
C21	3.5243000000	-3.8686000000	-0.1552000000
C22	4.2153000000	-3.1092000000	-1.0721000000
C23	5.5255000000	-3.5817000000	-1.3296000000
C24	5.8486000000	-4.7168000000	-0.6231000000
S25	4.5191000000	-5.2059000000	0.3983000000
C26	7.0791000000	-5.5160000000	-0.7843000000
C27	8.3848000000	-4.9702000000	-0.6837000000
C28	8.7084000000	-3.7130000000	0.0071000000
C29	7.8528000000	-3.1100000000	0.9419000000
C30	9.4596000000	-5.6899000000	-1.2981000000
C31	10.7498000000	-5.0897000000	-1.4682000000
C32	10.9691000000	-3.7448000000	-1.0356000000
C33	9.9779000000	-3.1018000000	-0.2295000000
C34	6.8985000000	-6.8292000000	-1.2541000000
C35	7.9551000000	-7.5773000000	-1.7374000000
C36	9.2373000000	-6.9960000000	-1.8160000000
C37	10.2988000000	-7.6766000000	-2.4752000000

C38	11.5338000000	-7.0978000000	-2.6017000000
C39	11.8121000000	-5.8057000000	-2.0754000000
C40	10.2821000000	-1.8491000000	0.3739000000
C41	9.3710000000	-1.2596000000	1.2757000000
C42	8.1807000000	-1.9104000000	1.5710000000
C43	12.1708000000	-3.0752000000	-1.3803000000
C44	12.4313000000	-1.8139000000	-0.7714000000
C45	11.5362000000	-1.2308000000	0.0907000000
C46	-2.9061000000	-4.9731000000	0.1535000000
N47	-2.1354000000	-6.1349000000	0.1525000000
C48	-0.7474000000	-6.2476000000	0.2189000000
C49	4.1227000000	2.5219000000	1.4392000000
N50	3.3356000000	3.6609000000	1.2656000000
C51	1.9860000000	3.7335000000	0.9311000000
C52	11.9018000000	0.0527000000	0.7517000000
N53	10.9344000000	0.5703000000	1.6109000000
C54	9.6932000000	0.0274000000	1.9441000000
C55	7.7038000000	-8.9405000000	-2.2744000000
N56	8.7962000000	-9.5382000000	-2.9006000000
C57	10.0741000000	-9.0139000000	-3.0851000000
O58	-4.1209000000	-5.0280000000	0.0490000000
O59	-0.2045000000	-7.3399000000	0.1976000000
O60	1.4190000000	4.8100000000	0.8392000000
O61	5.3016000000	2.6167000000	1.7370000000
O62	8.9552000000	0.5880000000	2.7378000000
O63	12.9601000000	0.6336000000	0.5758000000
O64	6.6289000000	-9.5132000000	-2.2061000000
O65	10.9236000000	-9.6356000000	-3.7014000000
C66	-2.1462000000	1.1441000000	-0.0230000000
C67	-2.8600000000	-0.0100000000	0.3670000000
C68	13.0885000000	-5.1554000000	-2.3018000000
C69	13.1566000000	-3.7482000000	-2.2068000000
C70	14.2904000000	-5.8839000000	-2.6550000000
C71	15.3737000000	-5.2014000000	-3.2605000000
C72	15.2863000000	-3.7914000000	-3.4839000000
C73	14.1925000000	-3.0585000000	-2.9514000000
C74	-2.8792000000	2.2449000000	-0.6120000000
C75	-4.2879000000	2.3103000000	-0.4743000000
C76	-4.9768000000	1.2845000000	0.2454000000
C77	-4.2718000000	0.1289000000	0.6711000000
C78	-5.0242000000	3.4039000000	-1.0344000000
C79	-6.4286000000	3.5380000000	-0.8135000000
C80	-7.1175000000	2.5395000000	0.0079000000
C81	-6.3763000000	1.4286000000	0.5157000000

C82	16.5461000000	-5.9162000000	-3.6680000000
C83	17.5962000000	-5.2662000000	-4.3828000000
C84	17.4616000000	-3.8437000000	-4.7012000000
C85	16.3127000000	-3.1331000000	-4.2350000000
C86	16.1797000000	-1.7468000000	-4.5258000000
C87	15.0211000000	-1.0495000000	-4.0688000000
C88	14.0734000000	-1.6828000000	-3.3045000000
C89	18.4235000000	-3.1438000000	-5.4439000000
C90	18.2803000000	-1.7893000000	-5.7351000000
C91	17.1686000000	-1.0878000000	-5.2866000000
C92	14.4752000000	-7.2510000000	-2.3000000000
C93	15.6150000000	-7.9358000000	-2.6313000000
C94	16.6626000000	-7.3005000000	-3.3600000000
C95	17.8132000000	-8.0200000000	-3.7433000000
C96	18.8255000000	-7.3774000000	-4.4444000000
C97	18.7140000000	-6.0252000000	-4.7599000000
C98	-7.0373000000	0.4456000000	1.3045000000
C99	-6.2814000000	-0.6468000000	1.8246000000
C100	-4.9550000000	-0.7959000000	1.5121000000
C101	-2.2415000000	3.1979000000	-1.4564000000
C102	-2.9409000000	4.2163000000	-2.0508000000
C103	-4.3409000000	4.3724000000	-1.8234000000
C104	-8.4850000000	2.6219000000	0.3113000000
C105	-9.1229000000	1.6579000000	1.0899000000
C106	-8.4125000000	0.5745000000	1.5918000000
C107	-5.0500000000	5.4522000000	-2.3914000000
C108	-6.4159000000	5.5734000000	-2.1660000000
C109	-7.0910000000	4.6325000000	-1.3901000000
C110	17.0243000000	0.3483000000	-5.6264000000
N111	15.8500000000	0.9503000000	-5.1723000000
C112	14.8125000000	0.3776000000	-4.4394000000
C113	15.7441000000	-9.3565000000	-2.2116000000
N114	16.9036000000	-9.9939000000	-2.6506000000
C115	17.9577000000	-9.4536000000	-3.3879000000
C116	-9.1023000000	-0.4309000000	2.4398000000
N117	-8.2850000000	-1.4457000000	2.9386000000
C118	-6.9204000000	-1.6379000000	2.7301000000
C119	-2.2190000000	5.1510000000	-2.9529000000
N120	-2.9946000000	6.1926000000	-3.4574000000
C121	-4.3494000000	6.4483000000	-3.2419000000
O122	-1.0391000000	5.0461000000	-3.2474000000
O123	-4.8910000000	7.4193000000	-3.7462000000
O124	-10.2921000000	-0.3956000000	2.7113000000
O125	-6.3284000000	-2.5640000000	3.2607000000

133

O126	14.9136000000	-9.9508000000	-1.5436000000
O127	18.9200000000	-10.1383000000	-3.6962000000
O128	13.8237000000	1.0262000000	-4.1380000000
O129	17.8460000000	0.9859000000	-6.2651000000
H130	-0.5152000000	3.3487000000	0.3148000000
H131	5.1091000000	0.0760000000	1.8301000000
H132	-3.8905000000	-2.5715000000	0.2002000000
H133	1.8582000000	-5.9081000000	0.0454000000
H134	5.9025000000	-7.2577000000	-1.2962000000
H135	12.2654000000	-7.6405000000	-3.1821000000
H136	7.5164000000	-1.4644000000	2.3036000000
H137	13.3794000000	-1.3116000000	-0.9123000000
H138	-2.6486000000	-7.0068000000	0.0796000000
H139	3.8052000000	4.5481000000	1.4101000000
H140	11.1673000000	1.4494000000	2.0599000000
H141	8.6331000000	-10.4591000000	-3.2934000000
H142	13.1963000000	-1.1099000000	-3.0327000000
H143	19.3036000000	-3.6553000000	-5.8118000000
H144	19.0267000000	-1.2590000000	-6.3167000000
H145	13.7422000000	-7.7810000000	-1.7081000000
H146	19.7001000000	-7.9500000000	-4.7341000000
H147	19.5248000000	-5.5618000000	-5.3075000000
H148	-4.4323000000	-1.6170000000	1.9825000000
H149	-1.1918000000	3.1122000000	-1.7025000000
H150	-9.0748000000	3.4512000000	-0.0593000000
H151	-10.1798000000	1.7351000000	1.3217000000
H152	-6.9412000000	6.4119000000	-2.6105000000
H153	-8.1558000000	4.7624000000	-1.2410000000
H154	15.7318000000	1.9274000000	-5.4171000000
H155	16.9988000000	-10.9698000000	-2.3913000000
H156	-8.7414000000	-2.1273000000	3.5351000000
H157	-2.5123000000	6.8527000000	-4.0576000000
H158	3.9963000000	-2.0917000000	1.4479000000
H159	3.7777000000	-2.2502000000	-1.5660000000
H160	6.2044000000	-3.1237000000	-2.0382000000
H161	6.9220000000	-3.5909000000	1.2026000000

excitation   X coeff.
------------ ---------
 426 => 429   -0.12841
 428 => 429   -0.97924

Transition dipole moment (debye):
   X= -5.4165   Y=   2.2351   Z=   0.3293 Tot=   5.8688

Oscillator strength, f=   0.2411

Restricted Singlet Excited State   2:   1.9607 eV   632.34 nm

 excitation   X coeff.
------------ ---------
 426 => 430   -0.10524
 428 => 430   -0.98105

Transition dipole moment (debye):
  X=   0.9696   Y=   3.9707   Z=   0.2075 Tot=   4.0927

Oscillator strength, f=   0.1245

Restricted Singlet Excited State   3:   2.1287 eV   582.44 nm

 excitation   X coeff.
------------ ---------
 426 => 430   0.20079
 427 => 429   -0.95472

Transition dipole moment (debye):
  X=   1.4254   Y=   5.1980   Z= -0.2368 Tot=   5.3952

Oscillator strength, f=   0.2350

Restricted Singlet Excited State   4:   2.1911 eV   565.86 nm

 excitation   X coeff.
------------ ---------
 426 => 429   0.56186
 426 => 431   -0.11287
 427 => 430   -0.78806
 427 => 432   -0.11270

Transition dipole moment (debye):
  X=   4.5075   Y= -1.4674   Z= -1.5876 Tot=   4.9992

Oscillator strength, f=   0.2077

Restricted Singlet Excited State   5:   2.2547 eV   549.88 nm

 excitation   X coeff.
------------ ---------
 425 => 430   -0.23255
 426 => 429   -0.61933
 426 => 430   -0.12390
 427 => 430   -0.43890
 427 => 432   0.13358
 428 => 431   -0.54585
 428 => 432   0.14138

Transition dipole moment (debye):
   X=   0.2108   Y=   -0.6926   Z=   -0.0696 Tot=   0.7273

Oscillator strength, f=   0.0045

Restricted Singlet Excited State   6:   2.2902 eV   541.37 nm

 excitation   X coeff.
------------ ---------
 424 => 429   0.16160
 426 => 429   -0.42347
 426 => 431   0.10201
 427 => 430   -0.39086
 427 => 432   -0.11942
 428 => 429   0.15874
 428 => 431   0.72847
 428 => 432   -0.17516

Transition dipole moment (debye):
   X=   -3.7724   Y=   1.5341   Z=   0.7422 Tot=   4.1395

Oscillator strength, f=   0.1488

Restricted Singlet Excited State   7:   2.3102 eV   536.67 nm

 excitation   X coeff.
------------ ---------
 425 => 429   -0.42568
 426 => 430   -0.44077

```
427 => 431   -0.24682
428 => 431    0.23219
428 => 432    0.68984
```

Transition dipole moment (debye):
   X= -0.5094   Y= -0.8892   Z= -0.0457 Tot=   1.0258

Oscillator strength, f=   0.0092

Restricted Singlet Excited State   8:   2.3723 eV   522.63 nm

 excitation   X coeff.
 -----------   ---------
```
426 => 430   -0.77593
426 => 432   -0.14670
427 => 429   -0.24568
428 => 430    0.10692
428 => 432   -0.51753
```

Transition dipole moment (debye):
   X=   0.0589   Y=   0.2077   Z=   1.6706 Tot=   1.6844

Oscillator strength, f=   0.0255

Restricted Singlet Excited State   9:   2.4453 eV   507.02 nm

 excitation   X coeff.
 -----------   ---------
```
423 => 430   -0.41717
424 => 429   -0.75020
424 => 430   -0.18804
425 => 430   -0.28505
427 => 432    0.10610
427 => 434    0.14803
428 => 431    0.19162
428 => 433    0.14991
```

Transition dipole moment (debye):
   X=   6.5241   Y= -1.8029   Z= -0.6479 Tot=   6.7996

Oscillator strength, f=   0.4287

Restricted Singlet Excited State 10:   2.4711 eV   501.75 nm

excitation   X coeff.
------------ ---------
 423 => 429   -0.57531
 423 => 430   0.14082
 424 => 430   -0.45710
 425 => 429   -0.47297
 426 => 430   0.10094
 427 => 431   -0.14191
 427 => 433   0.17559
 428 => 432   -0.28822
 428 => 434   0.17192

Transition dipole moment (debye):
  X=   -0.3425   Y=   0.5570   Z=   2.7801 Tot=   2.8560

Oscillator strength, f=   0.0764

Conformation **2j**

B3LYP/6-31G** optimized geometry
Final total energy = -6022.852427

angstroms

atom	x	y	z
C1	-0.0263000000	0.0346000000	0.2845000000
C2	1.3923000000	0.0621000000	0.4547000000
C3	2.0520000000	1.3204000000	0.5595000000
C4	1.2924000000	2.5184000000	0.4020000000
C5	-0.0542000000	2.4672000000	0.1471000000
C6	-0.7545000000	1.2295000000	0.0633000000
C7	2.1456000000	-1.1466000000	0.5817000000
C8	3.4909000000	-1.0365000000	0.9726000000
C9	4.1225000000	0.1977000000	1.1112000000
C10	3.4271000000	1.3751000000	0.8683000000
C11	-0.7153000000	-1.2121000000	0.3870000000
C12	0.0328000000	-2.4361000000	0.3999000000
C13	1.4665000000	-2.4341000000	0.3630000000
C14	-2.1328000000	-1.2199000000	0.4621000000
C15	-2.7976000000	-2.4772000000	0.4426000000
C16	-2.1024000000	-3.6579000000	0.4197000000
C17	-0.6794000000	-3.6671000000	0.4091000000
C18	0.0283000000	-4.8844000000	0.3508000000
C19	1.3980000000	-4.8737000000	0.1859000000
C20	2.1312000000	-3.6725000000	0.1336000000
C21	3.5293000000	-3.7924000000	-0.3091000000
C22	4.1890000000	-3.0724000000	-1.2801000000
C23	5.4891000000	-3.5609000000	-1.5619000000
C24	5.8322000000	-4.6678000000	-0.8193000000
S25	4.5333000000	-5.1162000000	0.2557000000
C26	7.0505000000	-5.4829000000	-0.9865000000
C27	8.3614000000	-4.9680000000	-0.8252000000
C28	8.6854000000	-3.7444000000	-0.0777000000
C29	7.8100000000	-3.1584000000	0.8497000000
C30	9.4407000000	-5.6875000000	-1.4301000000
C31	10.7467000000	-5.1083000000	-1.5366000000
C32	10.9782000000	-3.7857000000	-1.0463000000
C33	9.9738000000	-3.1522000000	-0.2490000000
C34	6.8585000000	-6.7765000000	-1.5037000000
C35	7.9153000000	-7.5286000000	-1.9810000000
C36	9.2099000000	-6.9701000000	-2.0001000000
C37	10.2785000000	-7.6480000000	-2.6495000000

C38	11.5272000000	-7.0899000000	-2.7171000000
C39	11.8133000000	-5.8231000000	-2.1368000000
C40	10.2822000000	-1.9298000000	0.4113000000
C41	9.3529000000	-1.3546000000	1.3037000000
C42	8.1401000000	-1.9901000000	1.5341000000
C43	12.2038000000	-3.1297000000	-1.3256000000
C44	12.4694000000	-1.8985000000	-0.6600000000
C45	11.5575000000	-1.3288000000	0.1936000000
C46	-2.8645000000	-4.9346000000	0.3682000000
N47	-2.0810000000	-6.0879000000	0.3687000000
C48	-0.6902000000	-6.1835000000	0.3634000000
C49	4.1258000000	2.6804000000	0.9775000000
N50	3.3146000000	3.8030000000	0.8085000000
C51	1.9473000000	3.8475000000	0.5496000000
C52	11.9262000000	-0.0789000000	0.9145000000
N53	10.9406000000	0.4275000000	1.7596000000
C54	9.6778000000	-0.1004000000	2.0302000000
C55	7.6563000000	-8.8681000000	-2.5718000000
N56	8.7569000000	-9.4649000000	-3.1851000000
C57	10.0491000000	-8.9585000000	-3.3123000000
O58	-4.0825000000	-5.0056000000	0.3332000000
O59	-0.1355000000	-7.2701000000	0.3545000000
O60	1.3611000000	4.9132000000	0.4519000000
O61	5.3183000000	2.8000000000	1.2031000000
O62	8.9244000000	0.4464000000	2.8191000000
O63	13.0016000000	0.4851000000	0.7961000000
O64	6.5699000000	-9.4226000000	-2.5558000000
O65	10.9062000000	-9.5744000000	-3.9238000000
C66	-2.1968000000	1.1781000000	-0.0719000000
C67	-2.8702000000	0.0286000000	0.3945000000
C68	13.1081000000	-5.1916000000	-2.3011000000
C69	13.2020000000	-3.7911000000	-2.1467000000
C70	14.3037000000	-5.9319000000	-2.6507000000
C71	15.4197000000	-5.2491000000	-3.1928000000
C72	15.3695000000	-3.8293000000	-3.3578000000
C73	14.2747000000	-3.0948000000	-2.8293000000
C74	-2.9792000000	2.2487000000	-0.6524000000
C75	-4.3799000000	2.2962000000	-0.4426000000
C76	-5.0122000000	1.2835000000	0.3439000000
C77	-4.2655000000	0.1547000000	0.7680000000
C78	-5.1645000000	3.3582000000	-0.9976000000
C79	-6.5583000000	3.4754000000	-0.7085000000
C80	-7.1851000000	2.4929000000	0.1795000000
C81	-6.3980000000	1.4120000000	0.6825000000

C82	16.5889000000	-5.9722000000	-3.5943000000
C83	17.6752000000	-5.3159000000	-4.2464000000
C84	17.5813000000	-3.8788000000	-4.5070000000
C85	16.4331000000	-3.1629000000	-4.0473000000
C86	16.3386000000	-1.7629000000	-4.2825000000
C87	15.1803000000	-1.0595000000	-3.8333000000
C88	14.1952000000	-1.7032000000	-3.1273000000
C89	18.5818000000	-3.1699000000	-5.1880000000
C90	18.4766000000	-1.8015000000	-5.4250000000
C91	17.3655000000	-1.0949000000	-4.9824000000
C92	14.4471000000	-7.3177000000	-2.3526000000
C93	15.5818000000	-8.0136000000	-2.6777000000
C94	16.6660000000	-7.3708000000	-3.3436000000
C95	17.8131000000	-8.0985000000	-3.7206000000
C96	18.8614000000	-7.4495000000	-4.3603000000
C97	18.7886000000	-6.0829000000	-4.6203000000
C98	-6.9985000000	0.4431000000	1.5352000000
C99	-6.1964000000	-0.6193000000	2.0479000000
C100	-4.8862000000	-0.7551000000	1.6708000000
C101	-2.4030000000	3.1852000000	-1.5565000000
C102	-3.1507000000	4.1721000000	-2.1448000000
C103	-4.5403000000	4.3115000000	-1.8515000000
C104	-8.5365000000	2.5609000000	0.5521000000
C105	-9.1147000000	1.6112000000	1.3930000000
C106	-8.3590000000	0.5567000000	1.8902000000
C107	-5.2982000000	5.3589000000	-2.4175000000
C108	-6.6531000000	5.4638000000	-2.1260000000
C109	-7.2701000000	4.5382000000	-1.2856000000
C110	17.2629000000	0.3569000000	-5.2647000000
N111	16.0872000000	0.9661000000	-4.8232000000
C112	15.0140000000	0.3865000000	-4.1490000000
C113	15.6666000000	-9.4541000000	-2.3173000000
N114	16.8269000000	-10.0977000000	-2.7456000000
C115	17.9160000000	-9.5486000000	-3.4234000000
C116	-8.9842000000	-0.4337000000	2.8037000000
N117	-8.1227000000	-1.4179000000	3.2897000000
C118	-6.7673000000	-1.5926000000	3.0153000000
C119	-2.4927000000	5.0890000000	-3.1105000000
N120	-3.3128000000	6.0990000000	-3.6092000000
C121	-4.6605000000	6.3372000000	-3.3358000000
O122	-1.3268000000	4.9954000000	-3.4602000000
O123	-5.2456000000	7.2801000000	-3.8453000000
O124	-10.1588000000	-0.4111000000	3.1362000000
O125	-6.1304000000	-2.4911000000	3.5417000000

O126	14.8017000000	-10.0581000000	-1.7036000000
O127	18.8738000000	-10.2404000000	-3.7298000000
O128	14.0295000000	1.0442000000	-3.8521000000
O129	18.1185000000	1.0024000000	-5.8487000000
H130	-0.5788000000	3.4115000000	0.0916000000
H131	5.1665000000	0.2634000000	1.4022000000
H132	-3.8739000000	-2.5451000000	0.3792000000
H133	1.8967000000	-5.8261000000	0.0414000000
H134	5.8565000000	-7.1846000000	-1.5867000000
H135	12.2660000000	-7.6265000000	-3.2935000000
H136	7.4600000000	-1.5572000000	2.2602000000
H137	13.4316000000	-1.4121000000	-0.7500000000
H138	-2.5867000000	-6.9671000000	0.3572000000
H139	3.7794000000	4.7003000000	0.8938000000
H140	11.1757000000	1.2843000000	2.2488000000
H141	8.5897000000	-10.3686000000	-3.6142000000
H142	13.3214000000	-1.1233000000	-2.8594000000
H143	19.4624000000	-3.6848000000	-5.5493000000
H144	19.2527000000	-1.2637000000	-5.9589000000
H145	13.6842000000	-7.8567000000	-1.8091000000
H146	19.7329000000	-8.0286000000	-4.6462000000
H147	19.6266000000	-5.6150000000	-5.1210000000
H148	-4.3250000000	-1.5524000000	2.1373000000
H149	-1.3656000000	3.1095000000	-1.8534000000
H150	-9.1607000000	3.3673000000	0.1876000000
H151	-10.1594000000	1.6773000000	1.6776000000
H152	-7.2163000000	6.2775000000	-2.5704000000
H153	-8.3283000000	4.6545000000	-1.0861000000
H154	15.9980000000	1.9550000000	-5.0294000000
H155	16.8931000000	-11.0858000000	-2.5267000000
H156	-8.5342000000	-2.0884000000	3.9298000000
H157	-2.8736000000	6.7472000000	-4.2537000000
H158	4.0643000000	-1.9296000000	1.1659000000
H159	3.7366000000	-2.2326000000	-1.7930000000
H160	6.1450000000	-3.1353000000	-2.3107000000
H161	6.8618000000	-3.6289000000	1.0611000000

Restricted Singlet Excited State   1:   1.8647 eV   664.89 nm

```
  excitation    X coeff.
 ------------  ---------
  426 => 429   -0.12728
  428 => 429   -0.97685
  428 => 431   -0.10114
```

Transition dipole moment (debye):
   X=   4.8052   Y=   -2.1364   Z=   -0.0107 Tot=   5.2588

Oscillator strength, f=   0.1956

Restricted Singlet Excited State   2:   1.9694 eV   629.57 nm

 excitation   X coeff.
 -----------   ---------
 426 => 430   0.10351
 428 => 430   0.98144

Transition dipole moment (debye):
   X=   0.5199   Y=   4.2220   Z=   0.1312 Tot=   4.2559

Oscillator strength, f=   0.1353

Restricted Singlet Excited State   3:   2.1440 eV   578.28 nm

 excitation   X coeff.
 -----------   ---------
 426 => 430   0.18587
 427 => 429   0.95593

Transition dipole moment (debye):
   X=   -1.0209   Y=   -5.2427   Z=   0.0954 Tot=   5.3421

Oscillator strength, f=   0.2320

Restricted Singlet Excited State   4:   2.2045 eV   562.41 nm

 excitation   X coeff.
 -----------   ---------
 426 => 429   0.47463
 426 => 430   0.14648
 426 => 431   0.10505
 427 => 430   0.82942
 427 => 432   -0.10063
 428 => 431   0.12609

Transition dipole moment (debye):
   X=   -4.2662   Y=   1.2341   Z=   1.8109 Tot=   4.7961

Oscillator strength, f=   0.1923

Restricted Singlet Excited State   5:   2.2641 eV   547.61 nm

 excitation   X coeff.
 ------------ ---------
 425 => 430   -0.24058
 426 => 429   -0.57788
 426 => 430   -0.19863
 427 => 430   0.29489
 427 => 432   0.15745
 428 => 431   0.61830
 428 => 432   -0.24034

Transition dipole moment (debye):
   X=   -0.0435   Y=   0.6549   Z=   -0.0792 Tot=   0.6611

Oscillator strength, f=   0.0038

Restricted Singlet Excited State   6:   2.2998 eV   539.11 nm

 excitation   X coeff.
 ------------ ---------
 424 => 429   -0.15101
 426 => 429   0.52075
 426 => 431   0.11947
 427 => 430   -0.43370
 428 => 429   -0.17440
 428 => 431   0.64758
 428 => 432   -0.13356

Transition dipole moment (debye):
   X=   -4.1226   Y=   1.4754   Z=   0.7606 Tot=   4.4442

Oscillator strength, f=   0.1723

Restricted Singlet Excited State   7:   2.3165 eV   535.23 nm

```
  excitation    X coeff.
 ------------  ---------
 425 => 429   -0.42874
 426 => 429    0.13570
 426 => 430   -0.38609
 427 => 431   -0.26421
 428 => 431   -0.23660
 428 => 432   -0.70510
```

Transition dipole moment (debye):
  X=   -0.0155   Y=   1.4147   Z=   0.3012 Tot=   1.4465

Oscillator strength, f=   0.0184

Restricted Singlet Excited State 8:   2.3790 eV   521.17 nm

```
  excitation    X coeff.
 ------------  ---------
 426 => 429    0.14453
 426 => 430   -0.77728
 426 => 432    0.15326
 427 => 429    0.24230
 428 => 430    0.10839
 428 => 432    0.48772
```

Transition dipole moment (debye):
  X=   0.5916   Y=   -0.4174   Z=   -1.8287 Tot=   1.9668

Oscillator strength, f=   0.0349

Restricted Singlet Excited State 9:   2.4492 eV   506.23 nm

```
  excitation    X coeff.
 ------------  ---------
 423 => 429   -0.23954
 423 => 430    0.42343
 424 => 429   -0.70823
 424 => 430   -0.16897
 425 => 430   -0.28031
 427 => 431    0.10289
 427 => 432    0.12365
 427 => 434    0.12650
```

428 => 431   -0.20265
428 => 433   0.13275

Transition dipole moment (debye):
  X= -6.5792   Y=   1.8129   Z=   1.0911 Tot=   6.9110

Oscillator strength, f=   0.4436

Restricted Singlet Excited State 10:   2.4724 eV   501.47 nm

 excitation   X coeff.
------------   ---------
 423 => 429   -0.50852
 424 => 429   0.13494
 424 => 430   0.51222
 425 => 429   0.46950
 426 => 430   -0.10560
 427 => 431   0.18635
 427 => 433   0.15299
 428 => 432   -0.29233
 428 => 434   0.18068

Transition dipole moment (debye):
  X=   1.0949   Y=   0.1635   Z=   2.2301 Tot=   2.4897

Oscillator strength, f=   0.0581

Conformation **2k**

B3LYP/6-31G** optimized geometry
Final total energy = -6022.853039

	angstroms		
atom	x	y	z
C1	-0.5753000000	-7.4790000000	-0.2398000000
C2	0.5197000000	-7.4953000000	-1.1583000000
C3	0.4745000000	-8.3854000000	-2.2697000000
C4	-0.6250000000	-9.2840000000	-2.3963000000
C5	-1.6251000000	-9.3115000000	-1.4583000000
C6	-1.6222000000	-8.4316000000	-0.3401000000
C7	1.6277000000	-6.6004000000	-1.0119000000
C8	2.5755000000	-6.5666000000	-2.0487000000
C9	2.5044000000	-7.4151000000	-3.1516000000
C10	1.4793000000	-8.3402000000	-3.2606000000
C11	-0.6253000000	-6.4680000000	0.7702000000
C12	0.5197000000	-5.6375000000	1.0013000000
C13	1.6981000000	-5.7397000000	0.1838000000
C14	-1.8147000000	-6.3025000000	1.5267000000
C15	-1.8035000000	-5.3828000000	2.6107000000
C16	-0.7016000000	-4.6159000000	2.8843000000
C17	0.4706000000	-4.7072000000	2.0792000000
C18	1.5961000000	-3.9154000000	2.3772000000
C19	2.7541000000	-4.0804000000	1.6426000000
C20	2.8385000000	-4.9860000000	0.5721000000
C21	4.1709000000	-5.0197000000	-0.0771000000
C22	4.7076000000	-4.0319000000	-0.8618000000
C23	6.0284000000	-4.3073000000	-1.3021000000
C24	6.5160000000	-5.5138000000	-0.8706000000
S25	5.3313000000	-6.3165000000	0.1485000000
C26	7.8515000000	-6.0870000000	-1.1641000000
C27	9.0900000000	-5.3974000000	-1.0398000000
C28	9.2802000000	-4.1443000000	-0.2889000000
C29	8.3467000000	-3.6488000000	0.6346000000
C30	10.2312000000	-5.9427000000	-1.7274000000
C31	11.4677000000	-5.2183000000	-1.8259000000
C32	11.5505000000	-3.8950000000	-1.2870000000
C33	10.4850000000	-3.3969000000	-0.4747000000
C34	7.8168000000	-7.3572000000	-1.7704000000
C35	8.9376000000	-7.9366000000	-2.3324000000
C36	10.1511000000	-7.2192000000	-2.3545000000
C37	11.2809000000	-7.7441000000	-3.0487000000

C38	12.4652000000	-7.0522000000	-3.0925000000
C39	12.6117000000	-5.7884000000	-2.4541000000
C40	10.6460000000	-2.1431000000	0.1848000000
C41	9.6523000000	-1.6673000000	1.0652000000
C42	8.5244000000	-2.4381000000	1.2994000000
C43	12.6921000000	-3.0985000000	-1.5449000000
C44	12.8230000000	-1.8588000000	-0.8570000000
C45	11.8450000000	-1.3978000000	-0.0156000000
C46	-0.7433000000	-3.7022000000	4.0593000000
N47	0.3970000000	-2.9257000000	4.2433000000
C48	1.5742000000	-2.9406000000	3.4987000000
C49	1.4244000000	-9.2382000000	-4.4413000000
N50	0.3300000000	-10.0997000000	-4.4771000000
C51	-0.7164000000	-10.2013000000	-3.5652000000
C52	12.0698000000	-0.1151000000	0.7066000000
N53	11.0169000000	0.2936000000	1.5199000000
C54	9.8173000000	-0.3710000000	1.7703000000
C55	8.8184000000	-9.2697000000	-2.9797000000
N56	9.9640000000	-9.7068000000	-3.6385000000
C57	11.1849000000	-9.0491000000	-3.7638000000
O58	-1.6963000000	-3.6073000000	4.8143000000
O59	2.5050000000	-2.2010000000	3.7771000000
O60	-1.6288000000	-10.9930000000	-3.7399000000
O61	2.2559000000	-9.2405000000	-5.3345000000
O62	8.9864000000	0.1038000000	2.5262000000
O63	13.0848000000	0.5544000000	0.6086000000
O64	7.8013000000	-9.9437000000	-2.9738000000
O65	12.0890000000	-9.5372000000	-4.4206000000
C66	-2.7415000000	-8.3733000000	0.5801000000
C67	-2.9505000000	-7.1705000000	1.2865000000
C68	13.8374000000	-5.0117000000	-2.5733000000
C69	13.7605000000	-3.6174000000	-2.3691000000
C70	15.1386000000	-5.5748000000	-2.8891000000
C71	16.1917000000	-4.7267000000	-3.3289000000
C72	15.9685000000	-3.3192000000	-3.4527000000
C73	14.7584000000	-2.7615000000	-2.9744000000
C74	-3.6620000000	-9.4705000000	0.8006000000
C75	-4.9055000000	-9.2301000000	1.4406000000
C76	-5.2535000000	-7.9001000000	1.8380000000
C77	-4.2881000000	-6.8670000000	1.7499000000
C78	-5.8265000000	-10.3017000000	1.6735000000
C79	-7.1167000000	-10.0570000000	2.2365000000
C80	-7.5102000000	-8.6786000000	2.5459000000
C81	-6.5676000000	-7.6275000000	2.3351000000

C82	17.4757000000	-5.2667000000	-3.6657000000
C83	18.5064000000	-4.4411000000	-4.2116000000
C84	18.2393000000	-3.0171000000	-4.4305000000
C85	16.9744000000	-2.4853000000	-4.0393000000
C86	16.7068000000	-1.1008000000	-4.2316000000
C87	15.4338000000	-0.5853000000	-3.8495000000
C88	14.5039000000	-1.3853000000	-3.2377000000
C89	19.1815000000	-2.1462000000	-4.9973000000
C90	18.9069000000	-0.7944000000	-5.1949000000
C91	17.6784000000	-0.2647000000	-4.8215000000
C92	15.4512000000	-6.9392000000	-2.6280000000
C93	16.6950000000	-7.4578000000	-2.8856000000
C94	17.7274000000	-6.6507000000	-3.4491000000
C95	18.9925000000	-7.2003000000	-3.7524000000
C96	19.9795000000	-6.3900000000	-4.2994000000
C97	19.7359000000	-5.0371000000	-4.5274000000
C98	-6.9334000000	-6.2845000000	2.6324000000
C99	-5.9893000000	-5.2400000000	2.4012000000
C100	-4.7145000000	-5.5281000000	1.9867000000
C101	-3.2972000000	-10.8207000000	0.5308000000
C102	-4.1459000000	-11.8643000000	0.7982000000
C103	-5.4405000000	-11.6344000000	1.3519000000
C104	-8.7764000000	-8.3471000000	3.0496000000
C105	-9.1319000000	-7.0282000000	3.3256000000
C106	-8.2270000000	-5.9953000000	3.1135000000
C107	-6.3097000000	-12.7123000000	1.6306000000
C108	-7.5644000000	-12.4596000000	2.1712000000
C109	-7.9629000000	-11.1546000000	2.4576000000
C110	17.3925000000	1.1732000000	-5.0572000000
N111	16.1160000000	1.5909000000	-4.6827000000
C112	15.0897000000	0.8348000000	-4.1194000000
C113	16.9595000000	-8.8813000000	-2.5485000000
N114	18.2264000000	-9.3383000000	-2.8966000000
C115	19.2747000000	-8.6361000000	-3.4898000000
C116	-8.6315000000	-4.5941000000	3.3905000000
N117	-7.6680000000	-3.6292000000	3.0978000000
C118	-6.3813000000	-3.8168000000	2.5990000000
C119	-3.6859000000	-13.2519000000	0.5196000000
N120	-4.6173000000	-14.2464000000	0.8039000000
C121	-5.8875000000	-14.1139000000	1.3636000000
O122	-2.5838000000	-13.5321000000	0.0785000000
O123	-6.5806000000	-15.0925000000	1.5877000000
O124	-9.7236000000	-4.2731000000	3.8310000000
O125	-5.6538000000	-2.8660000000	2.3603000000

O126	16.1522000000	-9.6192000000	-2.0080000000
O127	20.3307000000	-9.1870000000	-3.7546000000
O128	14.0043000000	1.3344000000	-3.8732000000
O129	18.1889000000	1.9570000000	-5.5494000000
H130	-2.4544000000	-9.9815000000	-1.6425000000
H131	3.2501000000	-7.3681000000	-3.9388000000
H132	-2.6417000000	-5.3066000000	3.2921000000
H133	3.6260000000	-3.4990000000	1.9186000000
H134	6.8718000000	-7.8784000000	-1.8744000000
H135	13.2657000000	-7.4800000000	-3.6820000000
H136	7.7851000000	-2.0791000000	2.0070000000
H137	13.7315000000	-1.2747000000	-0.9217000000
H138	0.3708000000	-2.2777000000	5.0237000000
H139	0.2849000000	-10.7237000000	-5.2734000000
H140	11.1485000000	1.1723000000	2.0092000000
H141	9.8941000000	-10.6044000000	-4.1055000000
H142	13.5437000000	-0.9392000000	-3.0143000000
H143	20.1530000000	-2.5193000000	-5.2986000000
H144	19.6410000000	-0.1327000000	-5.6426000000
H145	14.7357000000	-7.5939000000	-2.1492000000
H146	20.9408000000	-6.8323000000	-4.5377000000
H147	20.5326000000	-4.4419000000	-4.9555000000
H148	-4.0578000000	-4.6914000000	1.7876000000
H149	-2.3095000000	-11.0709000000	0.1668000000
H150	-9.5100000000	-9.1225000000	3.2285000000
H151	-10.1173000000	-6.7817000000	3.7064000000
H152	-8.2210000000	-13.3002000000	2.3706000000
H153	-8.9518000000	-11.0024000000	2.8730000000
H154	15.9020000000	2.5670000000	-4.8573000000
H155	18.4085000000	-10.3179000000	-2.7066000000
H156	-7.9418000000	-2.6664000000	3.2630000000
H157	-4.3240000000	-15.1958000000	0.5990000000
H158	3.3851000000	-5.8561000000	-2.0125000000
H159	4.1585000000	-3.1334000000	-1.1210000000
H160	6.6076000000	-3.6349000000	-1.9248000000
H161	7.4562000000	-4.2151000000	0.8511000000

Restricted Singlet Excited State   1:   2.0299 eV   610.79 nm

```
  excitation    X coeff.
 ------------  ---------
  426 => 429   0.13363
  428 => 429   0.96601
  428 => 430   0.11096
```

Transition dipole moment (debye):
   X= -3.8765   Y= -5.3545   Z= -1.0211 Tot=   6.6889

Oscillator strength, f=   0.3444

Restricted Singlet Excited State   2:   2.0797 eV   596.16 nm

 excitation   X coeff.
 -----------   ---------
 426 => 430   -0.12661
 427 => 429   0.16763
 428 => 429   0.10694
 428 => 430   -0.95503

Transition dipole moment (debye):
   X= -0.1161   Y= -0.4233   Z= -1.2134 Tot=   1.2903

Oscillator strength, f=   0.0131

Restricted Singlet Excited State   3:   2.1565 eV   574.93 nm

 excitation   X coeff.
 -----------   ---------
 426 => 430   -0.18613
 427 => 429   -0.86451
 427 => 430   0.40144
 428 => 430   -0.16130

Transition dipole moment (debye):
   X=   0.0404   Y=   1.9127   Z=   1.5558 Tot=   2.4658

Oscillator strength, f=   0.0497

Restricted Singlet Excited State   4:   2.2009 eV   563.33 nm

 excitation   X coeff.
 -----------   ---------
 426 => 429   0.27719
 427 => 429   0.39038
 427 => 430   0.85656

Transition dipole moment (debye):
  X= -2.3550   Y=   3.9699   Z=   1.5572 Tot=   4.8714

Oscillator strength, f=   0.1981

Conformation **2l**

B3LYP/6-31G** optimized geometry
Final total energy = -6022.852754

angstroms

atom	x	y	z
C1	-0.5671000000	-7.2395000000	-0.5294000000
C2	0.3653000000	-7.1689000000	-1.6112000000
C3	0.3673000000	-8.2051000000	-2.5892000000
C4	-0.5025000000	-9.3215000000	-2.4198000000
C5	-1.3323000000	-9.4085000000	-1.3326000000
C6	-1.3802000000	-8.3867000000	-0.3411000000
C7	1.2597000000	-6.0615000000	-1.7544000000
C8	2.0167000000	-5.9808000000	-2.9321000000
C9	1.9798000000	-6.9789000000	-3.9057000000
C10	1.1862000000	-8.1020000000	-3.7322000000
C11	-0.6903000000	-6.1245000000	0.3563000000
C12	0.2739000000	-5.0624000000	0.2988000000
C13	1.3193000000	-5.0496000000	-0.6875000000
C14	-1.7591000000	-6.0957000000	1.2909000000
C15	-1.7747000000	-5.0496000000	2.2552000000
C16	-0.8328000000	-4.0527000000	2.2543000000
C17	0.1982000000	-4.0248000000	1.2716000000
C18	1.1770000000	-3.0114000000	1.2944000000
C19	2.2383000000	-3.0665000000	0.4138000000
C20	2.3486000000	-4.0798000000	-0.5539000000
C21	3.5921000000	-4.0060000000	-1.3595000000
C22	3.9345000000	-3.1133000000	-2.3417000000
C23	5.2508000000	-3.3042000000	-2.8547000000
C24	5.9247000000	-4.3409000000	-2.2634000000
S25	4.9058000000	-5.1307000000	-1.0708000000
C26	7.2386000000	-4.9391000000	-2.6104000000
C27	8.5183000000	-4.4786000000	-2.1874000000
C28	8.7498000000	-3.4109000000	-1.1952000000
C29	7.7263000000	-2.8564000000	-0.4099000000
C30	9.6754000000	-5.1392000000	-2.7291000000
C31	11.0058000000	-4.6958000000	-2.4232000000
C32	11.2082000000	-3.5271000000	-1.6250000000
C33	10.0835000000	-2.9275000000	-0.9770000000
C34	7.1324000000	-6.0582000000	-3.4534000000
C35	8.2397000000	-6.7215000000	-3.9395000000
C36	9.5247000000	-6.2618000000	-3.5963000000
C37	10.6756000000	-6.9008000000	-4.1407000000

C38	11.9341000000	-6.4917000000	-3.7907000000
C39	12.1376000000	-5.4151000000	-2.8852000000
C40	10.3061000000	-1.8592000000	-0.0596000000
C41	9.2300000000	-1.3095000000	0.6693000000
C42	7.9564000000	-1.8284000000	0.5018000000
C43	12.5160000000	-2.9938000000	-1.4616000000
C44	12.6930000000	-1.9357000000	-0.5267000000
C45	11.6362000000	-1.3929000000	0.1582000000
C46	-0.8792000000	-3.0195000000	3.3237000000
N47	0.0907000000	-2.0208000000	3.2226000000
C48	1.1190000000	-1.9129000000	2.2907000000
C49	1.1784000000	-9.1659000000	-4.7700000000
N50	0.3232000000	-10.2383000000	-4.5133000000
C51	-0.5350000000	-10.4152000000	-3.4315000000
C52	11.9067000000	-0.3266000000	1.1624000000
N53	10.7782000000	0.1822000000	1.8004000000
C54	9.4504000000	-0.2157000000	1.6481000000
C55	8.0526000000	-7.8818000000	-4.8492000000
N56	9.2286000000	-8.4231000000	-5.3632000000
C57	10.5372000000	-8.0155000000	-5.1164000000
O58	-1.6931000000	-3.0082000000	4.2328000000
O59	1.9041000000	-0.9809000000	2.3253000000
O60	-1.2395000000	-11.4066000000	-3.3447000000
O61	1.8545000000	-9.1372000000	-5.7842000000
O62	8.5597000000	0.3115000000	2.2954000000
O63	13.0212000000	0.0948000000	1.4268000000
O64	6.9635000000	-8.3401000000	-5.1531000000
O65	11.4794000000	-8.5602000000	-5.6687000000
C66	-2.3441000000	-8.4214000000	0.7436000000
C67	-2.7048000000	-7.1980000000	1.3509000000
C68	13.4742000000	-4.9565000000	-2.5683000000
C69	13.6461000000	-3.6327000000	-2.1119000000
C70	14.6426000000	-5.7962000000	-2.7305000000
C71	15.9221000000	-5.2000000000	-2.8309000000
C72	16.0540000000	-3.7812000000	-2.7067000000
C73	14.9325000000	-2.9969000000	-2.3243000000
C74	-2.9725000000	-9.6406000000	1.2148000000
C75	-4.1513000000	-9.5703000000	2.0013000000
C76	-4.7056000000	-8.2949000000	2.3365000000
C77	-3.9950000000	-7.1105000000	2.0105000000
C78	-4.8061000000	-10.7666000000	2.4426000000
C79	-6.0414000000	-10.7140000000	3.1576000000
C80	-6.6431000000	-9.4099000000	3.4422000000
C81	-5.9648000000	-8.2260000000	3.0188000000

C82	17.0763000000	-6.0068000000	-3.0886000000
C83	18.3511000000	-5.4136000000	-3.3299000000
C84	18.4757000000	-3.9560000000	-3.2782000000
C85	17.3254000000	-3.1713000000	-2.9573000000
C86	17.4433000000	-1.7550000000	-2.8962000000
C87	16.2843000000	-0.9793000000	-2.6000000000
C88	15.0840000000	-1.5805000000	-2.3218000000
C89	19.6884000000	-3.2958000000	-3.5240000000
C90	19.7928000000	-1.9079000000	-3.4709000000
C91	18.6813000000	-1.1337000000	-3.1628000000
C92	14.5641000000	-7.2184000000	-2.6691000000
C93	15.6712000000	-8.0074000000	-2.8460000000
C94	16.9433000000	-7.4233000000	-3.1242000000
C95	18.0628000000	-8.2319000000	-3.4083000000
C96	19.2934000000	-7.6420000000	-3.6671000000
C97	19.4322000000	-6.2570000000	-3.6246000000
C98	-6.5462000000	-6.9550000000	3.2875000000
C99	-5.8770000000	-5.7799000000	2.8311000000
C100	-4.6509000000	-5.8622000000	2.2217000000
C101	-2.3725000000	-10.9190000000	1.0244000000
C102	-2.9666000000	-12.0711000000	1.4708000000
C103	-4.2177000000	-12.0308000000	2.1556000000
C104	-7.8602000000	-9.2738000000	4.1271000000
C105	-8.4214000000	-8.0259000000	4.3869000000
C106	-7.7808000000	-6.8670000000	3.9656000000
C107	-4.8508000000	-13.2197000000	2.5742000000
C108	-6.0565000000	-13.1552000000	3.2620000000
C109	-6.6379000000	-11.9220000000	3.5480000000
C110	18.8022000000	0.3443000000	-3.1351000000
N111	17.6187000000	1.0311000000	-2.8631000000
C112	16.3531000000	0.5060000000	-2.6137000000
C113	15.5334000000	-9.4841000000	-2.7390000000
N114	16.6884000000	-10.2020000000	-3.0449000000
C115	17.9371000000	-9.7095000000	-3.4282000000
C116	-8.4034000000	-5.5449000000	4.2263000000
N117	-7.7094000000	-4.4498000000	3.7096000000
C118	-6.5060000000	-4.4433000000	3.0060000000
C119	-2.2831000000	-13.3696000000	1.2333000000
N120	-2.9965000000	-14.4914000000	1.6513000000
C121	-4.2355000000	-14.5399000000	2.2912000000
O122	-1.1887000000	-13.4829000000	0.7057000000
O123	-4.7452000000	-15.6098000000	2.5865000000
O124	-9.4508000000	-5.3910000000	4.8333000000
O125	-6.0300000000	-3.4003000000	2.5892000000

O126	14.5048000000	-10.0552000000	-2.4158000000
O127	18.8448000000	-10.4687000000	-3.7254000000
O128	15.3965000000	1.2386000000	-2.4212000000
O129	19.8417000000	0.9481000000	-3.3428000000
H130	-2.0023000000	-10.2563000000	-1.3019000000
H131	2.5719000000	-6.8978000000	-4.8096000000
H132	-2.4868000000	-5.0454000000	3.0672000000
H133	3.0066000000	-2.3040000000	0.4900000000
H134	6.1521000000	-6.4132000000	-3.7517000000
H135	12.7654000000	-6.9819000000	-4.2775000000
H136	7.1451000000	-1.4201000000	1.0951000000
H137	13.6787000000	-1.5733000000	-0.2708000000
H138	0.0490000000	-1.2883000000	3.9223000000
H139	0.3221000000	-10.9805000000	-5.2086000000
H140	10.9456000000	0.9166000000	2.4794000000
H141	9.1176000000	-9.1992000000	-6.0069000000
H142	14.2391000000	-0.9253000000	-2.1620000000
H143	20.5763000000	-3.8654000000	-3.7662000000
H144	20.7336000000	-1.4074000000	-3.6704000000
H145	13.6345000000	-7.7157000000	-2.4261000000
H146	20.1382000000	-8.2830000000	-3.8954000000
H147	20.4085000000	-5.8368000000	-3.8275000000
H148	-4.2249000000	-4.9376000000	1.8562000000
H149	-1.4007000000	-11.0188000000	0.5610000000
H150	-8.3909000000	-10.1535000000	4.4694000000
H151	-9.3638000000	-7.9348000000	4.9158000000
H152	-6.5256000000	-14.0822000000	3.5714000000
H153	-7.5772000000	-11.9137000000	4.0857000000
H154	17.6857000000	2.0432000000	-2.8594000000
H155	16.6003000000	-11.2123000000	-3.0223000000
H156	-8.1351000000	-3.5435000000	3.8679000000
H157	-2.5596000000	-15.3871000000	1.4642000000
H158	2.6466000000	-5.1222000000	-3.1033000000
H159	3.2675000000	-2.3282000000	-2.6790000000
H160	5.6858000000	-2.6908000000	-3.6347000000
H161	6.7199000000	-3.2254000000	-0.5005000000

Restricted Singlet Excited State   1:   2.1282 eV   582.59 nm

    excitation   X coeff.
    ------------ ---------
    427 => 430   -0.26507
    428 => 429   0.92302
    428 => 430   -0.18888

156

Transition dipole moment (debye):
   X= -1.2510   Y= -6.0683   Z= -2.4731 Tot=   6.6713

Oscillator strength, f=   0.3592

Restricted Singlet Excited State   2:   2.1384 eV   579.80 nm

 excitation   X coeff.
 -----------   ---------
 427 => 429   0.61288
 428 => 430   -0.76581

Transition dipole moment (debye):
   X=   1.2047   Y=   0.3980   Z= -0.3063 Tot=   1.3052

Oscillator strength, f=   0.0138

Restricted Singlet Excited State   3:   2.1927 eV   565.44 nm

 excitation   X coeff.
 -----------   ---------
 426 => 429   -0.10207
 426 => 430   -0.14085
 427 => 429   -0.73761
 427 => 430   -0.19279
 428 => 429   -0.24221
 428 => 430   -0.55715

Transition dipole moment (debye):
   X=   0.4869   Y= -1.9148   Z= -0.6983 Tot=   2.0955

Oscillator strength, f=   0.0365

Restricted Singlet Excited State   4:   2.2207 eV   558.31 nm

 excitation   X coeff.
 -----------   ---------
 426 => 429   0.15022
 427 => 429   -0.17547
 427 => 430   0.91633

428 => 429   0.20601
428 => 430   -0.18121

Transition dipole moment (debye):
  X=   -1.1972   Y=   2.6417   Z=   1.1617 Tot=   3.1243

Oscillator strength, f=   0.0822

Conformation **2m** (final optimization)

B3LYP/6-31G** optimized geometry
Final total energy = -6022.854914

angstroms

atom	x	y	z
C1	0.0337000000	-7.8303000000	0.8002000000
C2	0.9614000000	-8.0313000000	-0.2674000000
C3	0.9703000000	-9.2772000000	-0.9537000000
C4	0.1233000000	-10.3279000000	-0.4934000000
C5	-0.6811000000	-10.1523000000	0.6047000000
C6	-0.7415000000	-8.9065000000	1.2940000000
C7	1.8364000000	-6.9849000000	-0.6869000000
C8	2.5744000000	-7.1788000000	-1.8639000000
C9	2.5395000000	-8.3833000000	-2.5643000000
C10	1.7707000000	-9.4432000000	-2.1042000000
C11	-0.1430000000	-6.5175000000	1.3386000000
C12	0.7869000000	-5.4854000000	0.9899000000
C13	1.8719000000	-5.7374000000	0.0870000000
C14	-1.2327000000	-6.2589000000	2.2116000000
C15	-1.3260000000	-4.9661000000	2.7993000000
C16	-0.4299000000	-3.9718000000	2.4997000000
C17	0.6389000000	-4.2038000000	1.5898000000
C18	1.5830000000	-3.1914000000	1.3201000000
C19	2.6930000000	-3.4854000000	0.5541000000
C20	2.8839000000	-4.7509000000	-0.0361000000
C21	4.2041000000	-4.9325000000	-0.6699000000
C22	4.8270000000	-4.0391000000	-1.5104000000
C23	6.1720000000	-4.3722000000	-1.8069000000
C24	6.6088000000	-5.5085000000	-1.1707000000
S25	5.3241000000	-6.2049000000	-0.2062000000
C26	7.9403000000	-6.1268000000	-1.3116000000
C27	9.1474000000	-5.3879000000	-1.1793000000
C28	9.2611000000	-4.1068000000	-0.4700000000
C29	8.2945000000	-3.6506000000	0.4381000000
C30	10.3414000000	-5.9374000000	-1.7455000000
C31	11.5460000000	-5.1624000000	-1.8397000000
C32	11.5562000000	-3.8047000000	-1.3895000000
C33	10.4387000000	-3.3144000000	-0.6449000000
C34	7.9802000000	-7.4530000000	-1.7780000000
C35	9.1547000000	-8.0278000000	-2.2285000000
C36	10.3364000000	-7.2594000000	-2.2690000000
C37	11.5155000000	-7.7740000000	-2.8790000000

C38	12.6643000000	-7.0282000000	-2.9329000000
C39	12.7344000000	-5.7229000000	-2.3732000000
C40	10.5300000000	-2.0384000000	-0.0203000000
C41	9.4993000000	-1.5962000000	0.8357000000
C42	8.4090000000	-2.4204000000	1.0810000000
C43	12.6830000000	-2.9790000000	-1.6408000000
C44	12.7253000000	-1.6978000000	-1.0170000000
C45	11.7004000000	-1.2477000000	-0.2235000000
C46	-0.5698000000	-2.6495000000	3.1710000000
N47	0.3728000000	-1.6927000000	2.7964000000
C48	1.4509000000	-1.8408000000	1.9265000000
C49	1.7556000000	-10.7237000000	-2.8554000000
N50	0.9165000000	-11.7072000000	-2.3313000000
C51	0.0776000000	-11.6256000000	-1.2226000000
C52	11.8426000000	0.0684000000	0.4583000000
N53	10.7606000000	0.4382000000	1.2535000000
C54	9.5951000000	-0.2824000000	1.5173000000
C55	9.1323000000	-9.4135000000	-2.7671000000
N56	10.3224000000	-9.8357000000	-3.3574000000
C57	11.5127000000	-9.1246000000	-3.4999000000
O58	-1.4384000000	-2.3855000000	3.9855000000
O59	2.2156000000	-0.9151000000	1.7079000000
O60	-0.6301000000	-12.5657000000	-0.9006000000
O61	2.4083000000	-10.9307000000	-3.8649000000
O62	8.7411000000	0.1633000000	2.2661000000
O63	12.8177000000	0.7935000000	0.3482000000
O64	8.1568000000	-10.1447000000	-2.7272000000
O65	12.4656000000	-9.6090000000	-4.0873000000
C66	-1.6864000000	-8.6721000000	2.3682000000
C67	-2.1130000000	-7.3458000000	2.6031000000
C68	13.9377000000	-4.9170000000	-2.4683000000
C69	13.8230000000	-3.5150000000	-2.3616000000
C70	15.2556000000	-5.4864000000	-2.6580000000
C71	16.3254000000	-4.6652000000	-3.0939000000
C72	16.0985000000	-3.2735000000	-3.3306000000
C73	14.8583000000	-2.6923000000	-2.9595000000
C74	-2.2120000000	-9.7308000000	3.2045000000
C75	-3.3608000000	-9.4928000000	4.0001000000
C76	-4.0068000000	-8.2175000000	3.9480000000
C77	-3.3998000000	-7.1466000000	3.2421000000
C78	-3.8914000000	-10.5250000000	4.8370000000
C79	-5.1029000000	-10.3337000000	5.5674000000
C80	-5.8226000000	-9.0649000000	5.4288000000
C81	-5.2559000000	-8.0303000000	4.6230000000

C82	17.6282000000	-5.2188000000	-3.3089000000
C83	18.6862000000	-4.4296000000	-3.8527000000
C84	18.4213000000	-3.0323000000	-4.2037000000
C85	17.1350000000	-2.4798000000	-3.9205000000
C86	16.8740000000	-1.1164000000	-4.2311000000
C87	15.5834000000	-0.5796000000	-3.9478000000
C88	14.6227000000	-1.3368000000	-3.3268000000
C89	19.3859000000	-2.2044000000	-4.7976000000
C90	19.1181000000	-0.8739000000	-5.1151000000
C91	17.8719000000	-0.3243000000	-4.8386000000
C92	15.5543000000	-6.8238000000	-2.2736000000
C93	16.8112000000	-7.3512000000	-2.4106000000
C94	17.8723000000	-6.5789000000	-2.9693000000
C95	19.1535000000	-7.1390000000	-3.1530000000
C96	20.1737000000	-6.3621000000	-3.6881000000
C97	19.9395000000	-5.0325000000	-4.0329000000
C98	-5.9434000000	-6.7915000000	4.4846000000
C99	-5.3782000000	-5.7732000000	3.6605000000
C100	-4.1516000000	-5.9475000000	3.0715000000
C101	-1.5199000000	-10.9657000000	3.3713000000
C102	-1.9823000000	-11.9425000000	4.2149000000
C103	-3.1966000000	-11.7621000000	4.9430000000
C104	-7.0502000000	-8.8191000000	6.0626000000
C105	-7.7218000000	-7.6072000000	5.9146000000
C106	-7.1831000000	-6.5955000000	5.1294000000
C107	-3.6943000000	-12.7801000000	5.7826000000
C108	-4.8720000000	-12.5812000000	6.4910000000
C109	-5.5642000000	-11.3785000000	6.3806000000
C110	17.5944000000	1.0883000000	-5.2002000000
N111	16.3014000000	1.5283000000	-4.9175000000
C112	15.2520000000	0.8145000000	-4.3415000000
C113	17.0567000000	-8.7421000000	-1.9468000000
N114	18.3455000000	-9.2167000000	-2.1816000000
C115	19.4231000000	-8.5457000000	-2.7605000000
C116	-7.9282000000	-5.3229000000	4.9604000000
N117	-7.3277000000	-4.3940000000	4.1095000000
C118	-6.1235000000	-4.5070000000	3.4178000000
C119	-1.1909000000	-13.1920000000	4.3769000000
N120	-1.7675000000	-14.1453000000	5.2129000000
C121	-2.9608000000	-14.0593000000	5.9306000000
O122	-0.1193000000	-13.3993000000	3.8320000000
O123	-3.3371000000	-14.9860000000	6.6303000000
O124	-8.9960000000	-5.0770000000	5.4991000000
O125	-5.7366000000	-3.6145000000	2.6816000000

O126	16.2167000000	-9.4427000000	-1.4049000000
O127	20.5009000000	-9.0996000000	-2.9053000000
O128	14.1565000000	1.3279000000	-4.1835000000
O129	18.4104000000	1.8338000000	-5.7181000000
H130	-1.3313000000	-10.9734000000	0.8759000000
H131	3.1141000000	-8.5159000000	-3.4747000000
H132	-2.0701000000	-4.7414000000	3.5494000000
H133	3.4540000000	-2.7211000000	0.4446000000
H134	7.0658000000	-8.0324000000	-1.8491000000
H135	13.4999000000	-7.4553000000	-3.4690000000
H136	7.6502000000	-2.0831000000	1.7787000000
H137	13.6051000000	-1.0715000000	-1.0834000000
H138	0.2765000000	-0.7822000000	3.2331000000
H139	0.8964000000	-12.5855000000	-2.8382000000
H140	10.8408000000	1.3351000000	1.7203000000
H141	10.3136000000	-10.7693000000	-3.7539000000
H142	13.6529000000	-0.8782000000	-3.1849000000
H143	20.3695000000	-2.5959000000	-5.0265000000
H144	19.8693000000	-0.2461000000	-5.5818000000
H145	14.8122000000	-7.4491000000	-1.7967000000
H146	21.1512000000	-6.8120000000	-3.8239000000
H147	20.7622000000	-4.4608000000	-4.4430000000
H148	-3.8009000000	-5.1560000000	2.4222000000
H149	-0.5722000000	-11.1453000000	2.8822000000
H150	-7.5049000000	-9.5831000000	6.6804000000
H151	-8.6750000000	-7.4308000000	6.4011000000
H152	-5.2336000000	-13.3799000000	7.1293000000
H153	-6.4784000000	-11.2622000000	6.9481000000
H154	16.0941000000	2.4865000000	-5.1774000000
H155	18.5252000000	-10.1713000000	-1.8900000000
H156	-7.8383000000	-3.5288000000	3.9697000000
H157	-1.2476000000	-15.0094000000	5.3220000000
H158	3.1809000000	-6.3728000000	-2.2518000000
H159	4.3171000000	-3.1738000000	-1.9184000000
H160	6.8044000000	-3.7968000000	-2.4712000000
H161	7.4311000000	-4.2636000000	0.6530000000

Restricted Singlet Excited State   1:   1.9151 eV   647.42 nm

```
  excitation    X coeff.
 ------------  ---------
  426 => 429    0.13690
  428 => 429    0.97744
```

Transition dipole moment (debye):
   X= -5.8327   Y= -5.4998   Z=   0.2976 Tot=   8.0223

Oscillator strength, f=   0.4674

Restricted Singlet Excited State 2:   1.9962 eV   621.10 nm

 excitation   X coeff.
------------   ---------
 426 => 430   -0.10588
 428 => 430   -0.98341

Transition dipole moment (debye):
   X=   0.7615   Y= -0.2214   Z= -0.0293 Tot=   0.7935

Oscillator strength, f=   0.0048

Restricted Singlet Excited State 3:   2.1367 eV   580.27 nm

 excitation   X coeff.
------------   ---------
 426 => 430   -0.20014
 427 => 429   -0.96106

Transition dipole moment (debye):
   X= -0.5808   Y= -0.0195   Z=   0.3574 Tot=   0.6822

Oscillator strength, f=   0.0038

Restricted Singlet Excited State 4:   2.2048 eV   562.34 nm

 excitation   X coeff.
------------   ---------
 426 => 429   0.45027
 426 => 431   0.11408
 427 => 430   0.85811
 428 => 431   0.12277

Transition dipole moment (debye):
   X= -4.0009   Y=   4.8248   Z=   1.0356 Tot=   6.3529

Oscillator strength, f=   0.3374

Restricted Singlet Excited State   5:   2.2742 eV   545.19 nm

 excitation   X coeff.
 ------------ ---------
 425 => 430   -0.25399
 426 => 429   -0.73368
 427 => 430   0.35843
 427 => 432   0.16458
 428 => 429   0.10093
 428 => 431   0.44908

Transition dipole moment (debye):
   X=   0.9856   Y=   -0.0057   Z=   -0.1889 Tot=   1.0035

Oscillator strength, f=   0.0087

Restricted Singlet Excited State   6:   2.3235 eV   533.61 nm

 excitation   X coeff.
 ------------ ---------
 424 => 429   0.17898
 425 => 429   -0.19833
 425 => 430   0.13745
 426 => 429   -0.29877
 426 => 430   -0.26139
 427 => 430   0.27780
 427 => 431   -0.10897
 427 => 432   -0.15483
 428 => 429   0.12942
 428 => 431   -0.73234
 428 => 432   -0.19403

Transition dipole moment (debye):
   X=   4.7700   Y=   1.4796   Z=   -0.1721 Tot=   4.9971

Oscillator strength, f=   0.2200

Restricted Singlet Excited State   7:   2.3274 eV   532.72 nm

excitation   X coeff.
------------ ---------
 424 => 429   0.14795
 425 => 429   0.39956
 426 => 429   -0.18124
 426 => 430   0.45617
 427 => 430   0.14460
 427 => 431   0.25786
 428 => 431   -0.27994
 428 => 432   0.61375

Transition dipole moment (debye):
   X=   2.2913   Y=   0.6369   Z=   -0.1010 Tot=   2.3803

Oscillator strength, f=   0.0500

Restricted Singlet Excited State   8:   2.3966 eV   517.33 nm

 excitation   X coeff.
------------ ---------
 424 => 430   0.13633
 426 => 430   -0.72260
 426 => 432   0.14646
 427 => 429   0.20473
 428 => 430   0.12245
 428 => 432   0.58513

Transition dipole moment (debye):
   X=   -1.6115   Y=   -0.8706   Z=   1.0018 Tot=   2.0877

Oscillator strength, f=   0.0396

Restricted Singlet Excited State   9:   2.4499 eV   506.08 nm

 excitation   X coeff.
------------ ---------
 423 => 430   0.33168
 424 => 429   -0.65283
 424 => 430   0.37852
 425 => 429   0.25156
 425 => 430   -0.23127
 426 => 429   -0.11425

```
427 =>  433    0.10602
427 =>  434    0.12910
428 =>  431   -0.24828
428 =>  432   -0.16851
428 =>  433    0.15489
```

Transition dipole moment (debye):
  X= -4.1464   Y= -0.9229   Z=   4.2199 Tot=   5.9876

Oscillator strength, f=   0.3331

Restricted Singlet Excited State 10:   2.4734 eV   501.27 nm

 excitation   X coeff.
------------   ---------
```
423 =>  429    0.65692
423 =>  430    0.33858
424 =>  429   -0.22372
424 =>  430   -0.37004
425 =>  429   -0.31457
427 =>  433   -0.14449
428 =>  431   -0.11668
428 =>  432    0.22780
428 =>  434   -0.18170
```

Transition dipole moment (debye):
  X= -3.3654   Y=   0.2630   Z=   1.4528 Tot=   3.6750

Oscillator strength, f=   0.1267

Conformation **2n**

B3LYP/6-31G** optimized geometry
Final total energy = -6022.852027

angstroms

atom	x	y	z
C1	0.2542000000	-7.6626000000	0.7858000000
C2	1.1671000000	-7.7654000000	-0.3089000000
C3	1.4721000000	-9.0519000000	-0.8353000000
C4	0.9223000000	-10.2068000000	-0.2040000000
C5	0.1090000000	-10.0897000000	0.8934000000
C6	-0.2381000000	-8.8215000000	1.4388000000
C7	1.7442000000	-6.6013000000	-0.9082000000
C8	2.4697000000	-6.7692000000	-2.0987000000
C9	2.7315000000	-8.0306000000	-2.6322000000
C10	2.2692000000	-9.1731000000	-1.9938000000
C11	-0.1834000000	-6.3681000000	1.2037000000
C12	0.4794000000	-5.1989000000	0.6980000000
C13	1.5311000000	-5.2939000000	-0.2759000000
C14	-1.2582000000	-6.2624000000	2.1257000000
C15	-1.5846000000	-4.9694000000	2.6226000000
C16	-0.9377000000	-3.8428000000	2.1834000000
C17	0.0915000000	-3.9280000000	1.2032000000
C18	0.7723000000	-2.7684000000	0.7772000000
C19	1.8647000000	-2.8840000000	-0.0603000000
C20	2.2935000000	-4.1248000000	-0.5665000000
C21	3.5708000000	-4.0781000000	-1.3118000000
C22	3.9339000000	-3.1619000000	-2.2720000000
C23	5.2786000000	-3.2911000000	-2.7207000000
C24	5.9652000000	-4.2990000000	-2.0944000000
S25	4.9502000000	-5.0828000000	-0.8943000000
C26	7.2940000000	-4.8875000000	-2.4128000000
C27	8.5807000000	-4.3734000000	-2.0882000000
C28	8.8290000000	-3.2083000000	-1.2205000000
C29	7.8125000000	-2.5669000000	-0.4952000000
C30	9.7293000000	-5.0827000000	-2.5881000000
C31	11.0654000000	-4.6184000000	-2.3449000000
C32	11.2836000000	-3.3832000000	-1.6594000000
C33	10.1677000000	-2.7157000000	-1.0633000000
C34	7.1784000000	-6.0741000000	-3.1580000000
C35	8.2759000000	-6.7671000000	-3.6232000000
C36	9.5661000000	-6.2782000000	-3.3477000000
C37	10.7062000000	-6.9650000000	-3.8547000000

C38	11.9698000000	-6.5337000000	-3.5579000000
C39	12.1879000000	-5.3836000000	-2.7530000000
C40	10.4045000000	-1.5645000000	-0.2566000000
C41	9.3361000000	-0.9354000000	0.4173000000
C42	8.0565000000	-1.4532000000	0.3045000000
C43	12.5970000000	-2.8486000000	-1.5561000000
C44	12.7878000000	-1.7096000000	-0.7240000000
C45	11.7399000000	-1.0931000000	-0.0895000000
C46	-1.2990000000	-2.5310000000	2.7833000000
N47	-0.6261000000	-1.4325000000	2.2475000000
C48	0.3791000000	-1.4263000000	1.2802000000
C49	2.5828000000	-10.5105000000	-2.5563000000
N50	2.0327000000	-11.5897000000	-1.8606000000
C51	1.2155000000	-11.5644000000	-0.7334000000
C52	12.0243000000	0.0618000000	0.8070000000
N53	10.9027000000	0.6425000000	1.3939000000
C54	9.5704000000	0.2474000000	1.2817000000
C55	8.0696000000	-7.9942000000	-4.4362000000
N56	9.2357000000	-8.5798000000	-4.9235000000
C57	10.5495000000	-8.1581000000	-4.7297000000
O58	-2.1232000000	-2.3878000000	3.6725000000
O59	0.8853000000	-0.3785000000	0.9100000000
O60	0.7984000000	-12.5979000000	-0.2340000000
O61	3.2650000000	-10.6933000000	-3.5521000000
O62	8.6876000000	0.8468000000	1.8744000000
O63	13.1435000000	0.4945000000	1.0285000000
O64	6.9734000000	-8.4663000000	-4.6869000000
O65	11.4817000000	-8.7508000000	-5.2482000000
C66	-1.1928000000	-8.6912000000	2.5242000000
C67	-1.8771000000	-7.4628000000	2.6649000000
C68	13.5304000000	-4.9125000000	-2.4881000000
C69	13.7190000000	-3.5559000000	-2.1501000000
C70	14.6867000000	-5.7777000000	-2.5854000000
C71	15.9739000000	-5.2103000000	-2.7391000000
C72	16.1254000000	-3.7883000000	-2.7353000000
C73	15.0145000000	-2.9588000000	-2.4212000000
C74	-1.4883000000	-9.7614000000	3.4583000000
C75	-2.6557000000	-9.6980000000	4.2618000000
C76	-3.5317000000	-8.5726000000	4.1518000000
C77	-3.1542000000	-7.4610000000	3.3545000000
C78	-2.9776000000	-10.7618000000	5.1674000000
C79	-4.1922000000	-10.7547000000	5.9179000000
C80	-5.1219000000	-9.6354000000	5.7521000000
C81	-4.7738000000	-8.5695000000	4.8678000000

C82	17.1161000000	-6.0517000000	-2.9309000000
C83	18.3993000000	-5.4986000000	-3.2196000000
C84	18.5453000000	-4.0443000000	-3.2889000000
C85	17.4054000000	-3.2195000000	-3.0376000000
C86	17.5428000000	-1.8047000000	-3.0972000000
C87	16.3936000000	-0.9904000000	-2.8725000000
C88	15.1850000000	-1.5495000000	-2.5444000000
C89	19.7684000000	-3.4245000000	-3.5857000000
C90	19.8925000000	-2.0385000000	-3.6498000000
C91	18.7907000000	-1.2258000000	-3.4120000000
C92	14.5885000000	-7.1887000000	-2.4090000000
C93	15.6834000000	-8.0059000000	-2.5240000000
C94	16.9631000000	-7.4642000000	-2.8495000000
C95	18.0713000000	-8.3090000000	-3.0638000000
C96	19.3099000000	-7.7603000000	-3.3700000000
C97	19.4681000000	-6.3788000000	-3.4433000000
C98	-5.6731000000	-7.4782000000	4.7023000000
C99	-5.3304000000	-6.4340000000	3.7936000000
C100	-4.1181000000	-6.4306000000	3.1529000000
C101	-0.5718000000	-10.8261000000	3.6978000000
C102	-0.8465000000	-11.8321000000	4.5881000000
C103	-2.0719000000	-11.8496000000	5.3174000000
C104	-6.3425000000	-9.5608000000	6.4406000000
C105	-7.2170000000	-8.4887000000	6.2738000000
C106	-6.8966000000	-7.4515000000	5.4058000000
C107	-2.3738000000	-12.9095000000	6.2004000000
C108	-3.5612000000	-12.8936000000	6.9215000000
C109	-4.4526000000	-11.8318000000	6.7802000000
C110	18.9331000000	0.2474000000	-3.5081000000
N111	17.7581000000	0.9720000000	-3.3033000000
C112	16.4833000000	0.4875000000	-3.0165000000
C113	15.5247000000	-9.4669000000	-2.2980000000
N114	16.6689000000	-10.2238000000	-2.5431000000
C115	17.9251000000	-9.7811000000	-2.9608000000
C116	-7.8484000000	-6.3259000000	5.2206000000
N117	-7.4585000000	-5.3698000000	4.2831000000
C118	-6.2901000000	-5.3304000000	3.5230000000
C119	0.1606000000	-12.9083000000	4.7888000000
N120	-0.2352000000	-13.9268000000	5.6560000000
C121	-1.4291000000	-14.0409000000	6.3708000000
O122	1.2527000000	-12.9337000000	4.2442000000
O123	-1.6464000000	-15.0147000000	7.0795000000
O124	-8.9091000000	-6.2213000000	5.8170000000
O125	-6.1009000000	-4.4397000000	2.7121000000

O126	14.4888000000	-9.9965000000	-1.9315000000
O127	18.8224000000	-10.5751000000	-3.1904000000
O128	15.5366000000	1.2479000000	-2.8946000000
O129	19.9829000000	0.8178000000	-3.7575000000
H130	-0.3158000000	-11.0034000000	1.2828000000
H131	3.3070000000	-8.1425000000	-3.5448000000
H132	-2.3049000000	-4.8370000000	3.4167000000
H133	2.4252000000	-1.9870000000	-0.2948000000
H134	6.1941000000	-6.4606000000	-3.3970000000
H135	12.7932000000	-7.0673000000	-4.0108000000
H136	7.2519000000	-0.9754000000	0.8529000000
H137	13.7780000000	-1.3349000000	-0.5075000000
H138	-0.8886000000	-0.5266000000	2.6201000000
H139	2.2573000000	-12.5091000000	-2.2229000000
H140	11.0797000000	1.4381000000	1.9971000000
H141	9.1127000000	-9.4055000000	-5.4998000000
H142	14.3484000000	-0.8726000000	-2.4443000000
H143	20.6482000000	-4.0250000000	-3.7775000000
H144	20.8406000000	-1.5688000000	-3.8872000000
H145	13.6530000000	-7.6518000000	-2.1243000000
H146	20.1456000000	-8.4299000000	-3.5428000000
H147	20.4505000000	-5.9909000000	-3.6799000000
H148	-3.9441000000	-5.6360000000	2.4423000000
H149	0.3973000000	-10.8497000000	3.2194000000
H150	-6.6261000000	-10.3498000000	7.1248000000
H151	-8.1592000000	-8.4441000000	6.8094000000
H152	-3.7700000000	-13.7203000000	7.5927000000
H153	-5.3670000000	-11.8554000000	7.3582000000
H154	17.8404000000	1.9796000000	-3.3867000000
H155	16.5673000000	-11.2276000000	-2.4372000000
H156	-8.1083000000	-4.6038000000	4.1378000000
H157	0.4248000000	-14.6875000000	5.7769000000
H158	2.8310000000	-5.9007000000	-2.6286000000
H159	3.2448000000	-2.4218000000	-2.6618000000
H160	5.7170000000	-2.6697000000	-3.4913000000
H161	6.8021000000	-2.9324000000	-0.5482000000

Restricted Singlet Excited State   1:   2.0202 eV   613.71 nm

```
 excitation    X coeff.
------------  ---------
 426 => 429   -0.16415
 428 => 429    0.96399
 428 => 430    0.11237
```

Transition dipole moment (debye):
   X= -2.4581   Y= -4.6548   Z= -0.1326 Tot=   5.2656

Oscillator strength, f=   0.2124

Restricted Singlet Excited State   2:   2.0733 eV   597.99 nm

 excitation   X coeff.
------------ ---------
 426 => 430   0.10038
 427 => 429   0.13134
 428 => 430   -0.96840

Transition dipole moment (debye):
   X= -0.7879   Y=   2.5285   Z= -0.4321 Tot=   2.6834

Oscillator strength, f=   0.0566

Restricted Singlet Excited State   3:   2.1479 eV   577.23 nm

 excitation   X coeff.
------------ ---------
 426 => 430   -0.11938
 427 => 429   0.95377
 427 => 430   -0.15092
 428 => 430   0.10917

Transition dipole moment (debye):
   X= -1.2960   Y= -4.2297   Z= -0.8430 Tot=   4.5034

Oscillator strength, f=   0.1652

Restricted Singlet Excited State   4:   2.2188 eV   558.80 nm

 excitation   X coeff.
------------ ---------
 426 => 429   0.26159
 426 => 430   0.23195
 427 => 429   -0.14039
 427 => 430   -0.90644

Transition dipole moment (debye):
   X=   2.7209   Y= -2.8519   Z= -1.0031 Tot=   4.0673

Oscillator strength, f=   0.1392

Restricted Singlet Excited State   5:   2.2936 eV   540.57 nm

 excitation   X coeff.
 -----------   ---------
 425 => 430   -0.19052
 426 => 429   -0.62894
 426 => 430   -0.52488
 427 => 430   -0.33104
 428 => 429   -0.10374
 428 => 431   0.25647
 428 => 432   -0.25137

Transition dipole moment (debye):
   X= -2.3929   Y= -0.3923   Z=   0.3238 Tot=   2.4464

Oscillator strength, f=   0.0521

Restricted Singlet Excited State   6:   2.3544 eV   526.61 nm

 excitation   X coeff.
 -----------   ---------
 425 => 429   0.45932
 426 => 429   -0.49478
 426 => 430   0.50079
 427 => 429   0.12084
 427 => 431   0.29050
 427 => 432   0.14290
 428 => 429   -0.12688
 428 => 431   -0.10487
 428 => 432   0.30924

Transition dipole moment (debye):
   X= -2.0625   Y= -0.6555   Z=   0.1103 Tot=   2.1670

Oscillator strength, f=   0.0419

Restricted Singlet Excited State   7:   2.3945 eV   517.79 nm

  excitation   X coeff.
------------   ---------
 423 => 429   -0.14731
 423 => 430   0.12036
 424 => 429   0.32386
 424 => 430   0.18266
 425 => 429   0.27360
 425 => 430   -0.27876
 426 => 429   0.21297
 426 => 431   -0.10139
 427 => 431   0.23098
 427 => 432   0.26245
 428 => 429   0.11105
 428 => 431   0.64776
 428 => 432   -0.13692

Transition dipole moment (debye):
   X=   5.4252   Y=   0.8649   Z=   -1.4099 Tot=   5.6717

Oscillator strength, f=   0.2921

Restricted Singlet Excited State   8:   2.4258 eV   511.11 nm

  excitation   X coeff.
------------   ---------
 424 => 429   -0.14338
 424 => 430   -0.35070
 425 => 429   0.37670
 426 => 429   0.30832
 426 => 430   -0.49884
 426 => 432   -0.11653
 427 => 431   0.19890
 428 => 432   0.49113
 428 => 434   0.10462

Transition dipole moment (debye):
   X=   -3.2305   Y=   -1.7430   Z=   1.5387 Tot=   3.9801

Oscillator strength, f=   0.1457

Restricted Singlet Excited State 9:   2.4748 eV   500.99 nm

 excitation   X coeff.
------------ ---------
 423 => 429   0.30505
 423 => 430   -0.29418
 424 => 429   -0.47094
 424 => 430   -0.39132
 425 => 430   0.11976
 426 => 429   0.11899
 426 => 430   0.24671
 428 => 431   0.40341
 428 => 432   -0.31728
 428 => 434   0.12878

Transition dipole moment (debye):
   X= -3.3967   Y= -0.1239   Z=   3.6290 Tot=   4.9722

Oscillator strength, f=   0.2320

Restricted Singlet Excited State 10:   2.4878 eV   498.37 nm

 excitation   X coeff.
------------ ---------
 423 => 429   -0.73578
 423 => 430   0.21400
 424 => 430   -0.44767
 425 => 429   0.11227
 425 => 430   0.10751
 427 => 433   -0.22417
 428 => 432   -0.24433
 428 => 434   0.16764

Transition dipole moment (debye):
   X=   3.1459   Y= -0.9863   Z=   0.7357 Tot=   3.3780

Oscillator strength, f=   0.1077

Compound **3**

B3LYP/6-31G** optimized geometry
Final total energy = -5702.103341

angstroms

atom	x	y	z
C1	-0.0754070000	-0.1291650000	0.1347610000
C2	1.3569270000	-0.1996010000	0.1912860000
C3	2.0903380000	1.0213810000	0.2180720000
C4	1.4008570000	2.2680980000	0.2564910000
C5	0.0352780000	2.3119780000	0.1472900000
C6	-0.7352130000	1.1223750000	0.0095670000
C7	2.0498950000	-1.4592640000	0.1594460000
C8	3.4594910000	-1.4376740000	0.0075990000
C9	4.1495870000	-0.2157840000	0.0798240000
C10	3.4976830000	0.9951880000	0.2113890000
C11	-0.8522000000	-1.3300530000	0.1667250000
C12	-0.1846220000	-2.5952020000	0.2065240000
C13	1.2435680000	-2.6854420000	0.2660660000
C14	-2.2700980000	-1.2577190000	0.2180440000
C15	-3.0079760000	-2.4728240000	0.1246510000
C16	-2.3859160000	-3.6951170000	0.1388890000
C17	-0.9656070000	-3.7869690000	0.2421570000
C18	-0.3430450000	-5.0453230000	0.3819770000
C19	1.0338310000	-5.1111800000	0.5376100000
C20	1.8063890000	-3.9516340000	0.4877250000
C21	4.3486520000	-2.5991090000	-0.3233630000
C22	6.2377610000	-4.0360760000	0.2059090000
C23	7.1444270000	-5.6901110000	-1.4854880000
C24	8.1482270000	-5.5798640000	-2.4795720000
C25	8.5747680000	-4.3104730000	-3.0892030000
C26	8.2678280000	-3.0544560000	-2.5440920000
C27	8.8041170000	-6.7803740000	-2.9184290000
C28	9.6967680000	-6.7759500000	-4.0412050000
C29	9.8833940000	-5.5734460000	-4.7927610000
C30	9.3756380000	-4.3423780000	-4.2749880000
C31	6.9204750000	-6.9254930000	-0.8535650000
C32	7.6049280000	-8.0726280000	-1.2160580000
C33	8.5389770000	-8.0195250000	-2.2702100000
C34	9.1823850000	-9.2093160000	-2.7205780000
C35	10.0767850000	-9.1707500000	-3.7602760000
C36	10.3867070000	-7.9535880000	-4.4310190000
C37	9.7190390000	-3.1236660000	-4.9287220000

175

C38	9.3324470000	-1.8848350000	-4.3717450000
C39	8.6344430000	-1.8639460000	-3.1731050000
C40	10.5983970000	-5.6048750000	-6.0166340000
C41	10.9091320000	-4.3670630000	-6.6480720000
C42	10.5014630000	-3.1675720000	-6.1207390000
C43	-3.2185890000	-4.9276500000	0.0433400000
N44	-2.5169720000	-6.1216000000	0.1839890000
C45	-1.1464430000	-6.2949990000	0.3764410000
C46	4.2924260000	2.2480880000	0.3018160000
N47	3.5418600000	3.4155650000	0.4128640000
C48	2.1547810000	3.5433730000	0.4168130000
C49	10.9166020000	-1.9071320000	-6.7991100000
N50	10.4612040000	-0.7376160000	-6.1964440000
C51	9.6973140000	-0.6063530000	-5.0366620000
C52	7.3147640000	-9.3510290000	-0.5146360000
N53	7.9776130000	-10.4669250000	-1.0211300000
C54	8.8726720000	-10.5224900000	-2.0875330000
O55	-4.4250890000	-4.9219430000	-0.1361520000
O56	-0.6692550000	-7.4091250000	0.5114110000
O57	1.6265820000	4.6352450000	0.5390610000
O58	5.5114870000	2.2796240000	0.2947310000
O59	9.3758300000	0.4939670000	-4.6199390000
O60	11.6006540000	-1.8704720000	-7.8085280000
O61	6.5471760000	-9.4479690000	0.4280510000
O62	9.3560160000	-11.5829920000	-2.4469460000
C63	-2.1784210000	1.1724640000	-0.1322080000
C64	-2.9308010000	0.0334260000	0.2344320000
C65	11.2639120000	-7.9283690000	-5.5903230000
C66	11.1365430000	-6.8593760000	-6.5053060000
C67	12.2623750000	-8.9452980000	-5.8596110000
C68	12.8165670000	-9.0617720000	-7.1608980000
C69	12.4022220000	-8.1625580000	-8.1935910000
C70	11.5632680000	-7.0648490000	-7.8756310000
C71	-2.8853970000	2.3320780000	-0.6426730000
C72	-4.2845610000	2.4488710000	-0.4406430000
C73	-4.9902310000	1.4208820000	0.2621190000
C74	-4.3216640000	0.2186760000	0.6101150000
C75	-4.9968060000	3.5910870000	-0.9285140000
C76	-6.3875140000	3.7678140000	-0.6546880000
C77	-7.0827620000	2.7725290000	0.1655640000
C78	-6.3693530000	1.6131200000	0.5986030000
C79	13.7817340000	-10.0785630000	-7.4528080000
C80	14.2719720000	-10.2742840000	-8.7799270000
C81	13.7714090000	-9.4154480000	-9.8562180000

C82	12.8506880000	-8.3711980000	-9.5372680000
C83	12.3686980000	-7.5210910000	-10.5724400000
C84	11.4391700000	-6.4870560000	-10.2475870000
C85	11.0607690000	-6.2692210000	-8.9466720000
C86	14.1664030000	-9.5715430000	-11.1917210000
C87	13.6856400000	-8.7398620000	-12.2009030000
C88	12.7904360000	-7.7191000000	-11.9051610000
C89	12.8115070000	-9.7534170000	-4.8227850000
C90	13.7758380000	-10.6952520000	-5.0748830000
C91	14.2580120000	-10.9099350000	-6.4003670000
C92	15.2143360000	-11.9136970000	-6.6634950000
C93	15.6799550000	-12.0966530000	-7.9597150000
C94	15.2145740000	-11.2897940000	-8.9966660000
C95	-7.0395970000	0.6294050000	1.3785330000
C96	-6.3167960000	-0.5203500000	1.8158810000
C97	-5.0121200000	-0.7146980000	1.4372770000
C98	-2.2425770000	3.3003220000	-1.4680660000
C99	-2.9206780000	4.3722590000	-1.9901150000
C100	-4.3064170000	4.5627340000	-1.7082980000
C101	-8.4274350000	2.9073560000	0.5384630000
C102	-9.0731920000	1.9445350000	1.3122690000
C103	-8.3931900000	0.8094340000	1.7372810000
C104	-4.9953660000	5.6831140000	-2.2199570000
C105	-6.3490480000	5.8412500000	-1.9489250000
C106	-7.0295000000	4.8992170000	-1.1787490000
C107	12.2816560000	-6.8501500000	-12.9971380000
N108	11.3522450000	-5.8886990000	-12.6028960000
C109	10.8554670000	-5.6407230000	-11.3251380000
C110	14.3211360000	-11.4844800000	-3.9381050000
N111	15.2447900000	-12.4645480000	-4.2941160000
C112	15.7338180000	-12.7687590000	-5.5648300000
C113	-9.0946730000	-0.1993590000	2.5731260000
N114	-8.3096860000	-1.2758330000	2.9864970000
C115	-6.9671090000	-1.5212540000	2.7066170000
C116	-2.1910050000	5.3278060000	-2.8701940000
N117	-2.9458780000	6.4113030000	-3.3122550000
C118	-4.2888070000	6.6882850000	-3.0556860000
O119	-1.0214570000	5.2008760000	-3.1927700000
O120	-4.8190060000	7.6888750000	-3.5103040000
O121	-10.2676220000	-0.1156030000	2.8987810000
O122	-6.3977660000	-2.4965020000	3.1683620000
O123	13.9989200000	-11.3162050000	-2.7737380000
O124	16.5401650000	-13.6702740000	-5.7265980000
O125	10.0109400000	-4.7820460000	-11.1361500000

O126	12.6246080000	-6.9507040000	-14.1637310000
H127	-0.4401100000	3.2788720000	0.2141230000
H128	5.2301290000	-0.2057580000	0.0096500000
H129	-4.0811680000	-2.4646860000	0.0011050000
H130	1.4958410000	-6.0783660000	0.6937880000
H131	6.1730290000	-7.0020120000	-0.0735880000
H132	10.4879020000	-10.1116600000	-4.0923040000
H133	8.3767400000	-0.9056160000	-2.7386890000
H134	11.5370910000	-4.3305920000	-7.5264940000
H135	-3.0680660000	-6.9729920000	0.1524420000
H136	4.0647250000	4.2813510000	0.4955570000
H137	10.7233550000	0.1311930000	-6.6505200000
H138	7.7796070000	-11.3522180000	-0.5662840000
H139	10.3199510000	-5.5025880000	-8.7691550000
H140	14.8628590000	-10.3540160000	-11.4634600000
H141	13.9981400000	-8.8718980000	-13.2295410000
H142	12.5224140000	-9.6099340000	-3.7923800000
H143	16.4112040000	-12.8744470000	-8.1427570000
H144	15.6055910000	-11.4645340000	-9.9905610000
H145	-4.5083180000	-1.5800880000	1.8408790000
H146	-1.2079530000	3.1870680000	-1.7557170000
H147	-8.9918560000	3.7772640000	0.2291840000
H148	-10.1117410000	2.0617350000	1.5967200000
H149	-6.8600310000	6.7075080000	-2.3509060000
H150	-8.0828130000	5.0596870000	-0.9945150000
H151	10.9801230000	-5.2982450000	-13.3395200000
H152	15.6113920000	-13.0306780000	-3.5359020000
H153	-8.7686780000	-1.9658190000	3.5719510000
H154	-2.4622600000	7.0850590000	-3.8969460000
H155	7.7371960000	-2.9903900000	-1.6075150000
C156	4.3071060000	-3.1734530000	-1.6017230000
C157	5.2190250000	-4.1557340000	-1.9717590000
C158	6.2056380000	-4.5953270000	-1.0780070000
C159	5.3286370000	-3.0437060000	0.5742970000
H160	5.1745310000	-4.5833830000	-2.9679780000
H161	5.3905180000	-2.5990120000	1.5624120000
H162	3.5652000000	-2.8330950000	-2.3165500000
H163	6.9869790000	-4.3691020000	0.9173780000
H164	2.8688330000	-4.0464010000	0.6366290000

Restricted Singlet Excited State   1:   2.1416 eV   578.94 nm

  excitation   X coeff.
  ------------ ---------

```
426 => 428    0.21715
426 => 429   -0.33885
427 => 428   -0.89305
```

Transition dipole moment (debye):
  X=   3.7429   Y=   4.5116   Z=   -3.1969 Tot=   6.6772

Oscillator strength, f=   0.3621

Restricted Singlet Excited State   2:   2.1458 eV   577.81 nm

```
 excitation    X coeff.
------------   ---------
 426 => 428    0.54213
 426 => 429    0.18658
 427 => 428    0.14743
 427 => 429    0.78828
```

Transition dipole moment (debye):
  X=   1.3671   Y=   -1.2683   Z=   2.4088 Tot=   3.0463

Oscillator strength, f=   0.0755

Restricted Singlet Excited State   3:   2.2113 eV   560.68 nm

```
 excitation    X coeff.
------------   ---------
 425 => 429   -0.13221
 426 => 428    0.78924
 427 => 428    0.11590
 427 => 429   -0.57344
```

Transition dipole moment (debye):
  X=   0.3457   Y=   0.3838   Z=   -0.0888 Tot=   0.5241

Oscillator strength, f=   0.0023

Restricted Singlet Excited State   4:   2.2222 eV   557.93 nm

```
 excitation    X coeff.
------------   ---------
```

```
425 => 428   -0.12654
426 => 429    0.90116
427 => 428   -0.37045
427 => 429   -0.10473
```

Transition dipole moment (debye):
  X=   0.2429   Y= -2.6343   Z=   1.2135 Tot=   2.9105

Oscillator strength, f=   0.0714

Restricted Singlet Excited State   5:   2.3736 eV   522.35 nm

```
 excitation    X coeff.
 ------------  ---------
 424 => 429   -0.44500
 425 => 428    0.62889
 425 => 429    0.25285
 426 => 430    0.12315
 426 => 431    0.34740
 427 => 430    0.42971
```

Transition dipole moment (debye):
  X= -1.2990   Y=   0.5457   Z=   0.0796 Tot=   1.4113

Oscillator strength, f=   0.0179

Restricted Singlet Excited State   6:   2.3805 eV   520.84 nm

```
 excitation    X coeff.
 ------------  ---------
 424 => 428    0.53699
 425 => 428    0.18687
 425 => 429   -0.55671
 426 => 430   -0.37766
 426 => 431    0.12504
 427 => 431   -0.43257
```

Transition dipole moment (debye):
  X= -0.0279   Y=   0.4387   Z= -0.2946 Tot=   0.5292

Oscillator strength, f=   0.0025

Restricted Singlet Excited State   7:   2.4553 eV   504.97 nm

 excitation   X coeff.
 ------------   ---------
 422 => 428   0.21567
 422 => 429   -0.55096
 423 => 428   -0.64647
 423 => 429   -0.21384
 424 => 429   0.15566
 425 => 428   0.18015
 426 => 431   -0.11660
 426 => 433   -0.14054
 427 => 430   -0.18296
 427 => 432   0.14555

Transition dipole moment (debye):
   X=   -6.9126   Y=   4.7119   Z=   2.4833 Tot=   8.7266

Oscillator strength, f=   0.7091

Restricted Singlet Excited State   8:   2.4847 eV   499.00 nm

 excitation   X coeff.
 ------------   ---------
 422 => 428   -0.64190
 423 => 429   -0.64581
 424 => 428   0.14741
 425 => 429   0.17110
 426 => 432   0.17736
 426 => 433   -0.11488
 427 => 432   -0.11685
 427 => 433   -0.17883

Transition dipole moment (debye):
   X=   0.7898   Y=   -0.0986   Z=   2.5585 Tot=   2.6795

Oscillator strength, f=   0.0676

Restricted Singlet Excited State   9:   2.5476 eV   486.67 nm

 excitation   X coeff.

```
------------   ---------
 422 => 428    0.12856
 422 => 429   -0.21637
 423 => 428   -0.19102
 424 => 428    0.12069
 424 => 429   -0.30567
 425 => 428   -0.67818
 426 => 429   -0.10133
 426 => 431    0.14780
 427 => 430    0.49552
 427 => 431   -0.11149
```

Transition dipole moment (debye):
   X=   0.4325   Y=   1.1981   Z=   1.3948 Tot=   1.8889

Oscillator strength, f=   0.0345

Restricted Singlet Excited State 10:   2.5556 eV   485.15 nm

```
 excitation    X coeff.
------------   ---------
 422 => 428   -0.17269
 423 => 429   -0.14142
 424 => 428   -0.37371
 424 => 429   -0.12940
 425 => 429   -0.72693
 426 => 430    0.15279
 427 => 430    0.19027
 427 => 431    0.40367
```

Transition dipole moment (debye):
   X=   1.3838   Y=   0.3714   Z=   0.3500 Tot=   1.4749

Oscillator strength, f=   0.0211

Restricted Singlet Excited State 11:   2.5972 eV   477.38 nm

```
 excitation    X coeff.
------------   ---------
 424 => 428   -0.71667
 426 => 430   -0.45574
 427 => 431   -0.49547
```

Transition dipole moment (debye):
   X=   -1.2024   Y=   -0.2531   Z=   1.2462 Tot=   1.7501

Oscillator strength, f=   0.0302

Restricted Singlet Excited State 12:   2.6106 eV   474.93 nm

 excitation   X coeff.
 -----------   ---------
 424 => 429   0.80174
 426 => 431   0.22666
 427 => 430   0.52459

Transition dipole moment (debye):
   X=   2.2288   Y=   0.8224   Z=   1.8689 Tot=   3.0228

Oscillator strength, f=   0.0905

Restricted Singlet Excited State 13:   2.6475 eV   468.31 nm

 excitation   X coeff.
 -----------   ---------
 425 => 429   0.16353
 426 => 430   -0.75665
 427 => 431   0.59886

Transition dipole moment (debye):
   X=   -0.4639   Y=   -0.0540   Z=   0.0290 Tot=   0.4679

Oscillator strength, f=   0.0022

Restricted Singlet Excited State 14:   2.6542 eV   467.12 nm

 excitation   X coeff.
 -----------   ---------
 425 => 428   0.17384
 426 => 431   -0.85985
 427 => 430   0.43935

Transition dipole moment (debye):

X=   -0.3011   Y=   -0.1048   Z=   -1.4808 Tot=   1.5147

Oscillator strength, f=   0.0231

Restricted Singlet Excited State 15:   2.7158 eV   456.53 nm

 excitation   X coeff.
------------ ---------
 422 => 428   0.50682
 422 => 429   -0.26032
 423 => 428   0.59292
 423 => 429   -0.55661

Transition dipole moment (debye):
  X=   -0.1406   Y=   0.0210   Z=   -0.2430 Tot=   0.2816

Oscillator strength, f=   0.0008

1.8. References

(1)   Smith, K. R.; Frumkin, H.; Balakrishnan, K.; Butler, C. D.; Chafe, Z. A.; Fairlie, I.; Kinney, P.; Kjellstrom, T.; Mauzerall, D. L.; McKone, T. E.; McMichael, A. J.; Schneider, M. *Annu. Rev. Public Health* **2013**, *34* (1), 159–188.

(2)   Xie, S.-P.; Deser, C.; Vecchi, G. A.; Collins, M.; Delworth, T. L.; Hall, A.; Hawkins, E.; Johnson, N. C.; Cassou, C.; Giannini, A.; Watanabe, M. *Nat. Clim. Chang.* **2015**, *5* (10), 921–930.

(3)   *BP Statistical Review of World Energy 2017*; BP: London, UK, 2017.

(4)   *Compendium of Scientific, Medical, and Media Findings Demonstrating Risks and Harms of Fracking (Unconventional Gas and Oil Extraction) (5ᵗʰ ed.)*; Concerned Health Professionals of NY, Physicians for Social Responsibility: New York, NY, 2018.

(5)   Green, M. A.; Hishikawa, Y.; Dunlop, E. D.; Levi, D. H.; Hohl-Ebinger, J.; Ho-Baillie, A. W. Y. *Prog. Photovoltaics Res. Appl.* **2018**, *26* (1), 3–12.

(6)   Mori, S.; Oh-Oka, H.; Nakao, H.; Gotanda, T.; Nakano, Y.; Jung, H.; Iida, A.; Hayase, R.; Shida, N.; Saito, M.; Todori, K.; Asakura, T.; Matsui, A.; Hosoya, M. *MRS Proceedings* **2015**, *1737*, mrsf14-1737-u17-02.

(7)   He, Y.; Li, Y. *Phys. Chem. Chem. Phys.* **2011**, *13* (6), 1970–1983.

(8)   Chen, W.; Xu, T.; He, F.; Wang, W.; Wang, C.; Strzalka, J.; Liu, Y.; Wen, J.; Miller, D. J.; Chen, J.; Hong, K.; Yu, L.; Darling, S. B. *Nano Lett.* **2011**, *11* (9), 3707–3713.

(9)   Zhang, J.; Li, Y.; Huang, J.; Hu, H.; Zhang, G.; Ma, T.; Chow, P. C. Y.; Ade, H.; Pan, D.; Yan, H. *J. Am. Chem. Soc.* **2017**, *139* (45), 16092–16095.

(10)   Hedley, G. J.; Ruseckas, A.; Samuel, I. D. W. *Chem. Rev.* **2017**, *117* (2), 796-837.

(11)   Liu, Y.; Mu, C.; Jiang, K.; Zhao, J.; Li, Y.; Zhang, L.; Li, Z.; Lai, J. Y. L.; Hu, H.; Ma, T.; Hu, R.; Yu, D.; Huang, X.; Tang, B. Z.; Yan, H. *Adv. Mater.* **2015**, *27* (6), 1015–1020.

(12)   Lin, H.; Chen, S.; Hu, H.; Zhang, L.; Ma, T.; Lai, J. Y. L.; Li, Z.; Qin, A.; Huang, X.; Tang, B.; Yan, H. *Adv. Mater.* **2016**, *28* (38), 8546–8551.

(13)   Wu, Q.; Zhao, D.; Schneider, A. M.; Chen, W.; Yu, L. *J. Am. Chem. Soc.* **2016**, *138* (23), 7248–7251.

(14)   Meng, D.; Sun, D.; Zhong, C.; Liu, T.; Fan, B.; Huo, L.; Li, Y.; Jiang, W.; Choi, H.; Kim, T.; Kim, J. Y.; Sun, Y.; Wang, Z.; Heeger, A. J. *J. Am. Chem. Soc.* **2015**, *138* (1), 375–380.

(15)   Foertig, A.; Kniepert, J.; Gluecker, M.; Brenner, T.; Dyakonov, V.; Neher, D.; Deibel, C. *Adv. Funct. Mater.* **2014**, *24* (9), 1306–1311.

(16)   Dou, L.; You, J.; Hong, Z.; Xu, Z.; Li, G.; Street, R. A.; Yang, Y. *Adv. Mater.* **2013**, *25* (46), 6642–6671.

(17)   Thompson, B. C.; Fréchet, J. M. J. *Angew. Chemie Int. Ed.* **2008**, *47* (1), 58–77.

(18)   Pivrikas, A.; Sariciftci, N. S.; Juška, G.; Osterbacka, R. *Photovolt Res. Appl* **2007**, *15*, 677–696.

(19)   Holcombe, T. W.; Norton, J. E.; Rivnay, J.; Woo, C. H.; Goris, L.; Piliego, C.; Griffini, G.; Sellinger, A.; Brédas, J.-L.; Salleo, A.; Fréchet, J. M. J. *J. Am. Chem. Soc.* **2011**, *133* (31), 12106–12114.

(20)   Rolczynski, B. S.; Szarko, J. M.; Jung Son, H.; Liang, Y.; Yu, L.; Chen, L. X. *J. Am. Chem. Soc.* **2012**, *134* (9), 4142-4152.

(21)   Liu, J.; Chen, S.; Qian, D.; Gautam, B.; Yang, G.; Zhao, J.; Bergqvist, J.; Zhang, F.; Ma, W.; Ade, H.; Inganäs, O.; Gundogdu, K.; Gao, F.; Yan, H. *Nature Energy* **2016**, *1*, 16089.

(22)   Lu, L.; Yu, L. *Adv. Mater.* **2014**, *26* (26), 4413–4430.

(23)   Graham, K. R.; Cabanetos, C.; Jahnke, J. P.; Idso, M. N.; El Labban, A.; Ngongang Ndjawa, G. O.; Heumueller, T.; Vandewal, K.; Salleo, A.; Chmelka, B. F.; Amassian, A.; Beaujuge, P. M.; McGehee, M. D. *J. Am. Chem. Soc.* **2014**, *136* (27), 9608–9618.

(24)   Zhan, C.; Yao, J. *Chem. Mater.* **2016**, *28* (7), 1948-1964.

(25)   Park, S.; Jeong, J.; Hyun, G.; Kim, M.; Lee, H.; Yi, Y. *Sci. Rep.* **2016**, *6* (1), 35262.

(26)   Ye, T.; Singh, R.; Rgen Butt, H.-J.; Floudas, G.; Keivanidis, P. E. *ACS Appl. Mater. Interfaces* **2013**, *5* (22), 11844-11857.

(27)   Chen, Z.; Baumeister, U.; Tschierske, C.; Würthner, F. *Chem. - A Eur. J.* **2007**, *13* (2), 450–465.

(28)   Keivanidis, P. E.; Howard, I. A.; Friend, R. H. *Adv. Funct. Mater.* **2008**, *18* (20), 3189-3202.

(29)   Howard, I. A.; Laquai, F.; Keivanidis, P. E.; Friend, R. H.; Greenham, N. C. *J. Phys. Chem. C* **2009**, *113* (50), 21225–21232.

(30)   Foster, S.; Finlayson, C. E.; Keivanidis, P. E.; Huang, Y.-S.; Hwang, I.; Friend, R. H.; Otten, M. B. J.; Lu, L.-P.; Schwartz, E.; Nolte, R. J. M.; Rowan, A. E. *Macromolecules* **2009**, *42* (6), 2023–2030.

(31)   Chen, Y.; Zhang, X.; Zhan, C.; Yao, J. *Phys. status solidi* **2015**, *212* (9), 1961–1968.

(32)   Hedley, G. J.; Ward, A. J.; Alekseev, A.; Howells, C. T.; Martins, E. R.; Serrano, L. A.; Cooke, G.; Ruseckas, A.; Samuel, I. D. W. *Nat. Commun.* **2013**, *4*, 2867.

(33)   Hammond, M. R.; Kline, R. J.; Herzing, A. A.; Richter, L. J.; Germack, D. S.; Ro, H.-W.; Soles, C. L.; Fischer, D. A.; Xu, T.; Yu, L.; Toney, M. F.; DeLongchamp, D. M. *ACS Nano* **2011**, *5* (10), 8248–8257.

(34)   Khokhlov, K.; Schuster, N. J.; Ng, F.; Nuckolls, C. *Org. Lett.* **2018**, *20* (7), 1991–1994.

(35)   Zhang, A.; Li, C.; Yang, F.; Zhang, J.; Wang, Z.; Wei, Z.; Li, W. *Angew. Chemie Int. Ed.* **2017**, *56* (10), 2694–2698.

(36)   Li, S.; Liu, W.; Li, C.-Z.; Liu, F.; Zhang, Y.; Shi, M.; Chen, H.; Russell, T. P. *J. Mater. Chem. A* **2016**, *4* (27), 10659–10665.

(37)   Duan, Y.; Xu, X.; Yan, H.; Wu, W.; Li, Z.; Peng, Q. *Adv. Mater.* **2017**, *29* (7), 1605115.

(38)   Jiang, W.; Ye, L.; Li, X.; Xiao, C.; Tan, F.; Zhao, W.; Hou, J.; Wang, Z. *Chem. Commun. (Camb).* **2014**, *50* (8), 1024–1026.

(39)   Zhang, G.; Zhao, J.; Chow, P. C. Y.; Jiang, K.; Zhang, J.; Zhu, Z.; Zhang, J.; Huang, F.; Yan, H. *Chem. Rev.* **2018**, *118* (7), 3447–3507.

(40)   Nakazono, S.; Easwaramoorthi, S.; Kim, D.; Shinokubo, H.; Osuka, A. *Org. Lett.* **2009**, *11* (23), 5426-5429.

(41)   Li, X.; Wang, H.; Schneider, J. A.; Wei, Z.; Lai, W.-Y.; Huang, W.; Wudl, F.; Zheng, Y. *J. Mater. Chem. C* **2017**, *5* (11), 2781–2785.

(42)   Hartnett, P. E.; Timalsina, A.; Matte, H. S. S. R.; Zhou, N.; Guo, X.; Zhao, W.; Facchetti, A.; Chang, R. P. H.; Hersam, M. C.; Wasielewski, M. R.; Marks, T. J. *J. Am. Chem. Soc.* **2014**, *136* (46), 16345–16356.

(43)   Teraoka, T.; Hiroto, S.; Shinokubo, H. *Org. Lett.* **2011**, *13* (10), 2532–2535.

(44)   Zhang, J.; Singh, S.; Hwang, D. K.; Barlow, S.; Kippelen, B.; Marder, S. R. *J. Mater. Chem. C* **2013**, *1*, 5093-5100.

(45)   Wu, J.; He, D.; Zhang, L.; Liu, Y.; Mo, X.; Lin, J.; Zhang, H. *Org. Lett.* **2017**, *19* (19), 5438–5441.

(46)   Zhao, D.; Wu, Q.; Cai, Z.; Zheng, T.; Chen, W.; Lu, J.; Yu, L. *Chem. Mater.* **2016**, *28* (4), 1139–1146.

(47)   Hendsbee, A. D.; Sun, J.-P.; Law, W. K.; Yan, H.; Hill, I. G.; Spasyuk, D. M.; Welch, G. C. *Chem. Mater.* **2016**, *28* (19), 7098–7109.

(48)   Meng, D.; Fu, H.; Xiao, C.; Meng, X.; Winands, T.; Ma, W.; Wei, W.; Fan, B.; Huo, L.; Doltsinis, N. L.; Li, Y.; Sun, Y.; Wang, Z. *J. Am. Chem. Soc.* **2016**, *138* (32), 10184-10190.

(49)   Fan, W.; Liang, N.; Meng, D.; Feng, J.; Li, Y.; Hou, J.; Wang, Z. *Chem. Commun. Chem. Commun* **1150**, *52* (52), 11500–11503.

(50)   Duan, Y.; Xu, X.; Li, Y.; Li, Z.; Peng, Q. *Macromol. Rapid Commun.* **2017**, *38* (23), 1700405.

(51)   Sun, D.; Meng, D.; Cai, Y.; Fan, B.; Li, Y.; Jiang, W.; Huo, L.; Sun, Y.; Wang, Z. *J. Am. Chem. Soc.* **2015**, *137* (34), 11156–11162.

(52)   Hartnett, P. E.; Matte, H. S. S. R.; Eastham, N. D.; Jackson, N. E.; Wu, Y.; Chen, L. X.; Ratner, M. A.; Chang, R. P. H.; Hersam, M. C.; Wasielewski, M. R.; Marks, T. J. *Chem. Sci.* **2016**, *7*, 3543-3555.

(53)   Zhong, H.; Wu, C. H.; Li, C. Z.; Carpenter, J.; Chueh, C. C.; Chen, J. Y.; Ade, H.; Jen, A. K. Y. *Adv. Mater.* **2015**, *28* (5), 951–958.

(54)   Zhong, Y.; Kumar, B.; Oh, S.; Trinh, M. T.; Wu, Y.; Elbert, K.; Li, P.; Zhu, X.; Xiao, S.; Ng, F.; Steigerwald, M. L.; Nuckolls, C. *J. Am. Chem. Soc.* **2014**, *136* (22), 8122–8130.

(55)   Liao, S.-H.; Jhuo, H.-J.; Cheng, Y.-S.; Chen, S.-A. *Adv. Mater.* **2013**, *25* (34), 4766–4771.

(56)   Bhatta, R. S.; Perry, D. S.; Tsige, M. *J. Phys. Chem. A* **2013**, *117* (47), 12628–12634.

(57)   Liang, Y.; Feng, D.; Wu, Y.; Tsai, S.-T.; Li, G.; Ray, C.; Yu, L. *J. Am. Chem. Soc.* **2009**, *131* (22), 7792–7799.

(58)   Lu, L.; Yu, L. *Adv. Mater.* **2014**, *26* (26), 4413–4430.

(59)   Liang, Y.; Xu, Z.; Xia, J.; Tsai, S.-T.; Wu, Y.; Li, G.; Ray, C.; Yu, L. *Adv. Mater.* **2010**, *22* (20), E135–E138.

(60)   Szarko, J. M.; Rolczynski, B. S.; Lou, S. J.; Xu, T.; Strzalka, J.; Marks, T. J.; Yu, L.; Chen, L. X. *Adv. Funct. Mater.* **2014**, *24* (1), 10–26.

(61)   Guo, J.; Liang, Y.; Szarko, J.; Lee, B.; Son, H. J.; Rolczynski, B. S.; Yu, L.; Chen, L. X. *J. Phys. Chem. B* **2010**, *114* (2), 742–748.

(62)   Liu, C.; Wang, K.; Hu, X.; Yang, Y.; Hsu, C.-H.; Zhang, W.; Xiao, S.; Gong, X.; Cao, Y. *ACS Appl. Mater. Interfaces* **2013**, *5* (22), 12163–12167.

(63)   Son, H. J.; Wang, W.; Xu, T.; Liang, Y.; Wu, Y.; Li, G.; Yu, L. *J. Am. Chem. Soc.* **2011**, *133* (6), 1885–1894.

(64)   Rolczynski, B. S.; Szarko, J. M.; Son, H. J.; Liang, Y.; Yu, L.; Chen, L. X. *J. Am. Chem. Soc.* **2012**, *134* (9), 4142–4152.

(65)   Huo, L.; Liu, T.; Sun, X.; Cai, Y.; Heeger, A. J.; Sun, Y. *Adv. Mater.* **2015**, *27* (18), 2938–2944.

(66)   Vandewal, K.; Tvingstedt, K.; Gadisa, A.; Inganäs, O.; Manca, J. V. *Nat. Mater.* **2009**, *8* (11), 904–909.

(67)   Burke, T. M.; Sweetnam, S.; Vandewal, K.; McGehee, M. D. *Adv. Energy Mater.* **2015**, *5* (11), 1500123.

(68)   Tvingstedt, K.; Vandewal, K.; Gadisa, A.; Zhang, F.; Manca, J.; Inganäs, O. *J. Am. Chem. Soc.* **2009**, *131* (33), 11819–11824.

(69)   Heumueller, T.; Burke, T. M.; Mateker, W. R.; Sachs-Quintana, I. T.; Vandewal, K.; Brabec, C. J.; McGehee, M. D. *Adv. Energy Mater.* **2015**, *5* (14), 1500111.

(70)   Vandewal, K.; Albrecht, S.; Hoke, E. T.; Graham, K. R.; Widmer, J.; Douglas, J. D.; Schubert, M.; Mateker, W. R.; Bloking, J. T.; Burkhard, G. F.; Sellinger, A.; Fréchet, J. M. J.; Amassian, A.; Riede, M. K.; McGehee, M. D.; Neher, D.; Salleo, A. *Nat. Mater.* **2014**, *13* (1), 63–68.

(71)   Li, Y.; Wang, C.; Li, C.; Di Motta, S.; Negri, F.; Wang, Z. *Org. Lett.* **2012**, *14* (20), 5278–5281.

(72)   Sisto, T. J.; Zhong, Y.; Zhang, B.; Trinh, M. T.; Miyata, K.; Zhong, X.; Zhu, X.-Y.; Steigerwald, M. L.; Ng, F.; Nuckolls, C. *J. Am. Chem. Soc.* **2017**, *139* (16), 5648-5651.

(73)   Zhong, Y.; Trinh, M. T.; Chen, R.; Wang, W.; Khlyabich, P. P.; Kumar, B.; Xu, Q.; Nam, C.-Y.; Sfeir, M. Y.; Black, C.; Steigerwald, M. L.; Loo, Y.-L.; Xiao, S.; Ng, F.; Zhu, X.-Y.; Nuckolls, C. *J. Am. Chem. Soc.* **2014**, *136* (43), 15215–15221.

(74)   Zhong, Y.; Trinh, M. T.; Chen, R.; Purdum, G. E.; Khlyabich, P. P.; Sezen, M.; Oh, S.; Zhu, H.; Fowler, B.; Zhang, B.; Wang, W.; Nam, C.-Y.; Sfeir, M. Y.; Black, C. T.; Steigerwald, M. L.; Loo, Y.-L.; Ng, F.; Zhu, X.-Y.; Nuckolls, C. *Nat. Commun.* **2015**, *6*, 8242.

(75)   Castro, E.; Sisto, T. J.; Romero, E. L.; Liu, F.; Peurifoy, S. R.; Wang, J.; Zhu, X.; Nuckolls, C.; Echegoyen, L. *Angew. Chemie Int. Ed.* **2017**, *56* (46), 14648–14652.

(76)   Zhong, Y.; Sisto, T. J.; Zhang, B.; Miyata, K.; Zhu, X.-Y.; Steigerwald, M. L.; Ng, F.; Nuckolls, C. *J. Am. Chem. Soc.* **2017**, *139* (16), 5644-5647.

(77)   McAfee, S. M.; Topple, J. M.; Hill, I. G.; Welch, G. C. *J. Mater. Chem. A* **2015**, *3* (32), 16393–16408.

(78)   Namepetra, A.; Kitching, E.; Eftaiha, A. F.; Hill, I. G.; Welch, G. C. *Phys. Chem. Chem. Phys.* **2016**, *18* (18), 12476–12485.

(79)   Lin, H.; Chen, S.; Hu, H.; Zhang, L.; Ma, T.; Lai, J. Y. L.; Li, Z.; Qin, A.; Huang, X.; Tang, B.; Yan, H. *Adv. Mater.* **2016**, *28* (38), 8546–8551.

(80)   Meng, D.; Sun, D.; Zhong, C.; Liu, T.; Fan, B.; Huo, L.; Li, Y.; Jiang, W.; Choi, H.; Kim, T.; Kim, J. Y.; Sun, Y.; Wang, Z.; Heeger, A. J. *J. Am. Chem. Soc.* **2016**, *138* (1), 375–380.

(81)   Shastry, T. A.; Hartnett, P. E.; Wasielewski, M. R.; Marks, T. J.; Hersam, M. C. *ACS Energy Lett.* **2016**, *1* (3), 548–555.

(82)   Hartnett, P. E.; Mauck, C. M.; Harris, M. A.; Young, R. M.; Wu, Y.-L.; Marks, T. J.; Wasielewski, M. R. *J. Am. Chem. Soc.* **2017**, *139* (2), 749–756.

(83)   Logsdon, J. L.; Hartnett, P. E.; Nelson, J. N.; Harris, M. A.; Marks, T. J.; Wasielewski, M. R. *ACS Appl. Mater. Interfaces* **2017**, *9* (39), 33493–33503.

(84)   Mickley Conron, S. M.; Shoer, L. E.; Smeigh, A. L.; Ricks, A. B.; Wasielewski, M. R. *J. Phys. Chem. B* **2013**, *117* (7), 2195–2204.

(85)   Fukuzumi, S.; Ohkubo, K.; Suenobu, T. *Acc. Chem. Res.* **2014**, *47* (5), 1455–1464.

(86)   Guldi, D. M. *Chem. Soc. Rev.* **2002**, *31* (1), 22–36.

(87)   Zhou, H.; Yang, L.; You, W. *Macromolecules* **2012**, *45* (2), 607–632.

(88)   Ajayaghosh, A. *Chem. Soc. Rev.* **2003**, *32* (4), 181–191.

(89)   Busby, E.; Xia, J.; Wu, Q.; Low, J. Z.; Song, R.; Miller, J. R.; Zhu, X.-Y.; Campos, L. M.; Sfeir, M. Y. *Nat. Mater.* **2015**, *14* (4), 426–433.

(90)   Fukuzumi, S.; Kotani, H.; Ohkubo, K.; Ogo, S.; Tkachenko, N. B.; Lemmetyinen, H. *J. Am. Chem. Soc.* **2004**, *126* (6), 1600-1601.

189

(91)   Fukuzumi, S.; Doi, K.; Itoh, A.; Suenobu, T.; Ohkubo, K.; Yamada, Y.; Karlin, K. D. *Proc. Natl. Acad. Sci. U. S. A.* **2012**, *109* (39), 15572–15577.

(92)   Sasaki, S.; Drummen, G. P. C.; Konishi, G. *J. Mater. Chem. C* **2016**, *4* (14), 2731–2743.

(93)   Yang, W.; Zhao, J.; Sonn, C.; Escudero, D.; Karatay, A.; Yaglioglu, H Gul; Küçüköz, B.; Hayvali, M.; Li, C.; Jacquemin, D. *J Phys. Chem. C* **2016**, *120* (19), 10162-10175.

(94)   Smith, M. B.; Michl, J. *Chem. Rev.* **2010**, *110* (11), 6891–6936.

(95)   Chan, W.-L.; Ligges, M.; Zhu, X.-Y. *Nat. Chem.* **2012**, *4* (10), 840–845.

(96)   Lee, J. K.; Ma, W. L.; Brabec, C. J.; Yuen, J; Moon, J. S.; Kim, J. Y.; Lee, K.; Bazan, G. C.; Heeger, A. J. *J. Am. Chem. Soc.* **2008**, *130* (11), 3619-3623.

(97)   Graham, K. R.; Wieruszewski, P. M.; Stalder, R.; Hartel, M. J.; Mei, J.; So, F.; Reynolds, J. R. *Adv. Funct. Mater.* **2012**, *22* (22), 4801–4813.

(98)   Guo, X.; Cui, C.; Zhang, M.; Huo, L.; Huang, Y.; Hou, J.; Li, Y. *Energy Environ. Sci.* **2012**, *5* (7), 7943.

Chapter 2. Controlling the Morphology of Perylene Diimide-Based Materials via Facile Side Chain Engineering

Diverge at first step: inefficient

Diverge at final step: efficient
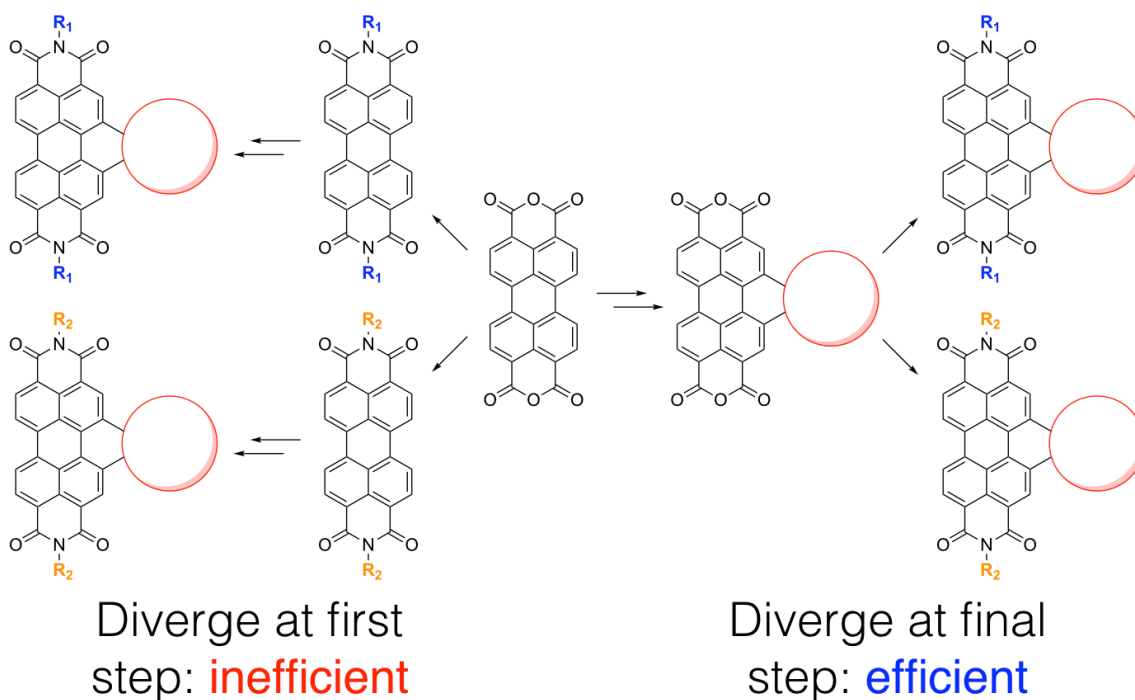
2.1. Preface

This chapter presents work on the side chain engineering of N-type organic semiconductors based on perylene-3,4,9,10-tetracarboxylic acid diimide (PDI). The imide side chains of these materials have a profound effect on their processing characteristics and solid-state properties. However, these side chains are installed in the first step of making PDI-based materials, and there are no known methods for swapping one side chain for another. Therefore, making multiple variations of the same material with different side chains to optimize their properties for applications in devices is an onerous task. Here, we build up the aromatic core of PDI-based materials using perylene-3,4,9,10-tetracarboxylic acid tetraester (PTE). This allows us to make PDI-based materials in

which the imide side chain is installed in the final step, enabling the rapid screening of various side chains. We apply this strategy to cove-edge graphene nanoribbons of PDI that we call hPDI. The resulting materials exhibit stark differences in their solubility, aggregation, conductivity in thin films, and phase transitions, demonstrating the value of this technique in tuning the side chains of PDI-based materials.

This chapter is based on a publication in preparation entitled "Controlling Aggregation in PDI-Based Materials via Facile Side Chain Engineering" by Grisha Etkin, Neil Foegen, Raúl Hernández Sánchez, Fay Ng, Michael L. Steigerwald, and Colin Nuckolls. For this work, I synthesized all of the compounds. Neil Foegen and I performed UV-Vis experiments. Neil Foegen fabricated all devices. Sebastian Russell performed all differential scanning calorimetry.

2.2. Side Chain Engineering of Organic Materials

Here we present a method for controlling the bulk morphology and processing characteristics of organic semiconductors based on perylene-3,4,9,10-tetracarboxylic acid diimide (PDI). We have developed a strategy for synthesizing these materials in which the imide side chains are introduced in the final synthetic step, allowing us to readily study the effect of these side chains on aggregation, optical properties, electron mobility, and phase transitions in the solid state. PDI has numerous advantageous properties for organic electronics as result of its aromatic core consisting of electron-rich perylene with electron-withdrawing imide substituents (Figure 2.1). (1) It is highly absorbent, with a sharp absorption edge. (2) It is highly fluorescent, with quantum yield greater than 90%.[1] (3) It is reversibly reducible and its radical anion PDI$^-$ is stabilized by delocalization.[2] (4) It acts as an N-type semiconductor, with electron mobilities greater than 1 cm^2 V^{-1} s^{-1}.[3] (5) It is thermally, chemically, and photochemically stable.[4] The latter property has been especially advantageous for its use as an industrial pigment and as an electron acceptor for organic photovoltaics (OPVs).[5,6] PDI-based materials have also been used in many other applications such as photoredox catalysis,[7] ultra-narrowband photodectors,[8] as the cathodic material in batteries,[9] as the electron transport material in perovskite solar cells,[10,11] fluorescence spectroscopy,[12] organic field effect transistors (OFETs),[13] and supramolecular chemistry.[14]
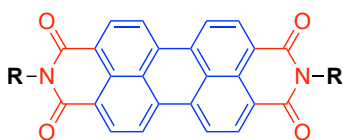
Figure 2.1. Structure of PDI, highlighting the electron-rich perylene core in blue and the electron-withdrawing imides in red. Although the imide side chains R have minimal influence on the frontier orbitals associated with the all-sp^2 perylene-imide core, they influence the solubility and solid state properties of the molecule.
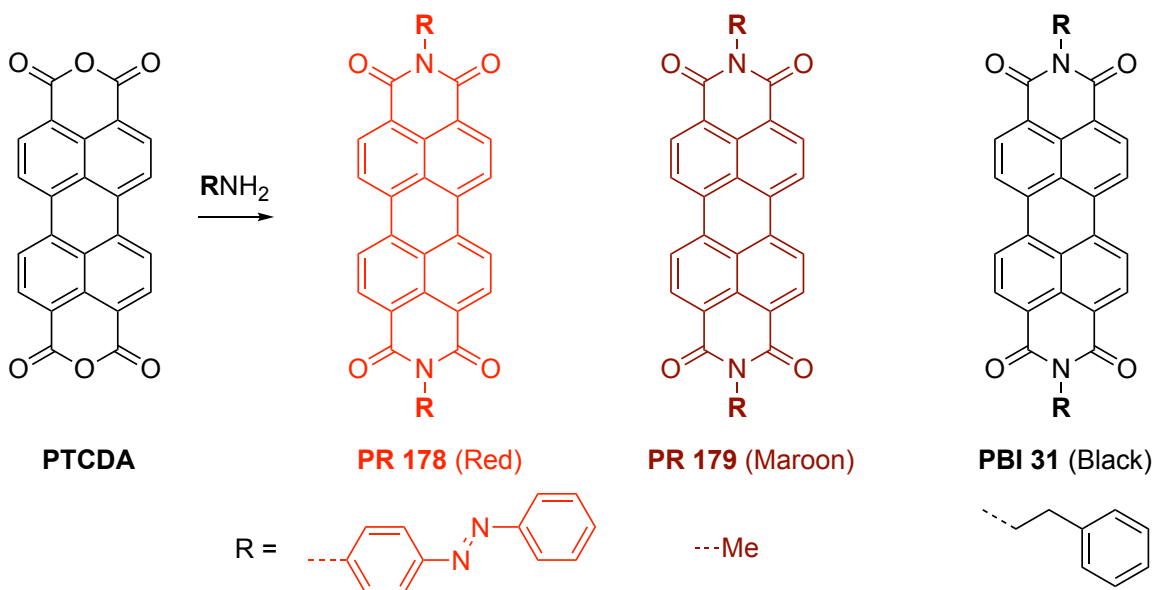
Figure 2.2. PDI is prepared from perylene-3,4,9,10-tetracarboxylic acid dianhydride (PTCDA) and a primary amine. The imide side chains R influence packing in the solid state. As a result, commercial PDI pigments such as these examples range in color from bright red to black.

Any number of primary amines can be used to prepare PDI with various imide side chains (Figure 2.2). These side chains have minimal effect on the energies of orbitals associated with the PDI aromatic core, but heavily influence solubility and bulk properties that are important for applications. For example, commercial PDI pigments may be red, maroon, or black despite differing only in their side chains (Figure 2.2).[15,16] This drastic color difference results from changes in how the dye molecules pack in the

solid state.[17] Depending on the relative orientation of molecules within aggregates of PDI, UV-Vis absorption may be either hypsochromically shifted (H-aggregates) or bathochromically shifted (J-aggregates).[18,19] Either type of aggregation leads to fluorescence quenching via excimer formation. Excimer formation is a potential loss mechanism in OPVs, which is why all PDI-based materials used as electron acceptors in high-performance devices feature branched alkyl chains that inhibit aggregation (Figure 2.3).
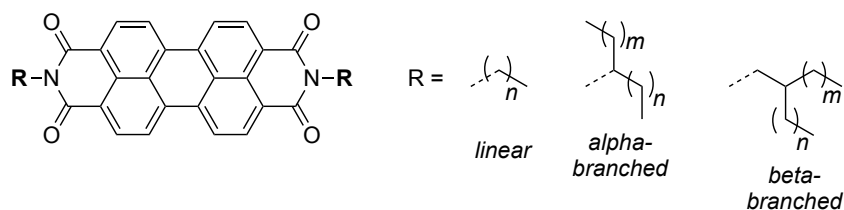
Figure 2.3. Branching in PDI side chains. PDI-based materials for OPVs typically feature symmetrical ($m = n$) alpha-branched side chains. Some feature asymmetrical ($m \neq n$) beta-branched side chains.

Although the importance of branched side chains in PDI-based materials is widely recognized, very little work has been done on more subtle side chain engineering of these materials. This is especially striking given the performance enhancements attained in electron donating polymers simply by lengthening or shortening their side chains by as little as one methylene group. For example, independently changing the two side chains of **PBDTTPD** (Figure 2.4) led to a range of PCEs from 2.5% to 8.3%.[20] Notably, lengthening or shortening R_2 by a single methylene unit reduced PCE by up to 2%. Sun et. al., prepared random donor-acceptor terpolymers in which acceptor subunits alternate with one of two donor subunits that differ only in the length of their branching alkyl side chains (Figure 2.5).[21] By varying the proportions of these two different side chains along

the polymer backbone, the performance improved from PCE = 9.8% to 11.8%. Lengthening one of the side chains in **PDBT-FT** from *n*-octyl to *n*-decyl (Figure 2.6) improved PCE in devices made with a small molecule acceptor from 11.5 to 14.2%.[22] The subtle changes in the side chains of these and many other classes of polymers leads to improved order, in turn improving charge transport and reducing recombination.
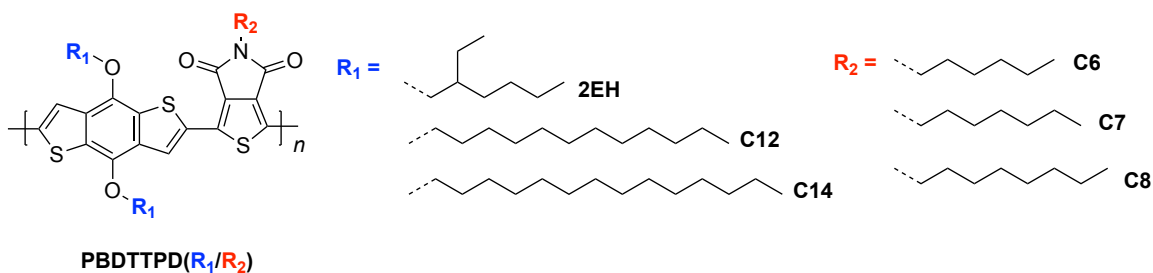
Figure 2.4. Side chain engineering of **PBDTTPD**. Linear R_1 chains reduced performance over the **2EH/C8** variant. Shortening **2EH/C8** to **2EH/C7** improved PCE from 7.3% to 8.3%, but further shortening to **2EH/C6** reduced PCE to 6.3%.
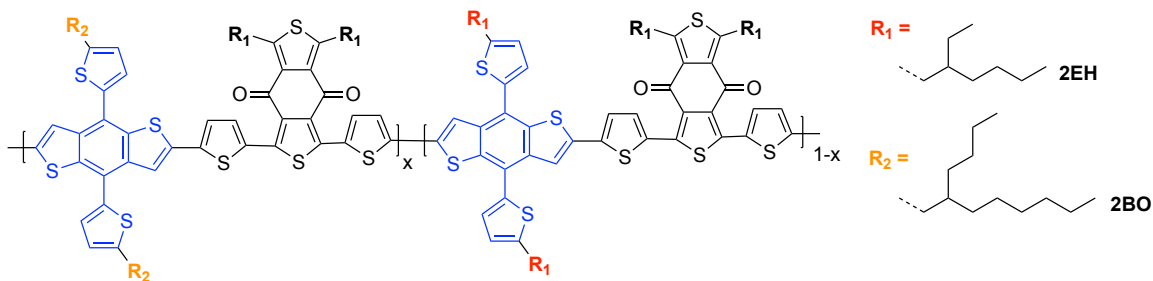
Figure 2.5. Terpolymers with random distribution of side chains. Donor segments (blue) with beta-branched side chains of different lengths randomly alternate with acceptor segments (red). The lowest performance in OPVs was seen at x = 0 and x = 1, with best performance at x = 0.5.
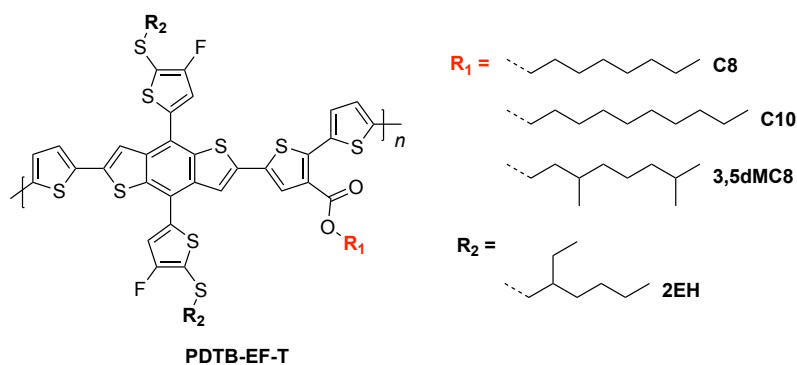
Figure 2.6. Side chain engineering of **PDTB-EF-T**. Hyperbranching the **C8** ester side chain (R$_1$, in red) to the 3,5-dimethyloctyl side chain reduced PCE slightly from 11.5% to 11.2%, whereas a linear extension of two methylene groups to **C10** improved the PCE to 14.2%.

Besides changing their length, incorporating novel functionality into the side chains of organic semiconductors can lead to beneficial properties for a wide variety of applications. Introducing small percentages (0.25% by weight) of **P1-6**, which feature pendant aromatic rings on every other alkyl chain, into **P3HT**/**PC$_{61}$BM** (Figure 2.7) devices improves contact between the fullerene acceptor phase and the mixed polymer donor phase, reducing recombination and improving PCE from 3.9% top 5.1%.[23] Fluoralkyl side chains are rigid, and effectively exclude both water and oxygen, improving the thermal and chemical stability of thin films of materials featuring fluorinated side chains.[24] These features, along with the unique self-organization[25–30] of fluorinated materials improves the performance and stability of OFETs made from PDI with fluorinated side chains.[31–33] PDI-based acceptor **TPH** featuring fluorinated side chains was not incorporated into OPVs like its high-performance analog **TPH** with alkyl side chains (Figure 2.8),[34] likely due to the poor solubility of fluorinated materials in organic solvents used for fabrication. However, single crystals of **TPH** with fluorinated side chains were grown to better understand the packing of **TPH** in the solid state. The

reduced aggregation of materials with branched alkyl chains often inhibits the growth of single crystals for X-ray diffraction. Water-soluble materials with ionic side chains or oligoethylene glycol side chains effectively segregate from materials that are soluble in organic solvents, facilitating the preparation of multi-layer devices.[35]
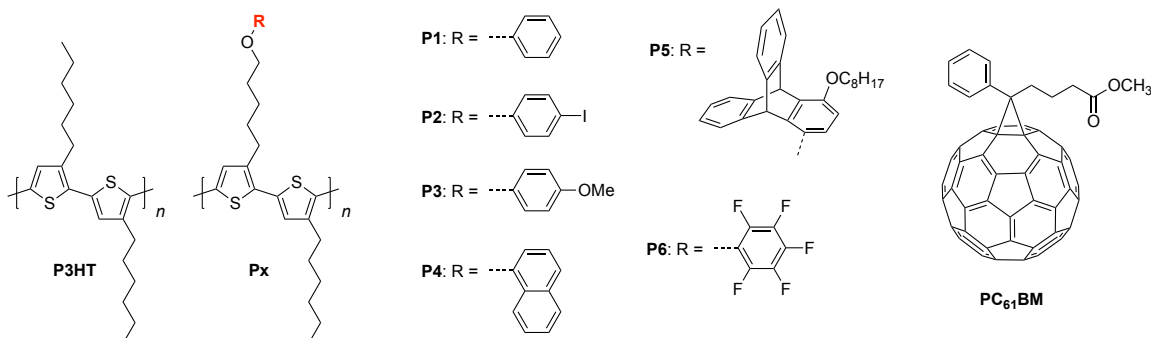
Figure 2.7. Aryl-alkyl side chains for polymer additives in **P3HT** OPVs. Incorporating 0.25% of any of the polymers **P1-6** improved the performance of OPVs using **P3HT** as the donor material. Aromatic side chains improved the interfaces between donor polymer and fullerene acceptor. **PC$_{61}$BM** was used as the electron acceptor materials in that study.
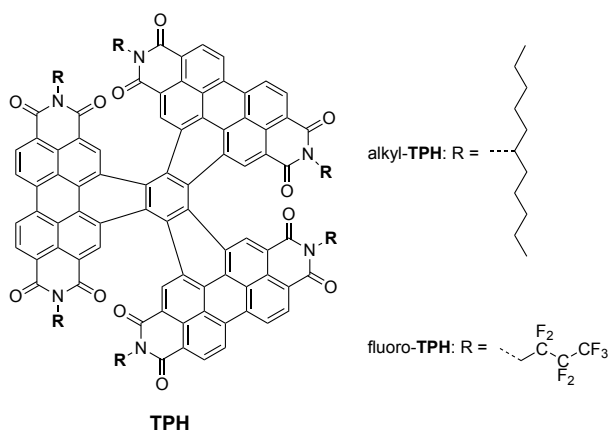
Figure 2.8. Side chain variation in high-performance electron acceptor **TPH**. Although fluoro-**TPH** was not incorporated into devices, it was more suitable for growing single crystals, providing insight on intermolecular interactions and packing of **TPH** in the solid state.

Given the importance of side chain engineering on the morphology of PDI and PDI-based materials, and on the performance of organic electronics in general, we were

interested in varying the side chains on cove-edge graphene nanoribbons of PDI that we call **hPDI** (Figure 2.9).[36] **hPDI** exhibits PCEs up to 8.3% in OPVs,[37] and can be used as a parent material for larger ribbons and nanostructures that are highly effective in ultra-narrowband photodectors[8,38] and as electron transporting layers in perovskite solar cells.[10,11] Subtle changes in side chain length or branching could be used to improve device performance, while materials with entirely new side chains could be used as ternary additives for solar cells or to promote self-assembly. We developed a method that allows us to incorporate the side chain of the dimeric PDI ribbon **hPDI2** in the final synthetic step, facilitating our efforts. This method was also applied to the thiophene-fused PDI dimer FPDI-T,[39,40] demonstrating its general utility for the side chain engineering of PDI-based materials.
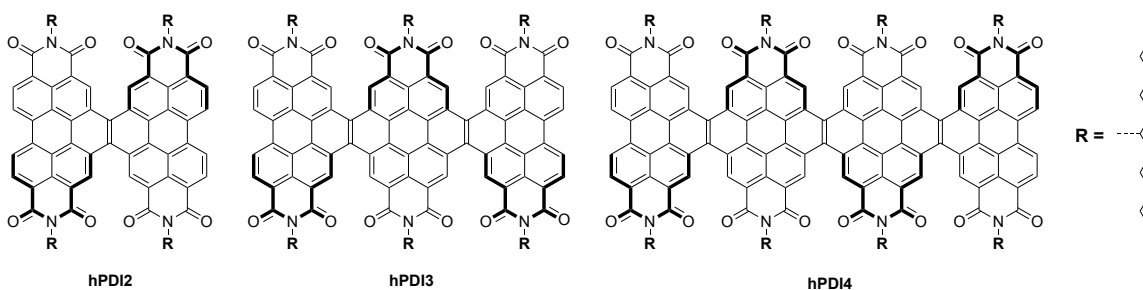
Figure 2.9. Structure of **hPDI**. The use of an alpha-branched side chain improves the solubility of these materials and their derivatives.

2.3. Divergent Synthesis of PDI-Based Materials

To create a series of analogs of **hPDI2** with varying imide side chains, we first looked towards previous syntheses of **hPDI2**. Our group prepared **hPDI2** (**1**) using the sequence presented in Scheme 2.1.[36] Monomeric PDI is prepared from a primary amine and perylene-3,4,9,10-tetracarboxylic acid dianhydride (PTCDA), then brominated. Two equivalents of brominated **3** are bridged with an ethylene linker using an organometallic cross-coupling reaction and the final bonds are closed under oxidative photocyclization conditions first developed by Mallory.[41] With optimization, we can prepare **hPDI2** in batches of nearly 10g.
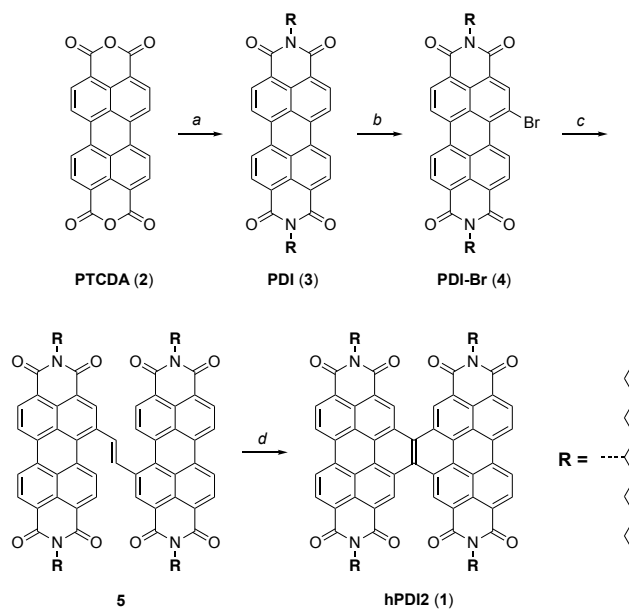
Scheme 2.1. Synthesis of **hPDI2** (**1**). (a) RNH_2, imidazole, 140 °C; (b) Br_2, DCM, RT; (c) bis(tributylstannyl)ethylene, $Pd(PPh_3)_4$, PhMe, 110 °C; (d) I_2, air, hv, PhH.

Introducing the imide side chain in the first step of the synthesis has several disadvantages for screening a large number of variants of **1** with different side chains. (1) Each desired product is produced in a separate route despite having the same aromatic

core. Building a library of **1** with varying side chains is step-inefficient. (2) Many types of side chains are not compatible with subsequent steps. In particular, aromatic side chains are difficult to include because all but the most extremely electron-deficient aromatic groups would be brominated under the conditions required to brominate the electron-poor PDI. Although methods exist of producing halogenated PDI with aromatic side chains, they introduce additional steps into the procedure.[42] (3) Depending on the choice of side chain, intermediates may be unfeasible to purify in sufficient quantity. (4) Many highly desirable side chains are prepared from expensive amines, including many branched alkyl amines. Although yields for most synthetic steps are good, the overall yield is approximately 30% from starting PTCDA and the first step uses excess of the amine side chain. As a result, preparing derivatives of **1** with a wide variety of side chains can become prohibitively expensive.

Given the overall efficiency and scalability of our existing synthesis, we considered a strategy based on removing the 6-undecyl side chains of **hPDI2**, creating a divergent synthetic pathway in which imide side chains are introduced in the final synthetic step (Scheme 2.2). The only known procedure for returning the imides of PDI back to their respective anhydrides involves refluxing the material under basic conditions. However, this procedure often suffers from low yields and long reaction times. Our attempts to perform this reaction on **hPDI2** were similarly plagued.
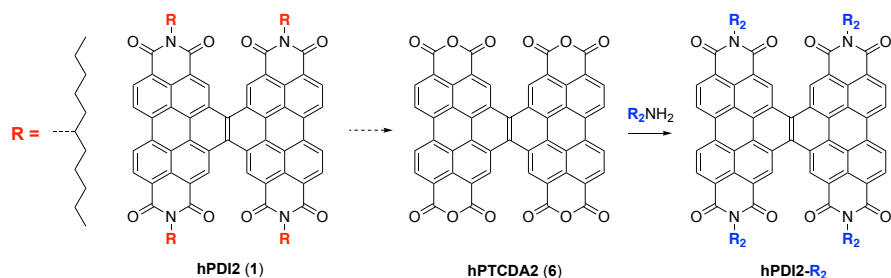
Scheme 2.2. Strategy for divergent synthesis of **hPDI2** via removal of imide side chains. **1** can be made on multi-gram scale, potentially making this an efficient route for preparing derivatives with varying side chains. However, no suitable methods for preparing rylene anhydrides (such as **6**) from their corresponding imides (**1**) are known.

To achieve a divergent synthesis in which the imide side chains could be introduced in the last step, we prepared the intermediate dianhydride dimer **6** by a different route (Scheme 2.3). We built up the aromatic core by subjecting perylene-3,4,9,10-tetracarboxylic acid tetraester (PTE, **7**) to the same sequence of reactions used to prepare **1**: bromination, cross-coupling, and oxidative photocyclization. The esters of the resulting intermediate can be readily condensed to their corresponding anhydrides under strongly acidic conditions to yield **6**. This can then be followed by the same reaction used to prepare PDI from PTCDA to yield derivatives of **1** with any desired imide side chain in a sequence that only diverges at the last synthetic step. This method can potentially be applied to any other PDI-based material prepared by a similar sequence of cross-coupling and oxidative cyclization (Scheme 2.4). This includes the high-performance OPV materials **TPH**, **FPDI-T**, and **FTTB-PDI4** discussed in Chapter 1.2.2 of this work,[34,39,40,43] as well as PDI-helicenes with unprecedented chiroptical properties.[44]
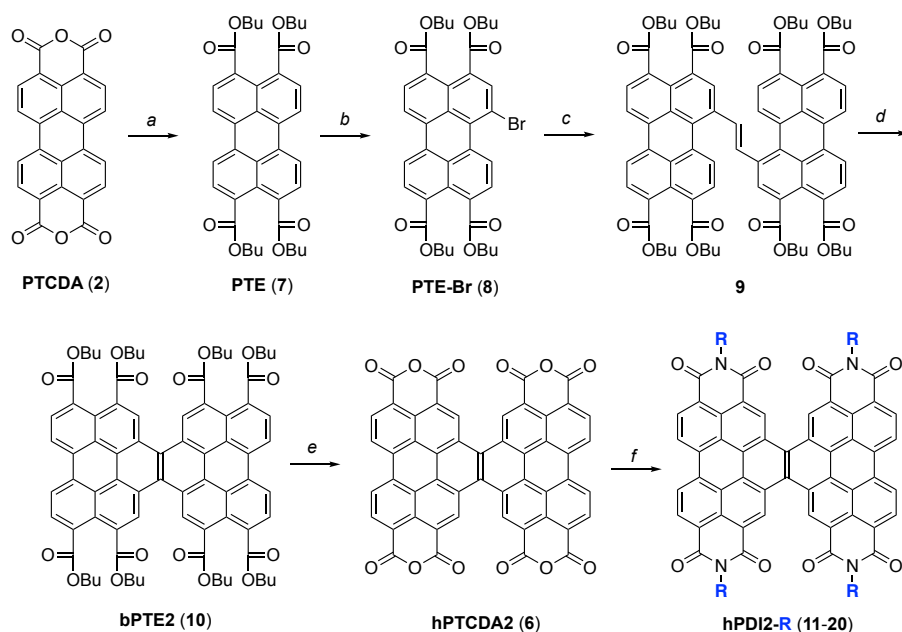
Scheme 2.3. Divergent synthesis of **hPDI2** via a perylene tetraester intermediate. (a) BuOH, DBU, DMF 70 ºC, 45 min; BuBr, 70 ºC, 90 min, 89%; (b) Br$_2$, K$_2$CO$_3$, DCM, RT, 2 hr, 46%; (c) bis(tributylstannyl)ethylene, Pd$_2$dba$_3$, AsPh$_3$, PhMe, 105 ºC, 2 hr, 54%; (d) I$_2$, K$_2$CO$_3$, PhH, *hv*, 3 d, 81%; (e) H$_2$SO$_4$, RT, 5 min, 97%; (f) **R**NH$_2$, imidazole, 120-140 ºC, 3-4 d, 17-100%. See Figure 2.10 for the structures of **11**-**20**.
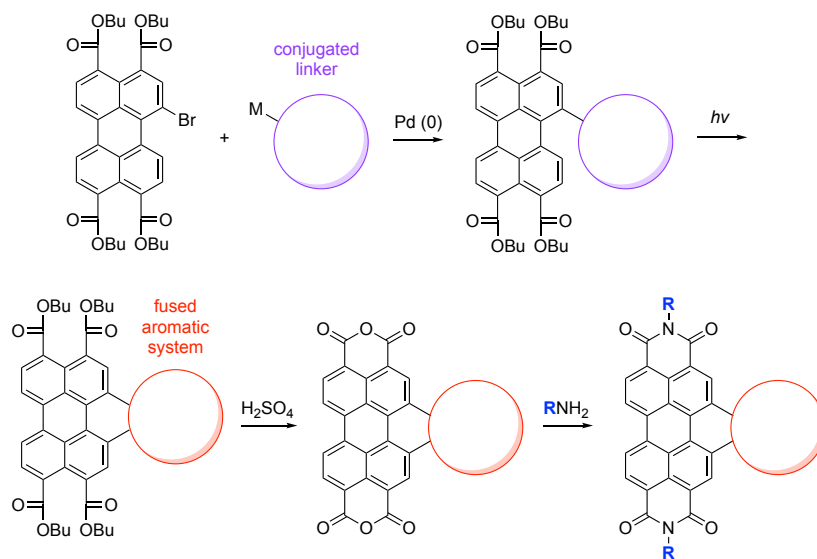
Scheme 2.4. Generalized concept for divergent synthesis of PDI-based materials with varying side chains. Many high-performance PDI-based materials for OPVs and other applications could be prepared via this strategy.

This sequence proved effective, yielding the divergent anhydride intermediate **6** on multi-gram scale, which could then be converted into a library of **hPDI2** with varying side chains. We were able to increase the scale of the first step, preparation of **7**, by changing the purification from column chromatography to a simple filtration. This was followed by bromination and then cross-coupling with bis(tributylstannyl)ethylene to yield intermediate **9**. Subjecting **9** to the same photocyclization conditions used to prepare **1** led to condensation of the esters to their corresponding anhydrides and addition of oxygen. **10** decomposed on silica and alumina, so we could not isolate it from undesired side products in large scale. Oxygenation was eliminated by running the reaction under inert atmosphere, and condensation was eliminated by using potassium carbonate to quench the hydrogen iodide produced in the reaction. Although these changes preclude the use of high-throughput flow photochemistry, we obtain high yields of **10** on multi-gram scale in batch reactions using a high-power UV lamp. We unambiguously identify **10** as the product of this reaction by single-crystal X-ray diffraction, which is discussed in Chapter 3 of this text. Briefly stirring **10** in sulfuric acid lead to quantitative conversation to **6**. Like its monomeric analog **2**, black **6** is insoluble. However, reaction of **6** with multiple equivalents of any primary amine in molten imidazole formed **11-20** with the desired side chains.
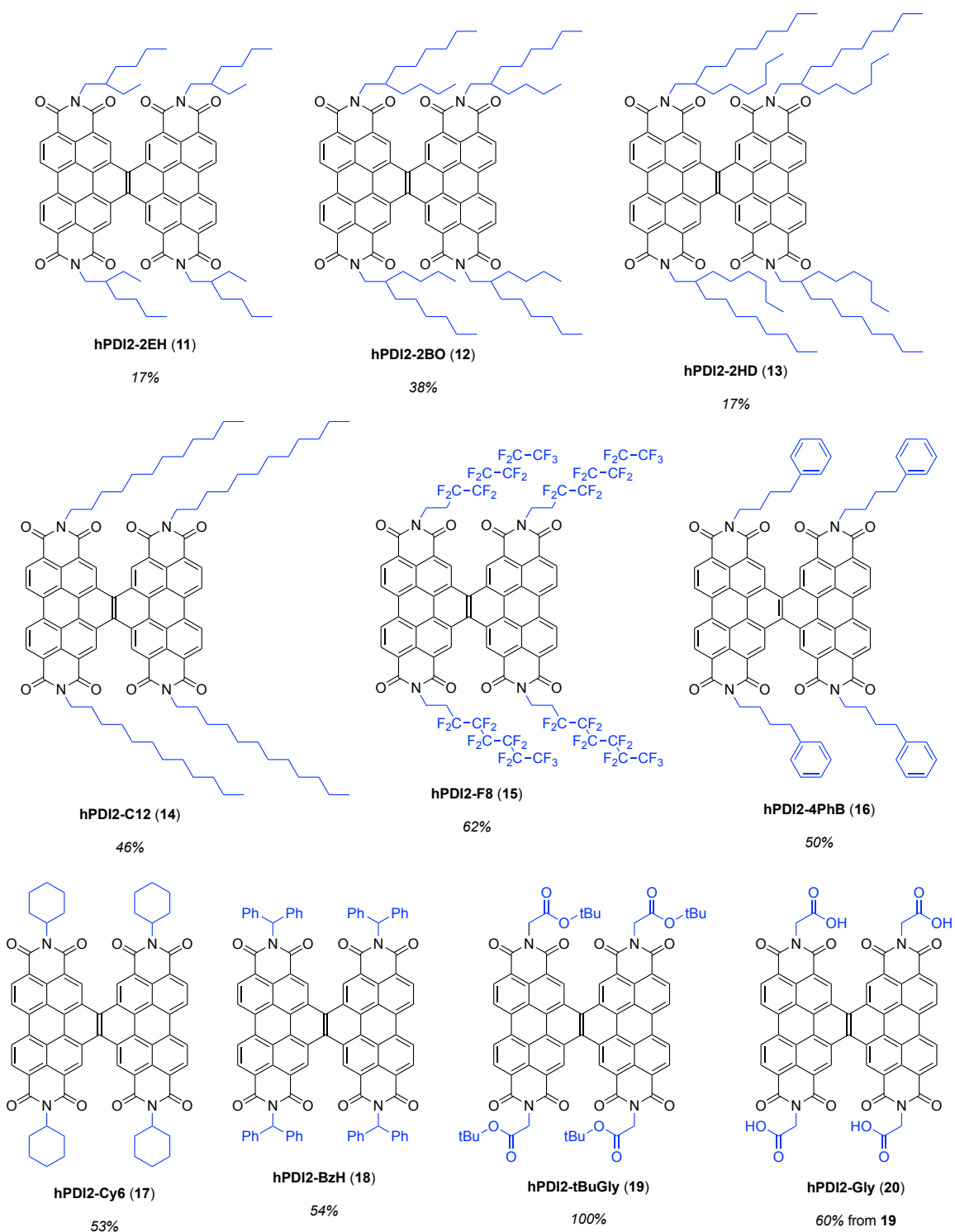
Figure 2.10. Library of **hPDI2** with varying side chains (highlighted in blue). **11-19** were prepared directly from **6** (Scheme 2.3). **20** was prepared from **19** by reaction with trifluoroacetic acid.

The library of **hPDI2** prepared using this method is depicted in Figure 2.10, along with the yields of the final reaction. Compounds **11-13** with beta-branched side chains and compound **14** with linear side chains were prepared to investigate the effects of branching on **hPDI2**. Compound **15** with 1*H*,1*H*,2*H*,2*H*-perfluoroalkyl chains was prepared to investigate **hPDI2** featuring the beneficial properties of fluorinated side chains described above. Compound **16** was prepared to investigate the effect of pendant aryl side chains. Compounds **17** and **18** were prepared in the hopes of growing single crystals of **hPDI2** of sufficient quality for X-ray diffraction. Single crystals of **17** were successfully grown and the crystal structure of **hPDI2** is discussed in Chapter 3 of this work. Lastly, we prepared **19** featuring *t*-butyl glycyl side chains. **19** is readily deprotected to form **20**, which is soluble in water or water/methanol mixtures containing mild base.

To show that this synthetic strategy can be applied to the synthesis of other PDI-based materials, we prepared **FPDI-T** (**21**) via the same method (Scheme 2.5). In particular, we were concerned that subjecting intermediate **22** to concentrated sulfuric acid might lead to oxidation of the central thiophene ring. To our delight, **21** was successfully produced from **23**, with no sign by mass spectrometry or NMR of oxidation in the isolated product.
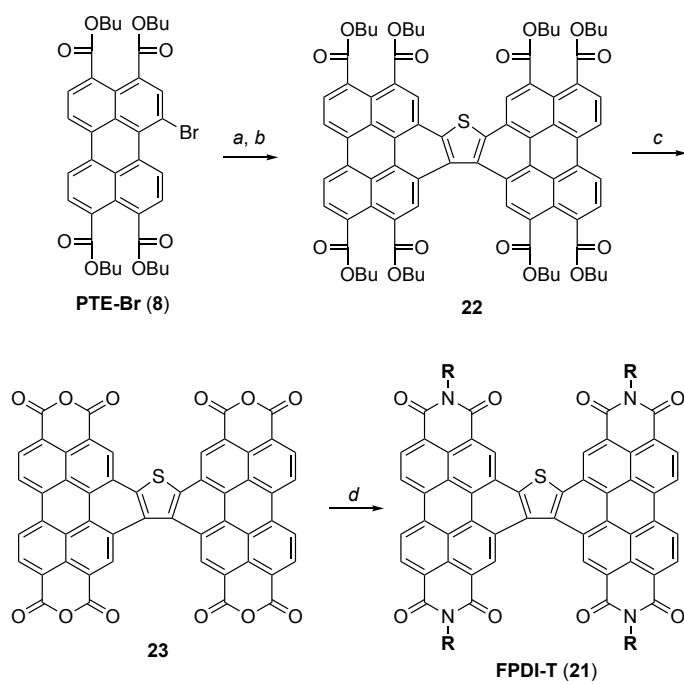
Scheme 2.5. Synthesis of **FPDI-T** via a perylene tetraester intermediate. R = 6-undecyl. (a) bis(tributylstannyl)thiophene, Pd$_2$dba$_3$, AsPh$_3$, PhMe, 110 °C, 2 hrs, 71%. (b) I$_2$, K$_2$CO$_3$, PhH, *hv*, 24 hr, 85%; (c) H$_2$SO$_4$, RT, 30 min, 99%; (d) 6-undecylamine, imidazole, 130 °C, 3 d, 42%.

2.4. Side Chain Variation in hPDI2

The most immediately striking difference between **11-20** is their variation in color and solubility. **14**, with a linear side chain, as well as **16**, **19**, and **20**, featuring linear side chains with various pendant functional groups, are all black, suggesting intense aggregation in the solid state. **14** and **16** are only in moderately soluble in common solvents used for materials processing, such as chloroform and chlorobenzene. This limits their potential for applications that demand high solubility, such as bulk heterojunction OPVs. However, **16** is sufficiently soluble to be incorporated as a low weight percentage additive for ternary devices.[ref] **19** is moderately soluble in DMSO, or mixtures of DMSO with polar solvents. **20** is soluble in basic solutions of water or water/alcohol. Despite also featuring a linear side chain, fluorinated **15** is a maroon color, indicating that chain functionality, as well as topology, influences solid state packing. **15** is modestly soluble in α,α,α-trifluorotoluene or mixtures of α,α,α-trifluorotoluene with THF, and moderately soluble in trifluoroacetic acid. The poor solubility even in highly specialized solvents suggests that future investigation of PDI-based materials with fluorinated side chains will depend on developing new techniques for facile access to branched fluorinated side chains. **11-13**, with beta-branched side chains are all maroon. Solubility in solvents like chloroform and chlorobenzene improves dramatically with increasing side chain length. Variable temperature NMR experiments (Figure 2.12) on **12** and **13** show a dramatic difference in aggregation between the two molecules at identical temperatures. Just as with the donor polymers discussed above, subtle changes in side chain length can significantly affect the properties of PDI-based materials.
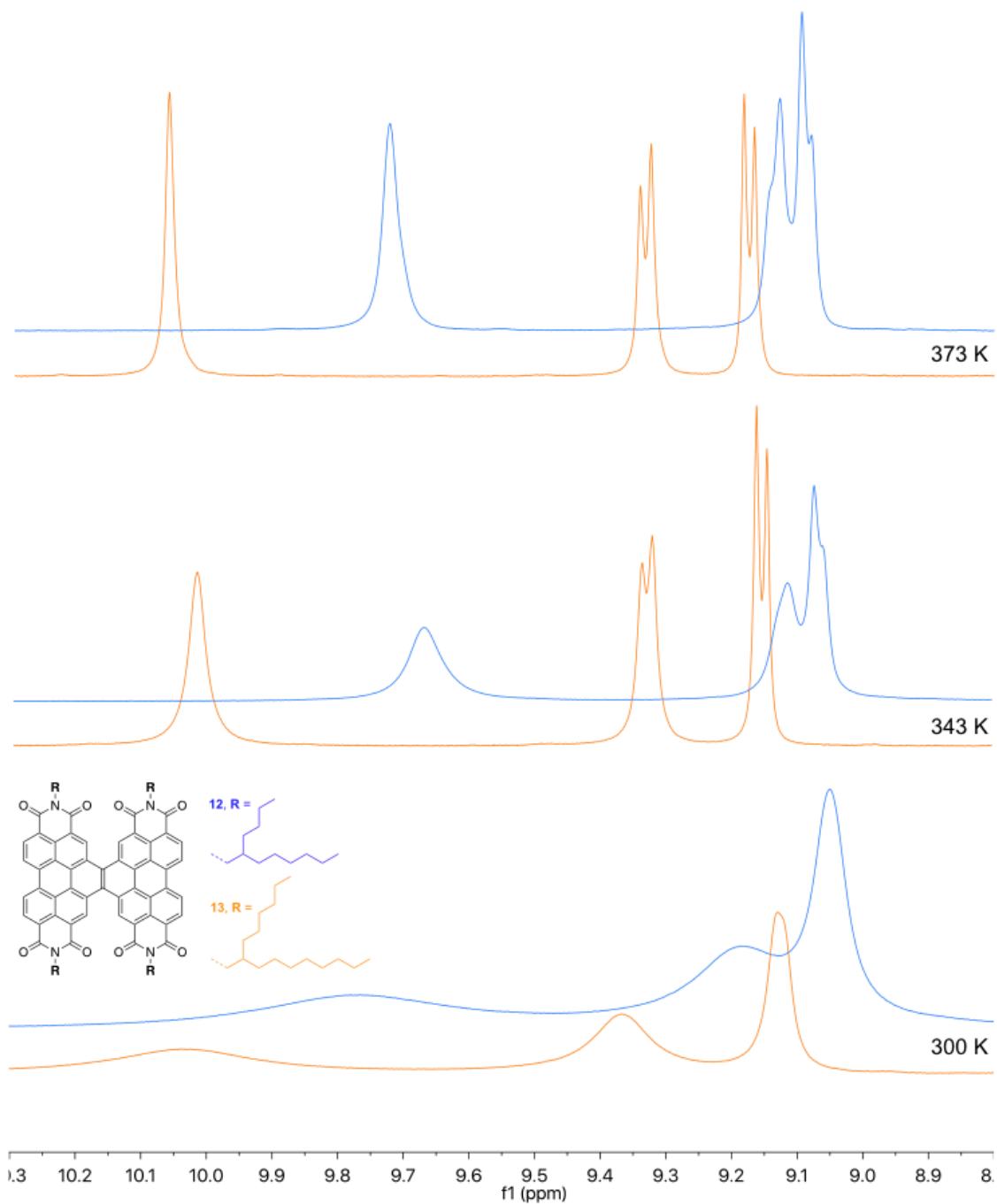
Figure 2.11. VT NMR of the aromatic region of **12** (blue) and **13** (orange) at 300 K (bottom), 343 K (middle) and 373 K (top). Even at 373 K, **12** is broadened and shifted upfield, indicating significant aggregation. NMR spectra were recorded in $C_2D_2Cl_4$.

17, with a cyclic alpha-branched side chain, and **18**, with an alpha-branched diphenylmethyl side chain, are both red. **17** has good solubility in chloroform and chlorobenzene, while **18** is only moderately soluble. Of all the materials **11-20**, **17** was the promising in our initial attempts at growing single crystals for X-ray diffraction. After refining the growth conditions by diffusion of cyclohexane vapor into a solution of **17** in chlorobenzene, we obtained single crystals. The structure is discussed in Chapter 3. The other materials **11-20** tended either to precipitate far too rapidly or not at all, while **17** grew crystals of nearly sufficient quality under a wide variety of conditions. Most new PDI-based materials are prepared with long alpha- or beta-branched side chains that inhibit π-π contact, which is useful for preparing thin film devices, but impedes attempts at growing single crystals. The balance between solubility and order provided by the cyclohexyl side chain may make it an ideal candidate for growing single crystals of PDI-based materials.

Consistent with our observations on solubility, branching closer to the imide nitrogen reduced aggregation in solution. Even with a shorter alpha-branched side chain, **17** shows no aggregation up to 10^{-3} M in DCM (Figure 2.12.a). **12** and **14** both have the same length of side chain, but **12** is beta-branched and **14** is linear. As a result **12** only begins to aggregate at 10^{-3} M (Figure 2.12.b), while **14** aggregates strongly even at 10^{-4} M in DCM (Figure 2.12.c). Previously, we attributed the solubility of **1**, with long alpha-branched chains, in part to the non-planar aromatic core.[8,36,45] These studies suggest that the choice of side chain is just as important in maintaining the solubility of contorted PDI-based materials.
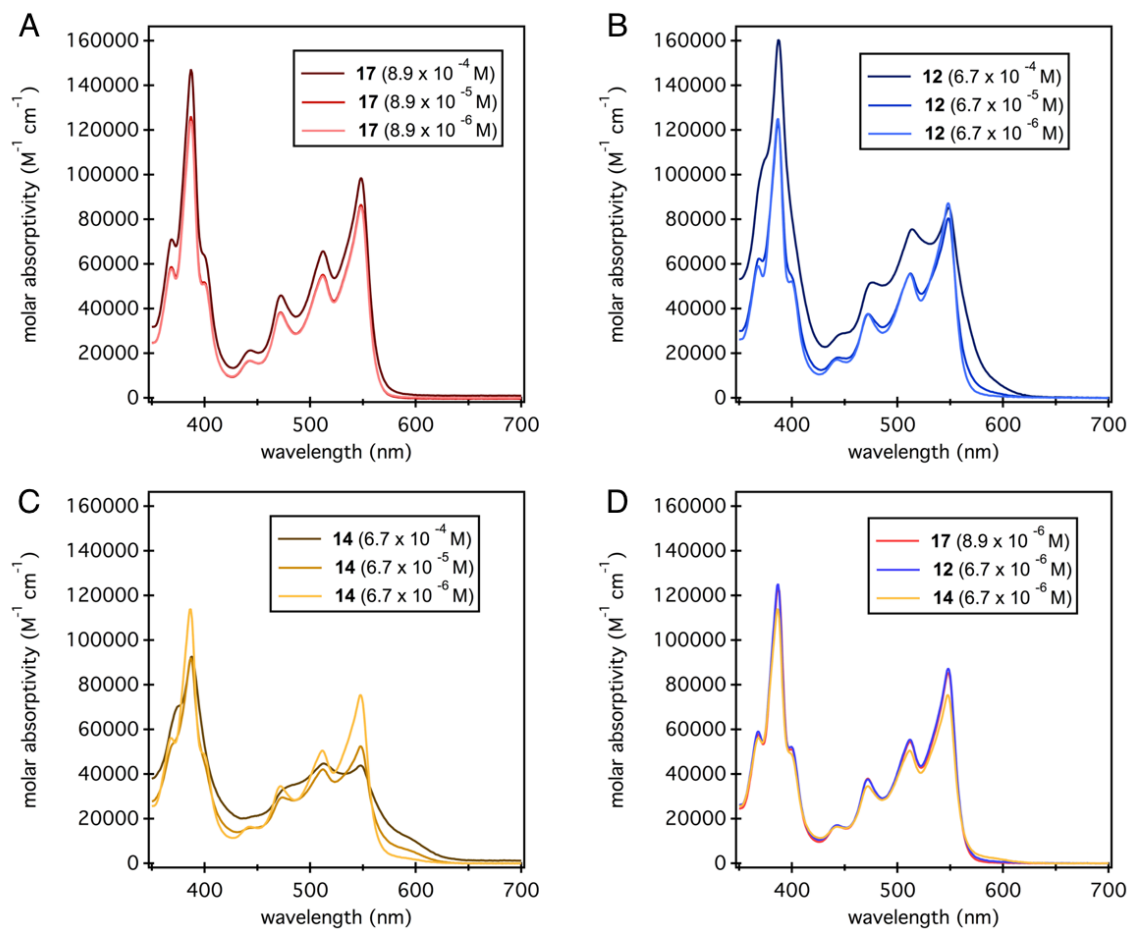
Figure 2.12. Concentration-dependent UV-Vis spectra of (A) **17**, (B) **12**, and (C) **14**. **17**, with alpha-branching, exhibits negligible aggregation even at high concentrations. Beta-branched and linear **12** and **14** exhibit more notable aggregation. (D) Low-concentration spectra of **17**, **12**, and **14**. All three are nearly identical in dilute solutions.

The color and charge mobility of PDI-based materials in the solid state are heavily influenced by how the side chains of these materials dictate packing. We investigated these properties by fabricating OFETs of these materials, and by investing their thin-film UV-Vis spectra. We chose to compare **1**, **12**, and **14**, because they have similar length of side chains that only differ in their branching point. We were also interested in whether or not **15** exhibited the same beneficial properties as monomeric

PDI bearing fluorinated side chains.[31–33] The electron mobility and optimal annealing temperatures of OFETs made from these materials are listed in Table 2.1. The optimal annealing temperature decreased with increasing branching. Similar to a more rigidly planar cousin of hPDI, the beta-branched **12** had the highest mobility.[46] The material **15** with a linear fluorinated side chain required an even high annealing temperature than **14** with a linear hydrocarbon side chain. It is not clear whether this difference is the result of the rigidifying effect of fluorination on hydrocarbons, the decreased length of the side chain, or both.

Table 2.1. Electron mobility and optimal annealing temperatures for OFETs.

	Side Chain	μ_e (cm^2 V^{-1} s^{-1})	Optimal Annealing Temperature (°C)[a]
1	6-undecyl (alpha-branched)	2 x 10^{-4}	160
12	2-butyloctyl (beta-branched)	1 x 10^{-2}	200
14	*n*-dodecyl (linear)	5 x 10^{-3}	240
15	1*H*,1*H*,2*H*,2*H*-perfluorooctyl	6 x 10^{-3}	310

[a] Optimal annealing temperatures were determined by measuring current as a function of gate voltage at progressively higher annealing temperatures. Films were allowed to anneal for 30 minutes to facilitate rearrangement.

We were interested in whether these electron mobility trends corresponded to aggregation effects in the solid state, so we studied the UV-Vis spectra of thin films before and after annealing each one at its optimal OFET annealing temperature. **1**, which featured the lowest mobility, exhibited little change in its absorption spectrum (Figure 2.13.a). The excitations do not change in energy, but the intensity of the 0-0 vibronic transition of the $S_0 \rightarrow S_1$ transition decreases relative to the 0-1 vibronic transition. In

folded oligomers of monomeric PDI, this change is associated with compact π-stacking and the formation of excimers at the expense of charge transfer states.[47,48] Annealing dramatically sharpened the features of **12**, the material with beta-branched side chains and highest mobility (Figure 2.13.b). Linear **14**, which exhibited the moderate mobility, had dramatically sharpened absorption features after annealing (Figure 2.13.c). Although both **12** and **14** maintained H-aggregation after annealing, the relative intensity of the 0-0 vibronic transition increased. Both before and after annealing, **15** exhibited the most intense aggregation in the solid state, with absorption extending into the near IR region (Figure 2.13.d). The wide variation in morphological changes after annealing in this series reinforces the importance of specifically tuning fabrication conditions for devices to each specific material.
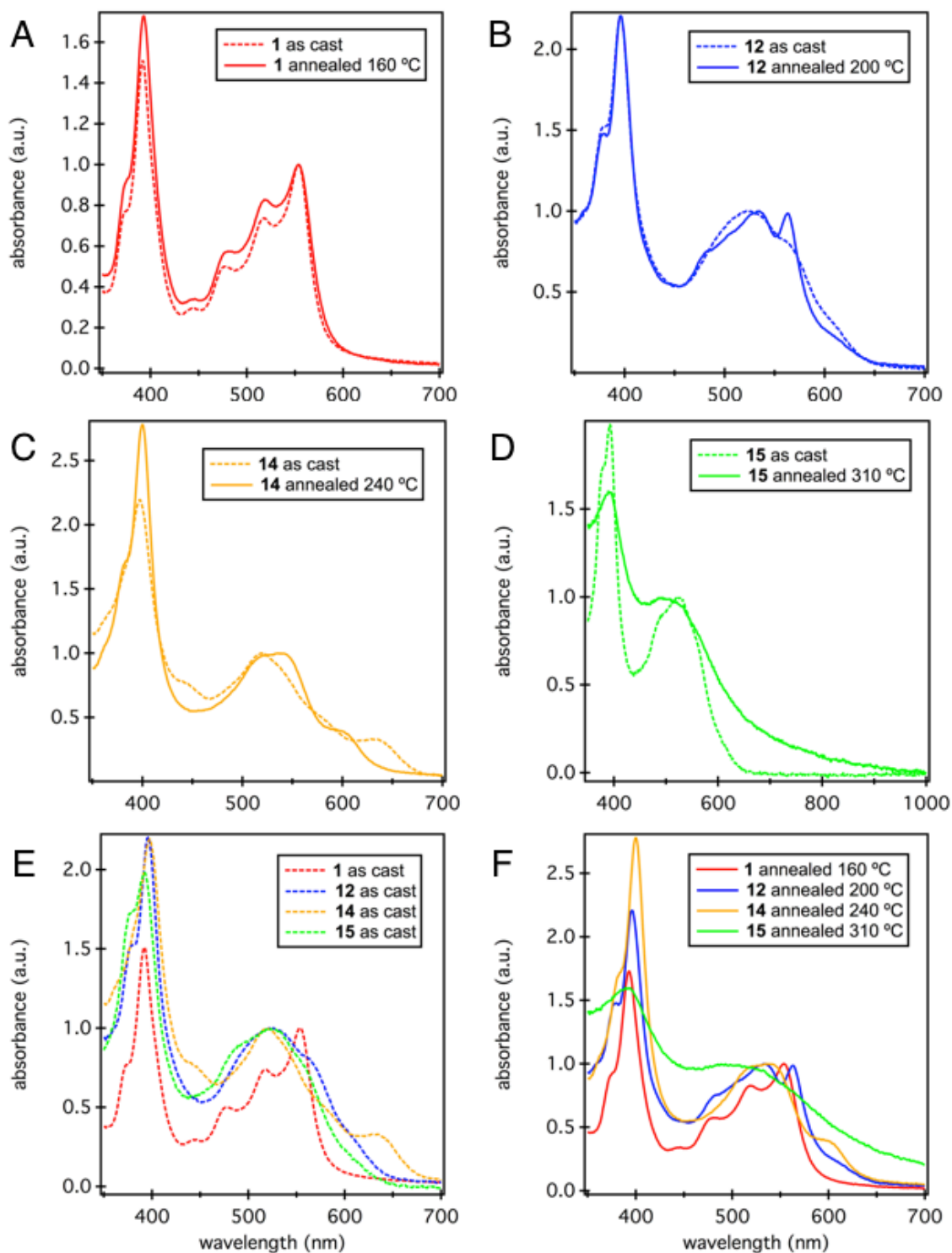
Figure 2.13. UV-Vis spectra before and after annealing thin films of (A) **1**, (B) **12**, (C) **4**, and (D) **15**. (E) All pre-annealing films overlaid. (F) All post-annealing films overlaid.

214

To further explore the relationship between optimal annealing conditions and morphological changes in **1**, **12**, **14**, and **15**, we performed differential scanning calorimetry (DSC). Powders of the materials were allowed to equilibrate at 250 ºC for 30 minutes, then cooled and heated in cycles. Heat flow plots **1** and **15** showed distinct crystalline transitions (Figure 2.14.a, 2.14.b), while **12** and **14** lacked any features under our conditions. Notably, **1** and **15** both underwent multiple crystallization events on the first cooling. **1** converged to a single crystallization event on the third cycle. **15** converged to a single crystallization event on the second cycle. Unlike in liquid-crystalline PDI derivatives,[49,50] the higher temperature crystallization events are not seen on heating and are not reversible. This suggests that, with certain side chains, disordered **hPDI2** passes through a series of metastable states on cooling. Continued DSC studies could be used to determine how to access these states in films of **hPDI** to study their behavior, and could also be used to optimize annealing conditions to ensure that thin films for devices are stable, minimizing changes in device performance over time.
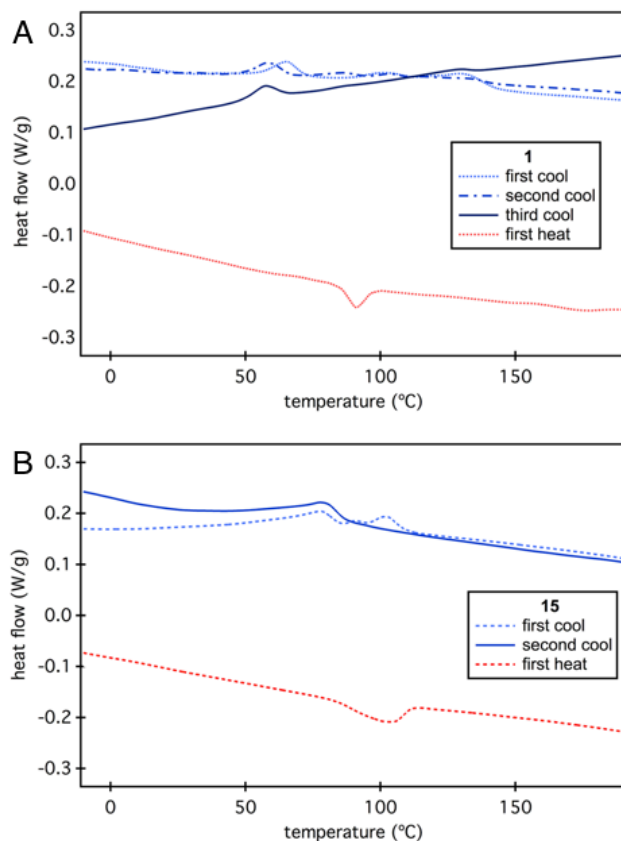
Figure 2.14. Differential scanning calorimetry. (A) Heat flow plot of **1**. Only one melting event is observed on heating, but multiple crystallization events are observed in the first two cooling cycles before reaching equilibrium. (B) Heat flow plot of **15**. **15** reaches equilibrium after the first cycle.

Here we have a demonstrated a synthetic technique for preparing PDI-based materials in which the imide side chains are installed in the final step. This method dramatically increases the throughput of producing PDI-based materials with various side chains. We applied this strategy prepare several derivatives of the high-performance OPV and narrowband photodetector material **hPDI**. We found that beta-branched imide side chains in derivative **12** improved the electron mobility by two orders of magnitude over the parent alpha-branched **1**. The facility of our new synthetic strategy will allow us to

further optimize **hPDI** for organic electronic applications and to include a wider variety of side chains for new applications.

2.5. General Experimental Details

General Synthetic Details. All reactions were performed under a nitrogen atmosphere. Anhydrous and anaerobic solvents were obtained from a Schlenck manifold with purification columns packed with activated alumina and supported copper catalyst (Glass Contour, Irvine, CA) and then sparged with nitrogen for 30 minutes before use. Reaction monitoring by thin layer chromatography (TLC) was performed on J.T. Baker Baker-flex Silica Gel IB2-F (25 mm x 75 mm) TLC plates. TLC visualization was accomplished by visible observation and irradiation with a UV lamp. Automated flash chromatography was performed with a Teledyne Isco Combiflash Rf200 using Redisep Rf Silica columns. Preparative high performance liquid chromatography (HPLC) was performed on a Waters Prep150 instrument equipped with a UV-vis detector (335 nm), an automated fraction collector, and a Nacalai Tesque COSMOSIL 5PBB column (20 mm I.D. x 250 mm, 5 μm).

Materials. All chemicals were purchased from commercial sources and used without further purification. **1** was prepared using previously published methods.[36]

Instrumentation. ^{1}H and ^{13}C NMR spectra were recorded on a Bruker DRX400 (400 MHz) or a Bruker DMX500 (500 MHz) spectrometer. Chemical shifts for protons are reported in parts per million downfield from tetramethylsilane and are referenced to residual protium in the NMR solvent ($C_2D_2Cl_4$ δ 6.0; $CHCl_3$: δ 7.26; CF_3CO_2H: δ 11.5).

Chemical shifts for carbon are reported in parts per million downfield from tetramethylsilane and are referenced to the carbon resonances of the solvent ($C_2D_2Cl_4$ δ 73.78; $CDCl_3$ δ 77.0;). Data are represented as follows: chemical shift, multiplicity (s = singlet, d = doublet, m = multiplet), coupling constants in Hertz, and integration.

High-resolution mass spectroscopic (HRMS) data were obtained on a Bruker UltrafleXtreme MALDI/TOF instrument using a dithranol matrix or an a Waters XEVO G2XS instrument equipped with a UPC2 SFC inlet, electrospray (ESI) and atmospheric pressure chemical (APCI) ionization, and a QToF mass spectrometer.

UV-Vis absorption spectra were obtained on Shimadzu UV 1800 UV-Vis spectrophotometer using a 1.0 cm or 0.1 quartz cell. Films of each molecule were spin-cast under inert (N2) conditions onto an amorphous glass substrate treated with OTS to mimic the conditions and films used in FETs.

Differential Scanning Calorimetry. A TA instrument DSC250 differential scanning calorimeter was used to measure thermal behavior. Each sample was cycled 3 times (3 cooling steps and 3 heating steps) between 250 °C and – 50 °C with a 5 °C/min ramp rate. Before each cooling step, the samples were held at 250 °C isothermally for 30 minutes to completely remove all previous thermal history. The slow ramp rate and multiple cycles were used to promote reproducible crystallization behavior.

Device Fabrication. FETs were fabricated using highly a doped Si substrate with 300 nm SiO2. The SiO2 surface was treated with OTS to passivate charge traps at the dielectric-semiconductor interface. Films of each molecule were then spin-cast under inert conditions (N2). Electrodes (5 nm Ti; 50 nm Au) were then deposited to produce FET with a top-contact architecture. The electronic measurements were performed under the same inert conditions after electrode deposition. Optimal annealing conditions were determined by measuring current as a function of gate voltage at progressively higher annealing temperatures. The films were allowed to anneal for about 30 minutes to facilitate solid-state rearrangement to its maximum extent for every temperature.

2.6. Synthetic Procedures and Details of Characterization

Preparation of Pd$_2$dba$_3$/AsPh$_3$ for Stille Coupling

Triphenylarsine (0.034 g, 0.110 mmol, 2 eq) and tris(dibenzylideneacetone)dipalladium(0) (0.050 g, 0.055 mmol, 1 eq) were ground together with a glass stir rod. The catalyst mixture was stored in a desiccator for up to 3 months with no apparent loss of catalytic activity.

PTE (7)

A 1 L round-bottom flask was charged with **2** (30.0 g, 76.5 mmol, 1 eq), 1,8-diazabicyclo[5.4.0]undec-7-ene (45 mL, 306 mmol, 4 eq), n-butanol (56 mL, 612 mmol, 8 eq), and dimethylformamide (400 mL). The mixture was stirred for 45 minutes at 70 ºC. 1-bromobutane (66 mL, 612 mmol, 8 eq) in 200 mL dimethylformamide was added and stirring was continued at 70 ºC for 90 minutes. The mixture was allowed to cool and then poured onto 3 L of water. The resulting slurry was filtered and the solids were washed with water, and then a minimal amount of methanol (approximately 1 L). The bright orange solids were dried and collected to yield pure **7** (44.4 g, 68.0 mmol, 89%) with ^{1}H NMR spectrum matching those previously reported.[51] **^{1}H NMR** (300 MHz, CDCl$_3$, 300K): δ 8.30 (d, J = 8 Hz, 4H), 8.05 (d, J = 8.0 Hz, 4H), 4.34 (t, J = 6.6 Hz, 8H), 1.83-1.73 (overlap, 8H), 1.55-1.42 (overlap, 8H), 0.99 (t, J = 7.4 Hz, 12H).

PTE-Br (8)

A 1 L round-bottom flask was charged with **7** (20.0 g, 30.7 mmol, 1 eq), bromine (20 mL, 390 mmol, 12.7 eq), potassium carbonate (20 g, 145 mmol, 4.7 eq), and dicholoromethane (300 mL). The mixture was stirred for 2 hours before cooling to 0 ºC and quenching with aqueous sodium thiosulfate. The organic layer was then washed once with additional sodium thiosulfate and once with water, dried over magnesium sulfate, filtered, and concentrated under reduced pressure. The mixture was purified by flash column chromatography (SiO$_2$, gradient mobile phase: hexane to 99:1 DCM:ethyl acetate), concentrated, triturated in methanol, filtered, and dried under vacuum to yield **8** as a yellow solid (10.26 g, 14.0 mmol, 46%) with ^{1}H NMR spectrum matching those previously reported.[51] **^{1}H NMR** (300 MHz, CDCl$_3$, 300K): δ 9.18 (d, J = 8.0 Hz, 1H), 8.32 (s, 1H), 8.27 (d, J = 1.6 Hz, 1H), 8.24 (d, J = 1.6 Hz, 1H), 8.12- 8.08 (overlap, 3H), 4.36-4.30 (overlap, 8H), 1.83-1.72 (overlap, 8H), 1.54-1.44 (overlap, 8H), 1.04-0.95 (overlap, 12H).

9

A 250 mL round-bottom flask was charged with **8** (8.03 g, 10.9 mmol, 2.1 eq), E-bis(tributylstannyl)ethylene (3.169 g, 5.2 mmol, 1 eq), and toluene (100 mL). The mixture was sparged with nitrogen for 30 minutes before adding tris(dibenzylideneacetone)dipalladium (0.045 g, 0.05 mmol, 1 mol%) and triphenylarsine (0.061 g, 0.20 mmol, 4 mol%) and sparging an additional 10 minutes. The mixture was then stirred under a nitrogen atmosphere at 105 ºC for 2 hours. The mixture was allowed

to cool, concentrated under reduced pressure, and then purified by flash column chromatography (SiO$_2$, gradient mobile phase: DCM to 97:3 DCM:THF). The resulting red-orange solid was dried thoroughly, triturated in methanol, filtered, washed with minimal additional methanol, and dried to yield **9** as a red-orange solid (3.75 g, 2.82 mmol, 54%). **^{1}H NMR** (500 MHz, CDCl$_3$, 323 K): δ 8.39 (s, 2H), 8.29-8.22 (multiplet, 6H), 8.18 (d, J = 7.9 Hz, 2H), 8.13 (d, J = 7.9 Hz, 2H), 8.09 (d, J = 7.9 Hz, 2H), 7.82 (s, 2H), 4.40-4.33 (multiplet, 16H), 1.83-1.75 (multiplet, 16H), 1.53-1.42 (multiplet, 16H), 1.02-0.89 (multiplet, 24H). **^{13}C NMR** (400 MHz, CDCl$_3$, 300 K): Numerous carbon resonances overlap, leading to fewer signals than the number of chemically distinct carbon nuclei. δ 168.61, 168.57, 168.45, 168.19, 134.00, 133.20, 132.86, 131.84, 130.94, 130.38, 130.33, 130.09, 130.07, 129.97, 129.91, 129.81, 129.17, 128.41, 122.42, 121.59, 65.61, 65.53, 65.49, 30.75, 30.67, 19.34, 19.26, 13.89, 13.87, 13.81 **HRMS** (QTOF, ESI$^+$) m/z [M + Na]$^+$ calculated for C$_{82}$H$_{88}$O$_{16}$Na: 1351.5970; found: 1351.5972.

bPTE2 (**10**)

A double-jacketed quartz photoreaction vessel was charged with **9** (3.289 g, 2.47 mmol, 1 eq), iodine (6.27 g, 24.7 mmol, 10 eq), potassium carbonate (6.83 g, 49.4 mmol, 20 eq), and benzene (450 mL). The mixture was stirred and irradiated with a broad-spectrum mercury UV-visible lamp for 3 days. The mixture was washed with sodium thiosulfate, then the organic phase was dried with magnesium sulfate, filtered, concentrated under reduced pressure, triturated with methanol, filtered, washed with minimal additional methanol, and dried to yield **10** as an orange solid (2.674 g, 2.0 mmol, 81%). **^{1}H NMR**

(500 MHz, CDCl$_3$, 300 K): δ 9.77 (s, 4H), 9.21 (d, J = 8.2 Hz, 4H), 8.62 (d, J = 8.2 Hz, 4H), 4.51 (t, J = 6.8 Hz, 8H), 4.45 (t, J = 6.9 Hz, 8H), 1.96-1.85 (multiplet, 16H), 1.63-1.46 (multiplet, 16H), 1.07 (t, J = 7.4 Hz, 12H), 0.96 (t, J = 7.4 Hz, 12H). **^{13}C NMR** (400 MHz, CDCl$_3$, 300K) δ 168.65, 168.18, 132.63, 132.59, 130.40, 129.76, 129.41, 127.06, 126.95, 126.00, 125.17, 125.04, 122.20, 65.59, 65.57, 30.78, 30.71, 19.34, 19.23, 13.85, 13.74. **HRMS** (QTOF, ESI$^+$) m/z [M + NH$_4$]$^+$ calculated for C$_{82}$H$_{84}$O$_{16}$Na: 1347.5657; found: 1347.5721. m/z [M + Na]$^+$ calculated for C$_{82}$H$_{88}$O$_{16}$N: 1342.6104; found: 1342.6130.

hPTCDA2 (6)

A scintillation vial was charged with **10** (1.50 g, 1.13 mmol, 1 eq) and concentrated sulfuric acid (5 mL). The mixture was stirred for 5 minutes, poured onto ice, and filtered. The solids were washed with water, methanol, and hexane, then dried under high vacuum to yield **6** as an insoluble black powder (0.884 g, 1.10 mmol, 97%). **6** proved insufficiently soluble to obtain NMR spectra. **HRMS** (MALDI$^-$) m/z [M]$^-$ calculated for C$_{50}$H$_{12}$O$_{12}$: 804.0323; found: 804.0288.

General Method for Formation of hPDI2 (11-20) from hPTCDA2 (6)

A scintillation vial was charged with **6** (1 eq), primary amine (10 eq), and imidazole. The vial was sealed with a PTFE septum cap with a needle to vent. The mixture was stirred at 120-140 ºC, depending on the boiling point of the amine, for 3-4 days. The mixture was removed from heat and dispersed by adding ethanol and stirring for 30 minutes. HCl (aq)

was added and the mixture was stirred an additional 30 minutes before filtering. Solids were then washed with various solvents, depending on their solubility. If sufficiently soluble, materials were subjected to flash column chromatography.

hPDI2-2EH (11)

A scintillation vial was charged with **6** (0.200 g, 0.25 mmol 1 eq), 2-ethylhexylamine (0.645 g, 5 mmol, 20 eq), and imidazole (2.0 g). The vial was sealed with a PTFE septum cap with a needle to vent. The mixture was stirred at 130 ºC for 4 days. The mixture was removed from heat and dispersed by adding ethanol and stirring for 30 minutes. 6M HCl was added and the mixture was stirred an additional 30 minutes before filtering and washing with water, then ethanol. The solids were passed through plug of silica gel using 4:1 DCM:ethyl acetate. The solution was concentrated under reduced pressure, dissolved in minimal DCM, precipitated in methanol, filtered, and washed with hexanes to yield **11** as a maroon solid (0.052 g, 0.042 mmol, 17%). Poor solubility in common solvents limited attempts at further purification. Aggregation was observed in the ^{1}H NMR spectrum up to 383 K in $C_2D_2Cl_4$, with the clearest spectrum attained at 363 K. **^{1}H NMR** (500 MHz, $C_2D_2Cl_4$, 363K): δ 9.75 (broad singlet, 4H), 9.18-9.08 (multiplet, 8H), 4.27-4.17 (multiplet, 8H), 2.15-2.07 (multiplet, 4H), 1.59-1.41 (broad multiplet, 32H), 1.11-1.06 (multiplet, 12H), 1.02-0.96 (broad multiplet, 12H). **HRMS** (MALDI⁻) m/z [M]⁻ calculated for $C_{82}H_{80}N_4O_8$: 1248.5971; found: 1248.5508.

hPDI2-2BO (12)

A scintillation vial was charged with **6** (0.200 g, 0.25 mmol 1 eq), 2-butyloctylamine (0.462 g, 2.5 mmol, 10 eq), and imidazole (2.5 g). The vial was sealed with a PTFE septum cap with a needle to vent. The mixture was stirred at 130 ºC for 3 days. The mixture was removed from heat and dispersed by adding ethanol and stirring for 10 minutes. 6M HCl was added and the mixture was stirred an additional 10 minutes before filtering and washing with water, ethanol, and methanol. The solids were then purified by flash column chromatography (SiO_2, gradient mobile phase: DCM to 97:3 DCM:THF) to yield **12** as a maroon solid (0.140 g, 0.095 mmol, 38%). Aggregation was observed in the ^{1}H NMR spectrum up to 373 K in $C_2D_2Cl_4$. **^{1}H NMR** (500 MHz, $C_2D_2Cl_4$, 373K): δ 9.72 (broad singlet, 4H), 9.16-9.06 (multiplet, 8H), 4.20 (broad apparent singlet, 8H), 2.13 (broad apparent singlet, 4H), 1.48-1.30 (multiplet, 56H), 0.96 (broad apparent singlet, 16H), 0.88 (broad apparent singlet, 16H). **^{13}C NMR** (400 MHz, $C_2D_2Cl_4$, 300K): Numerous carbon resonances overlap or are broadened, leading to fewer signals than the number of chemically distinct carbon nuclei. δ 163.34, 163.13, 132.85, 129.94, 126.24, 125.38, 124.53, 123.73, 123.13, 122.65, 121.92, 44.80, 36.54, 31.74, 31.57, 31.08, 29.67, 28.40, 26.29, 23.03, 22.57, 14.13, 14.09. **HRMS** (QTOF, ESI$^+$) m/z [M + Na]$^+$ calculated for $C_{98}H_{112}N_4O_8Na$: 1495.8378; found: 1495.8337.

hPDI2-2HD (13)

A scintillation vial was charged with **6** (0.200 g, 0.25 mmol 1 eq), 2-butyloctylamine (0.601 g, 2.5 mmol, 10 eq), and imidazole (2.5 g). The vial was sealed with a PTFE

septum cap with a needle to vent. The mixture was stirred at 130 ºC for 3 days. The mixture was removed from heat and dispersed by adding ethanol and stirring for 10 minutes. 6M HCl was added and the mixture was stirred an additional 10 minutes before filtering and washing with water, ethanol, and methanol. The solids were then purified by flash column chromatography (SiO$_2$, gradient mobile phase: hexane to 3:7 hexane:A, A = 99:1 DCM:Ethyl Acetate) to yield **13** as a maroon solid (0.075 g, 0.044 mmol, 17%). Aggregation was observed in the ^{1}H NMR spectrum up to 373 K in C$_2$D$_2$Cl$_4$. **^{1}H NMR** (500 MHz, C$_2$D$_2$Cl$_4$, 373K): δ 10.06 (s, 4H), 9.33 (d, *J* = 8.1 Hz, 4H), 9.18 (d, *J* = 8.1 Hz, 4H), 4.29 (d, *J* = 6.8 Hz, 8H), 2.16 (broad multiplet, 4H), 1.48-1.18 (multiplet, 96H), 0.89-0.79 (multiplet, 24H). **^{13}C NMR** (400 MHz, C$_2$D$_2$Cl$_4$, 300K): Numerous carbon resonances overlap or are broadened, leading to fewer signals than the number of chemically distinct carbon nuclei. δ 163.55, 133.38, 133.19, 130.20, 126.51, 126.12, 125.86, 125.09, 123.92, 123.55, 122.98, 122.02, 44.92, 36.59, 31.73, 31.70, 31.57, 29.97, 29.64, 29.44, 29.16, 22.52, 14.05, 14.02. **HRMS** (QTOF, ESI$^+$) m/z [M + Na]$^+$ calculated for C$_{110}$H$_{136}$N$_4$O$_8$Na: 1721.0916; found: 1721.0874.

hPDI2-nC12 (14)

A scintillation vial was charged with **hPTCDA2** (0.208 g, 0.26 mmol 1 eq), undecylamine (0.481 g, 2.6 mmol, 10 eq), and imidazole (1.5 g). The vial was sealed with a PTFE septum cap with a needle to vent. The mixture was stirred at 120 ºC for 4 days. The mixture was removed from heat and dispersed by adding ethanol and stirring for 30 minutes. 6M HCl was added and the mixture was stirred an additional 30 minutes before

filtering and washing with water, then ethanol. The mixture purified by flash column chromatography (SiO$_2$, gradient mobile phase: DCM to 97:3 DCM:THF) to yield **14** as a black solid (0.174 g, 0.12 mmol, 46% yield). **^{1}H NMR** (500 MHz, C$_2$D$_2$Cl$_4$, 373K): δ 9.83 (s, 4H), 9.17 (d, *J* = 8.1 Hz, 4H), 9.11 (d, *J* = 8.1 Hz, 4H), 4.28 (broad multiplet, 8H), 1.89 (broad multiplet, 8H), 1.57 (broad multiplet, 8H), 1.48-1.23 (mult, 64H), 0.92 (broad multiplet, 12H). **^{13}C NMR** (400 MHz, C$_2$D$_2$Cl$_4$, 300K) due to poor solubility, fewer signals than predicted are observed: δ 162.79, 162.53, 132.61, 129.97, 125.89, 125.30, 124.09, 123.96, 122.80, 121.79, 41.06, 31.81, 29.58, 29.56, 29.34, 29.26, 28.22, 27.26, 22.61, 14.12. **HRMS** (MALDI$^-$) m/z [M]$^-$ calculated for C$_{98}$H$_{112}$N$_4$O$_8$: 1472.8475; found: 1472.7692.

hPDI2-F8 (15)

A scintillation vial was charged with **6** (0.300 g, 0.37 mmol 1 eq), 1*H*,1*H*,2*H*,2*H*-perfluorooctylamine (1.26 g, 3.5 mmol, 9.5 eq), and imidazole (2.0 g). The vial was sealed with a PTFE septum cap with a needle to vent. The mixture was stirred at 120 ºC for 3 days. The mixture was removed from heat and dispersed by adding ethanol and stirring for 30 minutes. 6M HCl was added and the mixture was stirred an additional 30 minutes before filtering and washing with water, ethanol, and hexanes. The solids were filtered through a plug of silica gel using 2:3 α,α,α-trifluorotoluene:THF and then concentrated under reduced pressure to yield **15** as a maroon solid (0.404 g, 0.185 mmol, 62%). **^{1}H NMR** (500 MHz, CF$_3$CO$_2$H, 300K): δ 9.69 (broad singlet, 4H), 9.40-9.14

(multiplet, 8H), 4.48 (broad apparent singlet, 8H), 2.73 (broad apparent singlet, 8H). **HRMS** (MALDI⁻) m/z [M]⁻ calculated for $C_{82}H_{28}F_{52}N_4O_8$: 2184.1071; found: 2184.1309.

hPDI2-4PhB (16)

A scintillation vial was charged with **6** (0.195 g, 0.25 mmol 1 eq), 2-butyloctylamine (0.337 g, 2.5 mmol, 10 eq), and imidazole (1.5 g). The vial was sealed with a PTFE septum cap with a needle to vent. The mixture was stirred at 130 ºC for 3 days. The mixture was removed from heat and dispersed by adding ethanol and stirring for 10 minutes. 6M HCl was added and the mixture was stirred an additional 10 minutes before filtering and washing with water, ethanol, and hexanes. The solids were then purified by flash column chromatography (SiO₂, gradient mobile phase: DCM to 95:5 DCM:THF) to yield **16** as a black solid (0.167 g, 0.126 mmol, 50%). Aggregation was observed in the ¹H NMR spectrum up to 373 K in C₂D₂Cl₄. **¹H NMR** (500 MHz, C₂D₂Cl₄, 373K): δ 9.66 (s, 4H), 9.04 (apparent singlet, 8H), 7.32-7.24 (multiplet, 16H), 7.20-7.15 (multiplet, 4H), 4.31-4.23 (broad multiplet, 4.27), 2.80-2.73 (multiplet, 8H), 1.96-1.82 (multiplet, 16H). **¹³C NMR** (400 MHz, C₂D₂Cl₄, 300K): Numerous carbon resonances overlap or are broadened, leading to fewer signals than the number of chemically distinct carbon nuclei. δ 162.75, 162.48, 142.08, 132.51, 130.01, 128.35, 128.27, 125.69, 125.22, 123.99, 122.69, 121.61, 40.70, 35.56, 29.13, 27.95. **HRMS** (MALDI⁻) m/z [M]⁻ calculated for $C_{90}H_{64}N_4O_8$: 1328.4719; found: 1328.4204.

hPDI2-Cy6 (17)

A scintillation vial was charged with **6** (0.200 g, 0.25 mmol 1 eq), 2,6-diisopropylaniline (0.248 g, 2.5 mmol, 10 eq), and imidazole (1.5 g). The vial was sealed with a PTFE septum cap with a needle to vent. The mixture was stirred at 120 ºC for 3 days. The mixture was removed from heat and dispersed by adding ethanol and stirring for 30 minutes. 6M HCl was added and the mixture was stirred an additional 30 minutes before filtering and washing with water, ethanol, and hexanes. The solids were then purified by flash column chromatography (SiO_2, gradient mobile phase: DCM to 9:1 DCM:THF) to yield **17** as a red solid (0.149 g, 0.132 mmol, 53%). **^{1}H NMR** (500 MHz, $C_2D_2Cl_4$, 373K): δ 10.26 (s, 4H), 9.41 (d, J = 8.1 Hz, 4H), 9.19 (d, J = 8.1, 4H), 5.25-5.17 (multiplet, 4H), 2.72 (multiplet, 8H), 2.07-1.94 (multiplet, 16H), 1.88-1.78 (multiplet, 4H), 1.65-1.54 (multiplet, 8H), 1.47-1.40 (multiplet, 4H). **^{13}C NMR** (400 MHz, $C_2D_2Cl_4$, 300K) δ 164.09, 163.95, 133.69, 133.53, 130.18, 126.75, 126.53, 126.30, 125.51, 123.91, 123.88, 123.74, 122.63, 54.43, 29.16, 26.50, 25.40. **HRMS** (QTOF, ESI$^+$) m/z [M + Na]$^+$ calculated for $C_{74}H_{56}N_4O_8Na$: 1151.3995; found: 1151.3975.

hPDI2-BzH (18)

A scintillation vial was charged with **6** (0.201 g, 0.25 mmol 1 eq), benzhydrylamine (0.456 g, 2.5 mmol, 10 eq), and imidazole (1.5 g). The vial was sealed with a PTFE septum cap with a needle to vent. The mixture was stirred at 130 ºC for 3 days. The mixture was removed from heat and dispersed by adding ethanol and stirring for 10 minutes. 6M HCl was added and the mixture was stirred an additional 10 minutes before

filtering and washing with water, ethanol, and hexanes. The solids were then purified by flash column chromatography (SiO$_2$, gradient mobile phase: hexane to 99:1 DCM:ethyl acetate) to yield **18** as a bright red solid (0.199 g, 0.136 mmol, 54%). Aggregation was observed in the ^{1}H NMR spectrum up to 373 K in C$_2$D$_2$Cl$_4$. **^{1}H NMR** (500 MHz, C$_2$D$_2$Cl$_4$, 373K): δ 10.32 (s, 4H), 9.47 (d, J = 8.3 Hz, 4H), 9.23 (d, J = 8.3 Hz, 4H), 7.78 (broad singlet, 4H), 7.67-7.51 (broad multiplet, 16H), 7.48-7.24 (broad multiplet, 24H). **^{13}C NMR** (400 MHz, C$_2$D$_2$Cl$_4$, 300K): Numerous carbon resonances overlap or are broadened, leading to fewer signals than the number of chemically distinct carbon nuclei. δ 163.79, 163.64, 138.27, 134.19, 134.09, 130.61, 128.85, 128.21, 127.29, 127.02, 126.57, 126.39, 125.77, 124.17, 124.09, 123.58, 122.40, 59.43. **HRMS** (QTOF, ESI[+]) m/z [M + Na]$^+$ calculated for C$_{102}$H$_{56}$N$_4$O$_8$Na: 1487.3995; found: 1487.3994.

hPDI2-tBuGly (19)

A scintillation vial was charged with **hPTCDA2** (0.200 g, 0.25 mmol 1 eq), glycine *tert*-butyl ester hydrochloride (0.417 g, 2.5 mmol, 10 eq), and imidazole (1.5 g). The vial was sealed with a PTFE septum cap with a needle to vent. The mixture was stirred at 130 ºC for 4 days. The mixture was removed from heat and dispersed by adding ethanol and stirring for 30 minutes. 6M HCl was added and the mixture was stirred an additional 30 minutes before filtering and washing with water, methanol, and hexanes to yield crude **19** as a black solid (0.325 g, 0.25 mmol, 100%). Poor solubility in common solvents limited further attempts at purification. Aggregation was observed in the ^{1}H NMR spectrum up to 363 K in DMSO-D$_6$. **^{1}H NMR** (500 MHz, DMSO-D$_6$, 363K): δ 9.08 (broad singlet, 4H),

8.98-8.73 (broad multiplet, 8H), 4.68 (broad singlet, 8H), 2.54 (singlet, 36H). **HRMS** (MALDI⁻) m/z [M − 4tBu + 4H]⁻ calculated for $C_{58}H_{24}N_4O_{16}$: 1032.1182; found: 1032.1222.

hPDI2-Gly

A scintillation vial was charged with **hPDI2-tBuGly** (0.150 g, 0.12 mmol) and trifluoroacetic acid (5 mL). The mixture was stirred at room temperature for 18 hours, then precipitated in toluene and filtered. The solids were washed with toluene, DCM, ethanol, and hexanes to yield **hPDI2-Gly** as a black solid (0.074 g, 0.072 mmol, 60 %). **HRMS** (MALDI⁻) m/z [M]⁻ calculated for $C_{58}H_{24}N_4O_{16}$: 1032.1182; found: 1032.1550.
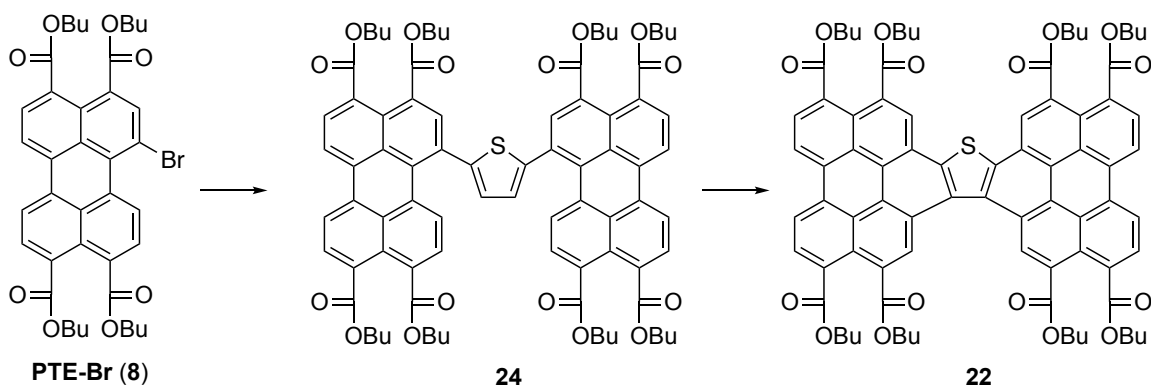
Scheme 2.6. Synthesis of intermediate **22.**

24

A 2-neck 50 mL roundbottom flask was charged with **PTE-Br** (1.498 g, 2.0 mmol, 2.2 eq), **Bis(tributylstannyl)thiophene** (0.600 g, 0.9 mmol, 1 eq), and toluene (20 mL). The

mixture was sparged with nitrogen for 30 minutes before adding adding $Pd_2dba_3/AsPh_3$ mixture (0.12 g, 0.09 mmol, 0.1 eq) and sparging for an additional 10 minutes. The mixture was then stirred at 110 ºC for 2 hrs. The mixture was cooled, concentrated under reduced pressure, and purified by flash column chromatography (SiO_2, gradient mobile phase: DCM to 99:3 DCM:THF) to yield **PTE-T** as an orange-red solid (0.884 g, 0.64 mmol, 71%). **¹H NMR** (500 MHz, $CDCl_3$, 300K): δ 8.30-8.25 (multiplet, 6H), 8.20 (s, 2H), 8.12-8.06 (multiplet, 4H), 7.80 (d, J = 8.1 Hz, 2H), 7.14 (s, 2H), 4.27-4.25 (multiplet, 16H), 1.82-1.68 (multiplet, 16H), 1.52-1.36 (multiplet, 16H), 1.01-0.94 (18H), 0.89 (t, J = 7.4 Hz, 6H). **¹³C NMR** (400 MHz, $CDCl_3$, 300K): δ 168.42, 168.38, 168.26, 168.00, 133.82, 133.02, 132.71, 132.69, 131.66, 130.77, 130.20, 130.16, 129.89, 129.80, 129.73, 129.63, 128.96, 128.23, 127.47, 122.24, 121.41, 65.42, 65.34, 65.30, 30.56, 30.48, 19.15, 19.07, 13.70, 13.62. **HRMS** (QTOF, ESI^+) m/z $[M + Na]^+$ calculated for $C_{84}H_{88}O_{16}SNa$: 1407.5691; found: 1407.5670.

22

A 200 mL roundbottom flask was charged with **24** (0.480 g, 0.35 mmol, 1 eq), iodine (0.349 g, 1.38 mmol, 4 eq), potassium carbonate (0.478 g, 3.47 mmol, 10 eq), and toluene (100 mL). The solution was sparged with nitrogen for 30 minutes and then sealed and placed under positive nitrogen pressure. The flask was stirred at room temperature while illuminating with two XXX lamps and the reaction was monitored using MALDI-TOF mass spectrometry. After 24 hours the lamps were turned off. The solution was washed with sodium thiosulfate then brine, dried with magnesium sulfate, and concentrated under

reduced pressure. The resulting solids were dissolved in a minimum amount of chloroform and precipitated in cold methanol, filtered, washed with additional methanol, and dried under vacuum to yield **22** as a bright orange solid (0.410 g, 0.296 mmol, 85%).

^{1}H NMR (500 MHz, CDCl$_3$, 300K): δ 9.80 (s, 2H), 9.18 (s, 2H), 9.09-9.01 (multiplet, 4H), 8.51 (d, J = 8.1 Hz, 2H), 8.41 (d, J = 8.0 Hz, 2H), 4.58-4.32 (multiplet, 16H), 2.00-1.91 (multiplet, 8H), 1.81-1.54 (multiplet, 16H), 1.50-1.42 (multiplet, 4H), 1.12-1.04 (multiplet, 16H), 0.96 (t, J = 7.4 Hz, 6H), 0.48 (t, J = 7.4, 6H). **^{13}C NMR** (400 MHz, CDCl$_3$, 300K): δ 168.51, 168.33, 168.26, 167.72, 139.18, 132.26, 131.58, 131.28, 130.76, 130.67, 130.11, 129.86, 129.06, 128.89, 128.66, 126.88, 126.73, 126.54, 126.45, 125.62, 123.95, 123.70, 123.48, 122.06, 121.98, 65.82, 65.54, 65.43, 30.80, 30.74, 30.64, 30.47, 19.36, 19.23, 19.00, 13.89, 13.86, 13.75, 13.38. **HRMS** (QTOF, ESI$^+$) m/z [M + Na]$^+$ calculated for C$_{84}$H$_{84}$O$_{16}$SNa: 1403.5377; found: 1403.5355.

23

A scintillation vial was charged with **FPTE-T** (0.410 g, 0.296 mmol, 1 eq) and sulfuric acid (3 mL). The mixture was stirred at room temperature for 30 minutes, then poured onto ice. The resulting solids were filtered and washed with water, methanol, ethanol, and hexanes. The solids were then dried under vacuum to yield **23** as a black powder (0.252 g, 0.295 mmol, 99%) which was carried forward without further purification. **HRMS** (MALDI$^-$) m/z [M]$^-$ calculated for C$_{52}$H$_{12}$O$_{12}$S: 860.0044; found: 859.9771.

FPDI-T (21)

A scintillation vial was charged with **23** (0.252 g, 0.295 mmol, 1 eq), 6-undecylamine (0.506 g, 2.96 mmol, 10 eq), and imidazole (3 g). The vial was sealed with a PTFE septum cap with a needle to vent. The mixture was stirred at 130 ºC for 3 days. The mixture was removed from heat and dispersed by adding ethanol and stirring for 30 minutes. 6M HCl was added and the mixture was stirred an additional 30 minutes before filtering and washing with water, then ethanol. The mixture was purified by flash column chromatography (SiO$_2$, gradient mobile phase: hexane to DCM) to yield **21** as a bright red-orange solid (0.185 g, 0.102 mmol, 42%). **^{1}H NMR** (500 MHz, CDCl$_3$, 323K): δ 10.51 (s, 2H), 9.73 (s, 2H), 9.26 (d, J = 8.0 Hz, 2H), 9.20 (d, J = 8.1 Hz, 2H), 8.99 (broad doublet, J = 7.3 Hz, 2H), 8.88 (broad doublet, J = 4.8 Hz, 2H), 5.29-5.28 (multiplet, 4H), 2.65-2.26 (broad multiplet, 8H), 2.10-1.92 (broad multiplet, 8H), 1.55-1.18 (broad multiplet, 48H), 1.02-0.67 (broad multiplet, 24H). **^{13}C NMR** (400 MHz, CDCl$_3$, 300K): δ 64.88, 164.61, 163.87, 163.27, 140.49, 133.21, 132.86, 132.00, 131.09, 129.89, 129.42, 128.79, 127.42, 126.97, 126.84, 126.59, 125.41, 124.29, 124.21, 123.76, 123.59, 123.41, 123.08, 122.33, 55.16, 54.69, 32.58, 32.39, 31.81, 26.80, 26.66, 22.88, 22.64, 22.51, 14.38, 14.09, 13.91. **HRMS** (MALDI⁻) m/z [M]⁻ calculated for C$_{96}$H$_{104}$N$_4$O$_8$S: 1472.7569; found: 1472.7078.

2.7 NMR Spectra
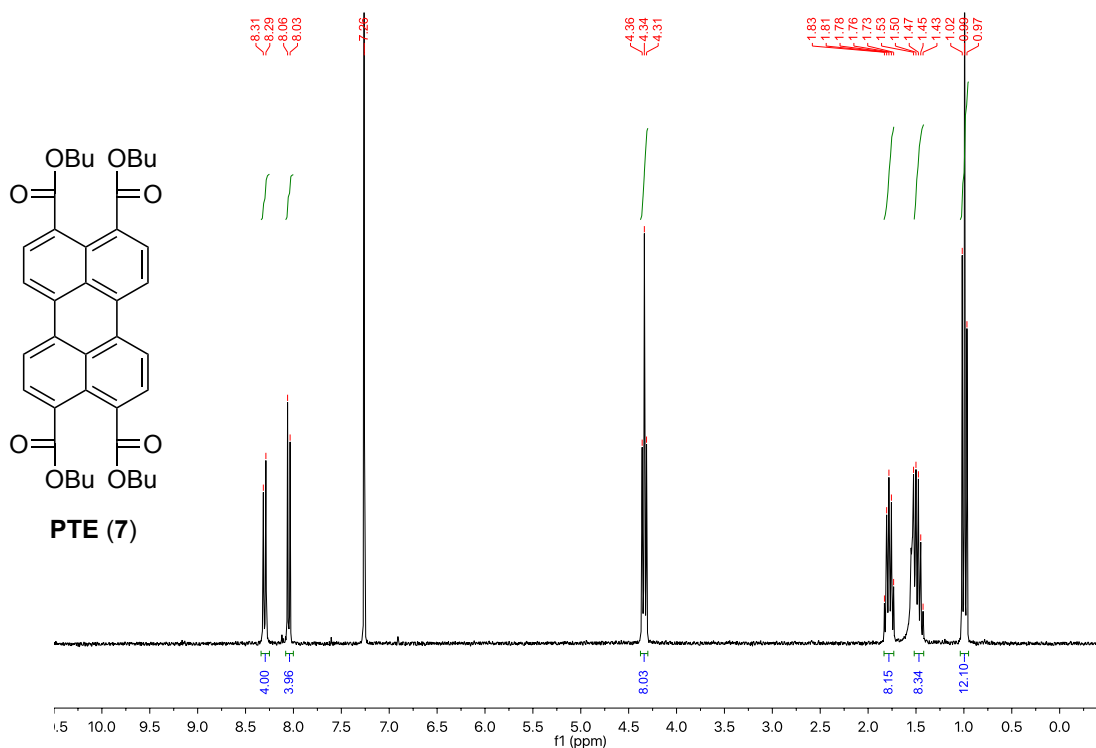
Figure 2.15. ^{1}H NMR spectrum of **7**.
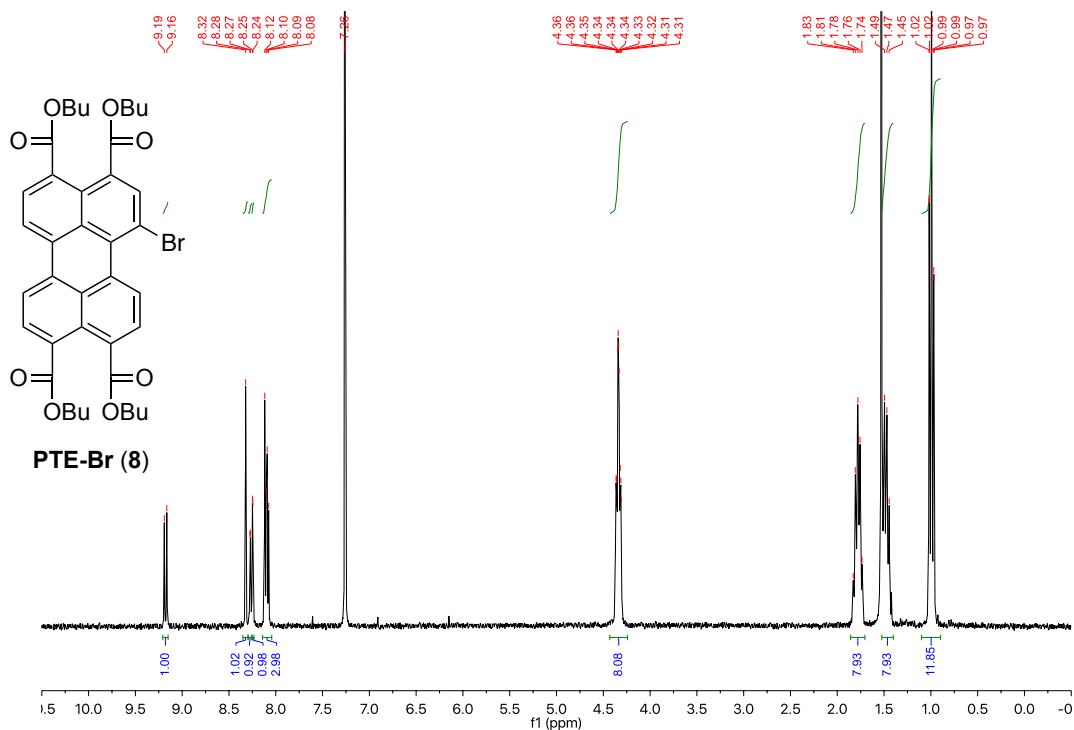
Figure 2.16. ^{1}H NMR spectrum of **8**.
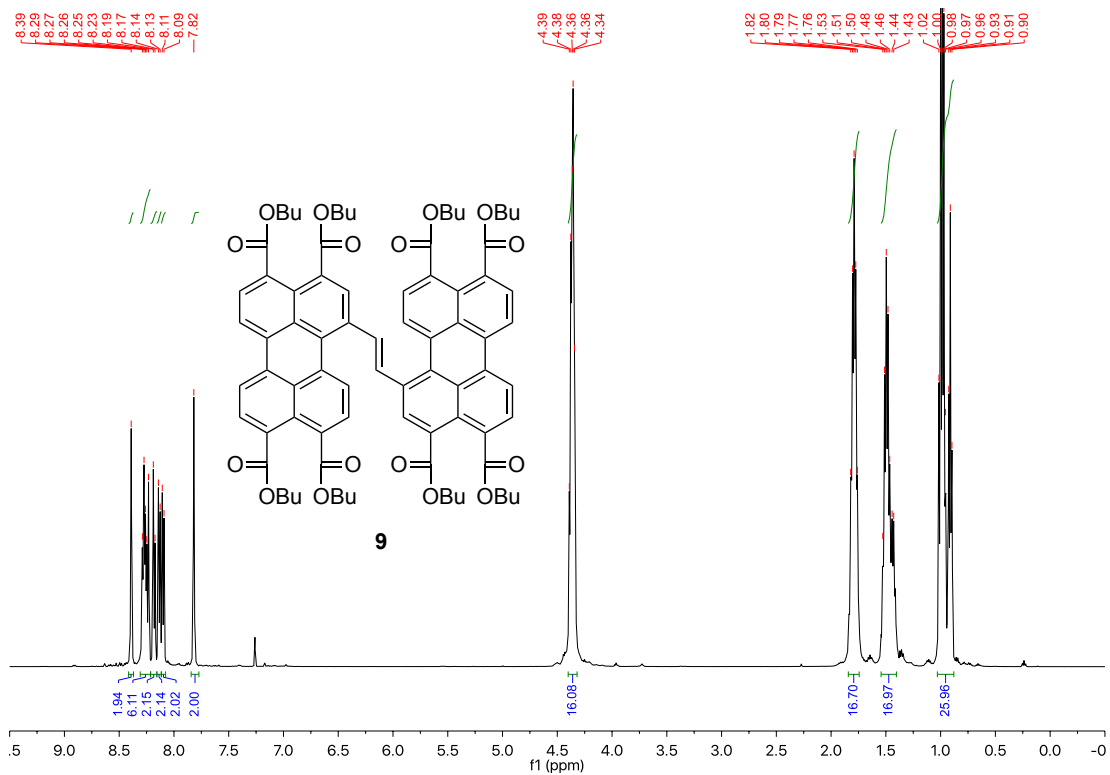
Figure 2.17. ^{1}H NMR spectrum of **9**.
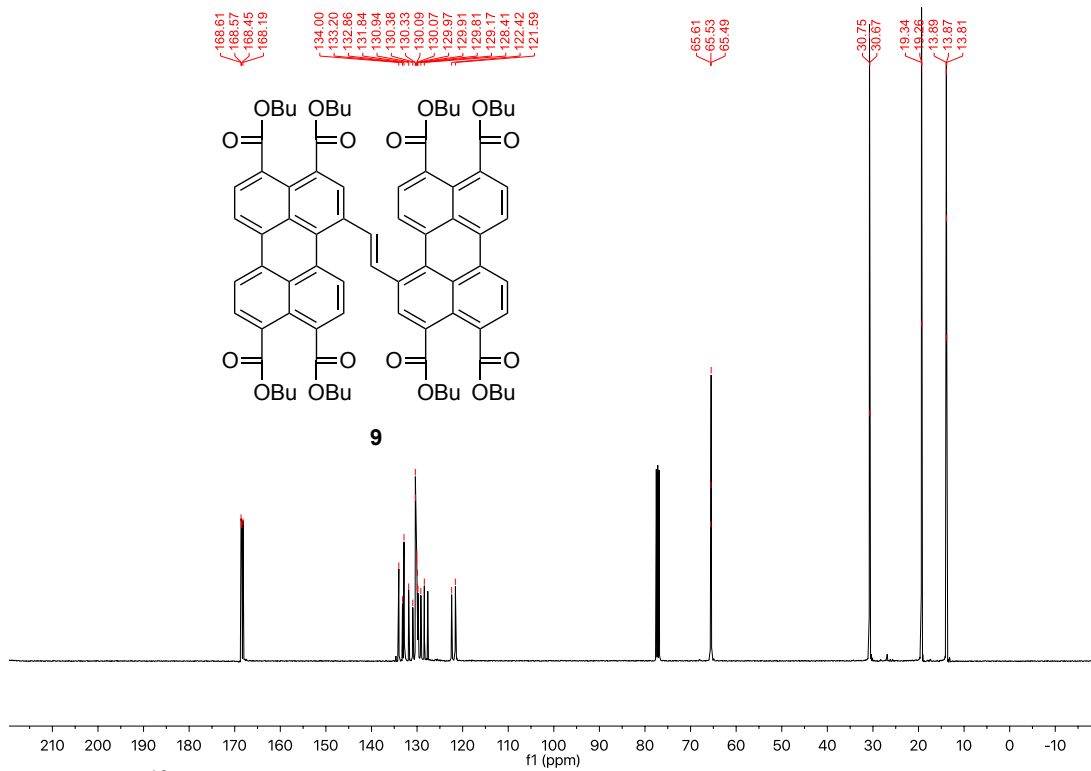
Figure 2.18. ^{13}C NMR spectrum of **9**.
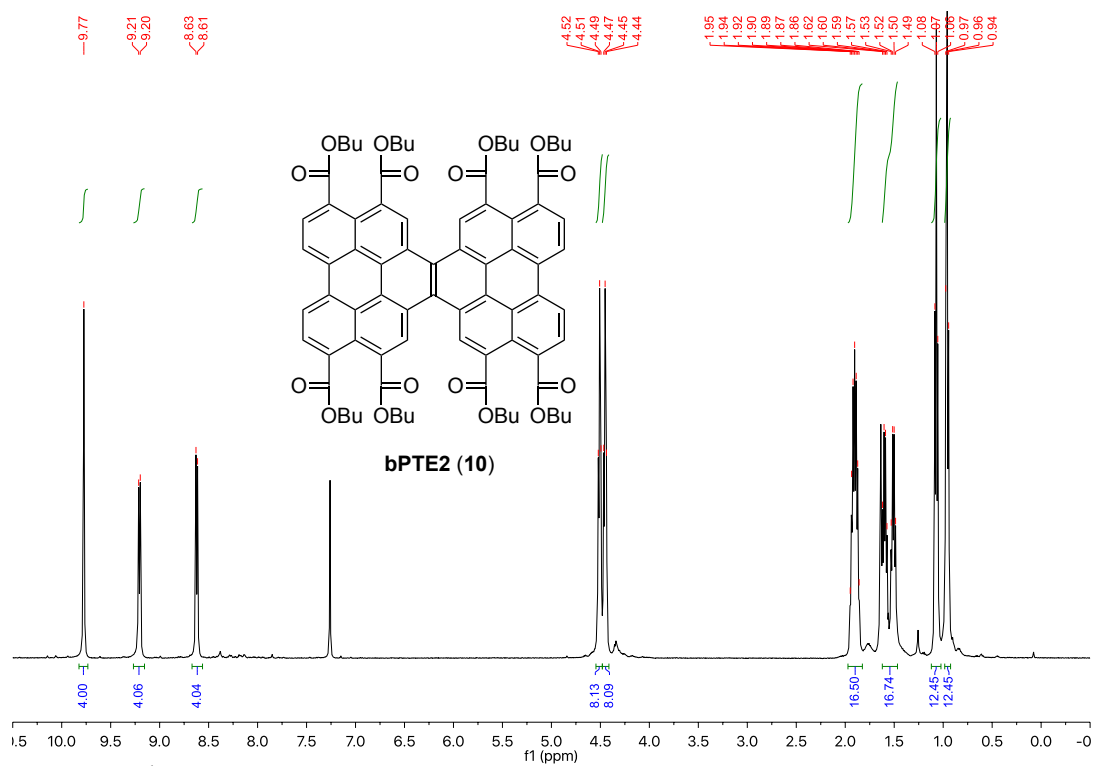
Figure 2.19. ¹H NMR spectrum of **10** .
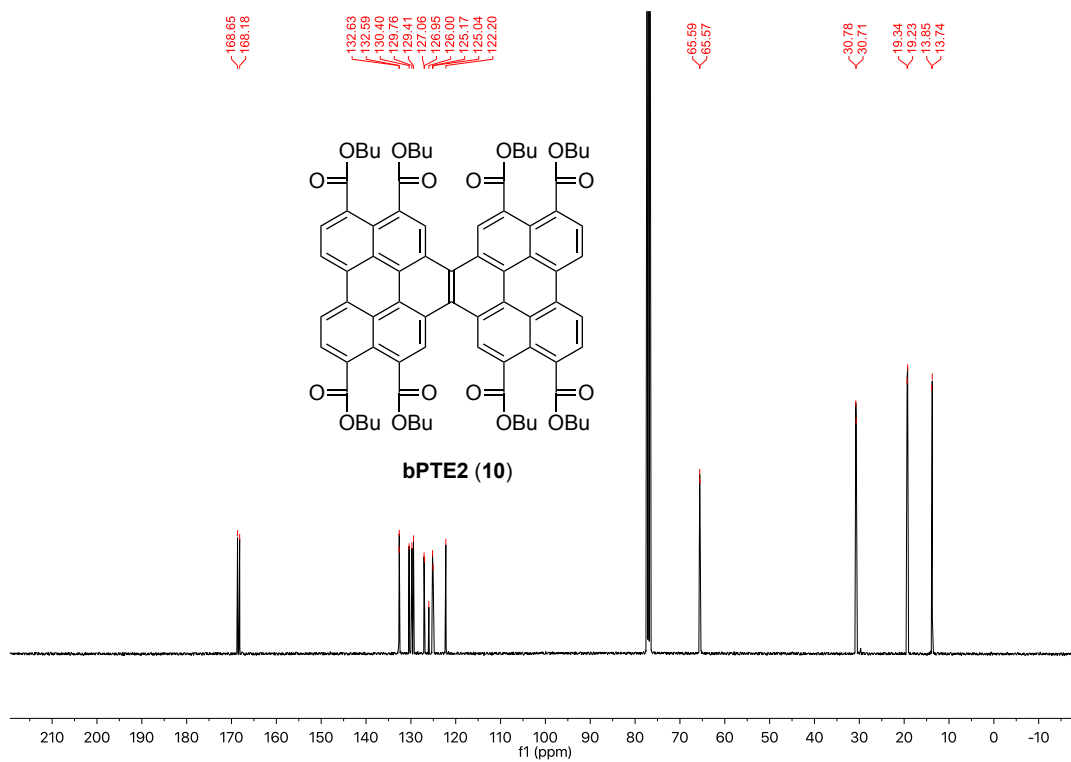
Figure 2.20. ¹³C NMR spectrum of **10**.
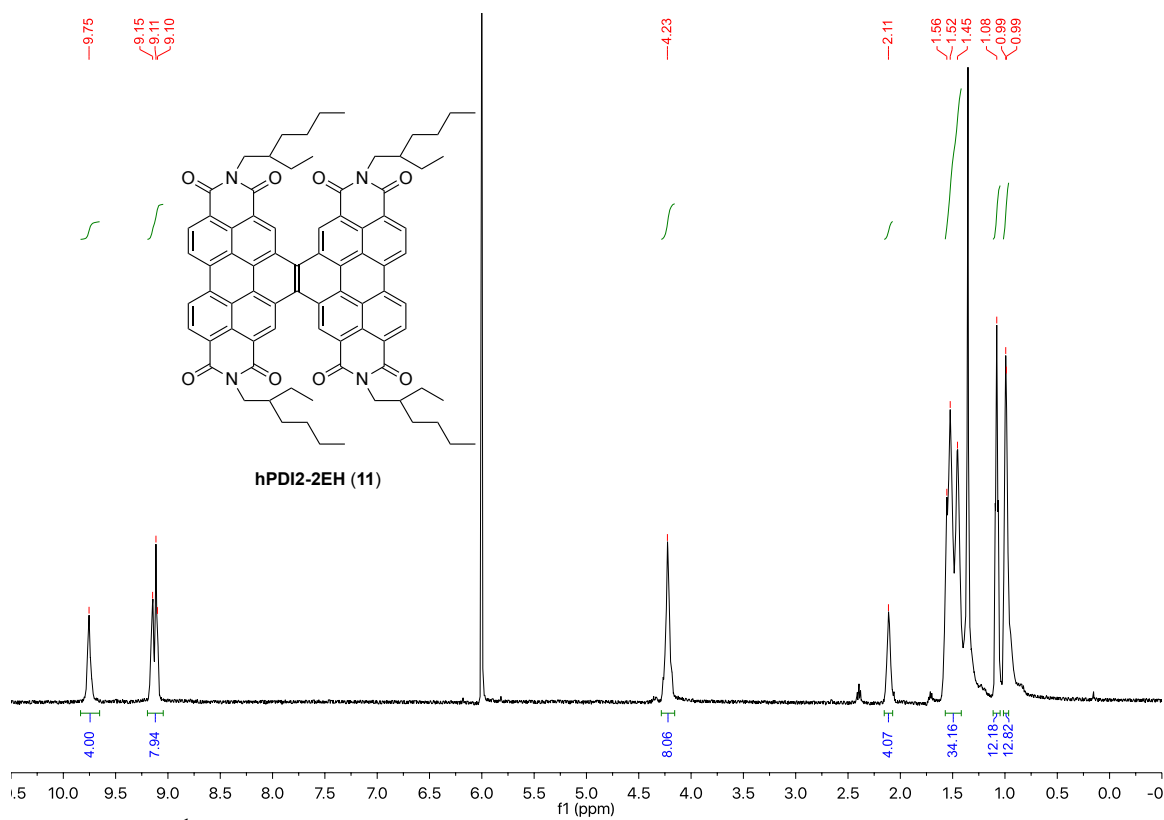
Figure 2.21. ^{1}H NMR spectrum of **11**.
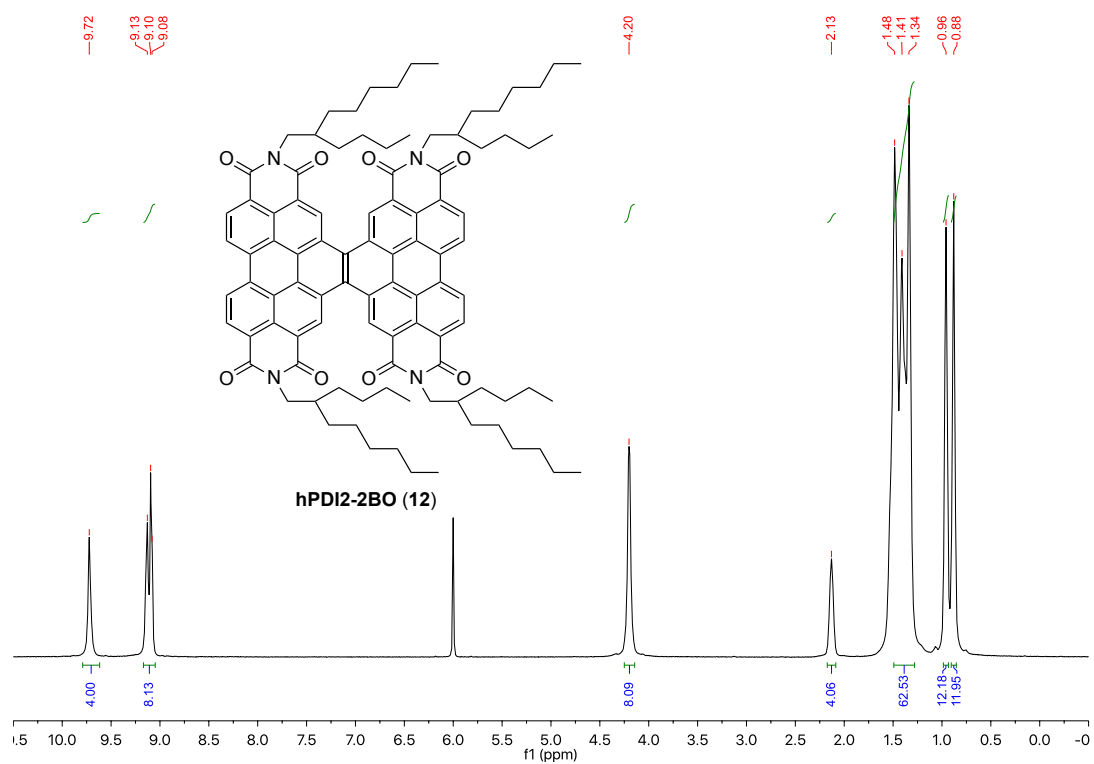
Figure 2.22. ^{1}H NMR spectrum of **12**.
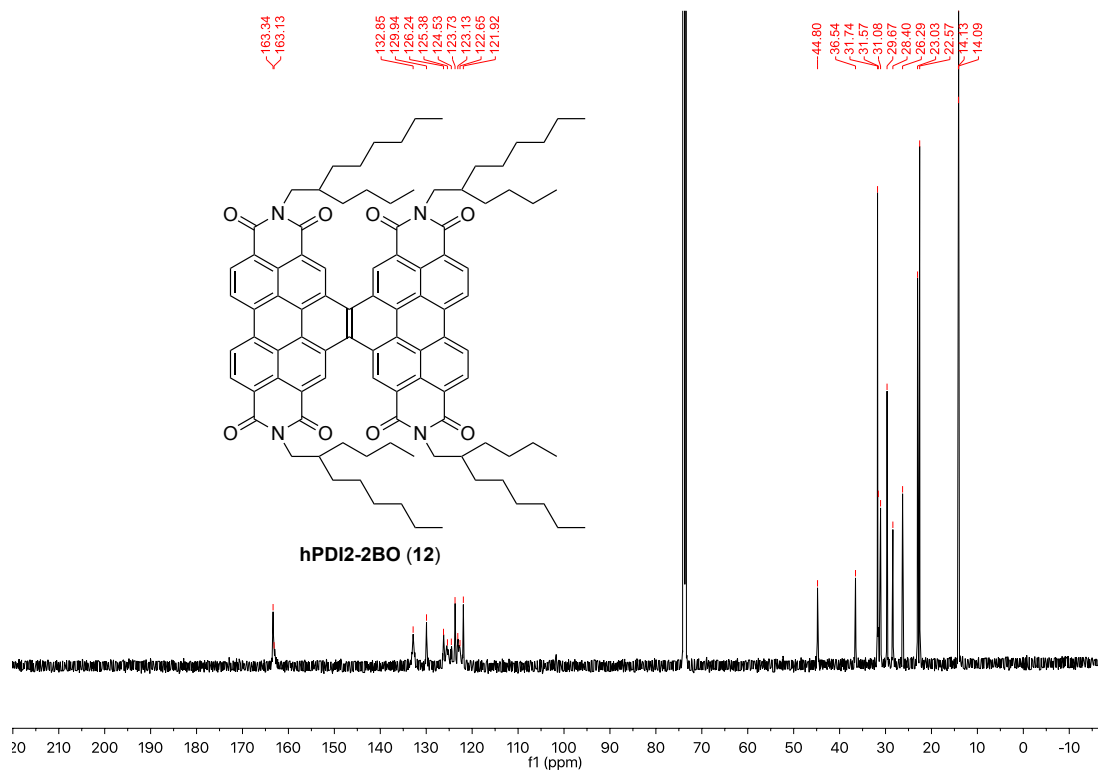
Figure 2.23. ^{13}C NMR spectrum of **11** .

240
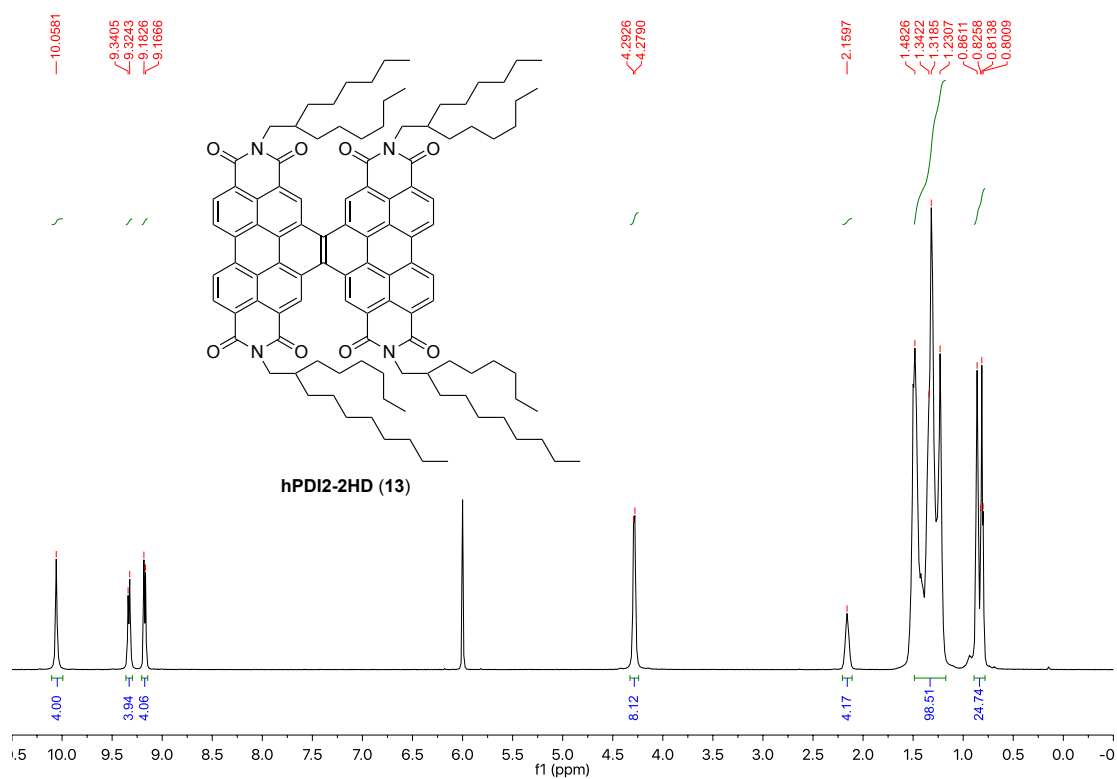
Figure 2.24. ^{1}H NMR spectrum of **13**.
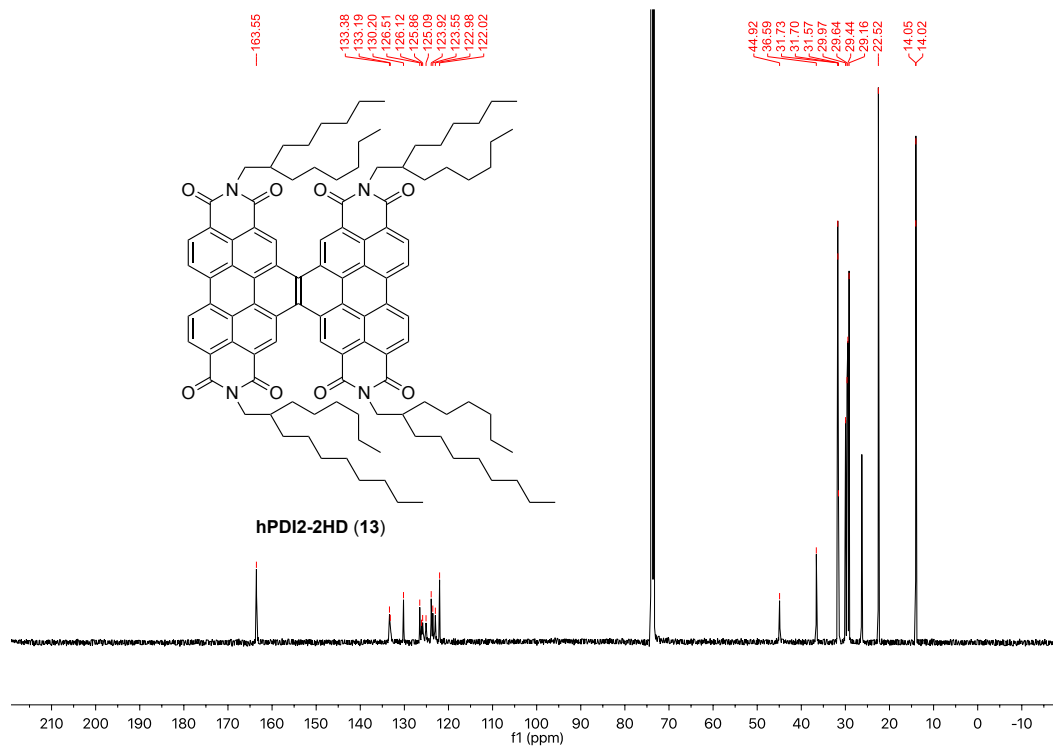
Figure 2.25. ^{13}C NMR spectrum of **13**.
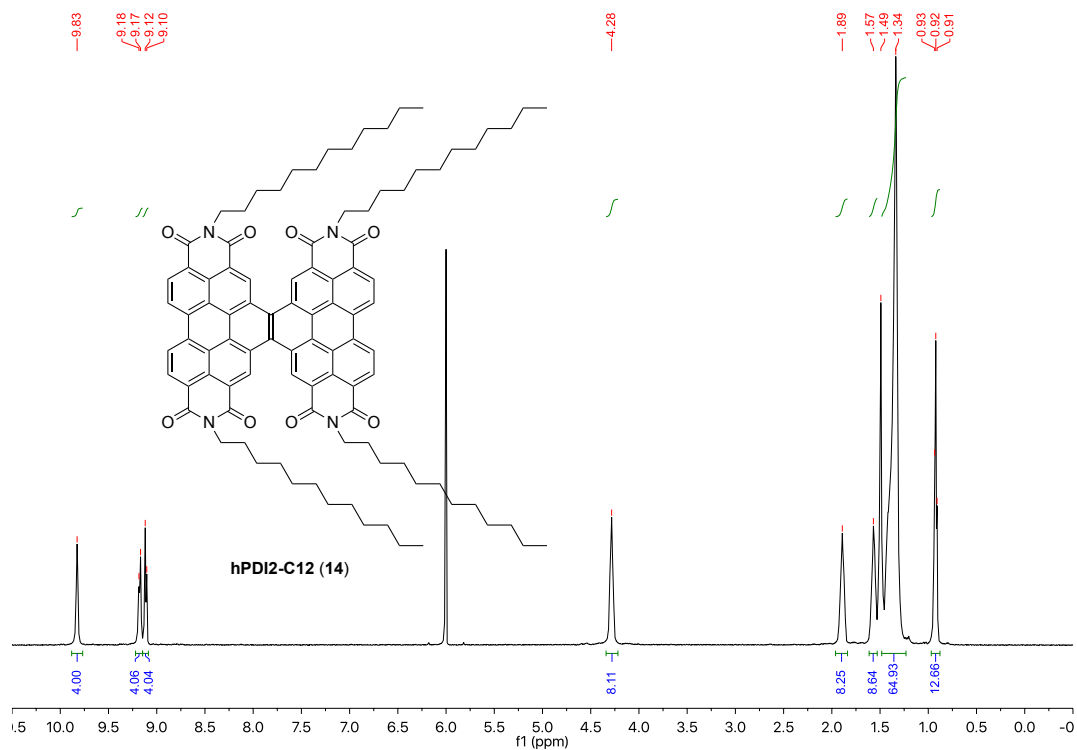
Figure 2.26. ^{1}H NMR spectrum of **14**.
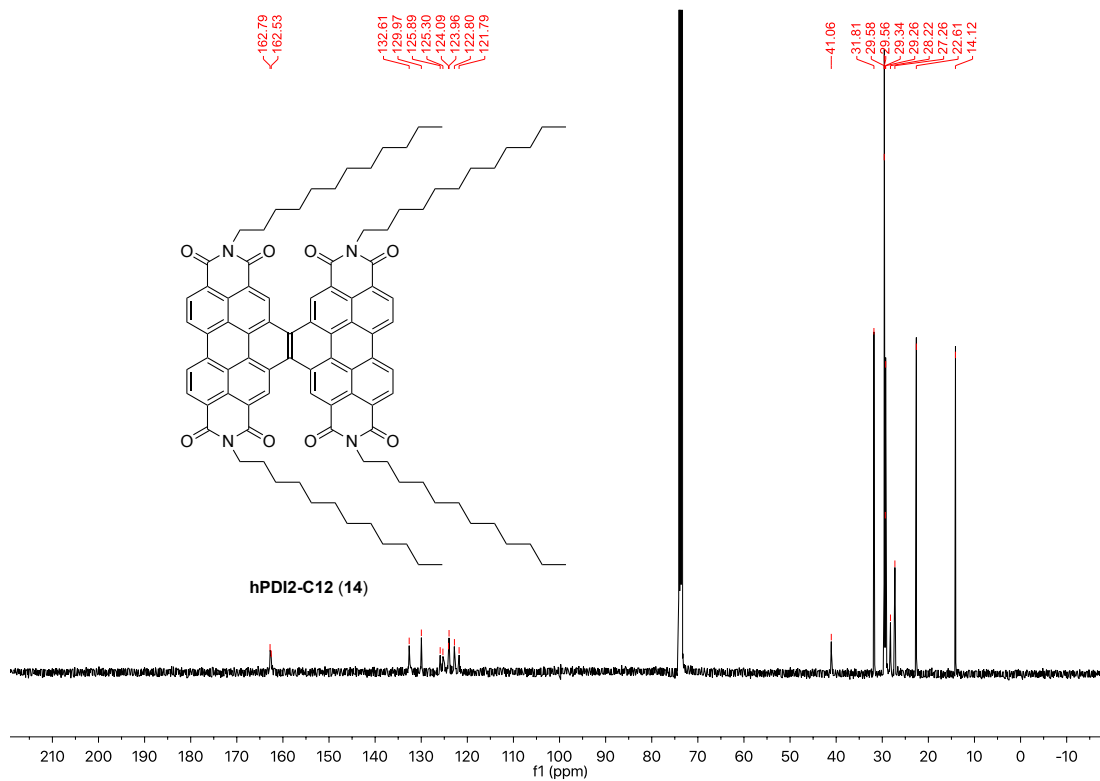
Figure 2.27. ^{13}C NMR spectrum of **14**.
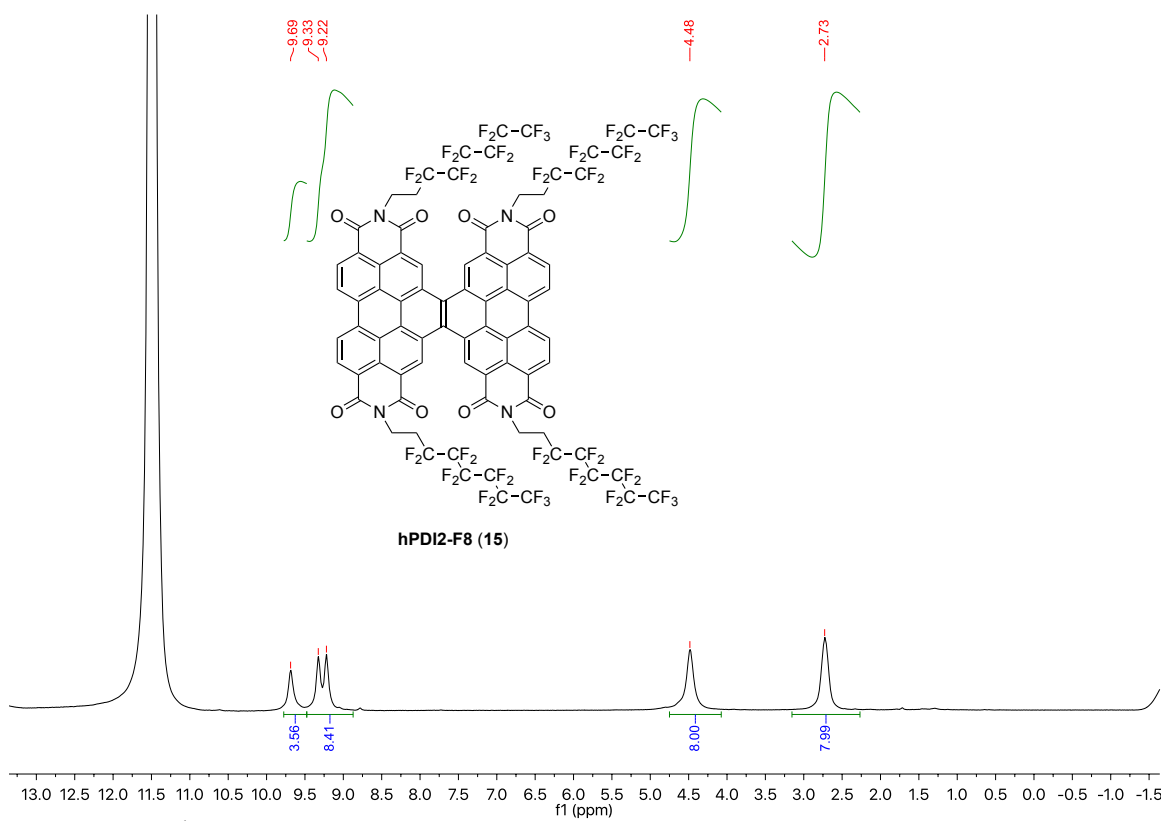
Figure 2.28. ^{1}H NMR spectrum of **15** .
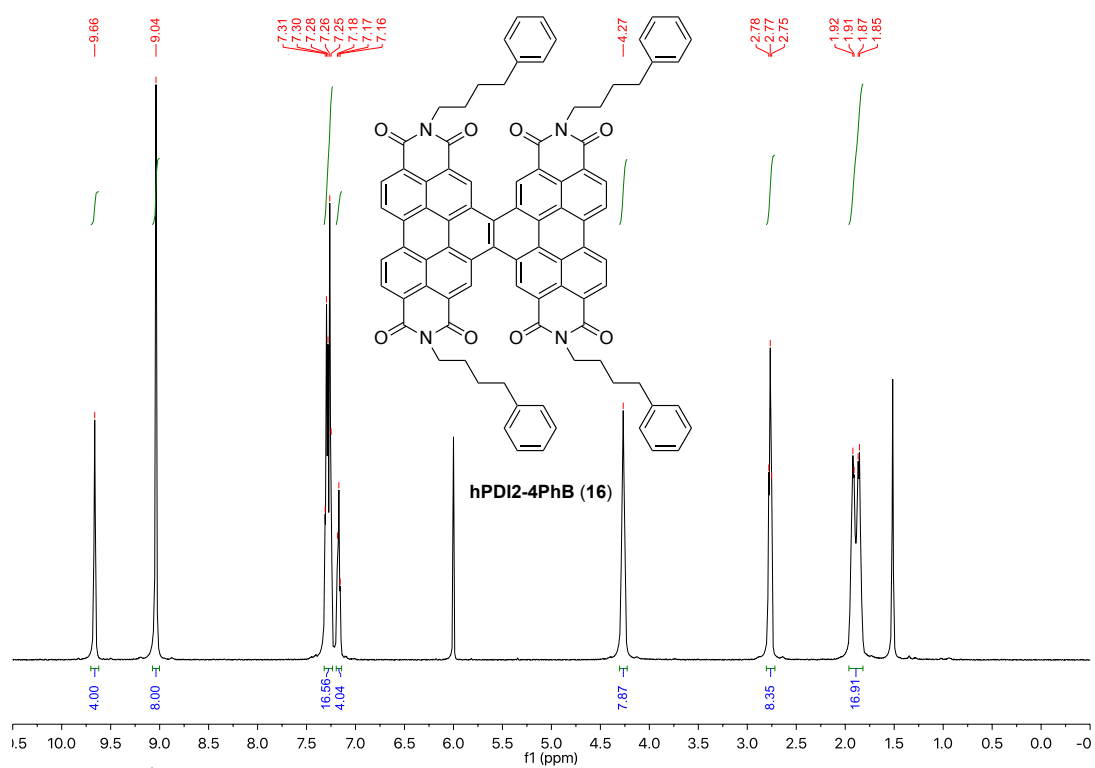
Figure 2.29. ^{1}H NMR spectrum of **16** .
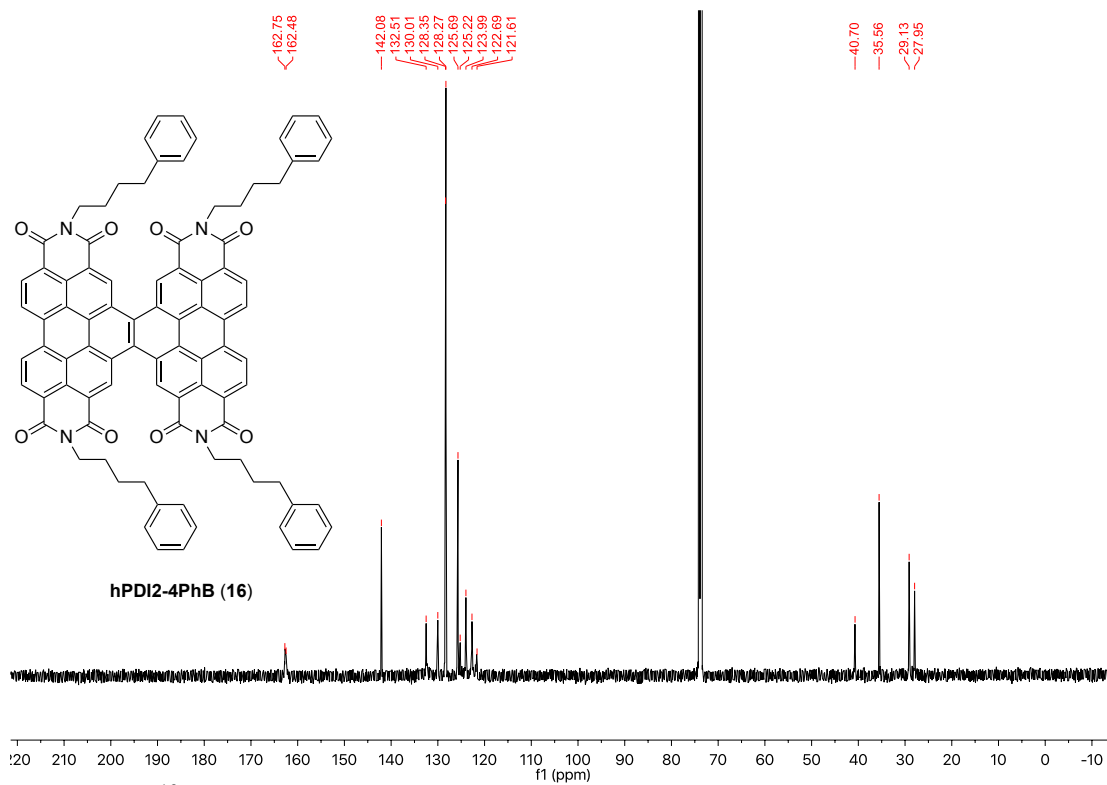
Figure 2.30. ^{13}C NMR spectrum of **16**.
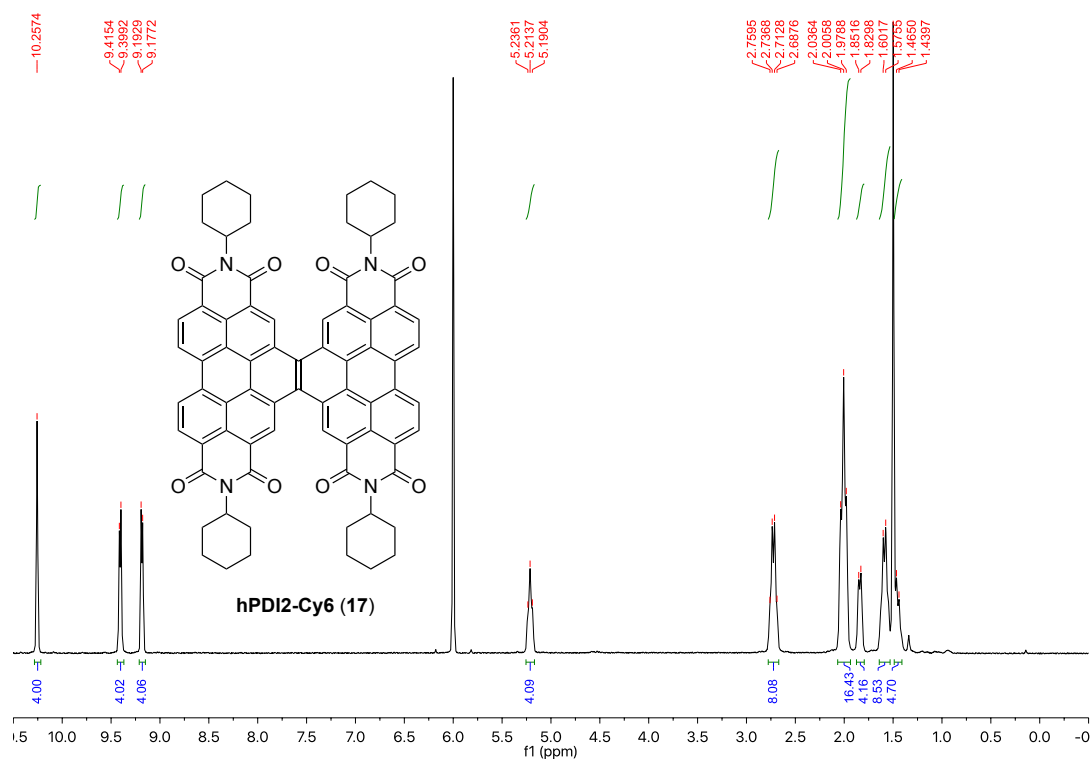
Figure 2.31. ^{1}H NMR spectrum of **17**.
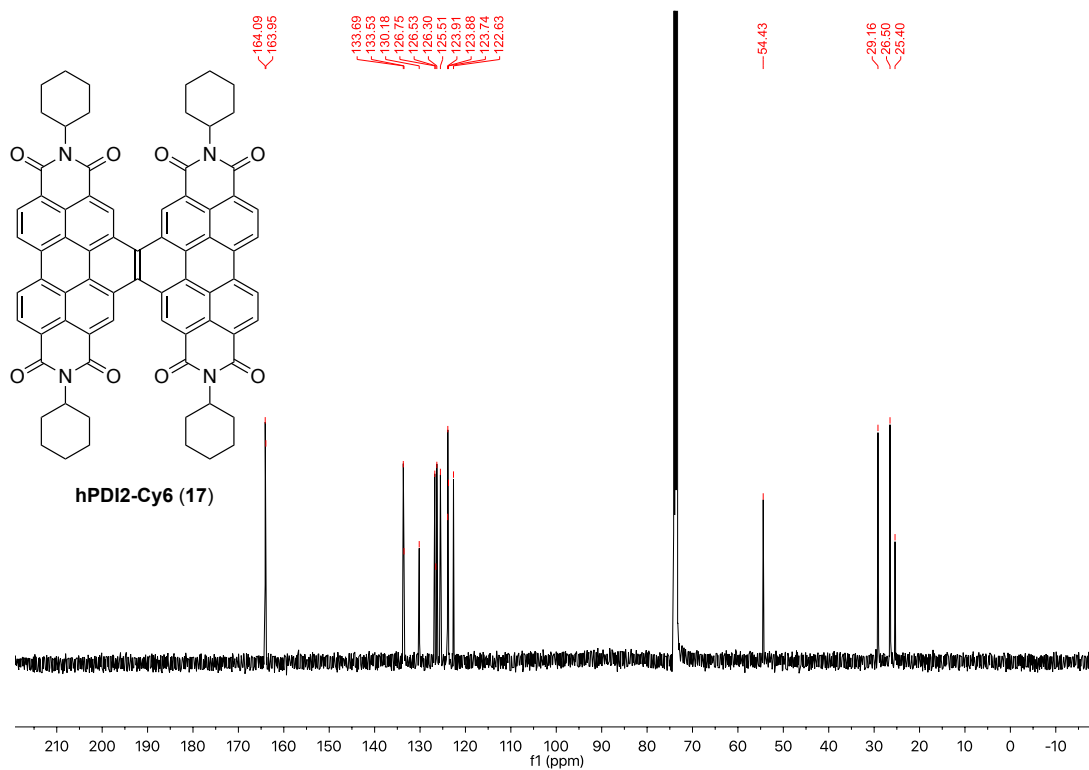
Figure 2.32. ^{13}C NMR spectrum of **17**.
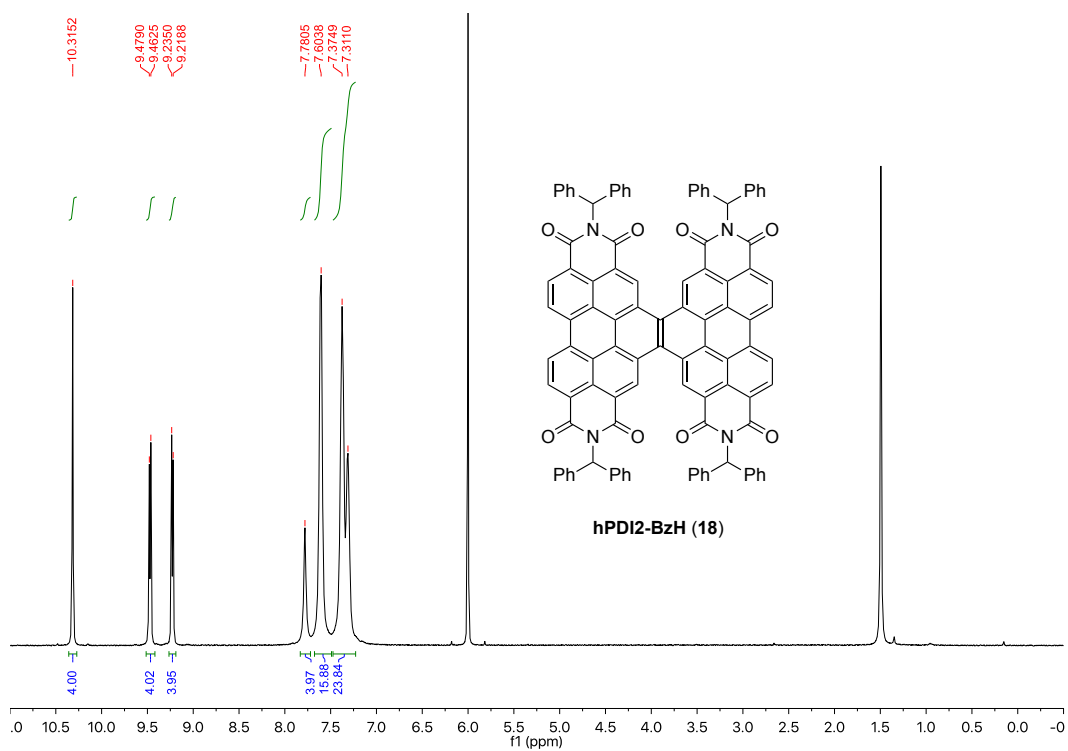
Figure 2.33. ^{1}H NMR spectrum of **18**.
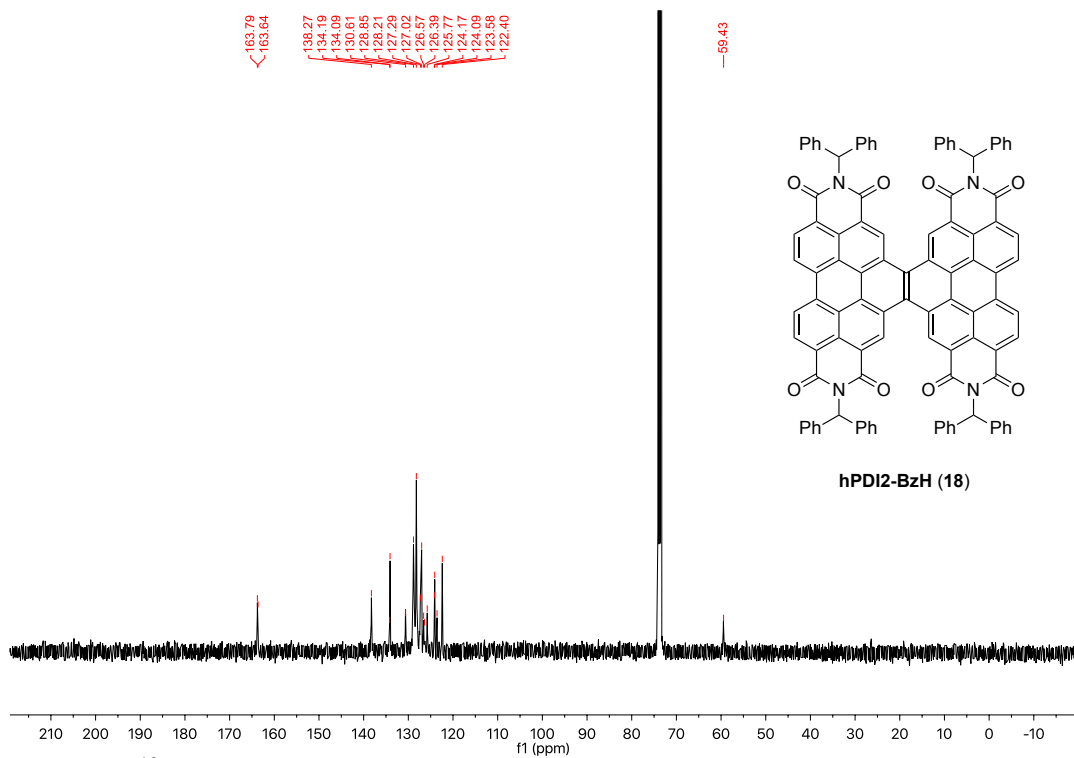
Figure 2.34. ^{13}C NMR spectrum of **18**.
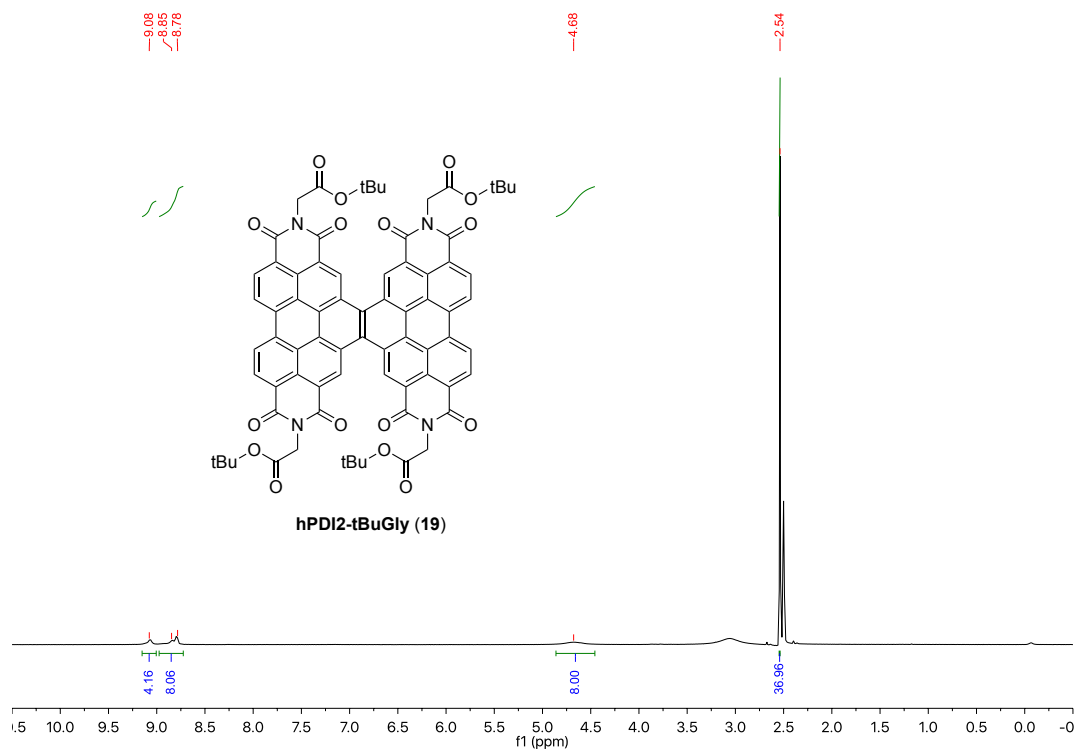
Figure 2.35. ^{1}H NMR spectrum of **19**.
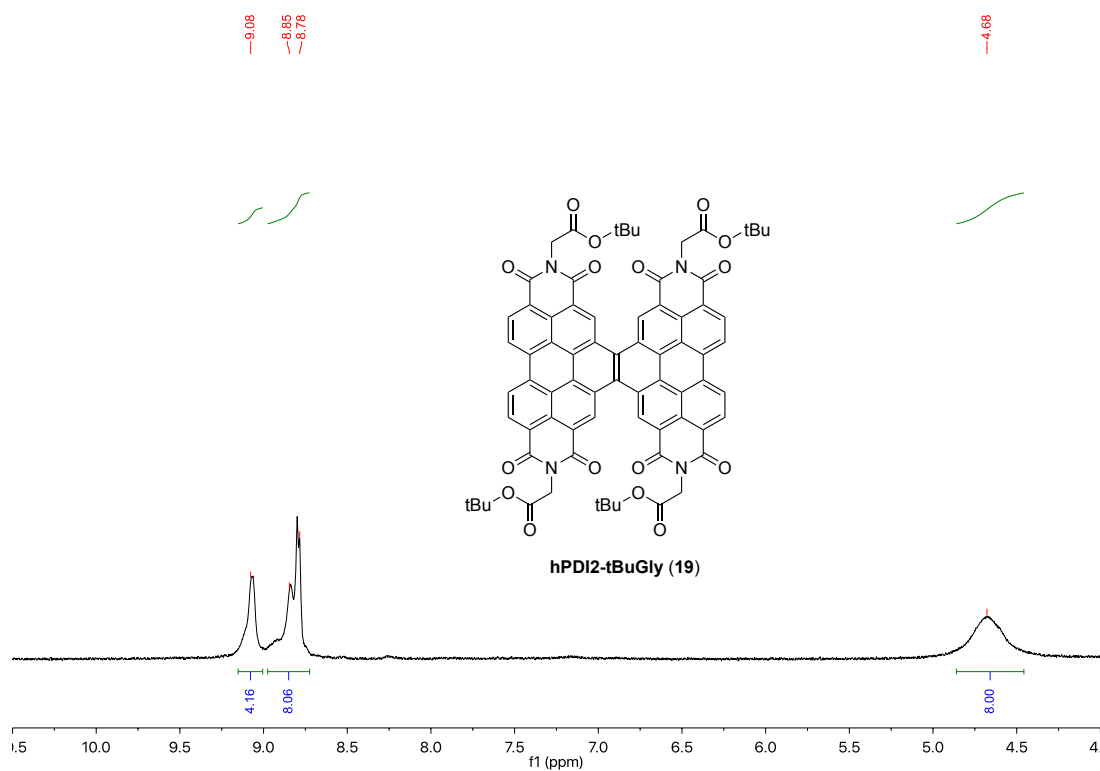
Figure 2.36. Detail of ^{1}H NMR spectrum of **19**.
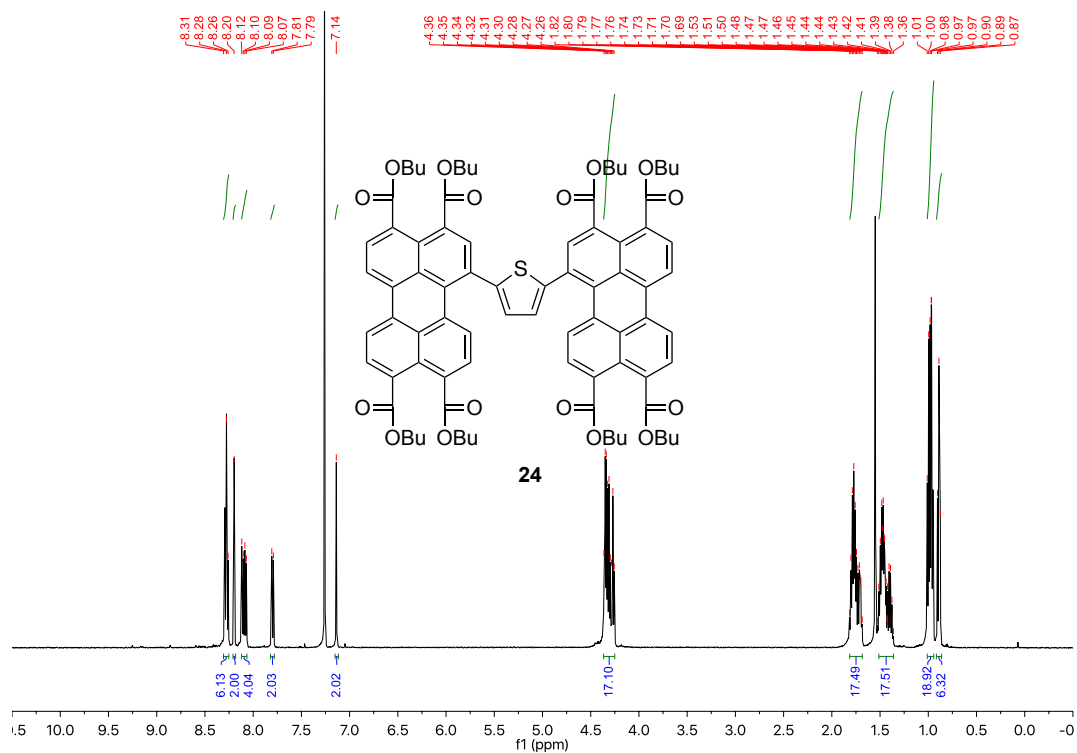
Figure 2.37. ^{1}H NMR spectrum of **24**.
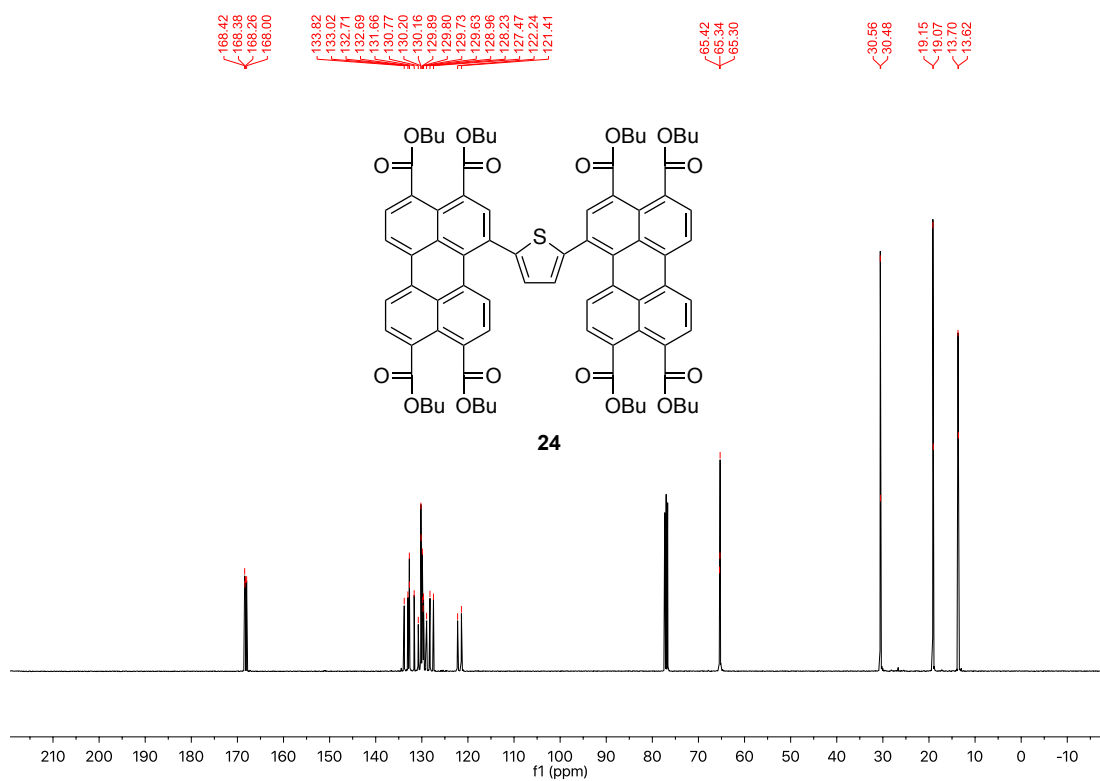
Figure 2.38. ^{13}C NMR spectrum of **24** .
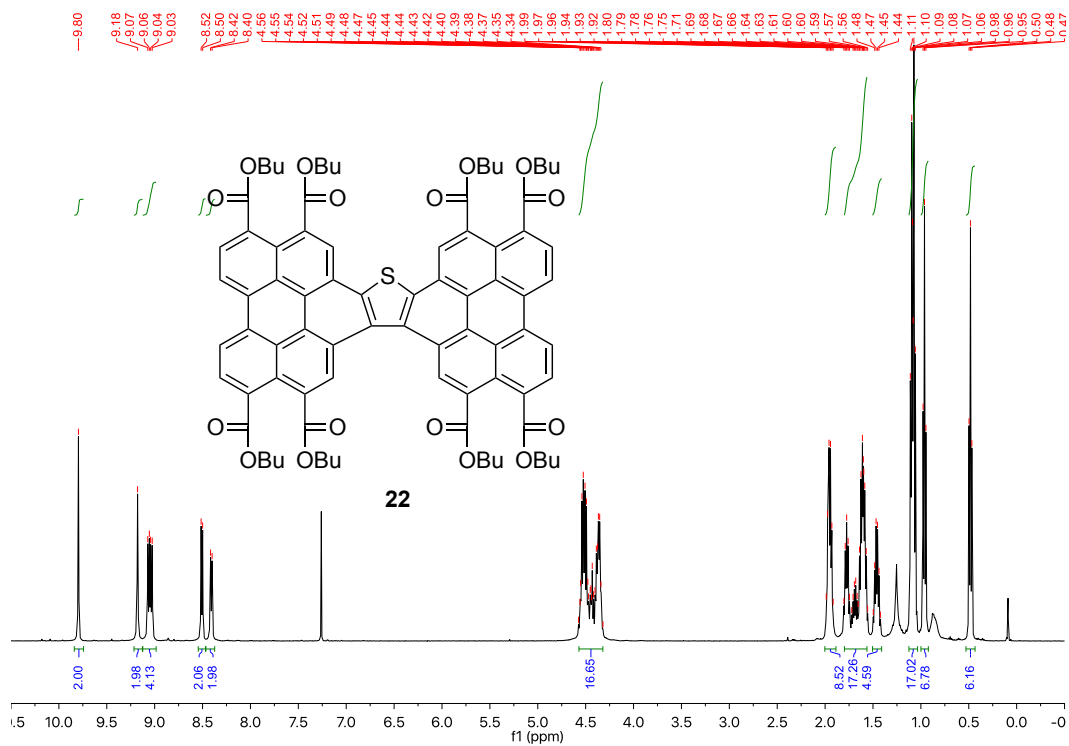
Figure 2.39. ^{1}H NMR spectrum of **22**.
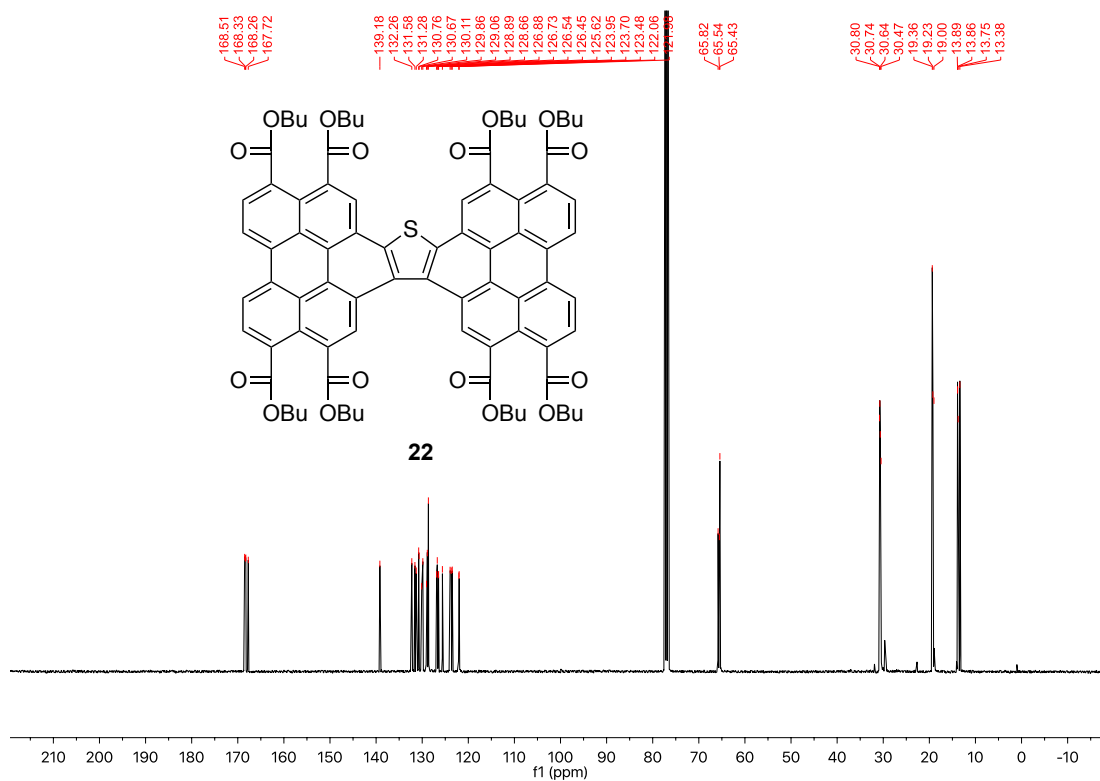
Figure 2.40. ^{13}C NMR spectrum of **22**.
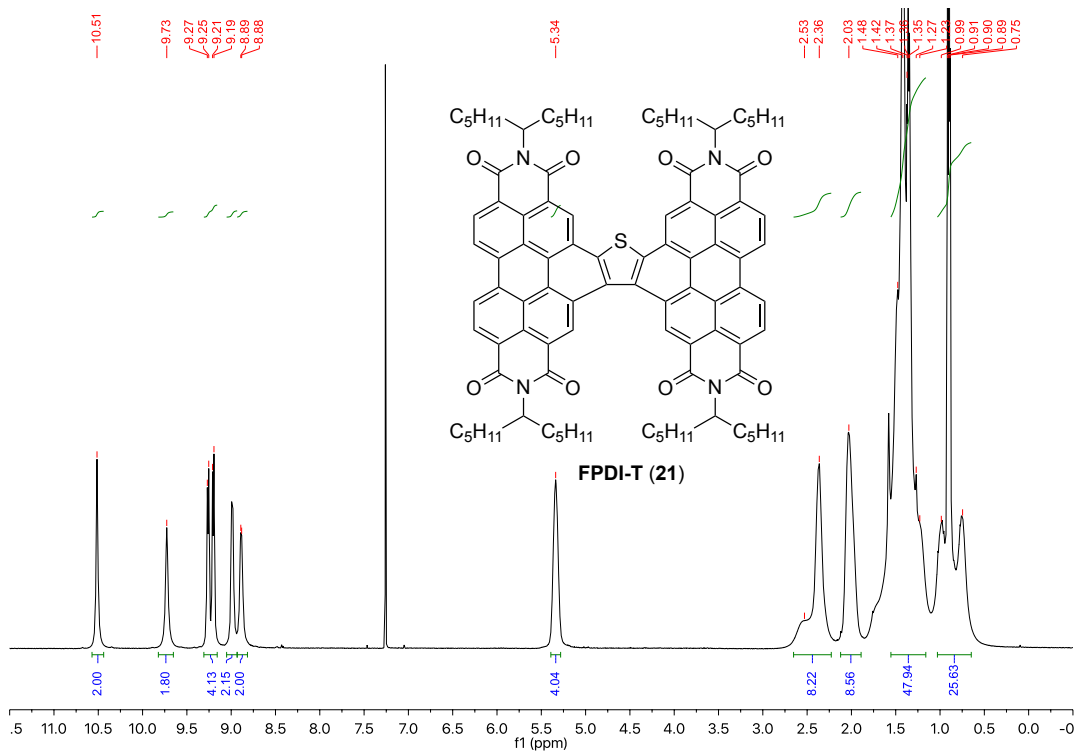
Figure 2.41. ^{1}H NMR spectrum of **21**.
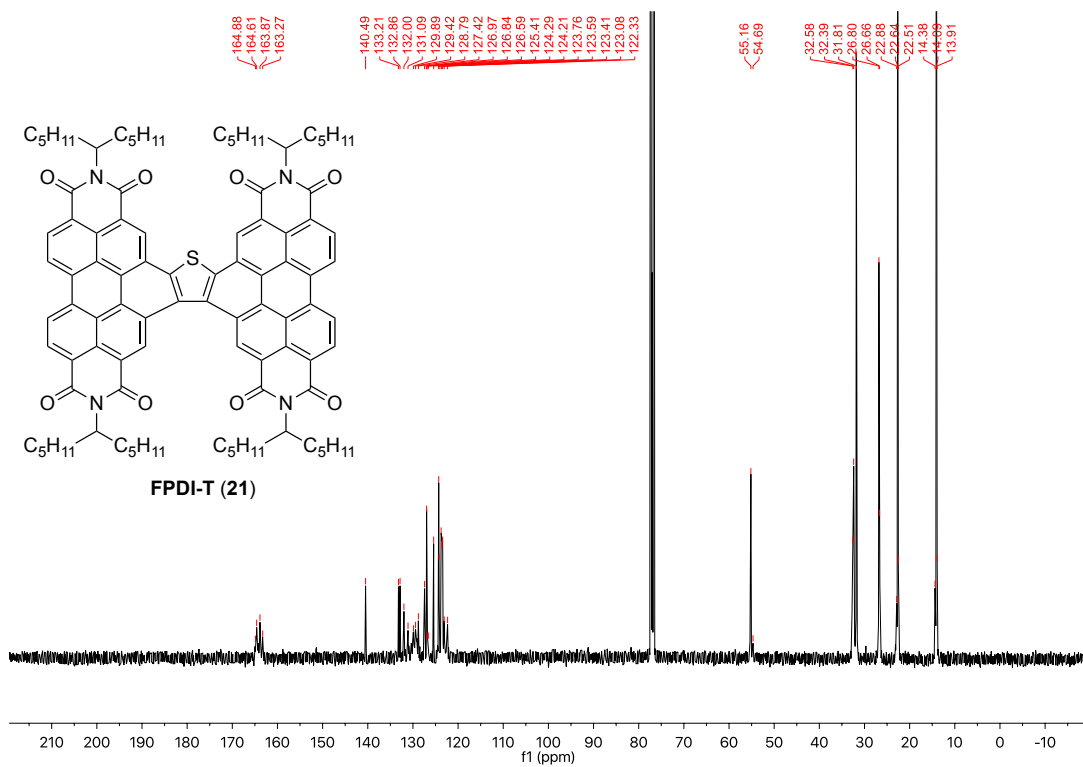
**Figure 2.42.** ^{13}C NMR spectrum of **21**.

2.8. References

(1)   Langhals, H. *Heterocycles* **1995**, *40* (1), 477–500.

(2)   Shirman, E.; Ustinov, A.; Ben-Shitrit, N.; Weissman, H.; Iron, M. A.; Cohen, R.; Rybtchinski, B. *J. Phys. Chem. B* **2008**, *112* (30), 8855–8858.

(3)   Liu, Z.; Zhang, G.; Cai, Z.; Chen, X.; Luo, H.; Li, Y.; Wang, J.; Zhang, D. *Adv. Mater.* **2014**, *26* (40), 6965–6977.

(4)   Zhan, X.; Facchetti, A.; Barlow, S.; Marks, T. J.; Ratner, M. A.; Wasielewski, M. R.; Marder, S. R. *Adv. Mater.* **2011**, *23* (2), 268–284.

(5)   Liang, N.; Jiang, W.; Hou, J.; Wang, Z. *Mater. Chem. Front.* **2017**, *1* (7), 1291–1303.

(6)   Zhang, G.; Zhao, J.; Chow, P. C. Y.; Jiang, K.; Zhang, J.; Zhu, Z.; Zhang, J.; Huang, F.; Yan, H. *Chem. Rev.* **2018**, *118* (7), 3447–3507.

(7)   Ghosh, I.; Ghosh, T.; Bardagi, J. I.; König, B. *Science* **2014**, *346* (6210), 725–728.

(8)   Zhong, Y.; Sisto, T. J.; Zhang, B.; Miyata, K.; Zhu, X.-Y.; Steigerwald, M. L.; Ng, F.; Nuckolls, C. *J. Am. Chem. Soc.* **2017**, *139* (16), 5644–5647.

(9)   Milton, M.; Cheng, Q.; Yang, Y.; Nuckolls, C.; Hernández Sánchez, R.; Sisto, T. J. *Nano Lett.* **2017**, *17* (12), 7859–7863.

(10)   Castro, E.; Sisto, T. J.; Romero, E. L.; Liu, F.; Peurifoy, S. R.; Wang, J.; Zhu, X.; Nuckolls, C.; Echegoyen, L. *Angew. Chemie Int. Ed.* **2017**, *56* (46), 14648–14652.

(11)   Peurifoy, S. R.; Castro, E.; Liu, F.; Zhu, X.-Y.; Ng, F.; Jockusch, S.; Steigerwald, M. L.; Echegoyen, L.; Nuckolls, C.; Sisto, T. J. *J. Am. Chem. Soc.* **2018**, jacs.8b04119.

(12)   Weil, T.; Vosch, T.; Hofkens, J.; Peneva, K.; Müllen, K. *Angew. Chemie Int. Ed.* **2010**, *49* (48), 9068–9093.

(13)   Würthner, F.; Stolte, M. *Chem. Commun.* **2011**, *47* (18), 5109.

(14)   Würthner, F.; Saha-Möller, C. R.; Fimmel, B.; Ogi, S.; Leowanawat, P.; Schmidt, D. *Chem. Rev.* **2016**, *116* (3), 962–1052.

(15)   Klebe, G.; Graser, F.; Hädicke, E.; Berndt, J. *Acta Crystallogr. Sect. B Struct. Sci.* **1989**, *45* (1), 69–77.

(16)   Würthner, F.; Saha-Möller, C. R.; Fimmel, B.; Ogi, S.; Leowanawat, P.; Schmidt, D. *Chem. Rev.* **2016**, *116* (3), 962–1052.

(17)   and, J. M.; Tojo, K. *J. Phys. Chem. B* **2002**, *106* (4), 767–772.

(18)   Würthner, F.; Saha-Möller, C. R.; Fimmel, B.; Ogi, S.; Leowanawat, P.; Schmidt, D. *Chem. Rev.* **2015**.

(19)   Hartnett, P. E.; Timalsina, A.; Matte, H. S. S. R.; Zhou, N.; Guo, X.; Zhao, W.; Facchetti, A.; Chang, R. P. H.; Hersam, M. C.; Wasielewski, M. R.; Marks, T. J. *J. Am. Chem. Soc.* **2014**, *136* (46), 16345–16356.

(20)   Cabanetos, C.; El Labban, A.; Bartelt, J. A.; Douglas, J. D.; Mateker, W. R.; Fréchet, J. M. J.; McGehee, M. D.; Beaujuge, P. M. *J. Am. Chem. Soc.* **2013**, *135* (12), 4656–4659.

(21)   Huo, L.; Xue, X.; Liu, T.; Xiong, W.; Qi, F.; Fan, B.; Xie, D.; Liu, F.; Yang, C.; Sun, Y. *Chem. Mater.* **2018**, *30* (10), 3294–3300.

(22)   Li, S.; Ye, L.; Zhao, W.; Yan, H.; Yang, B.; Liu, D.; Li, W.; Ade, H.; Hou, J. *J. Am. Chem. Soc.* **2018**, jacs.8b02695.

(23)   Lobez, J. M.; Andrew, T. L.; Bulović, V.; Swager, T. M. *ACS Nano* **2012**, *6* (4), 3044–3056.

(24)   Mei, J.; Bao, Z. *Chem. Mater.* **2014**, *26* (1), 604–615.

(25)   Hong, X. M.; Collard, D. M. *Macromolecules* **2000**, *33* (19), 6916–6917.

(26)   Wang, J.; Ober, C. K. *Macromolecules* **1997**, *30* (24), 7560–7567.

(27)   Robitaille, L.; Leclerc, M. *Macromolecules* **1994**, *27* (7), 1847–1851.

(28)   Yao, K.; Chen, L.; Chen, X.; Chen, Y. *Chem. Mater.* **2013**, *25* (6), 897–904.

(29)   Geng, Y.; Wei, Q.; Hashimoto, K.; Tajima, K. *Chem. Mater.* **2011**, *23* (18), 4257–4263.

(30)   Zhang, Q.; Kelly, M. A.; Bauer, N.; You, W. *Acc. Chem. Res.* **2017**, *50* (9), 2401–2409.

(31)   Schmidt, R.; Oh, J. H.; Sun, Y.-S.; Deppisch, M.; Krause, A.-M.; Radacki, K.; Braunschweig, H.; Könemann, M.; Erk, P.; Bao, Z.; Würthner, F. *J. Am. Chem. Soc.* **2009**, *131* (17), 6215–6228.

(32)   Oh, J. H.; Sun, Y.-S.; Schmidt, R.; Toney, M. F.; Nordlund, D.; Könemann, M.; Würthner, F.; Bao, Z. *Chem. Mater.* **2009**, *21* (22), 5508–5518.

(33)   Oh, J. H.; Liu, S.; Bao, Z.; Schmidt, R.; Würthner, F. *Appl. Phys. Lett.* **2007**, *91* (21), 212107.

(34)   Meng, D.; Fu, H.; Xiao, C.; Meng, X.; Winands, T.; Ma, W.; Wei, W.; Fan, B.; Huo, L.; Doltsinis, N. L.; Li, Y.; Sun, Y.; Wang, Z. .

(35)   Huang, F.; Wu, H.; Cao, Y. *Chem. Soc. Rev.* **2010**, *39* (7), 2500.

(36)   Zhong, Y.; Kumar, B.; Oh, S.; Trinh, M. T.; Wu, Y.; Elbert, K.; Li, P.; Zhu, X.; Xiao, S.; Ng, F.; Steigerwald, M. L.; Nuckolls, C. *J. Am. Chem. Soc.* **2014**, *136* (22), 8122–8130.

(37)   Zhong, Y.; Trinh, M. T.; Chen, R.; Purdum, G. E.; Khlyabich, P. P.; Sezen, M.; Oh, S.; Zhu, H.; Fowler, B.; Zhang, B.; Wang, W.; Nam, C.-Y.; Sfeir, M. Y.; Black, C. T.; Steigerwald, M. L.; Loo, Y.-L.; Ng, F.; Zhu, X.-Y.; Nuckolls, C. *Nat. Commun.* **2015**, *6*, 8242.

(38)   Sisto, T. J.; Zhong, Y.; Zhang, B.; Trinh, M. T.; Miyata, K.; Zhong, X.; Zhu, X.-Y.; Steigerwald, M. L.; Ng, F.; Nuckolls, C. *J. Am. Chem. Soc.* **2017**, jacs.6b13093.

(39)   Zhong, H.; Wu, C. H.; Li, C. Z.; Carpenter, J.; Chueh, C. C.; Chen, J. Y.; Ade, H.; Jen, A. K. Y.
         Adv. Mater. **2015**, 951–958.

(40)   Hartnett, P. E.; Matte, H. S. S. R.; Eastham, N. D.; Jackson, N. E.; Wu, Y.; Chen, L. X.; Ratner, M.
         A.; Chang, R. P. H.; Hersam, M. C.; Wasielewski, M. R.; Marks, T. J. *Chem. Sci.* **2016**.

(41)   Mallory, F. B.; Mallory, C. W. In *Organic Reactions*; John Wiley & Sons, Inc.: Hoboken, NJ,
         USA, 1984; pp 1–456.

(42)   Yongjun Li; Hao Li; Li, Y.; Huibiao Liu; Shu Wang; Xiaorong He; Ning Wang, A.; Zhu, D. *Org.
         Lett.* **2005**, *7* (22), 4835–4838.

(43)   Zhang, J.; Li, Y.; Huang, J.; Hu, H.; Zhang, G.; Ma, T.; Chow, P. C. Y.; Ade, H.; Pan, D.; Yan, H.
         J. Am. Chem. Soc. **2017**, *139* (45), 16092–16095.

(44)   Schuster, N. J.; Paley, D. W.; Jockusch, S.; Ng, F.; Steigerwald, M. L.; Nuckolls, C. *Angew.
         Chemie Int. Ed.* **2016**, *55* (43), 13519–13523.

(45)   Ball, M.; Zhong, Y.; Wu, Y.; Schenck, C.; Ng, F.; Steigerwald, M.; Xiao, S.; Nuckolls, C. *Acc.
         Chem. Res.* **2015**, *48* (2), 267–276.

(46)   Zeng, C.; Xiao, C.; Xin, R.; Jiang, W.; Wang, Y.; Wang, Z. *RSC Adv.* **2016**, *6* (61), 55946–55952.

(47)   Son, M.; Fimmel, B.; Dehm, V.; Würthner, F.; Kim, D. *ChemPhysChem* **2015**, *16* (8), 1757–1767.

(48)   Fimmel, B.; Son, M.; Sung, Y. M.; Grüne, M.; Engels, B.; Kim, D.; Würthner, F. *Chem. - A Eur. J.*
         2015, *21* (2), 615–630.

(49)   Struijk, C. W.; Sieval, A. B.; Dakhorst, J. E. J.; Van Dijk, M.; Kimkes, P.; Koehorst, R. B. M.;
         Donker, H.; Schaafsma, T. J.; Picken, S. J.; Van De Craats, A. M.; Warman, J. M.; Zuilhof, H.;
         Sudho, E. J. R. .

(50)   Balakrishnan, K.; Datar, A.; Naddo, T.; Huang, J.; Oitker, R.; Yen, M.; Zhao, J.; Zang, L. *J. A*
         2006, *128* (22), 7390–7398.

(50)   Li, Y.; Wang, C.; Li, C.; Di Motta, S.; Negri, F.; Wang, Z. *Org. Lett.* **2012**, *14* (20), 5278–5281.

Chapter 3. Conformational Control of Cove-Edge Graphene Nanoribbons
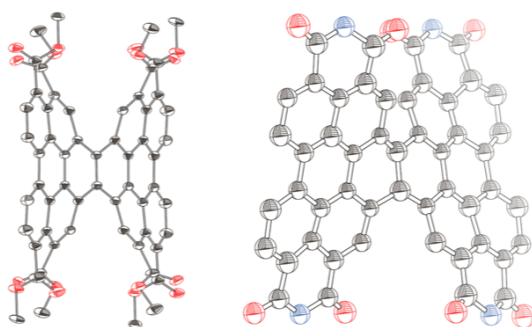

3.1. Preface

Here, the conformations of cove-edge graphene nanoribbons (GNRs) made from fusing perylene derivatives with ethylene bridges are investigated using density functional theory (DFT) calculations and single crystal X-ray diffraction (SCXRD). When adjacent edge positions of the GNRs are fused together as part of an all-sp^2 ring, the perylene cores of these ribbons are rigid. The strain of their cove edges is accommodated by twisting at the cove edge into a chiral helix. When substituents at the edge positions are no longer fused together, the perylene cores of these ribbons are flexible. The strain of their cove edges is accommodated throughout the aromatic core of the molecule, which contorts into an achiral butterfly conformation.

I synthesized the compounds **bPTE2 (8)** and **hPDI2-Cy6 (9)** using the protocols presented in Chapter 2 of this work. I grew SCXRD-quality single crystals of **bPTE2** and **hPDI2-Cy6**, the latter with significant advice from Prof. Raúl Hernández Sánchez. Dr. Fay Ng synthesized the compound **hPDI2-3C5 (10)** and grew SCXRD-quality single crystals. Prof. Raúl Hernández Sánchez, Taylor Hochuli, and Dr. Daniel Paley performed

SCXRD experiments and solved the crystal structures. Dr. Michael L. Steigerwald and I

performed DFT calculations. Neil Foegen and I performed UV-Vis experiments.

## 3.2. Conformation of Cove-Edge Graphene Nanoribbons

Here we present a method for controlling the conformation of cove-edge graphene nanoribbons (GNRs): changing their edge substituents tunes the flexibility of their aromatic cores, in turn dictating how they adapt to the strain induced by their cove edges. GNRs have been extensively investigated as organic semiconductors.[1–3] Their electronic properties can be readily tuned by (1) modifying their width or their carbon architecture, or by (2) incorporating heteroatoms in their aromatic cores or introducing substituents at their edges.[4–10] Recently, research has focused on GNRs or GNR fragments with atomically-precise structures.[11–15] Compared to GNRs of random length, this strategy reduces uncertainty due to defects and batch-to-batch variation. Periodically removing carbon atoms from the edges of GNRs introduces coves into their structure (Figure 3.1.a). The resulting cove-edge GNRs have improved solubility over their planar counterparts.[13,16] The carbon positions at their edges are no longer all identical to one another, opening up the possibility of regioselective functionalization (Figure 3.1.b). The aromatic core can be seen as a sequence of alternating motifs, rather than an uninterrupted chain of the same motif (Figure 3.1.b). This alternation of their aromatic cores leads to novel optoelectronic properties.[11]
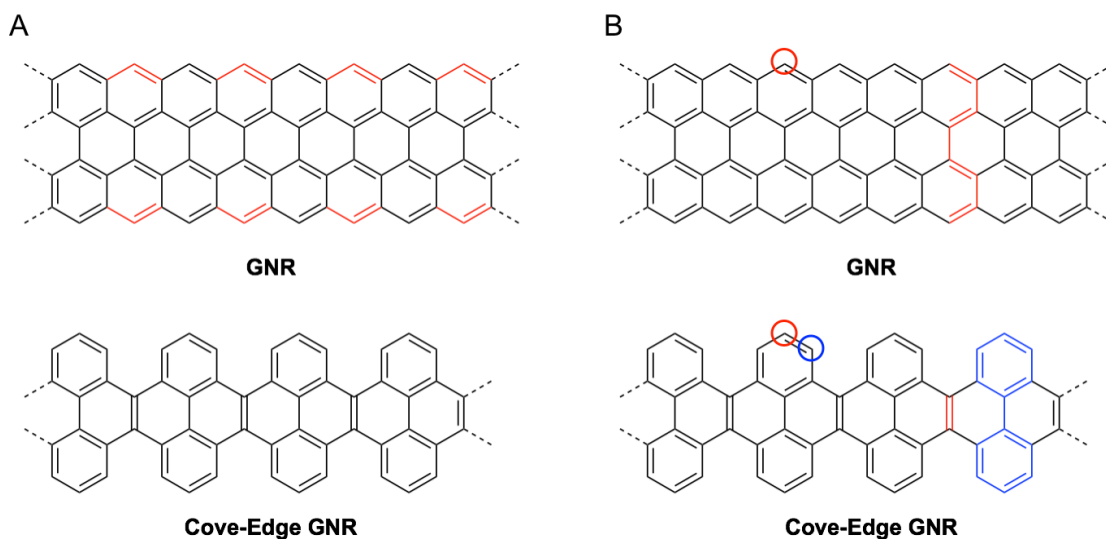
Figure 3.1. (A) When the alternating carbon atoms of a GNR (top) are removed, coves are introduced into the edges and we call it a cove-edge GNR (bottom). (B) Carbon atoms at the edges of standard GNRs (top, circled in red) are all chemically indistinct, while the cove-edge GNRs have chemically distinct carbon atoms at their edges (bottom, circled in red and blue). Standard GNRs consist of the same repeating motif of all-sp^2 carbon atoms (top, highlighted in red), while cove-edge GNRs alternate between two different motifs (bottom, highlighted in red and blue).

The coves of cove-edge GNRs can be seen as a repeating pattern of helicenes (Figure 3.2.a). Helicenes, molecules composed of continuously ortho-fused phenyl rings, adopt a helical conformation to accommodate atoms that would otherwise occupy the same space.[17,18] The three-dimensional structure of the helicenes along the edges of cove-edge GNRs and similar polyaromatic hydrocarbons results in them adopting unique conformations such as the structure in Figure 3.2.b.[19] Polyaromatic hydrocarbons such as cove-edge GNRs are a common motif in host-guest chemistry, self-assembly, and molecular recognition.[20–22] The self-assembly of these materials can affect their morphology and performance in bulk heterojunctions.[23–25] These applications are often sensitive to subtle changes in conformation. By studying the relationship between

structure and conformation in GNRs and other polyaromtic hydrocarbons, we may develop design principles for controlling their conformation for these applications.
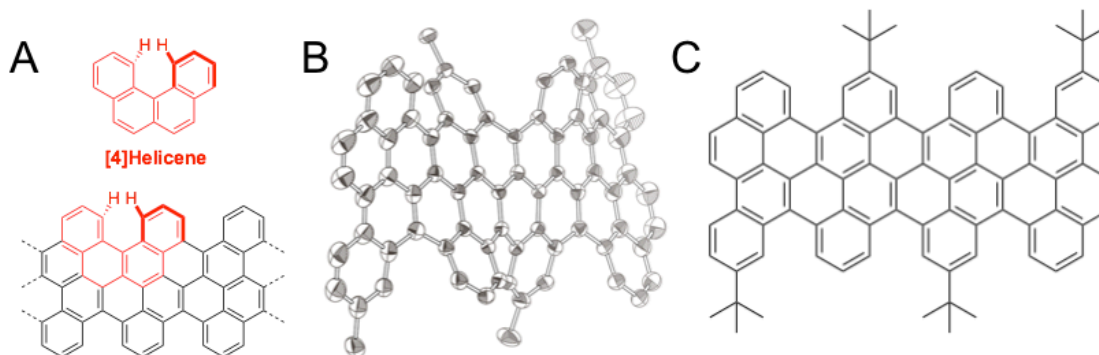
Figure 3.2. (A) [4]Helicene-edge GNR with helicene highlighted. (B) Steric repulsion between the highlighted hydrogen atoms contorts the edges of these ribbons such as in this single-crystal X-ray structure.[19] (C) Structure of the molecule in (B). t-Butyl groups are simplified as methyl groups for clarity.

One common cove-edge motif for GNRs is dibenzo[*g,p*]chrysene (**1**), which features two [4]helicenes fused back to back (Figure 3.3.a). In principle, **1** can adopt two conformations. In the chiral *helical* conformation, the molecule is twisted into a helix about the central ethylene bridge (Figure 3.3.b, 3.3.c). In the achiral *butterfly* conformation, two benzene "wings" on one side of the bridge bend one way, while the other two "wings" bend in the opposite direction (Figure 3.3.d-3.3.f).
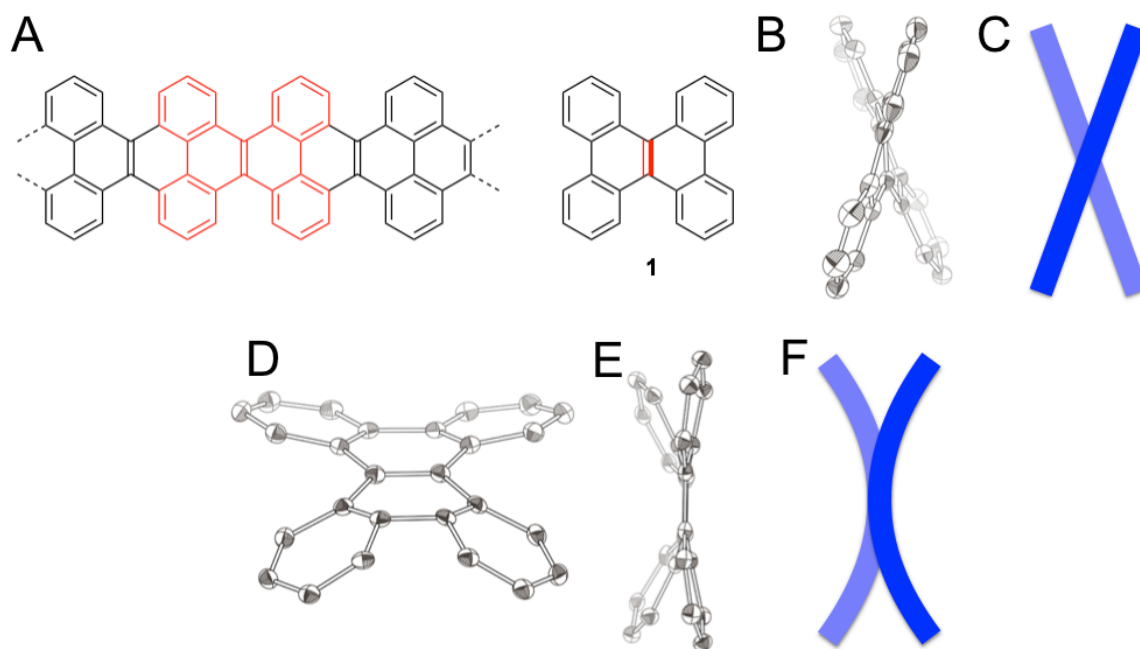
Figure 3.3. (A) Cove-edge GNR featuring the dibenzo[*g,p*]chrysene unit **1**. The ethylene bridge connecting the two [4]helicenes is highlighted in red. (B) SCXRD structure of **1** looking down the helical axis as indicated in (A).[26] (C) Schematic representation of the helical conformation of **1**. This helix has M chirality. (D) SCXRD of a butterfly conformation from a molecule with a **1** motif.[27] (E) A view of the butterfly conformation from the same view as in (B). (F) Schematic representation of the butterfly conformation.

All of the single crystal X-ray structures incorporating one or more **1** motifs that are reported in the Cambridge Structural Database (CSD) as of this writing are listed in Table 3.1.[28] There are 25 crystal structures representing 15 distinct aromatic cores. Of these structures, 27 are helical and 3 are butterfly. Two important parameters are defined here to quantify their contortion. (1) The *cove contortion* is defined here as the dihedral angle between the atoms on opposing sides of the cove as highlighted in Figure 3.4.a. (2) To quantify the planarity of these structures, first we calculate mean planes for the two phenyl rings on the same side of the bridging ethylene as highlighted in Figure 3.4.b. The
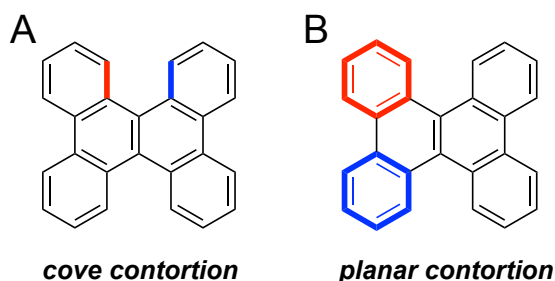
angle between these mean planes is the *planar contortion.* In a perfectly flat system, the cove contortion and planar contortion would both be 0º.

Table 3.1. Reported SCXRD structures of cove-edge GNRs featuring a **1** motif.[a]

BEFXES (**3**)	*unique*	butterfly	RUBWER	JOJSEI	helical
DATVUR	*unique*	helical	RUBWIV	JOJSEI	helical
DATWAY	DATVUR	helical	SEKQOR (**5**)	*unique*	butterfly
EVIWEN	*unique*	helical	SEKQUX (**6**)	*unique*	helical
JOJSEI (**1**)	*unique*	helical	TEBNAP	JOJSEI	helical
JOJSIM	JOJSEI	helical	UCEKOF	*unique*	helical
JOJSOS	JOJSEI	helical	UPAJIG	*unique*	helical
KAQLEV	*unique*	helical	URITUM	*unique*	helical
KEDQUI	*unique*	helical	VUFHUA (**4**)	*unique*	butterfly
KEFFEJ	*unique*	helical	WUFKOZ (**2**)	*unique*	helical
PASDOF	JOJSEI	helical	XUQXIR	PYRPYR10	helical
PUXCIU	JOJSEI	helical	ZZZAHA	JOJSEI	helical
PYRPYR10	*unique*	helical			

[a] Structures discussed in this text are highlighted in red. The number used to identify them is in parentheses.

[b] These structures differ only in substituents that are singly-bonded to the aromatic core.

cove contortion   *planar contortion*

Figure 3.4. (A) In this text, *cove contortion* of cove-edges with a **1** motif is defined as the torsion angle between the inner edges of the cove highlighted in red and blue. (B) To define *planar contortion*, the mean planes of two benzene rings on the same side of a **1** motif (highlighted in red and blue) are each separately defined. The plane normal-plane normal angle is the *planar contortion*.

Of the structures in Table 3.1, the π-extended perylene-3,4,9,10-tetracarboxylic acid diimide (PDI) material **2** is the only one containing a perylene core (Figure 3.5.a).[29] It consists of a central PDI unit flanked by two phenanthrene subunits. Both of the fusion

points adopt a helical conformation (Figure 3.5.b, 3.5.c). However, the two helical fusion points twist in opposing directions, rendering **2** achiral in the solid state (Figure 3.5.b, 3.5.c). The contortion of the coves is 41.51º and 44.36º. The planar contortion of the outer phenanthrene subunits is 13.77º, while the planar contortion of the central PDI is only 4.23º. (The asymmetric unit of single crystals of **2** contains half of one molecule.) The edges of PDI are locked into ring of all-sp^2 atoms, making the central perylene more rigidly planar than the flanking phenanthrenes.
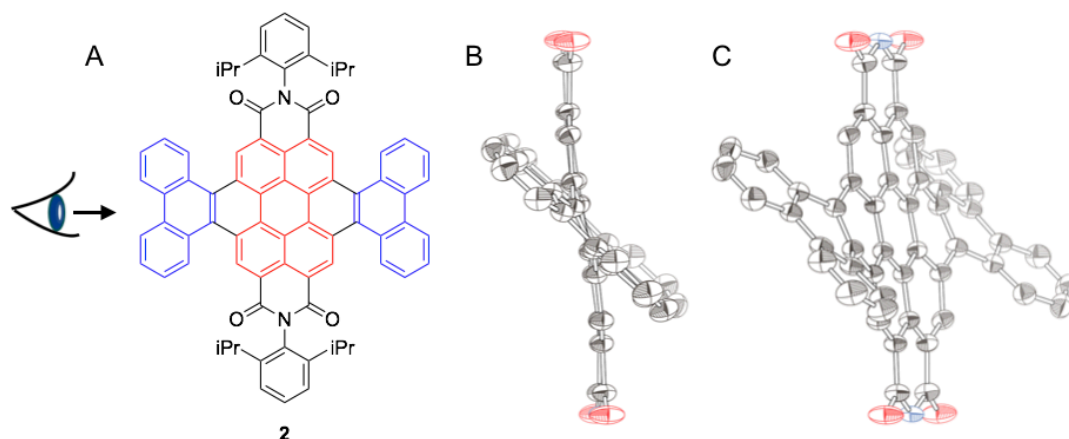
Figure 3.5. (A) Structure of **2** with perylene core highlighted in red and flanking phenanthrene units highlighted in blue. (B) SCXRD structure of **2** looking down its long axis as indicated in (A). The central PDI unit is only minimally distorted from planarity. The imide side chains are omitted for clarity. (C) A wider-angle view of **2** showing an alternating helical twist of the phenanthrene units.

Only three structures in the CSD that contain the **1** subunit adopt a butterfly conformation. Two of them are π-extended corannulenes (**3** and **4**, Figure 3.6.a).[27,30] The driving force for adopting this conformation is obvious: the corannulene core forms a bowl shape that would have to flatten out to adopt a planar conformation (Figure 3.6.b).
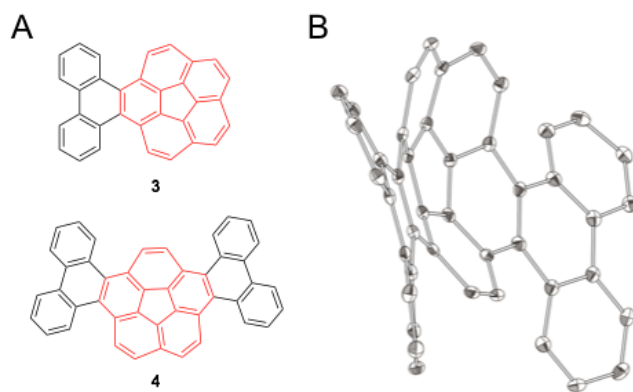
Figure 3.6. (A) Structure of π-extended corannulenes **3** and **4** with corannulene core highlighted in red. (B) SCXRD structure of **4**, showing the butterfly conformation of its **1** motifs.

The bis-dicarbacorrole ribbons **5** and **6** present a unique case (Figure 3.7.a).[31] When no metal is bound to the center of the dicarbacorrole subunits of **5**, the aromatic cores are flexible and **5** can adopt a butterfly conformation at its ethylene fusion point (Figure 3.7.b). Inserting square planar metal centers to create **6** rigidifies the dicarbacorrole subunits, forcing the molecule to adopt a helical conformation (Figure 3.7.c). Both molecules have similar degrees cove contortion: 35.53º in **5** and 32.70º in **6**. However, the planar contortion of **5** is much higher than in **6**: 35.37º compared to just 4.77º.
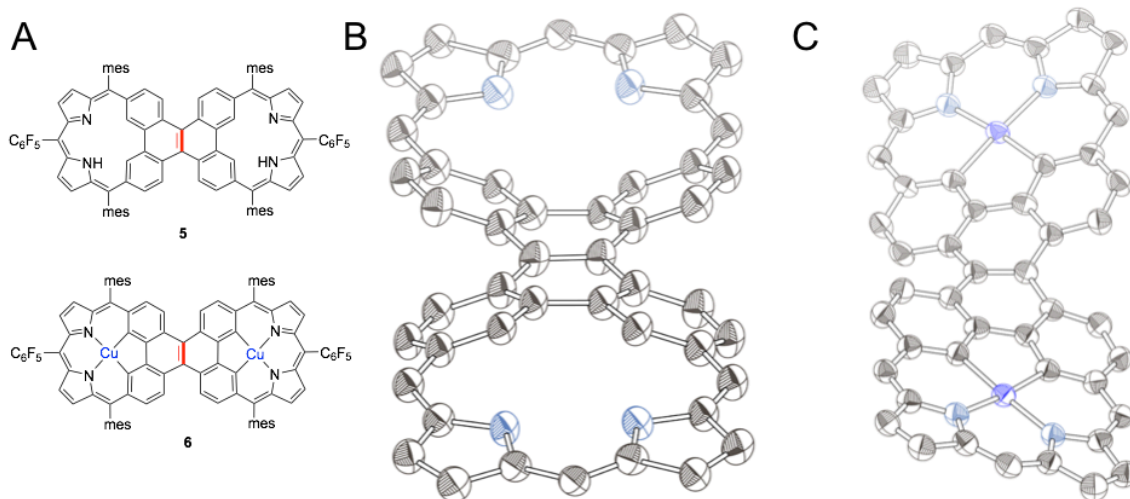
Figure 3.7. (A) Structure of bis-dicarbacorroles **5** and **6** with ethylene fusions between dicarbacorrole subunits highlighted in red. (B) SCXRD of **5**. Mesityl and pentafluorophenyl side chains are removed for clarity. With no metal centers, the dicarbacorrole subunits are flexible, allowing **5** to pucker into a butterfly formation. (C) SCXRD of **6**. Square planar copper centers rigidify the dicarbacorrole subunits, forcing them to be planar. In turn, this enforces the helical twist about the central ethylene fusion.

Together, these examples suggest that rigid aromatic subunits fused into cove-edge GNRs with a fusion as in **1** will dictate the conformation at the point of fusion. Flat subunits will prefer to remain flat, leading to a helical twist as in **2** and **6**. Bowl-shaped corannulenes will retain their curvature, leading to a butterfly conformation as in **3** and **4**. More flexible aromatic subunits, such as the free dicarbacorroles of **5**, can spread the strain of [4]helicene cove edges throughout the molecule, potentially leading to a butterfly conformation.

3.3. Strategy for Conformational Control

The cove-edge GNR **7** (Figure 3.8.a) discussed in Chapter 1 and Chapter 2 of this dissertation was initially predicted to adopt a helical conformation, hence the name helical perylene diimide dimer or **hPDI2**.[11] Calculations at the B3LYP/6-31-G** level by both our group and Wang predict that the butterfly conformation is disfavored by 6 kcal mol^{-1}.[11,32] The calculated structures are shown in Figure 3.8.b and Figure 3.8.c. The branched 6-undecyl side chains of **7** are reduced to methyl chains to simplify calculations. There are nodes at the imide nitrogen atoms in the frontier orbitals of PDI, so the exact identity of the side chains has minimal influence on the electronic structure of the aromatic core. The PDI units retain their planarity in this structure, with a planar contortion of only 4.67º on side and 6.03º on the other. The strain of the [4]helicene cove edges of **7** is accommodated therefore by twisting around the ethylene bridge between the two PDI units. This rigidity of the PDI subunits is enforced by the imide substituents that lock adjacent edge positions into an all-sp^2 ring.
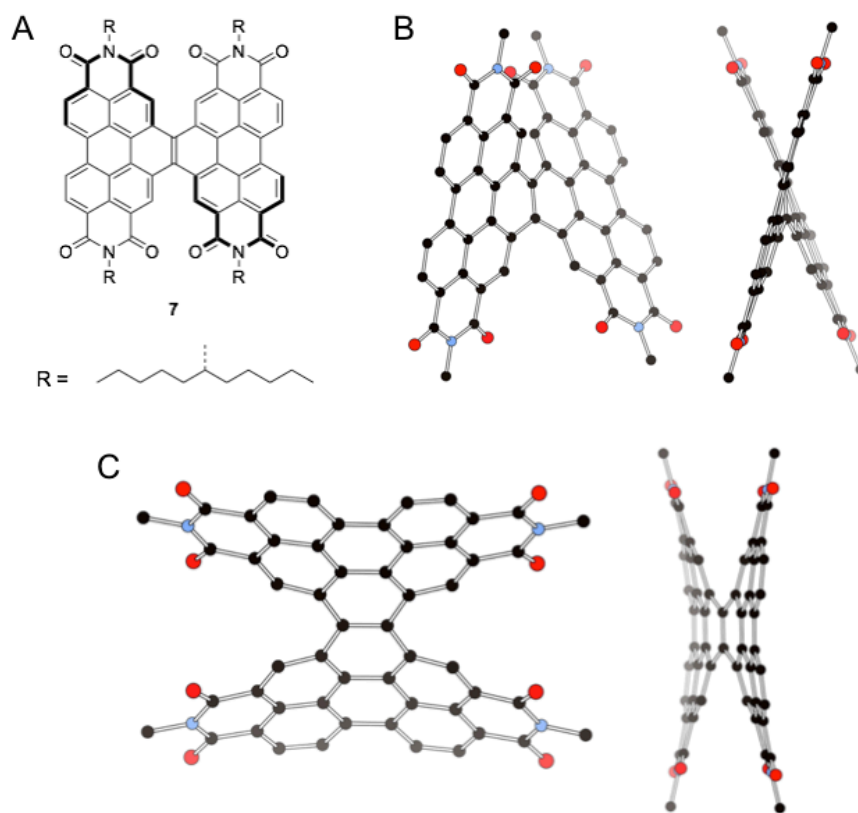
Figure 3.8. (A) Structure of **hPDI2** (**7**). (B) DFT-calculated structure of the favored helical conformation of **7**. DFT was performed at the B3LYP/6-31G** level of theory with imide side chains R simplified as methyl groups. (C) Disfavored butterfly conformation of **7**. This conformation is 6 kcal mol^{-1} higher in energy.

To better understand how substituents on the edges of GNRs influence conformation we sought to investigate an analog of **7** in which neighboring edge positions are no longer locked into all-sp^2 rings, making the perylene cores more flexible. First introduced in Chapter 2 of this work, the perylene-3,4,9,10-tetracarboxylic acid tetraester (PTE) dimer **8** retains a carbonyl moiety at all the peri- positions, but they are no longer fused into an all-sp^2 ring (Figure 3.9.a). This increases the flexibility of the aromatic perylene cores, with planar contortions of 22.75° and 22.87°, according to DFT

calculations at the B3LYP/6-31-G** level. The butterfly conformation is calculated to be 3 kcal mol^{-1} lower in energy than the helical conformation. As with **7**, we simplify the alkyl side chains to methyl groups for all calculations. The π-system of the carbonyls are no longer in plane with the aromatic core of **8**, so their pendant ester side chains have minimal influence on the structure of **8**. Because **8** favors the butterfly conformation, we call it butterfly perylene tetraester dimer or **bPTE2**.
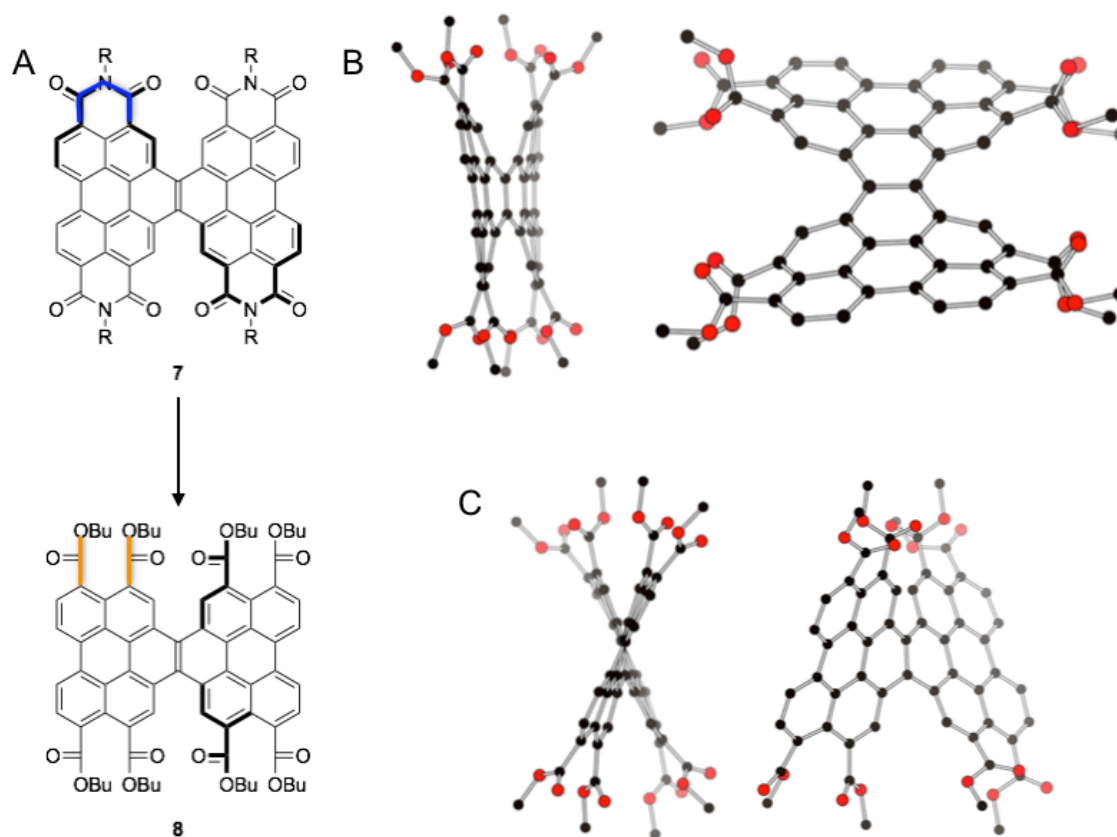
Figure 3.9. (A) Structure of **bPTE** (**8**). By breaking open the all-sp2 rings that fuse neighboring edge positions in **7**, the perylene cores of **8** are more flexible, allowing it to adopt a butterfly conformation. (B) DFT-calculated structure of the favored butterfly conformation of **8**. DFT was performed at the B3LYP/6-31G** level of theory with *n*-butyl ester simplified as methyl groups. (C) Disfavored helical conformation of **8**. This conformation is 3 kcal mol^{-1} higher in energy.

The comparison between **6** and **5** is analogous to the comparison between **7** and **8**. The flexible aromatic cores of butterfly **5** are rigidified to form helical **6**. A flexible aromatic core can distribute the strain of the [4]helicene cove edges throughout the molecule into a butterfly conformation, while rigidly planar aromatic cores must adopt a helical conformation to retain planarity of the aromatic cores. By opening up the all-sp^2 edges of **7** to form **8**, we increase the flexibility of the aromatic core, allowing **8** to adopt a butterfly conformation. The rigidly planar perylene subunits of **7** force the molecule into a helix to accommodate the strain of the **1** fusion.

To investigate these DFT predictions, we sought to grow crystals of **7** and **8** of sufficient quality for single crystal X-ray diffraction (SCXRD). Single crystals of **8** were grown by slow evaporation of a solution of **8** in hexane. Growing single crystals of **7** was considerably more difficult. The long alpha-branched imide side chains of **7** are highly favorable for preventing aggregation in the solid state,[33,34] improving the morphology of thin films made from **7** for device applications.[35] However, this inhibited aggregation makes it difficult to grow single crystals.

The method introduced in Chapter 2 of this work for readily varying the imide side chains of **7** gave us a library of hPDI2 materials to screen for growing single crystals. Ultimately, single crystals of **hPDI2-Cy6** (**9**, Figure 3.10) were grown by diffusion of cyclohexane vapor in to a solution of **9** in chlorobenzene. We also grew single crystals of **hPDI2-3C5** (**10**, Figure 3.10) by diffusing acetonitrile in to a solution of **10** in *p*-xylene. The structural and packing motifs of **9** and **10** are very similar, only differing slightly in specific angles and distances, but otherwise having identical crystal

structures. The details of all the crystallographic experiments are presented in Section 3.4 and all crystallographic data are summarized in Table 3.3.
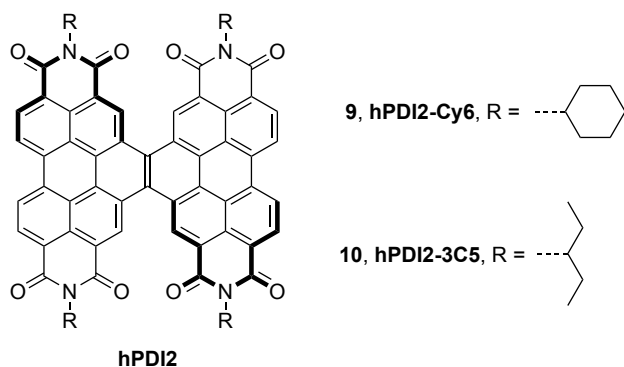
Figure 3.10. Structure of **9** and **10**.

The conformations of **8-10** match the DFT-calculated structures. **8** adopts a butterfly conformation, with the perylene subunits on each side of the ethylene bridge bending in opposite directions (Figure 3.11.a). **hPDI2** adopts a helical conformation with either cyclohexyl (**9**) or 3-pentyl (**10**) side chains at the imide positions (Figure 3.11.b). The asymmetric unit of **8** contains half of one molecule. The butterfly conformation has C_{2h} symmetry. The asymmetric unit of **9** contains half of two different molecules of **9**. The asymmetric unit of **10** contains four different complete molecules of **10**. The helical conformation has D_2 symmetry. The cove contortion and planar contortion of **8-10** are listed in Table 3.2 along with the DFT-calculated values.
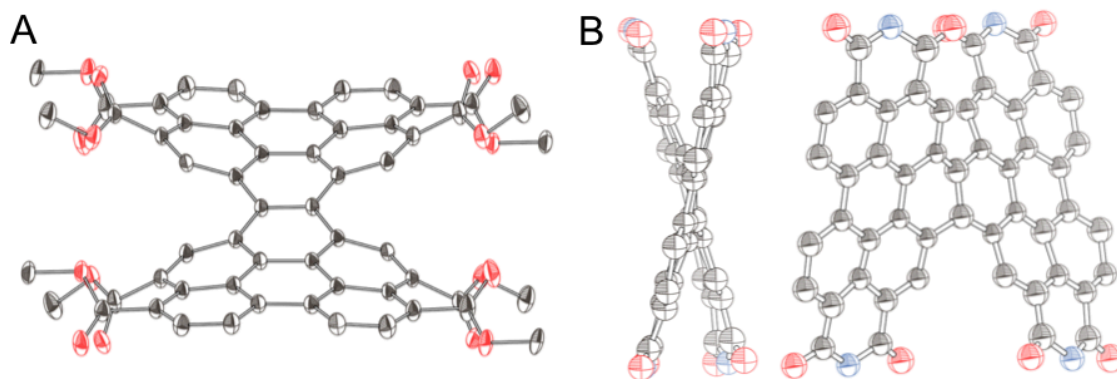
Figure 3.11. SCXRD structures of **8** (A) and **9** (B) emphasizing their respective butterfly and helical conformations in the solid state. Side chains or simplified or removed to emphasize the conformation of the aromatic cores. **10** adopts the same conformation

Table 3.2. Cove Contortion and Planar Contortion in **bPTE2** and **hPDI2**.

| | bPTE2 (8) | | hPDI2 | hPDI2-Cy6 (9)[d] | |
	DFT[a]	SCXRD[b]	DFT[c]	SCXRD	SCXRD
Cove Contortion °	27.33, 36.53	32.21	39.43, 39.89	38.13	38.44
Planar Contortion °	22.75, 22.87	23.40	4.67, 6.03	3.15	5.03

| | hPDI2-3C5 (10)[e] | | | |
	SCXRD	SCXRD	SCXRD	SCXRD
Cove Contortion °	35.76, 39.66	35.96, 42.55	34.78, 37.50	38.97, 41.75
Planar Contortion °	3.75, 4.98	4.12, 6.66	4.39, 5.07	3.44, 6.39

[a] Calculations were performed at the B3LYP/6-31G** level. Ester side chains were simplified as methyl groups. The calculated structure was asymmetrical. [b] Half of the molecule is in the asymmetric unit. [c] Calculations were performed at the B3LYP/6-31G** level. Imide side chains were simplified as methyl groups. The calculated structure was asymmetrical. [d] Half of two different molecules of **9** are in the asymmetric unit. Each column represents a different molecule. [e] Four different whole molecules of **10** are in the asymmetric unit. Each column represents a different molecule.

8 packs into parallel π-stacked columns. Adjacent columns are arranged into a lattice shown in Figure 3.12.a. The *n*-butyl side chains effectively insulate adjacent columns from each other. Molecules within a column have alternating orientation, with neighboring molecules skewed at 96º from each other (Figure 3.12.b, 3.12.c). Each half of the aromatic core of **8** faces half of the aromatic core of its nearest neighbor on each side, extending this packing motif down the length of the columns as shown in Figure 3.12.d and Figure 3.12.e. The distance between centroids of eclipsing aromatic rings is 3.6-3.8 Å. Steric repulsion between adjacent esters twists them out of plane with the aromatic core, preventing close π contact between neighboring molecules. Figure 3.13 shows UV-Vis spectra of **8** in solution and in amorphous thin films. There is only a small bathochromic shift from solution to the solid state, suggesting that amorphous films of **8** also have limited π-π contact.[36]
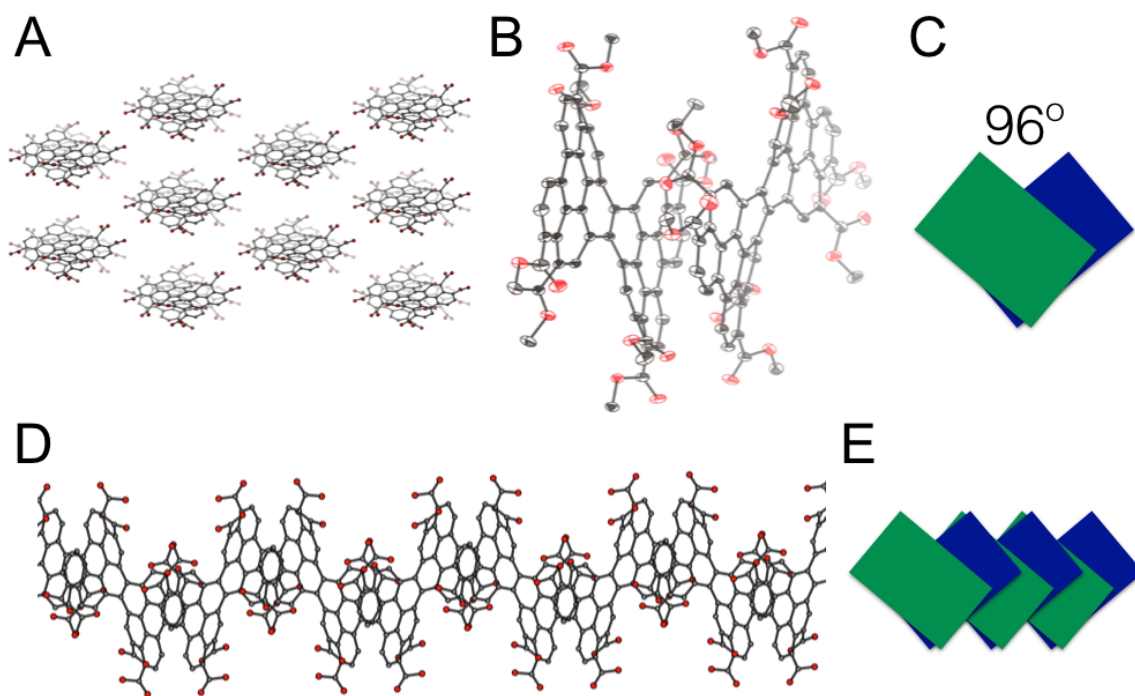
Figure 3.12. Long-rage order in **8**. Disordered side chains are simplified for clarity. (A) Columns of **8** pack into a lattice. (B) Relative orientations of neighboring molecules of **8**. (C) Schematic of how nearest neighbors pack. (D) This packing extends down the length of columns of **8**, with each half of the aromatic core of **8** facing half of the aromatic core of its neighbor on each side. (E) Schematic representation of this column packing.
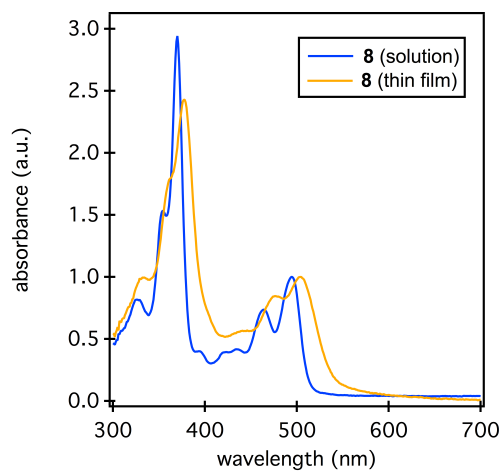
Figure 3.13. Solution and amorphous thin-film UV-Vis spectra of **8**.

Columns of **9/10** consist of closely packed pairs of molecules, with each pair separated by disordered solvent molecules (Figure 3.14.a, 3.14.b). All of the molecules within a column are homochiral and adjacent columns alternate their chirality (Figure 3.14.c, 3.14.d). Columns pack in parallel arrays similarly to **8** (Figure 3.14.d). The distance between centroids of eclipsing aromatic rings is 3.5-3.7 Å. Alpha-branched imide side chains such as cyclohexyl (in **9**) and 3-pentyl (in **10**) are known to disrupt close π contact between neighboring PDI molecules.[33,34] **7**, which bears long 6-undecyl side chains, has a nearly identical UV-Vis spectrum in solution and in amorphous films, with minimal bathochromic shift, minimal peak broadening, and minimal change in relative intensity of the peaks representing the vibronic progression of the PDI to PDI $S_0 \rightarrow S_1$ transition (Figure 3.15.a).[11,35] The shorter 3-pentyl side chains of **10** lead to a slight increase of these features (Figure 3.15.b). **9**, with cyclohexyl side chains, exhibits even greater H-aggregation. Although **9** and **10** form crystals with nearly identical contact between the π faces of neighboring molecules, thin films of the two materials behave differently, highlighting the importance that even subtle changes in side chains can have on the kinetics of crystal formation and the properties of amorphous films.
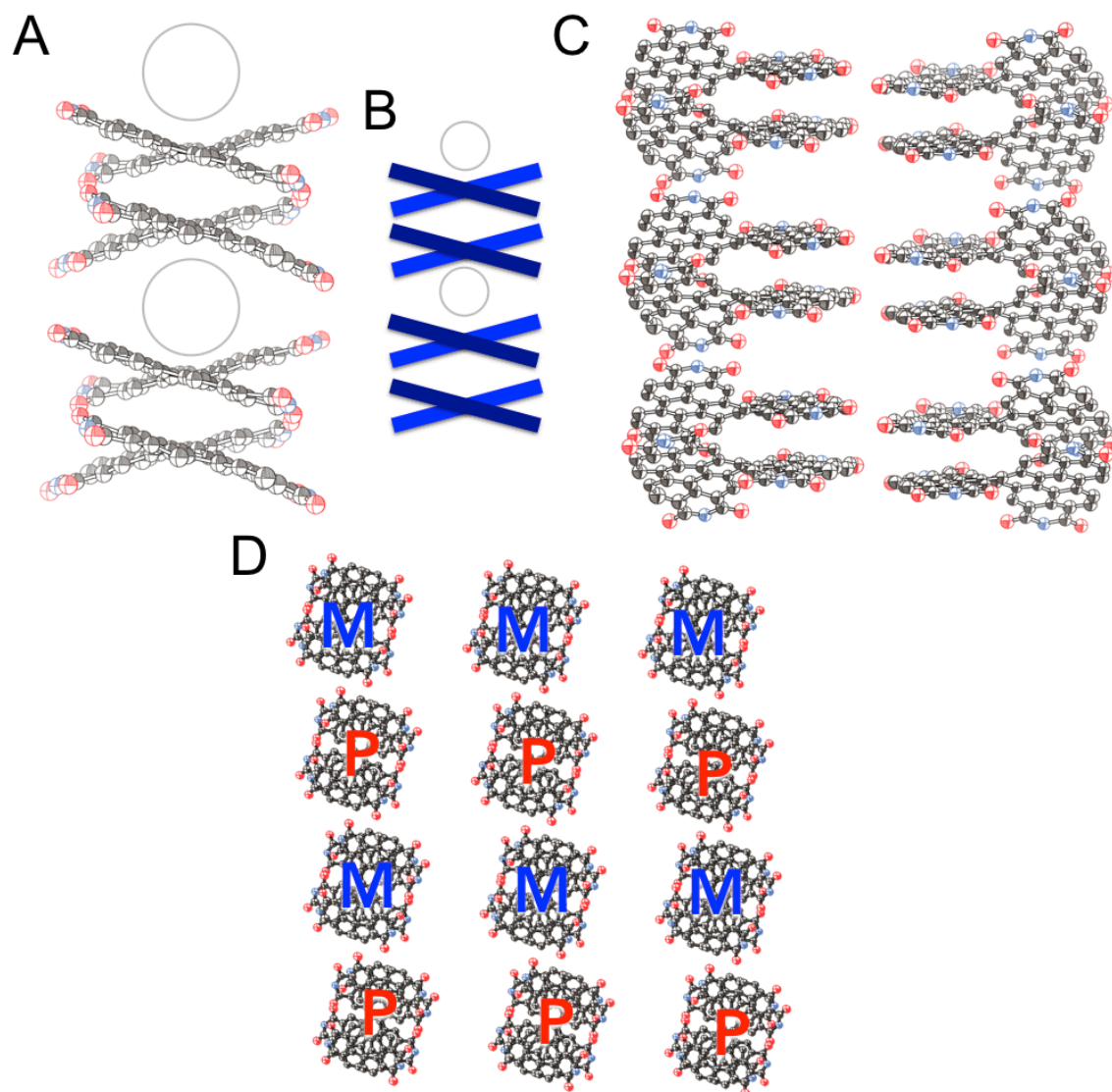
Figure 3.14. (A) Columns of **9** are composed of pairs of molecules separated by disordered solvent. Disordered side chains are removed for clarity. All of the molecules within this column have M helical chirality. (B) Schematic representation of this packing. (C) Neighboring columns have opposite chirality, with all the molecules in the column on the left being P helical and the molecules in the columns on the right being M helical. (D) Looking down the columns, demonstrating their alternating chirality.
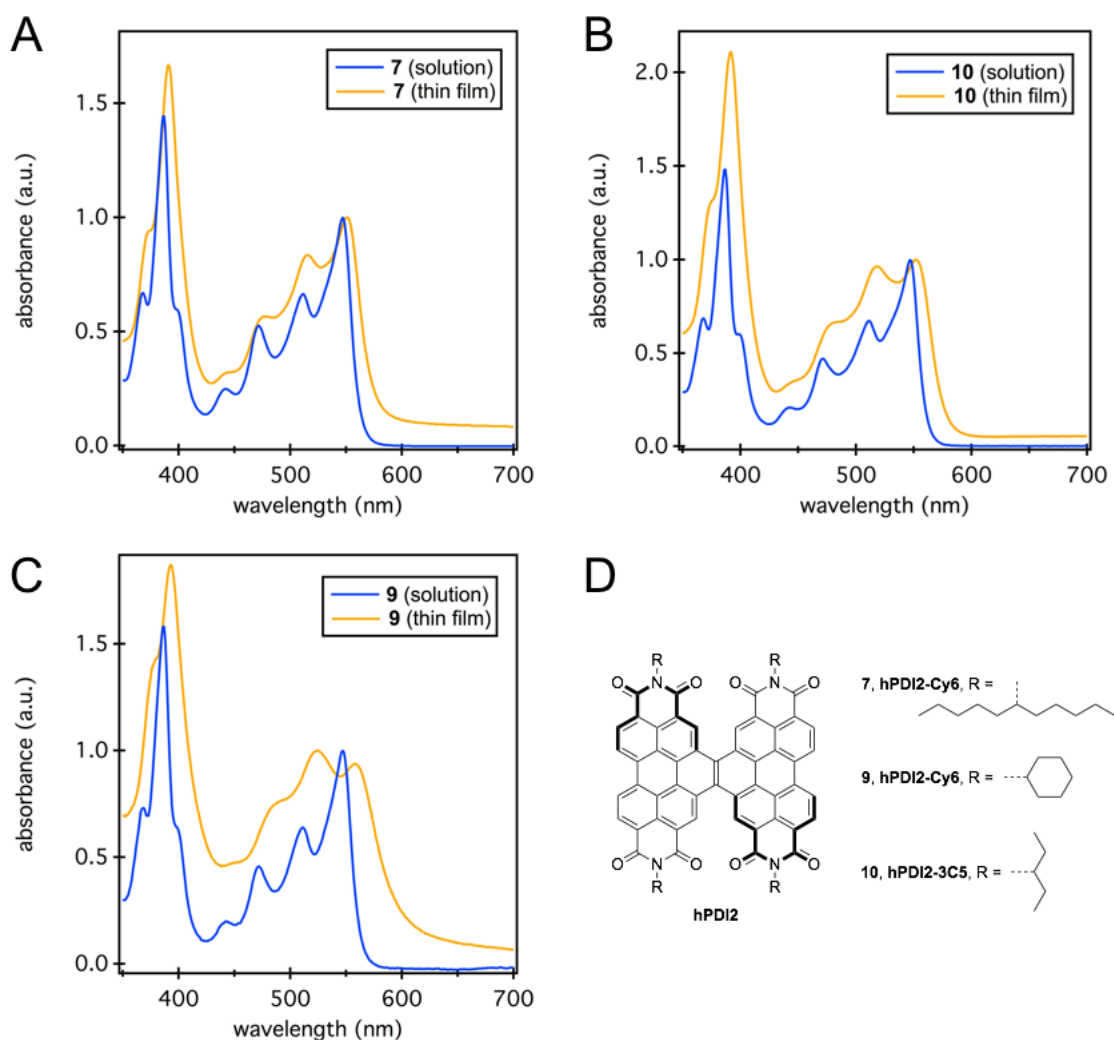
Figure 3.15. (A) Solution and thin film absorption spectra of **7**. (B) Solution and thin film absorption spectra of **10**. (C) Solution and thin film absorption spectra of **9**. (D) Structure of **7**, **9**, and **10**.

By modifying the edge substituents of cove-edge GNRs, we are able to dictate their conformation in the solid state. When adjacent edge positions are fused into all-sp^2 rings, the aromatic core of **9**/**10** is rigidly planar, forcing the ribbons to twist into a helical conformation to retain this rigidity. When adjacent edge positions are separated in **8**, the aromatic core is more flexible, and accommodates the cove-edges by adopting a butterfly conformation. This spreads the strain of the back-to-back [4]helicene **1** moiety across the

274

entire molecule, rather than concentrating it in the ethylene bridge. The design principle of controlling the conformation of cove-edge GNRs by synthetically modifying the rigidity of their aromatic cores is consistent with the small number of comparable systems that have been previously reported by other groups. This conformational control points the way forward for the rational application of these materials in host-guest chemistry, molecular recognition, and self-assembly.

3.4. Experimental Details

Synthesis. 8 and **9** were synthesized according to the protocols in Chapter 2 of this dissertation. **10** was synthesized using a previously reported protocol.[11]

UV-Vis Spectroscopy. UV-Vis spectra were obtained on a Shimadzu UV 1800 UV-Vis spectrophotometer.

General Crystallographic Information. All crystals were mounted on MiTeGen Kapton loops (polyimide) using paratone oil. Data for all compounds were collected on an Agilent SuperNova diffractometer using mirror-monochromated Cu Kα radiation. Data collection, integration, scaling (ABSPACK), and absorption correction were performed in CrysAlisPro.[37] Space group assignments were determined by examination of systematic absences, E-statistics, and successive refinement of the structures. Structures were solved by intrinsic phasing using SHELXT[38] and refined with SHELXL[39] using the OLEX2[40] interface. Successive cycles of least-square refinement followed by difference Fourier syntheses revealed the positions of the remaining non-hydrogen atoms. The program PLATON[41] was employed to confirm the absence of higher symmetry.

Structural Determination of 8. A solution of **8** in hexanes was placed in a sealed vial and a needle was placed through the cap to allow slow evaporation of the solvent. After two weeks, orange crystals of **8** formed. An irregular fragment (.17 x .11 x .06 mm) was

separated carefully, mounted with STP oil treatment, and cooled to 100 K on the diffractometer. Complete data were collected to 0.815 Å. 65078 reflections were collected (6526 unique, 5868 observed) with R(int) 5.5% and R(sigma) 2.4% after multiscan absorption correction (Tmin/Tmax 0.736).

The space group was assigned tentatively as C2/c based on the systematic absences and was solved readily using ShelXT. The aromatic core was located readily in the initial solution and refined with free anisotropic ADPs; the ester side chains were each disordered over 2, 3, or 4 positions and were refined with standard restraints on their geometry and ADPs. C-H hydrogens were placed in calculated positions and refined with riding coordinates and ADPs.

The final refinement (6526 data, 848 restraints, 706 parameters) converged with R_1 ($F_o > 4\sigma(F_o)$) = 5.6%, wR_2 = 15.9%, S = 1.04. The largest Fourier features were 0.54 and -0.34 $e^- A^{-3}$. Crystallographic data for **8** is given in Table 3.3.

Structural Determination of 9. Cyclohexane was introduced into a solution of **9** in chlorobenzene by vapor diffusion. After four days, fragile rod-like orange crystals formed. The crystals lost their solvent rapidly when removed from the mother liquor, so it was necessary to pick and mount them quickly. Data were collected at 100 K. All non-hydrogen atoms were refined with anisotropic displacement parameters. Hydrogen atoms were added in idealized positions. Crystallographic data for **9** is given in Table 3.3.

Structural Determination of **10**. Acetonitrile was introduced into a solution of **10** in *p*-xylene by vapor diffusion, producing fragile orange rods. The crystal was mounted on a MiTeGen Kapton loops (polyimide) using paratone oil. Data was collected at 100 K. The structure was processed as a regular 2-component twin with Squeeze to model disordered solvent. All non-hydrogen atoms were refined with anisotropic displacement parameters. Hydrogen atoms were added in idealized positions. Crystallographic data for X is given in Table 3.3.

Table 3.3. Crystallographic data for **8-10**.

	bPTE2 (8)	hPDI2-Cy6 (9)	hPDI2-3C5 (10)
Chemical formula	$C_{82}H_{84}O_{16}$	$2(C_{74}H_{56}N_4O_8)\cdot$ $3(C_6H_5Cl)$	$4(C_{70}H_{56}N_4O_8)$
Formula weight	1325.49	2596.10	4858.09
Space group	*C2/c*	*C2/c*	P-1
a (Å)	13.31393(13)	44.124 (5)	21.8288(7)
b (Å)	32.5646(2)	10.5998 (16)	23.5912(6)
c (Å)	15.43936(14)	33.308 (6)	29.8664(8)
α (deg)	90	90	93.285(2)
β (deg)	93.3923(8)	95.654 (12)	101.182(2)
γ (deg)	90	90	117.499(3)
V (Å^3)	6682.21(10)	15503 (4)	13191.6(7)
Z	4	4	2
μ (mm^{-1})	0.736	1.03	0.658
T (K)	100	100	100
$R1^a$ ($wR2^b$)	0.0564 (0.1587)	0.204 (0.540)	0.1593 (0.3834)
Reflections	65078	13685	54072
Radiation type	Cu Kα	Cu Kα	Cu Kα

[a]$R1 = [\Sigma w(F_o - F_c)^2/\Sigma wF_o^2]^{1/2}$; [b]$wR2 = [\Sigma[w(F_o^2 - F_c^2)^2]/\Sigma w(F_o^2)^2]^{1/2}]$, $w = 1/[\sigma^2(F_o^2) + (aP)^2 + bP]$, where $P = [\max(F_o^2,0) + 2(F_c^2)]/3$

3.5. Computational Details

Density functional theory calculations were performed using Jaguar, version 8.3, Schrodinger, Inc., New York NY, 2013. (See A. D. Bochevarov, E. Harder, T. F. Hughes, J. R. Greenwood, D. A. Braden, D. M. Philipp, D. Rinaldo, M. D. Halls, J. Zhang, R. A. Friesner, "Jaguar: A High-Performance Quantum Chemistry Software Program with Strengths in Life and Materials Sciences", Int. J. Quantum Chem., 2013, 113(18), 2110-2142).

All geometries were optimized using the B3LYP functional and the 6-31G** basis set.

hPDI2 (7) – helical conformation

B3LYP/6-31G** optimized geometry
Final total energy = -2893.38030281406 hartrees

angstroms

atom	x	y	z
C1	0.0238898930	0.0412417960	0.0020298530
C2	0.0060213119	0.0149274918	1.4047610645
C3	1.2528369856	0.0130849311	2.0979759708
C4	2.4633589357	0.0364683638	1.3537349141
C5	2.4378344326	0.0750480928	-0.0526706602
C6	1.2169371030	0.0733377675	-0.7174426566
C7	3.7063895387	0.0519202871	2.0448939650
C8	4.9883687333	0.1776153593	1.3002511689
N9	4.8967509920	0.1825624979	-0.0978310118
C10	3.7009134717	0.1286521851	-0.8280470392
C11	1.3118929585	-0.0183688096	3.5265829621
C12	2.5561042292	-0.1342648696	4.1930705336
C13	3.7454571979	-0.0382476461	3.4134862429
C14	-1.2330771595	-0.0255929810	2.1829098975
C15	-1.1547335889	-0.0039222780	3.6089984203
C16	0.1036401622	0.0429382413	4.2873680080
C17	0.1633577709	0.1661813400	5.7003779892
C18	1.4533189767	0.2245764798	6.3635633004
C19	2.5918579023	-0.1982891114	5.6410017069
C20	-1.0575430333	0.0763841227	6.4296128073
C21	-2.2708237458	-0.0297998911	5.7962861445
C22	-2.3509116268	-0.0330931577	4.3754357678
C23	-3.6041436894	-0.1000309576	3.7385418646
C24	-3.6695240802	-0.1173609736	2.3499047250
C25	-2.5030852278	-0.0773817058	1.5878913511
C26	-4.8519079621	-0.1677596317	4.5362786137
N27	-4.7171264509	-0.2005159270	5.9313503888
C28	-3.5008836702	-0.1605438634	6.6251601924
C29	1.6436656622	0.6955098202	7.7245337950
C30	2.8517012057	0.3989714238	8.4082374750
C31	3.8674048840	-0.3668666897	7.7583678604
C32	3.7419330769	-0.6742413341	6.3812858287
C33	5.0138997832	-0.7959035362	8.4979476303
C34	5.9728215138	-1.6312190375	7.8647896515
C35	5.7619577702	-2.0361833985	6.5186095727
C36	4.6904734736	-1.5661634918	5.8046067048
C37	5.2155326307	-0.4006908523	9.8532029746

C38	4.2281449411	0.4744167372	10.4865991093
C39	3.0624227012	0.8478988075	9.7500647560
C40	2.0912601213	1.6893316697	10.3575089599
C41	0.9389176333	2.0753086784	9.6163056437
C42	0.7227787098	1.5842136928	8.3524367669
C43	6.3633878793	-0.8599230380	10.5161972731
C44	7.2922542599	-1.6876710763	9.8888803088
C45	7.1053364365	-2.0812920420	8.5684805068
C46	8.0960485188	-2.9809497538	7.9246410540
N47	7.8168306187	-3.3815773033	6.6098015270
C48	6.6962247564	-2.9872647764	5.8676745168
C49	2.2812440621	2.1665003174	11.6680105913
C50	3.4183634930	1.7948103809	12.3770870437
C51	4.3719931265	0.9605074426	11.7954288349
C52	-0.0457043204	3.0349575683	10.1890964375
N53	0.1907834707	3.4572336348	11.5038920144
C54	1.2876377484	3.0754514122	12.2899599050
O55	3.7254219152	0.1390533189	-2.0517596094
O56	6.0695940851	0.2634203057	1.8640388091
O57	6.5231823146	-3.4138404824	4.7345303384
O58	9.1003088822	-3.3691149414	8.5042647491
O59	1.4039333290	3.4989682121	13.4324394496
O60	-1.0133310285	3.4361471181	9.5586838224
O61	-5.9620134506	-0.2080109463	4.0230640362
O62	-3.4646356589	-0.2253361931	7.8452630120
H63	-0.1482585566	1.9490537917	7.8253197710
H64	3.5455168353	2.1714101293	13.3861918791
H65	5.2441519627	0.6948578483	12.3802875511
C66	-0.7640519494	4.3763569720	12.1262467916
H67	8.1717187335	-2.0411696828	10.4156665708
H68	6.5456312524	-0.5759436081	11.5456080502
H69	4.5631447025	-1.9448983639	4.7999750797
C70	8.7498503742	-4.2906182485	5.9412718087
C71	-5.9588623351	-0.2941309537	6.7013672538
H72	-4.6447170313	-0.1662496047	1.8775807455
H73	-2.5968779214	-0.0921381275	0.5087866209
H74	-1.0606621447	0.0292522222	7.5102352799
C75	6.1310950821	0.2591005275	-0.8815832676
H76	1.2164125900	0.0995424313	-1.8017222492
H77	-0.9067828186	0.0395408609	-0.5524962147
H78	4.7171587514	0.0221341463	3.8829666971
H79	-1.5507099656	4.5742739052	11.4014176616
H80	-1.1719026953	3.9190126911	13.0296531845
H81	-0.2522329199	5.2990940213	12.4067842705

H82	-5.6925480471	-0.3053212526	7.7560771169
H83	-6.5951906177	0.5617328072	6.4686182869
H84	-6.4914875087	-1.2062292641	6.4248088226
H85	6.9640421869	0.2896175393	-0.1825258019
H86	6.2007554260	-0.6135849848	-1.5337795931
H87	6.1130501147	1.1553676257	-1.5048850267
H88	9.5627299479	-4.4970827076	6.6342562669
H89	8.2289107619	-5.2097583388	5.6662306173
H90	9.1244388403	-3.8201377050	5.0300813507

hPDI2 (7) – butterfly conformation

B3LYP/6-31G** optimized geometry
Final total energy = -2893.37034913593 hartrees

angstroms

atom	x	y	z
C1	-0.1207083661	0.6585517917	0.1745296997
C2	-0.0228332207	0.5294361203	1.5840954609
C3	1.2486121445	0.3412653527	2.2161814763
C4	2.4066034696	0.1872372139	1.4083742263
C5	2.2538545922	0.0970217842	-0.0030936873
C6	1.0326238607	0.3132260315	-0.5903970375
C7	3.6757904249	0.0427434479	1.9983792729
C8	4.8779953372	-0.1961738835	1.1614209744
N9	4.6579770449	-0.3548632045	-0.2181357962
C10	3.4145809223	-0.2606041864	-0.8566290656
C11	1.3736248307	0.2772312414	3.6360943512
C12	2.6625191294	0.1959093785	4.1868101528
C13	3.7972245794	0.0867171948	3.3840774477
C14	-1.2112985338	0.4692317441	2.3728122493
C15	-1.1075310939	0.2145902624	3.7785921542
C16	0.1554827501	0.2040015772	4.4433294093
C17	-2.2867956758	-0.0626850775	4.5207270779
C18	-3.5226401452	-0.1953537945	3.8287147375
C19	-3.6050287693	0.0837101166	2.4873607333
C20	-2.4792086646	0.5404251085	1.7400211455
C21	-2.2216331953	-0.2871567553	5.9079276351
C22	-0.9951489723	-0.2083649140	6.5591117147
C23	0.1728131666	0.0288846339	5.8358973153
C24	-4.7408011376	-0.6630220343	4.5415124052
N25	-4.6230658474	-0.8181779286	5.9320615931
C26	-3.4434290893	-0.6436185992	6.6696019948
C27	5.8024863319	-0.6667958484	-1.0814489661
O28	3.3205769633	-0.4592698928	-2.0594940674
O29	6.0003223867	-0.2805475782	1.6407099923
O30	-5.7918776580	-0.8913554137	3.9603992576
C31	-5.8089124452	-1.2223699987	6.6953890367
O32	-3.4442060229	-0.8080691980	7.8819991876
H33	1.1141379244	0.0399714541	6.3719153781
H34	-0.9660455881	-0.3696296002	7.6312108964
H35	-4.5574266883	-0.0981683959	2.0111788451
C36	-2.5668030955	1.0059851708	0.3657600415
H37	0.9747475779	0.1710282829	-1.6599359945

H38	2.7923994778	0.1800824180	5.2622142639
H39	4.7851747560	-0.0051902612	3.8213813740
H40	-6.6446407779	-1.2817125199	6.0028702021
H41	-5.6353040208	-2.1919314228	7.1677526739
H42	-6.0062441762	-0.4896777453	7.4799311252
H43	6.6919609195	-0.6935443378	-0.4572146448
H44	5.6449319591	-1.6314261069	-1.5688138506
H45	5.8976861886	0.0959896507	-1.8567855154
C46	-1.3834208598	1.0659937704	-0.4173683542
C47	-3.8287528422	1.4157582547	-0.2279378210
C48	-1.4648592758	1.5419960747	-1.7867576903
C49	-4.9889443527	1.7339084523	0.5398007167
C50	-6.2100070384	1.9578088426	-0.0454359851
C51	-6.3525734109	1.9143048063	-1.4601186977
C52	-5.1900014960	1.7858117204	-2.2664539547
C53	-3.9212526375	1.5746463874	-1.6352618566
H54	-4.9370539248	1.8464656844	1.6127969539
C55	-7.3784515478	2.2710572714	0.8218593431
C56	-7.6176564189	2.0793343919	-2.0522638410
C57	-0.3287470690	1.9858296898	-2.5258195625
C58	-0.4024214114	2.2859372831	-3.8622498848
C59	-1.6405306132	2.1946990154	-4.5562037667
C60	-2.8261051450	1.9273194065	-3.8200248633
C61	-2.7301414984	1.6415198358	-2.4198181830
H62	0.6265760553	2.1389842296	-2.0460107503
C63	0.8284859417	2.7322128988	-4.5664496421
C64	-1.6987969193	2.4488323265	-5.9382844821
C65	-7.7312601484	2.0923694081	-3.4383292217
C66	-8.8220050252	2.2745275411	-1.2101313459
H67	-8.7171731474	2.2027645386	-3.8764846730
C68	-6.5932348016	2.0081609753	-4.2386309952
C69	-5.3083625730	1.8966805221	-3.6842760808
H70	-6.7174898929	2.0634034739	-5.3132706739
C71	-2.9262092610	2.4159738011	-6.5907986005
C72	-0.4677581843	2.7851624302	-6.6937893314
H73	-2.9513582625	2.6008583852	-7.6591072266
C74	-4.0988156958	2.1906101736	-5.8723396401
C75	-4.0871357206	1.9779731744	-4.4853728541
H76	-5.0397519307	2.2127937075	-6.4087945691
O77	-7.2740234485	2.4239068998	2.0303768126
O78	-9.9484797190	2.3762972228	-1.6763444849
N79	-8.6200314088	2.3701599028	0.1747075673
C80	-9.8152464062	2.6187526853	0.9885587925
H81	-9.5072752891	2.6416220886	2.0308260267

H82	-10.2684429399	3.5707992966	0.7034049851
H83	-10.5464148919	1.8264249533	0.8181917279
O84	1.8851844847	2.9213400177	-3.9811995829
O85	-0.4622031339	2.9703075611	-7.9031950348
N86	0.7162314337	2.9129881540	-5.9540229044
C87	1.9136194723	3.2939520002	-6.7110046194
H88	2.7495944683	3.3220476698	-6.0168728814
H89	2.0920876323	2.5655852716	-7.5040876013
H90	1.7667843000	4.2733227139	-7.1719288243

bPTE2 (8) – helical conformation

B3LYP/6-31G** optimized geometry
Final total energy = -3435.67489478116 hartrees

angstroms

atom	x	y	z
C1	13.7931910369	1.7550156629	4.9554983110
C2	14.9923259830	1.0755812758	4.7443170874
C3	15.0274509766	-0.2282126759	4.0733368552
C4	13.9070336277	-0.7577062133	3.4324553607
C5	16.2059515809	1.6732241781	5.2061622025
C6	16.1890067763	2.9749555023	5.8053197430
C7	14.9255190715	3.5601923139	6.1152557963
C8	13.7605917433	2.9560077538	5.6574615742
C9	17.4616042108	3.5809218978	6.0930697737
C10	17.4340876575	0.9402454407	5.0889715742
C11	18.6674933383	1.5461396764	5.4201707487
C12	18.6254263603	2.8727365663	5.9288599608
C13	16.2294591265	-0.9987517633	4.0895950332
C14	17.4155456061	-0.4292473589	4.6598910429
C15	18.5804810624	-1.2107160623	4.8151257986
C16	19.7974365158	-0.6199556908	5.3309484722
C17	19.9023442607	0.7846115952	5.3515750365
C18	16.2530543530	-2.3180215140	3.5312787643
C19	17.4340315951	-3.1107820472	3.7635186948
C20	18.5402289345	-2.5562950181	4.3570040942
C21	21.2335705693	1.3617182849	5.3160174670
C22	22.3707844137	0.5691661092	5.6013829837
C23	22.1923498656	-0.8092359446	5.9608971984
C24	20.9146654403	-1.3940708838	5.8275164517
C25	23.6900472203	1.1323318117	5.5274121240
C26	23.8849784830	2.4670686565	5.0402716784
C27	22.7078251683	3.2572128264	4.7967033395
C28	21.4583139647	2.7014856012	4.8973978212
C29	24.8114424051	0.3429172270	5.9327068295
C30	24.6066251135	-1.0216187281	6.4316602185
C31	23.2996922661	-1.5970211984	6.4221444228
C32	23.1013025339	-2.9505464395	6.8547530136
C33	21.7380312455	-3.4121335781	6.9602677172
C34	20.7176592796	-2.6781771501	6.4119071836
C35	24.2401927303	-3.7336516568	7.1853822920
C36	25.4898570753	-3.1293338918	7.2494104129
C37	25.6697868969	-1.7977047246	6.8977781225

C38	25.2167487970	2.9134974669	4.8048335213
C39	26.2848549974	2.1494294958	5.2552508146
C40	26.0881584678	0.9008546484	5.8361166744
C41	13.9682073668	-1.9826424289	2.7757371972
C42	15.1239511988	-2.7531348976	2.7818178479
H43	26.3361039031	-3.7364722576	7.5511835492
H44	26.6685689988	-1.3862275425	6.9577129399
H45	26.9593356311	0.3444559904	6.1565330939
H46	27.2881925030	2.5322619519	5.1038802691
H47	20.6283457870	3.3318876752	4.6175459691
H48	19.7087236087	-3.0401008588	6.5484850933
H49	19.4152583841	-3.1794699296	4.4559854545
H50	13.1124832967	-2.3503054418	2.2203880392
H51	12.8076964953	3.4154326579	5.8907052103
H52	19.5314972028	3.3635547651	6.2496541429
C53	14.7764682136	4.6672533274	7.1071752399
C54	17.6858226246	5.0182355544	6.4620760199
C55	22.6884619428	4.7396970517	4.5683020642
C56	25.6062200726	4.0887516726	3.9648540216
C57	24.2645975151	-5.2169589828	7.3805240607
C58	21.3595312627	-4.5417226874	7.8624775652
C59	17.4474985737	-4.5961365377	3.5869207397
C60	15.0845162604	-3.9312604235	1.8592955805
H61	12.8539308570	1.3269034030	4.6304942934
H62	12.9801041779	-0.2003367704	3.3928836885
O63	26.6199855483	4.7385508968	4.1153203187
O64	24.7622482970	4.2602111403	2.9203678645
C65	25.1116513023	5.3110675214	2.0039770509
O66	21.8651863580	5.3249933623	3.8964870953
O67	23.6174891620	5.3682095119	5.3223179842
C68	23.5874646454	6.8053261252	5.2784324980
O69	25.0644172206	-5.7965072236	8.0836463832
O70	23.3875363372	-5.8594096201	6.5723841143
C71	23.3756470127	-7.2887852154	6.7199757951
O72	21.9803324381	-4.8816540601	8.8498825291
O73	20.1791891730	-5.1024471784	7.5102194057
C74	19.6712977975	-6.0845049729	8.4296808119
O75	16.4939318798	-5.3241084853	3.7805568081
O76	18.6809347002	-5.0617869357	3.2898589233
C77	18.8149892446	-6.4923745627	3.2923361809
O78	14.0845034276	-4.5698189528	1.6109937658
O79	16.2622285748	-4.1142745896	1.2153528889
C80	16.2857803780	-5.2280821157	0.3074196215
O81	18.5886915528	5.4095373176	7.1692173852

O82	16.8591548770	5.8463204443	5.7830703683
C83	17.0450171830	7.2439141911	6.0626855011
O84	15.5109031794	4.8552328784	8.0571753556
O85	13.6550284279	5.3927269297	6.8931191546
C86	13.3601572702	6.3744297441	7.9008103709
H87	24.2657380345	5.3967537010	1.3229940082
H88	25.2786120691	6.2501408979	2.5354765230
H89	26.0220965998	5.0491897086	1.4586868006
H90	24.4594833502	7.1317877000	5.8438964907
H91	23.6369572986	7.1637452671	4.2481485711
H92	22.6679079863	7.1762304672	5.7379997610
H93	22.6285304250	-7.6504508812	6.0133194657
H94	24.3579612450	-7.7074994434	6.4895979919
H95	23.1063766347	-7.5607381545	7.7435798081
H96	18.7093115494	-6.3960095929	8.0230124122
H97	20.3532629374	-6.9353539801	8.4991575402
H98	19.5473251098	-5.6527745610	9.4255590918
H99	19.8635029139	-6.6873690102	3.0679710390
H100	18.5474203370	-6.9023682483	4.2692044506
H101	18.1701370389	-6.9421495698	2.5338384193
H102	17.2915273171	-5.2416020060	-0.1125574816
H103	16.0745204663	-6.1565001870	0.8437483035
H104	15.5408052236	-5.0967564092	-0.4805982571
H105	16.3112050877	7.7651954316	5.4478404171
H106	16.8757081283	7.4417272724	7.1240253645
H107	18.0583659829	7.5555772855	5.7998212283
H108	12.4198628473	6.8334132131	7.5956760551
H109	13.2597230135	5.9030208239	8.8814052969
H110	14.1532783822	7.1240315489	7.9518512457

bPTE2 (8) – butterfly conformation

B3LYP/6-31G** optimized geometry
Final total energy = -3435.67968140964 hartrees

angstroms

atom	x	y	z
C1	13.9785046096	1.8735180629	4.5181204569
C2	15.1151251961	1.0700606618	4.6208285144
C3	15.0246115517	-0.3919899667	4.6604075818
C4	13.7958484768	-1.0557930584	4.6532995903
C5	16.3944654040	1.7019109305	4.6472369664
C6	16.5014005160	3.1197162407	4.4798956711
C7	15.3108235262	3.8977708692	4.4805701649
C8	14.0756203385	3.2590784474	4.4817678575
C9	17.8290214174	3.6551263432	4.3088315299
C10	17.5706005619	0.9071843492	4.8630163363
C11	18.8280302730	1.5310387215	5.0322169690
C12	18.9221446738	2.9000630462	4.6435993742
C13	16.2194668845	-1.1728471661	4.6682314770
C14	17.4888101792	-0.5223978436	4.8455655643
C15	18.6749172521	-1.2878249094	4.9505526450
C16	19.9145251086	-0.6616548484	5.3683508866
C17	19.9781254940	0.7534159554	5.4375064500
C18	16.1466297876	-2.5971815112	4.5400357219
C19	17.3905887622	-3.2857775554	4.3037830187
C20	18.5827581000	-2.6487344708	4.5306128956
C21	21.1982601218	1.3819028266	5.8961135236
C22	22.3997100790	0.6400939269	5.9552836310
C23	22.3503760527	-0.7856669969	5.8402735804
C24	21.0962860814	-1.4271305739	5.7091786359
C25	23.6494662668	1.3059343259	6.1884838158
C26	23.6741732181	2.7100548423	6.4602454897
C27	22.4079994178	3.3338890797	6.7587242475
C28	21.2365275144	2.7045171490	6.4270163817
C29	24.8664282147	0.5630146537	6.1206082907
C30	24.8177143902	-0.8966044037	5.9794241541
C31	23.5554904708	-1.5615557343	5.9284297195
C32	23.4915987381	-2.9928453409	5.9265838212
C33	22.1927875723	-3.5823486426	6.1430236183
C34	21.0616770127	-2.8174893008	6.0200500084
C35	24.6965646349	-3.7272254061	5.7667604978
C36	25.9128883339	-3.0564965206	5.8007809938
C37	25.9765633058	-1.6742050309	5.9341486605

C38	24.9251634191	3.3829618380	6.4443084793
C39	26.0980588682	2.6437265806	6.3539618905
C40	26.0731738566	1.2590946994	6.2292909078
C41	13.7247979991	-2.4432066626	4.6743404231
C42	14.8736018411	-3.2271265688	4.6322578995
H43	26.8207019586	-3.6418265787	5.7053448421
H44	26.9527821510	-1.2094356805	5.9719048035
H45	27.0176892395	0.7330846869	6.1859457220
H46	27.0416953098	3.1780493623	6.3654438643
H47	20.3146633922	3.2192758323	6.6658007611
H48	20.1149962715	-3.2876726127	6.2406070406
H49	19.4802156038	-3.2077853056	4.3084557231
H50	12.7606106087	-2.9308858257	4.7446450647
H51	13.1754520959	3.8610246214	4.4741019098
H52	19.8934143455	3.3553732543	4.5033472245
C53	15.3347067577	5.3785644763	4.6663631679
C54	18.1507699918	4.9425756898	3.6133006391
C55	22.2500981055	4.5779014810	7.5772667883
C56	25.0994053312	4.8664592938	6.3762746454
C57	24.7934700267	-5.1838864718	5.4381594452
C58	22.0333297143	-4.9659152344	6.6908844113
C59	17.5170544749	-4.6398912376	3.6759142846
C60	14.7342639626	-4.6922484045	4.8757498844
H61	12.9918474614	1.4308476688	4.4910898013
H62	12.8690606232	-0.4978845542	4.6674166886
O63	26.0960036640	5.4584104592	6.7384830186
O64	24.0635182018	5.4700103286	5.7512686830
C65	24.1764425987	6.8928363687	5.5829900527
O66	21.2716289392	5.2942833783	7.5635088586
O67	23.2827428721	4.7528668609	8.4361735103
C68	23.1664220644	5.8815704741	9.3176908922
O69	25.7419187242	-5.8841370354	5.7232500079
O70	23.7682169310	-5.6007251446	4.6608686635
C71	23.7990328853	-6.9947841377	4.3139598655
O72	22.8574465480	-5.5535928985	7.3642422199
O73	20.8170713941	-5.4673917640	6.4002711457
C74	20.5045781549	-6.7493147305	6.9650470923
O75	18.4384638536	-5.4037475043	3.8714856189
O76	16.5496388714	-4.8647704781	2.7557758810
C77	16.6181197685	-6.1463536703	2.1107865156
O78	15.5794690972	-5.4045434395	5.3830923512
O79	13.5050449787	-5.1477277836	4.5391076418
C80	13.2496619489	-6.5227960735	4.8672051871
O81	19.1688680612	5.5781482802	3.7793062636

O82	17.2372325944	5.2420420373	2.6571729574
C83	17.5011585613	6.4538530173	1.9331945480
O84	16.2224791446	6.0037695220	5.2113779117
O85	14.1957531855	5.9619667100	4.2243616950
C86	14.0907685612	7.3712942260	4.4836306761
H87	23.2225290209	7.2119320572	5.1649932869
H88	24.3628815861	7.3818522323	6.5416107976
H89	24.9976825444	7.1297261206	4.9018300600
H90	24.1057457724	5.9195440538	9.8683916835
H91	23.0133263732	6.8020931344	8.7501881578
H92	22.3234224580	5.7462653500	9.9999266649
H93	22.9117046888	-7.1635504232	3.7040209788
H94	24.7056311166	-7.2304167849	3.7516513674
H95	23.7721759359	-7.6086437518	5.2175758814
H96	19.5136015089	-6.9932695041	6.5844263132
H97	21.2363938557	-7.4964419004	6.6487795720
H98	20.5026643992	-6.6990943182	8.0571350132
H99	15.7832587774	-6.1673371699	1.4100701418
H100	17.5670632613	-6.2609136577	1.5818131528
H101	16.5254686530	-6.9467690984	2.8491557924
H102	12.2222707708	-6.7120786182	4.5565034847
H103	13.9387112055	-7.1807975500	4.3323955336
H104	13.3653694386	-6.6918154905	5.9404639433
H105	16.6902101541	6.5463207183	1.2105032276
H106	17.5128809830	7.3077864760	2.6151407916
H107	18.4657181043	6.3956561550	1.4235542810
H108	13.1199379701	7.6701967389	4.0885514441
H109	14.1496205030	7.5721495576	5.5560143084
H110	14.8934278814	7.9159626025	3.9810211909

3.6. References

(1)   Dutta, S.; Pati, S. K. *J. Mater. Chem.* **2010**, *20*, 8207–8223.

(2)   Terrones, M.; Botello-Méndez, A. R.; Campos-Delgado, J.; López-Urías, F.; Vega-Cantú, Y. I.; Rodríguez-Macías, F. J.; Elías, A. L.; Muñoz-Sandoval, E.; Cano-Márquez, A. G.; Charlier, J.-C.; Terrones, H. *Nano Today* **2010**, *5* (4), 351–372.

(3)   Novoselov, K. S.; Falʹko, V. I.; Colombo, L.; Gellert, P. R.; Schwab, M. G.; Kim, K. *Nature* **2012**, *490* (7419), 192–200.

(4)   Nakada, K.; Fujita, M.; Dresselhaus, G.; Dresselhaus, M. S. *Phys. Rev. B* **1996**, *54* (24), 17954–17961.

(5)   Cai, J.; Ruffieux, P.; Jaafar, R.; Bieri, M.; Braun, T.; Blankenburg, S.; Muoth, M.; Seitsonen, A. P.; Saleh, M.; Feng, X.; Müllen, K.; Fasel, R. *Nature* **2010**, *466*.

(6)   Zhang, H.; Lin, H.; Sun, K.; Chen, L.; Zagranyarski, Y.; Aghdassi, N.; Duhm, S.; Li, Q.; Zhong, D.; Li, Y.; Mü, K.; Fuchs, H.; Chi, L. *J. Am. Chem. Soc.* **2015**, *137* (12), 4022–4025.

(7)   Talirz, L.; So, H.; Dumslaff, T.; Wang, S.; Ramon Sanchez-Valencia, J.; Liu, J.; Shinde, P.; Pignedoli, C. A.; Liang, L.; Meunier, V.; Plumb, N. C.; Shi, M.; Feng, X.; Narita, A.; Mu, K.; Fasel, R.; Ruffieux, P. *ACS Nano* **2017**, *11* (2), 1380–1388.

(8)   Chen, Y.-C.; de Oteyza, D. G.; Pedramrazi, Z.; Chen, C.; Fischer, F. R.; Crommie, M. F. *ACS Nano* **2013**, *7* (7), 6123–6128.

(9)   Durr, R. A.; Haberer, D.; Lee, Y.-L.; Blackwell, R.; Kalayjian, A. M.; Marangoni, T.; Ihm, J.; Louie, S. G.; Fischer, F. R. *J. Am. Chem. Soc.* **2018**, *140* (2), 807–813.

(10)   Cloke, R. R.; Marangoni, T.; Nguyen, G. D.; Joshi, T.; Rizzo, D. J.; Bronner, C.; Cao, T.; Louie, S. G.; Crommie, M. F.; Fischer, F. R. *J. Am. Chem. Soc.* **2015**, *137* (28), 8872–8875.

(11)   Zhong, Y.; Kumar, B.; Oh, S.; Trinh, M. T.; Wu, Y.; Elbert, K.; Li, P.; Zhu, X.; Xiao, S.; Ng, F.; Steigerwald, M. L.; Nuckolls, C. *J. Am. Chem. Soc.* **2014**, *136* (22), 8122–8130.

(12)   Sisto, T. J.; Zhong, Y.; Zhang, B.; Trinh, M. T.; Miyata, K.; Zhong, X.; Zhu, X.-Y.; Steigerwald, M. L.; Ng, F.; Nuckolls, C. *J. Am. Chem. Soc.* **2017**, *139* (16), 5648–5651.

(13)   Narita, A.; Feng, X.; Hernandez, Y.; Jensen, S. A.; Bonn, M.; Yang, H.; Verzhbitskiy, I. A.; Casiraghi, C.; Hansen, M. R.; Koch, A. H. R.; Fytas, G.; Ivasenko, O.; Li, B.; Mali, K. S.; Balandina, T.; Mahesh, S.; De Feyter, S.; Müllen, K. *Nat. Chem.* **2014**, *6* (2), 126–132.

(14)   Cruz, C. M.; Márquez, I. R.; Mariz, I. F. A.; Blanco, V.; Sánchez-Sánchez, C.; Sobrado, J. M.; Martín-Gago, J. A.; Cuerva, J. M.; Maçôas, E.; Campaña, A. G. *Chem. Sci.* **2018**, *9* (16), 3917–3924.

(15)   Wang, Z.; Gu, P.; Liu, G.; Yao, H.; Wu, Y.; Li, Y.; Rakesh, G.; Zhu, J.; Fu, H.; Zhang, Q. *Chem. Commun.* **2017**, *53* (55), 7772–7775.

(16)   Narita, A.; Verzhbitskiy, I. A.; Frederickx, W.; Mali, K. S.; Jensen, S. A.; Hansen, M. R.; Bonn, M.; De Feyter, S.; Casiraghi, C.; Feng, X.; Müllen, K. *ACS Nano* **2014**, *8* (11), 11622–11630.

(17)   Gingras, M. *Chem. Soc. Rev.* **2013**, *42* (3), 1051–1095.

(18)   Hoffmann, R.; Hopf, H. *Angew. Chemie Int. Ed.* **2008**, *47* (24), 4474–4481.

(19)   Liu, J.; Li, B.-W.; Tan, Y.-Z.; Giannakopoulos, A.; Sanchez-Sanchez, C.; Beljonne, D.; Ruffieux, P.; Fasel, R.; Feng, X.; Mu, K. *J. Am. Chem. Soc.* **2015**, *137* (18), 6097–6103.

(20)   Bendikov, M.; Wudl, F.; Perepichka, D. F. *Chem. Rev.* **2004**, *104* (11), 4891–4946.

(21)   Ball, M.; Zhong, Y.; Wu, Y.; Schenck, C.; Ng, F.; Steigerwald, M.; Xiao, S.; Nuckolls, C. *Acc. Chem. Res.* **2015**, *48* (2), 267–276.

(22)   Spenst, P.; Sieblist, A.; Würthner, F. *Chem. - A Eur. J.* **2017**, *23* (7), 1667–1675.

(23)   Loser, S.; Bruns, C. J.; Miyauchi, H.; Ortiz, R. P.; Facchetti, A.; Stupp, S. I.; Marks, T. J. *J. Am. Chem. Soc.* **2011**, *133* (21), 8142–8145.

(24)   Bürckstümmer, H.; Tulyakova, E. V.; Deppisch, M.; Lenze, M. R.; Kronenberg, N. M.; Gsänger, M.; Stolte, M.; Meerholz, K.; Würthner, F. *Angew. Chemie Int. Ed.* **2011**, *50* (49), 11628–11632.

(25)   Troshin, P. A.; Sariciftci, N. S. Supramolecular chemistry for organic photovoltaics. In *Supramolecular Chemistry: From Molecules to Nanomaterials*; Gale, P. A.; Steed, J. W., Eds.; John Wiley & Sons: Hoboken, NJ, **2012**.

(26)   Herbstein, F. H. *Acta Cryst* **1979**, *35*, 1661–1670.

(27)   Kato, K.; Segawa, Y.; Itami, K. *Can. J. Chem.* **2017**, *95* (3), 329–333.

(28)   WebCSD - The Cambridge Crystallographic Data Centre (CCDC) https://www.ccdc.cam.ac.uk/solutions/csd-system/components/webcsd/ (accessed May 22, 2018).

(29)   Nagarajan, K.; Mallia, A. R.; Muraleedharan, K.; Hariharan, M. *Chem. Sci.* **2017**, *8* (3), 1776–1782.

(30)   Steinberg, B. D.; Jackson, E. A.; Filatov, A. S.; Wakamiya, A.; Petrukhina, M. A.; Scott, L. T. *J. Am. Chem. Soc.* **2009**, *131* (30), 10537–10545.

(31)   Ke, X.-S.; Hong, Y.; Tu, P.; He, Q.; Lynch, V. M.; Kim, D.; Sessler, J. L. *J. Am. Chem. Soc.* **2017**, *139* (42), 15232–15238.

(32)   Li, Y.; Wang, C.; Li, C.; Di Motta, S.; Negri, F.; Wang, Z. *Org. Lett.* **2012**, *14* (20), 5278–5281.

(33)   Sharenko, A.; Gehrig, D.; Laquai, F.; Nguyen, T.-Q. *Chem. Mater.* **2014**, *26* (14), 4109–4118.

(34)   Singh, R.; Aluicio-Sarduy, E.; Kan, Z.; Ye, T.; MacKenzie, R. C. I.; Keivanidis, P. E. *J. Mater. Chem. A* **2014**, *2* (35), 14348–14353.

(35)   Zhong, Y.; Trinh, M. T.; Chen, R.; Wang, W.; Khlyabich, P. P.; Kumar, B.; Xu, Q.; Nam, C.-Y.; Sfeir, M. Y.; Black, C.; Steigerwald, M. L.; Loo, Y.-L.; Xiao, S.; Ng, F.; Zhu, X.-Y.; Nuckolls, C. *J. Am. Chem. Soc.* **2014**, *136* (43), 15215–15221.

(36)   Würthner, F.; Saha-Möller, C. R.; Fimmel, B.; Ogi, S.; Leowanawat, P.; Schmidt, D. *Chem. Rev.* **2015**.

(37)   CrysAlisPro 1.171.38.41 Oxford Diffraction/Agilent Technologies UK Ltd: Yarnton, England.

(38)   Sheldrick, G. M. *Acta Crystallogr. Sect. A Found. Adv.* **2015**, *71* (1), 3–8.

(39)   Sheldrick, G. M. *Acta Crystallogr. Sect. C Struct. Chem.* **2015**, *71* (1), 3–8.

(40)   Dolomanov, O. V.; Bourhis, L. J.; Gildea, R. J.; Howard, J. A. K.; Puschmann, H.; IUCr. *J. Appl. Crystallogr.* **2009**, *42* (2), 339–341.

(41)   Spek, A. L.; IUCr. *Acta Crystallogr. Sect. D Biol. Crystallogr.* **2009**, *65* (2), 148–155.